NGU Report 2009.020

Barents Sea

Aeromagnetic Remapping 2008 – BASAR-08

Acquisition, processing and interpretation

M. Brönner, L. Gernigon, J. Ebbing, O. Olesen

D. Roberts, C. Barrère and J. Koziel

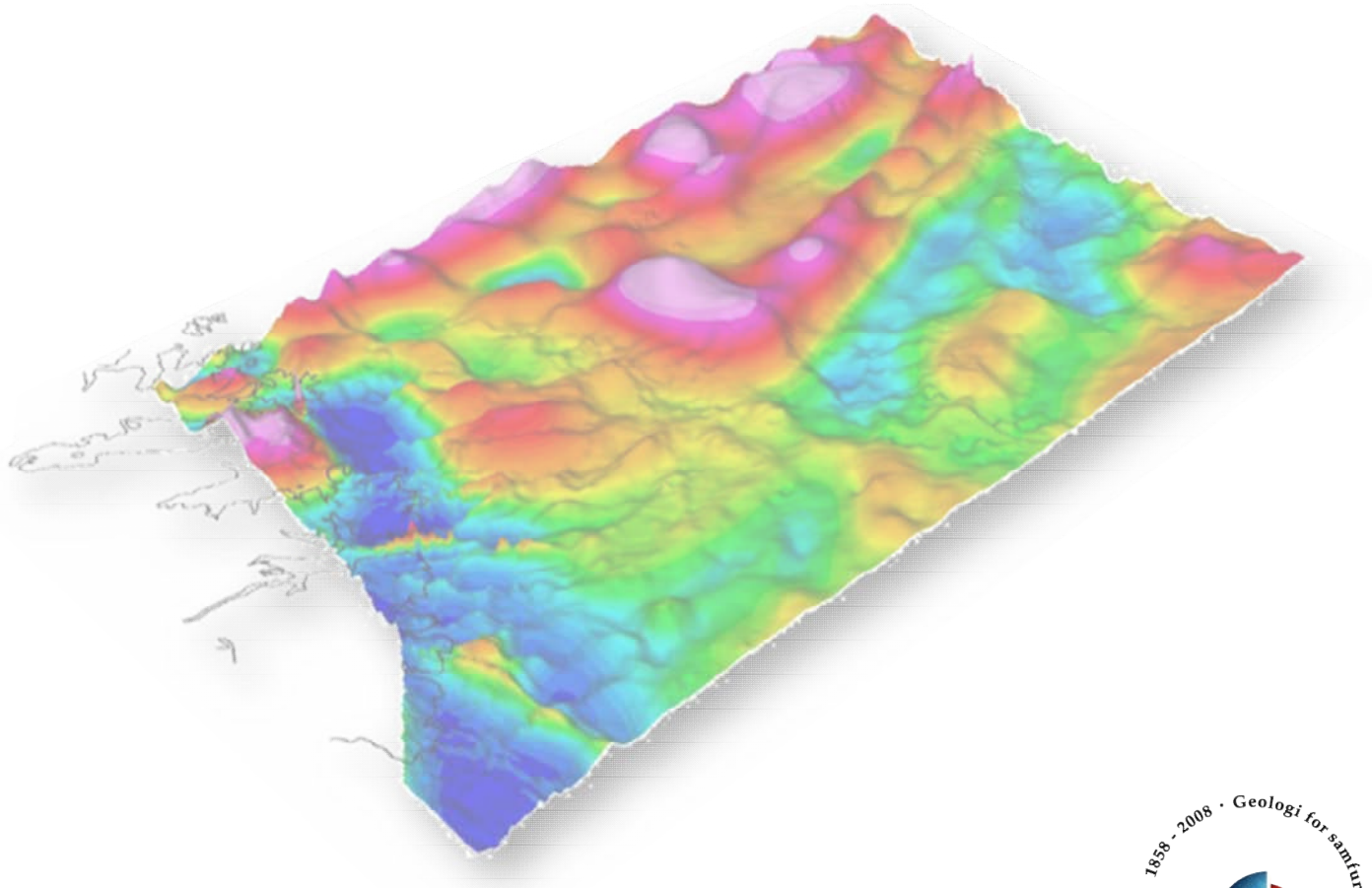

1858 - 2008 · Geologi for samfunnet i 150 år

NGU

Norges geologiske undersøkelse

150

NGU Report 2009.020

BArents Sea Aeromagnetic Remapping
BASAR-08 –Acquisition, processing and interpretation report

Geological Survey of Norway (NGU)
N-7441 Trondheim, Norway
Tel.: 47 73 90 40 00
Telefax 47 73 92 16 20

REPORT

Report no: 2009.020	ISSN 0800-3416	Grading: **Confidential to April 2014**

Title:
Barents Sea Aeromagnetic Remapping BASAR-08 – Acquisition, processing and interpretation

Authors: Marco Brönner, Laurent Gernigon, Jörg Ebbing, Odleiv Olesen, David Roberts, Cecile Barrère and Janusz Koziel	Clients: Det norske, ENI Norge, Norwegian Petroleum Directorate, StatoilHydro and Norges geologiske undersøkelse

Map-sheet name (M=1:250.000)		Map-sheet no. and -name (M=1:50.000)	
Deposit name and grid-reference:		Number of pages. 150 Price (NOK). 470 Map enclosures. x	
Fieldwork carried out: April - September 2008	Date of report: 23.04.2009	Project no.: 323600	Person responsible:

Summary:
A high-sensitivity aeromagnetic survey, BASAR-08, was carried out in an area of 80,600 km^2 in the Norwegian Barents Sea. Data processing comprised spike-removal and data editing, systematic corrections, statistical, and micro-levelling. Processing and interpretation of the new dataset included a reprocessing of the BAS-06 survey, covering the eastern Norwegian Barents Sea and the entire undisputed part of the Nordkapp Basin. Several potential field maps were produced from the survey area. Examples of various filters applied to the magnetic field have been illustrated. A depth-to-magnetic source was calculated, applying Euler deconvolution techniques.

Structural interpretation of the new magnetic data and 2D modelling along three regional seismic lines was carried out in conjunction with the existing gravity data. An existing 3D model of the Norwegian Barents Sea was updated and readjusted emplyibg the new magnetic data. The new and reprocessed magnetic data represent an important and beneficial improvement to the Norwegian shelf magnetic map, reflecting the regional basement settings with a significantly greater accuracy and providing new insights into the offshore prolongation of the Caledonides and the complex development of the southern Barents Sea. High-frequency anomalies from shallower structures were utilised to obtain a comprehensive overview of the distribution of dykes and salt diapirism in the area and were helpful in linking and identifying geological structures offshore by onshore-offshore correlations. Grav/Mag 2D and 3D modelling gave additional information of both the depth-to-basement, deeper crustal setting and the
crustal thickness.

Keywords. Geofysikk	Berggrunnsgeologi	Magnetometri
Kontinentalsokkel		Fagrapport

CONTENTS

INTRODUCTION

Laurent Gernigon, Marco Brönner & Odleiv Olesen

Like several countries (e.g. Australia, Canada, Finland, Sweden, U.S), Norway was one of the first to support a vigorous government programme to develop a countrywide, modern, high-resolution, aeromagnetic database. This programme includes continuous data acquisition, and the merging and re-processing of data from individual surveys. In this context, the Geological Survey of Norway (NGU) plays a crucial role in maintaining and continuously updating this national database. NGU's most recent aeromagnetic acquisitions proved the need for modern data in order to validate the first-order geophysical and geological features of the Norwegian continental shelf and contiguous oceanic domain. Comparing vintage and modern aeromagnetic surveys is like comparing 2D seismic lines from the 1970s with the most advanced 3D surveys and everybody usually agrees that the modern data provide much more detail and significantly improve our geological knowledge. Consequently, NGU has launched a series of remapping projects of the Norwegian continental shelf and adjacent oceanic basins with funding provided by the petroleum industry and governmental institutions. The need for a new generation of high-quality data has now become a reality for both academia and industry.

1.1 Aeromagnetic data and exploration

The delineation of gravity and magnetic anomalies should normally be the first geophysical method to be applied to a new basin or region under evaluation or re-evaluation. In frontier and under-explored areas, where seismic data are sparse or non-existent, aeromagnetic acquisition still remains the cheapest and easiest way to obtain and/or refine a picture of the structural setting of the study area. Aeromagnetic data can also be useful for the strategic planning of new seismic and electromagnetic acquisitions and define potential prospects. Large aeromagnetic surveys can be carried out efficiently and safely almost everywhere, in a short period of time and at a reasonable cost.

Also, when integrated with seismic and gravity interpretations, modern aeromagnetic information can reduce the risk of making faulty geological interpretations. Both gravity and magnetic data are independent of seismic data, both physically and from the technical measurement point of view. A joint interpretation that combines seismic and potential field data thus produces a synergy that helps to significantly improve and validate the geological and structural interpretation of potential prospects.

Modern aeromagnetic data are usually applied as a relevant complement for basin and geodynamic interpretation in Norway. If the seismic coverage is poor, it can be jointly combined with gravity data to confirm and/or estimate the lateral extent of basement features, lava flows, magmatic intrusions, salt structures or sand channels that may be observed in the sparse seismic sections (Fig. 0.1). High-resolution aeromagnetic surveys also represent relatively inexpensive tools for the 3D

mapping of faults and fracture systems propagating through hydrocarbon-bearing sedimentary successions.

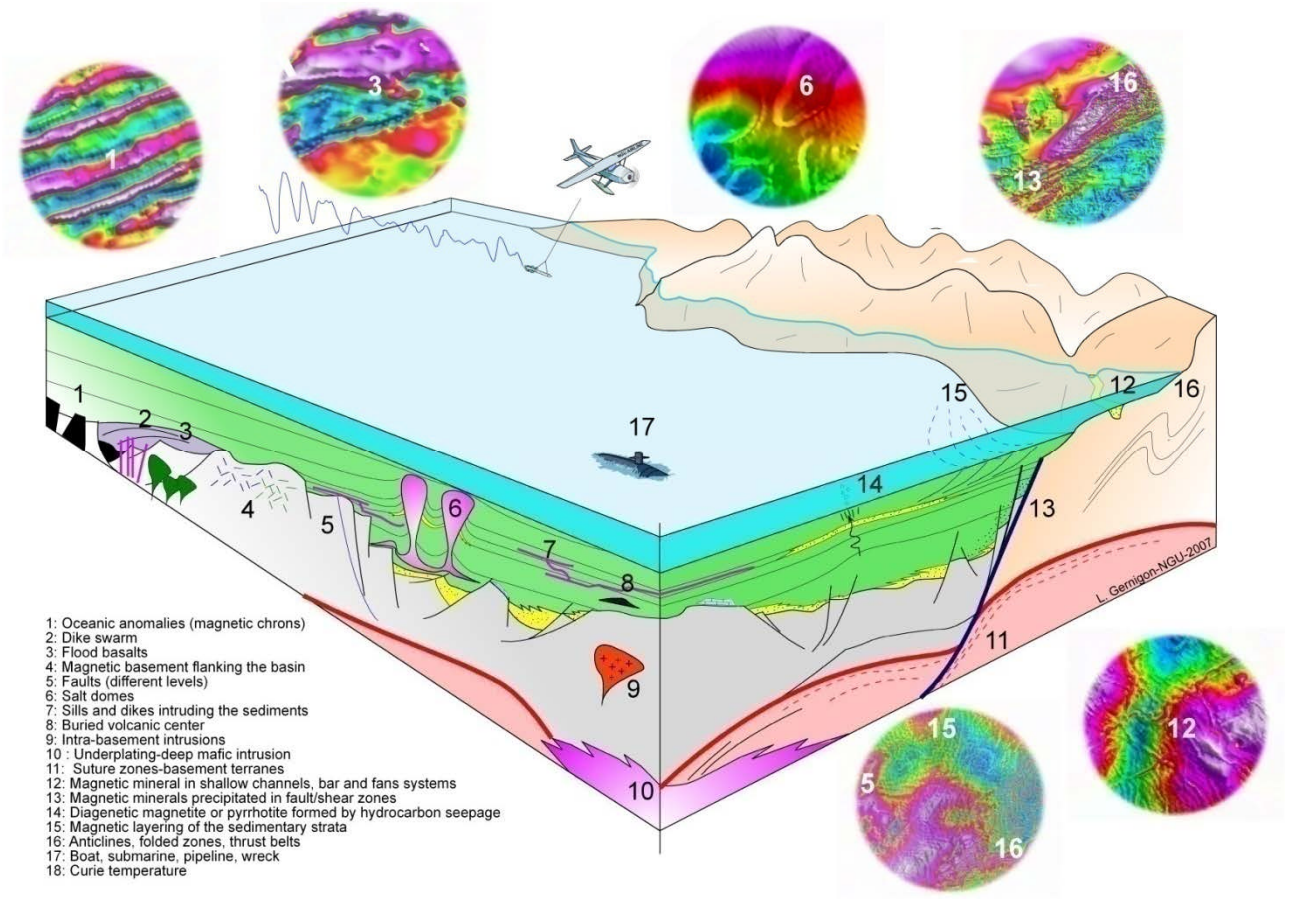

Figure 1.1 3D cartoon and examples of the application of modern NGU aeromagnetic surveys to basin or geodynamic studies. The cartoon illustrates structures and geological units that can cause observable magnetic responses (Gernigon et al. 2007).

A variety of modern techniques to process, display and model the magnetic anomalies are offered for basin analysis. Several magnetic techniques can support the basin analysis and permit geoscientists: 1) to identify and delineate in depth mafic intrusions and othe rocks volcanics, 2) to quantify and evaluate the top of the magnetic basement and infer the location of the thickest sedimentary section, 3) to detect subtle, intra-sedimentary, 'micro-magnetic' anomalies and 4) to evaluate, to some extent the temperature of the crust (Curie temperature).

1.2 Objective: BArents Sea Aero-magnetic Remapping 2008 (BASAR-08)

As part of the NGU mapping programme, a high-resolution aeromagnetic survey was acquired in the Norwegian Barents Sea in 2008 (BASAR-08). NGU initiated the BASAR-08 project as a follow-up of the successful Barents Sea Aeromagnetic Survey 2006 (BAS-06). The surveys provide state-of-the-art aeromagnetic data to replace the existing extremely sparse and poor-quality data.

The BASAR-08 is located to the west of BAS-06, which covered the area west of the Norwegian-Russian disputed area (Gernigon et al. 2007b).

Figure 0.2 shows the location of the new survey area and an outline of the previous magnetic acquisition in the study area. The existing aeromagnetic data in this region were acquired almost 40 years ago during the NGU-70 survey along parabolic Decca lines and with a small number of tie-lines, which were insufficent to consider and correct diurnal variations adequately and of low resolution. In the meantime, modern and more accurate magnetometers, navigation systems and recent advances in processing techniques allow us to seriously improve the quality of aeromagnetic mapping (Luyendyk 1997). Modern magnetometers, as used for the BASAR-08 survey, provide new total field measurements of high sensitivity, with virtually no drift and to all intents and purposes can be regarded as giving a reliable reading with typical noise envelopes of ±0.1 nT. The same cannot be said about the stinger-mounted proton magnetometers from the NGU-70 survey. They were not absolute and had to be manually calibrated, and were sensitive at best to about ±1 nT.

Advances in data acquisition techniques (more sensitive magnetometers, full release of modern Global Positioning Systems, pre-planned drape surveys, etc.), as well as data processing and displaying procedures (such as micro-levelling and advanced gridding techniques), have also significantly improved data quality and resolution, providing levels of detail that are compatible with those derived from seismic recording, well logging and surface geological mapping. Being aware of such major geophysical improvements, the primary objectives of the BASAR-08 project were multiple:

1) To provide a better and more reliable magnetic coverage of the study area.
2) To refine the tectonic and geodynamic setting of the Barents Sea, which are far from being well understood.
3) To interpret the tectonic framework, basement structure and lithology.
4) To correlate and combine these results with the known geology of the study area as an aid in the identification of new structural features.

The interpretation involves the application of improved processing techniques and cultural source removal from the total magnetic field. In order to enhance the signatures of the basement structures and lithological units, a number of processed images and interpretations have been produced during this project.

The first part of this report describes acquisition, processing, levelling and map production of the BASAR-08. Filtering techniques and data enhancement methods are described leading subsequently to an integrated study of the survey area and a discussion of the most interesting features revealed by this new dataset.

The second main part focuses on the geophysical and geological interpretation of the new survey, including also gravity and available and released seismic lines, kindly provided by the Norwegian

Petroleum Directorate (NPD). This leads to a preliminary interpretation of the survey area and opens discussions on onshore-offshore relationships and the development of the Barents Sea.

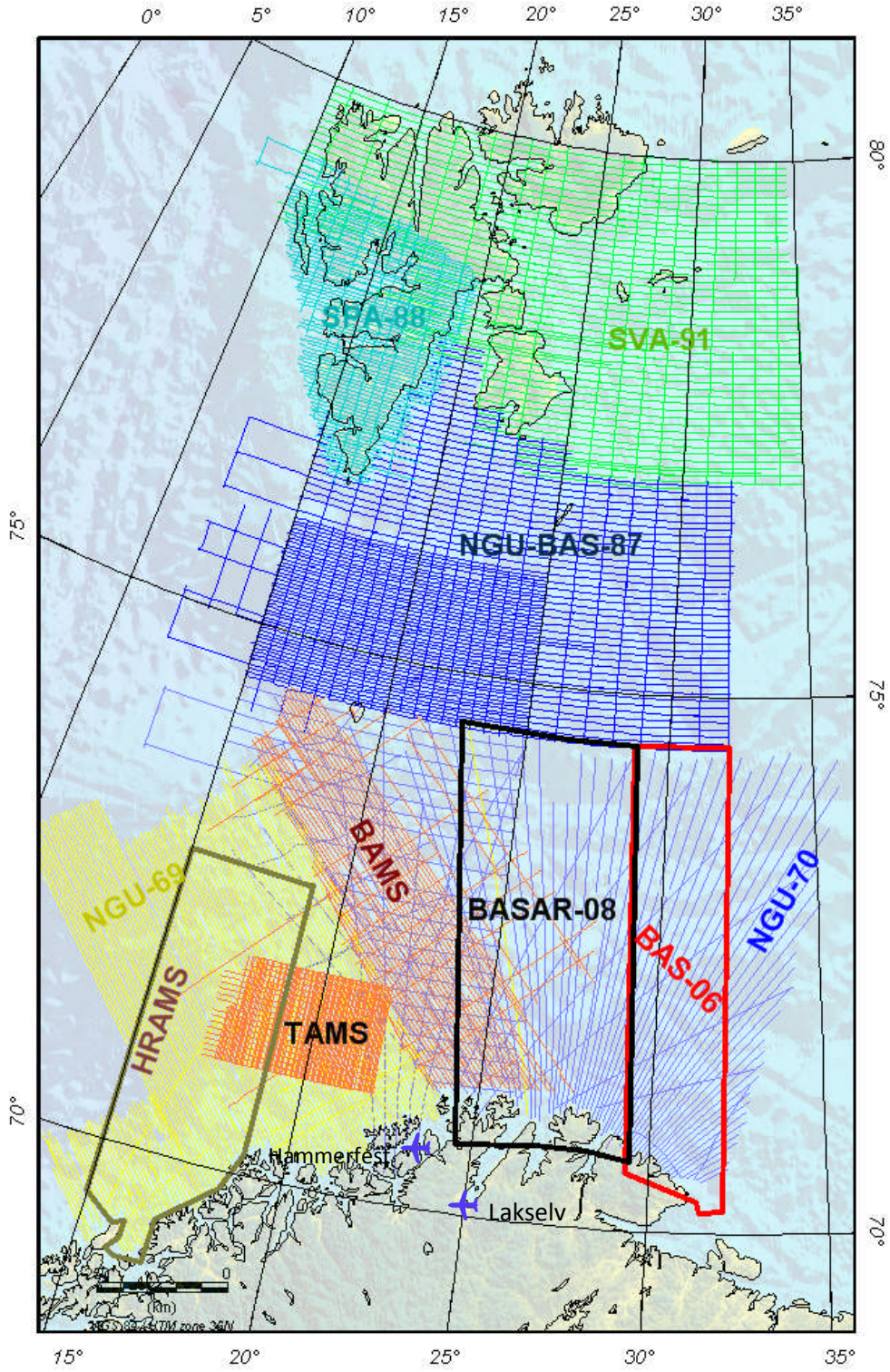

Figure 1.2 Geographic location of the BASAR-08 survey area and outline of the previous aeromagnetic surveys in and surround the Barents sea (Olesen et al. 2006, 2007, Gernigon et al. 2007b). Lakselv and Hammerfest airports were used during the survey acquisition.

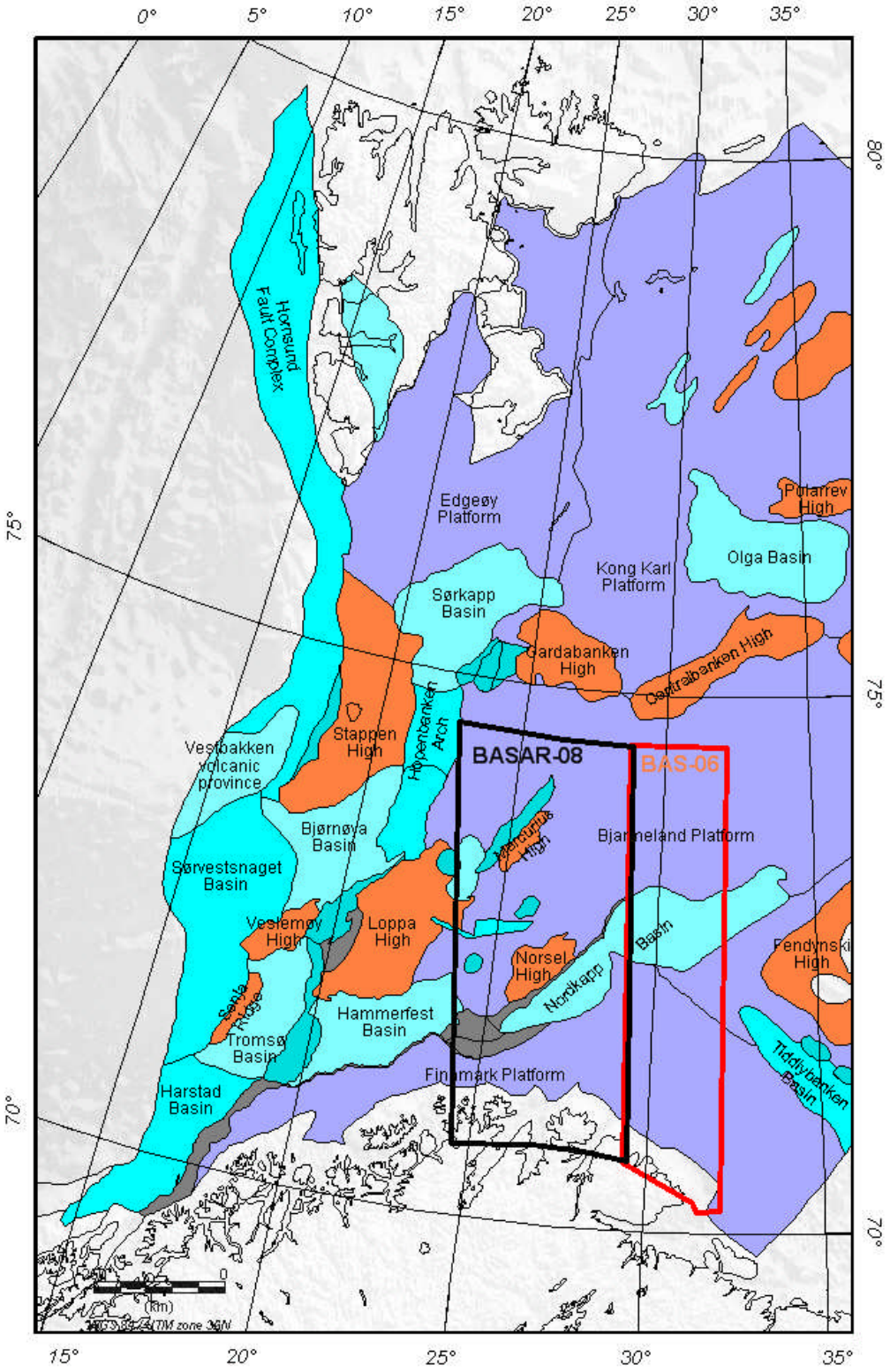

Figure 1.3 Location of the BASAR-08 survey area and outline of the adjacent BAS-06 aeromagnetic survey. The main structural elements of the western Barents Sea are from NPD (Gabrielsen et al. 1990).

The BASAR-08 acquisition was co-funded by the Norwegian Petroleum Directorate, StatoilHydro, Det norske and Eni Norge. The final compilation will certainly be welcomed by most researchers and explorationists working within the fields of geodynamics and geophysics and should provide a step further in our geodynamic knowledge of the Nordic seas.

2 SURVEY CHARACTERISTICS AND ACQUISITION

Marco Brönner and Janusz Koziel

2.1 Survey area and equipment

The survey area is approximately 435 km long by 185 km wide, extending southwards from 74°30'N to c. 40 km onshore northern Finnmark. It covers the area adjacent to the west of the BAS-06 survey and has an overlap with the latter of about 4 km to guarantee a proper coupling (Fig. 0.2). Onshore in Finnmark, the southern limit of the survey extends from Revsbotn in the west to Kongsfjorden on Varanger Peninsula in the east. The acquisition was carried out during the period 26 April – 2 September 2008. A total of 57 flight-days were necessary to cover the proposed area. For the data acquisition a cesium magnetometer was installed in a so-called 'bird' and towed at a sufficient distance from the aeroplane (70 m) to render the plane's magnetic effects negligible (Fig. 2.1).

The airborne magnetic survey was conducted with constant flight-line orientations, which were adapted from the BAS-06 survey. In-lines were running almost N-S (c. -5.85° off geogr. N) with perpendicular E-W oriented tie-lines (Fig. 2.2). Line spacing was slightly different from that of BAS-06 and was set to 2 km x 5 km instead of 2 km x 6 km to achieve a better control of diurnal variations of the magnetic field during the data processing.

Figure 2.1 Piper Chieftain from Fly Taxi Nord with the docking cradle for the bird containing a Scintrex Cesium Vapour MEP 410 high-sensitivity magnetometer.

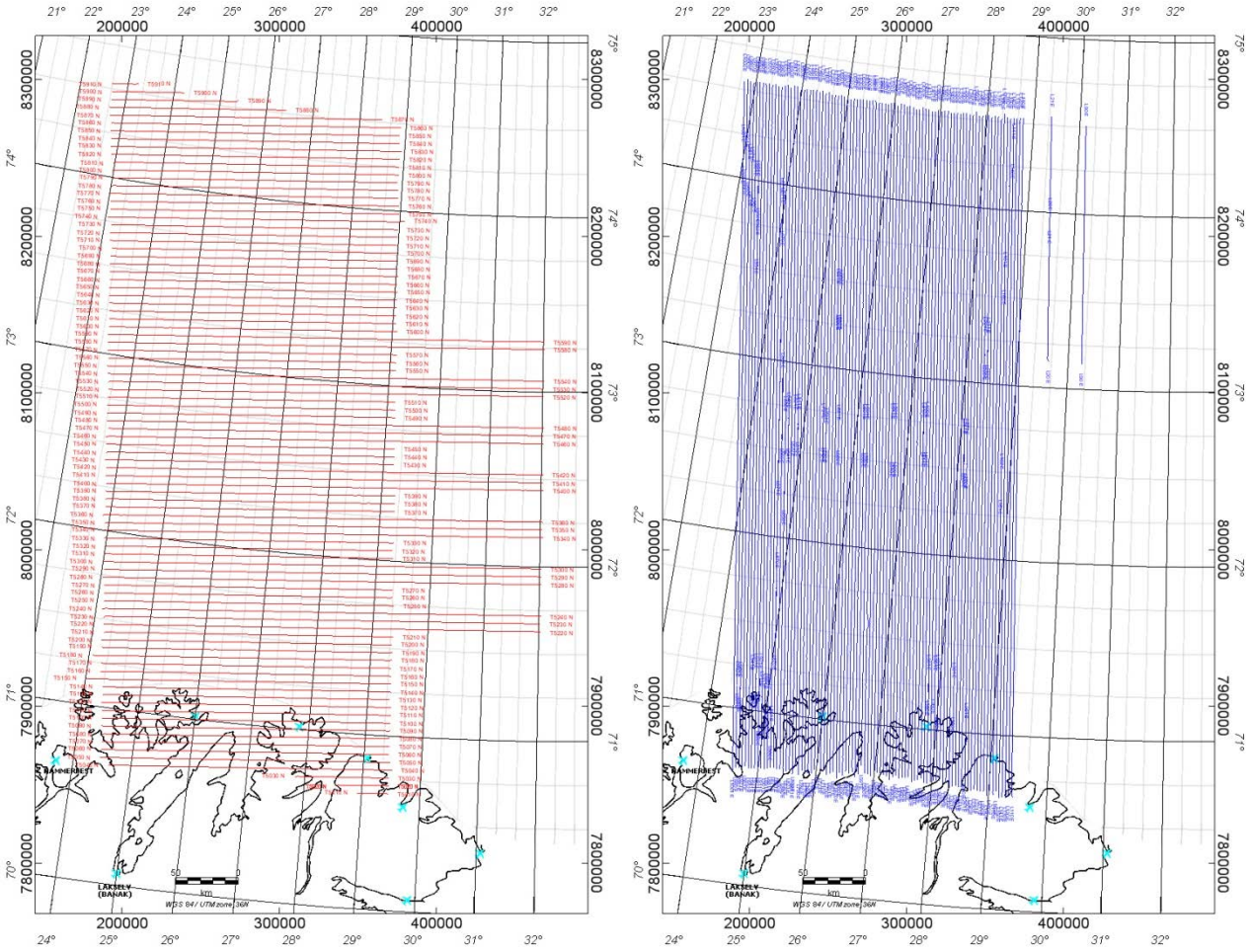

Figure 2.2: Flight pattern (blue lines and red tie-lines) of the BASAR-08 survey.

Table 2.1 defines the coordinates of the original survey area.

Longitude	*Latitude*	*X-UTM³6*	*Y-UTM³6*
22.42.36.75	74.33.12.74	195504	8300230
24.31.22.72	70.39.31.85	187551	7861206
26.45.41.67	70.44.03.97	270626	7859581
28.12.52.37	70.43.23.84	323838	7853484
29.27.03.81	70.38.59.85	368825	7842191
28.51.26.15	74.31.12.50	376671	8274367
26.25.15.19	74.31.27.59	304416	8281371
25.17.05.88	74.32.16.15	271005	8286925
22.42.33.64	74.32.52.05	195368	8299602
22.42.36.75	74.33.12.74	195504	8300230

Table 2.1 Coordinates of the BASAR-08 survey area.

The following summary provides the essence of the survey programme:

Base of operation	Lakselv and Hammerfest airports
Traverse line spacing and trend	2 km, north – south (5.85° cw from N)
Tie line spacing and trend	5 km, east – west
Flying height /sensor altitude	~300 m/230 m.
Speed	~225 km/h
Total line kilometres (in contract)	~52,000
Total line kilometres (acquired)	~57,600
Total flight-days	57
Data recorded	Magnetic field intensity, radar altitude and GPS positioning data

Table 2.2 Main characteristics of the BASAR-08 survey.

2.2 Personnel on board

Participants from NGU:

Senior engineer.	Janusz Koziel (leader of field operations)
Engineer:	Rolf Lynum
Engineer:	Geir Viken
Engineer:	Thomas Møller
Engineer:	Bjørn Wissing
Student:	Tore Vattekar
Geophysicist:	Marco Brönner

Participants from Fly Taxi Nord:

Captain:	Ronny Thorbjørnsen
Captain:	Ole Thorbjørnsen
Copilot:	Andreas Drevvatnet
Copilot:	Gard Pettersen

2.3 Equipment and technical specification

The following equipment was used in the survey:

- Aircraft: Piper Chieftain PA31 (registration. LN-ABZ) with long-range fuel tanks from Fly Taxi Nord in Tromsø (Fig. 2.1).

- Navigation: An Ashtech G12, 12 channel GPS receiver combined with a Trimble Navbeacon DGPS correctional receiver (SATREF) with flight guidance system from Seatex

ASA was used for real time differential navigation. The navigation accuracy was better than ±5 m throughout the survey.

- Altimeter: A KING KRA 405 radar altimeter is an integrated instrument of the aircraft and the data were both recorded and shown on the pilot's display. The altimeter has an accuracy of 0.25% with a resolution of 1 foot (0.3048 m) (Fig. 2.3).

- Magnetometer: A Scintrex Cesium Vapour MEP 410 high sensitivity magnetometer with a CS-2 sensor was applied in the data acquisition. The noise envelope of the onboard magnetometer was 0.1 nT. Most of the data fell within the limits of ±0.04 nT.

- Base magnetometer: A Scintrex MP-3 and an EnviMag proton magnetometer were used for recording diurnals at the base station at the Banak Airport, Lakselv and later at Hammerfest Airport during the last phase of the survey (Fig. 2.4). Data from the base magnetometer were used in the planning of flights and to decide on which lines were eventually to be reflown.

- Data logging: A DAS8 datalogger, GR33 chart recorder and a HDR150 tape station from RMS Instruments were used to record the different data from the survey.

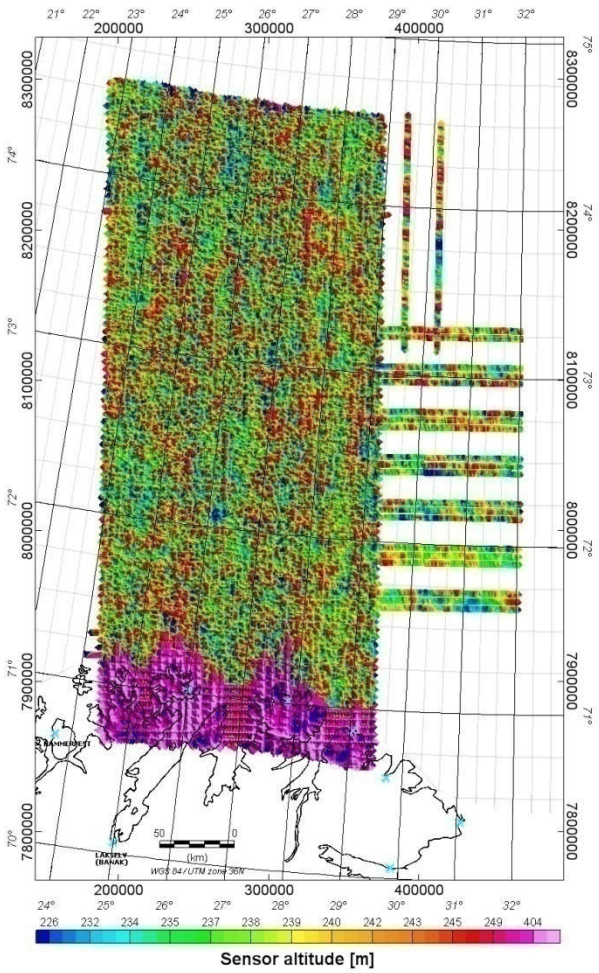

Figure 2.3 Sensor altitude (plane radar altitude – 70 m). In the offshore regions the sensor height was in a range of approximately 220 -250 m. In onshore Finnmark the ground clearance was generally higher on account of the steep coastal topography and poor weather conditions.

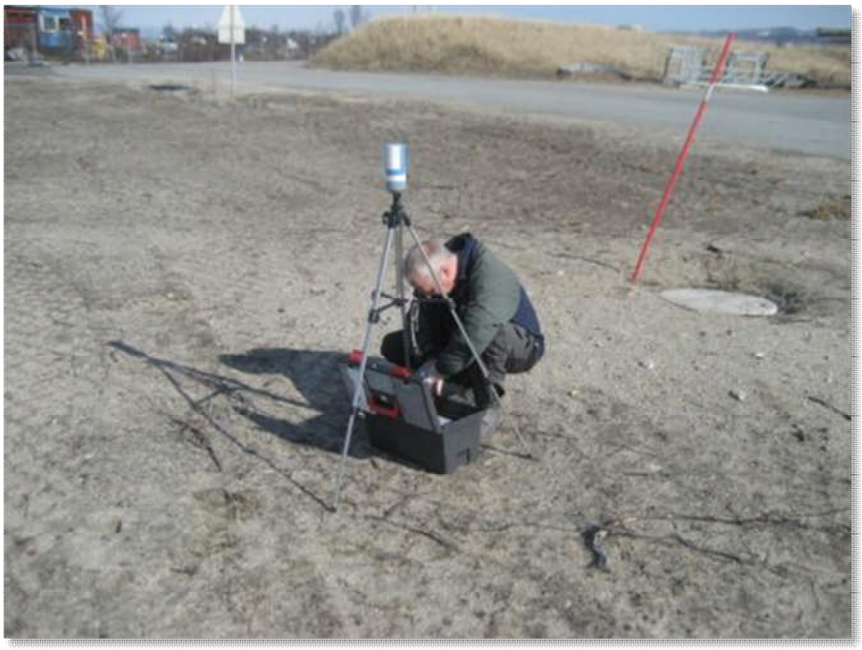

Figure 2.4 Geir Viken next to the base station magnetometer deployed in Lakselv during the BASAR-08 acquisition.

2.4 Acquisition

The whole area was covered with both tie-lines and traverse lines (Fig. 2.2). The total survey area covered c. 80,000 km^2 and consisted of 17,700 km tie-lines and 39,900 km ordinary profiles, of which approximately 2,300 km was flown within the BAS-06 survey area to improve the data quality and to allow a combined processing of both surveys. The aircraft altitude in the offshore area was 300 m a.s.l. on average (1000 feet) (Fig. 2.3). The magnetic sensor was towed approximately 70 m below and behind the aircraft, giving a sensor altitude of about 230±10 m. For the onshore areas, flight clearance was naturally greater due to topography and poor weather conditions. The flying speed was 225 km/h and magnetic data were sampled at a rate of 5 Hz, giving a spatial sampling interval of 11-14 m along the lines.

The acquisition period was initially planned for approximately 17 weeks but due to poor weather conditions, technical problems and some shorter periods with magnetic disturbances, the acquisition was extended by c. one month compared to the initial schedule.

2.5 Magnetic conditions

The most complex problem during magnetic acquisition is probably the diurnal variation of the Earth's magnetic field influenced by solar storms, which are particularly active at high latitudes (i.e. aurora borealis). This usually causes tie-lines and regular survey lines to have different readings at the same geographical point (crossover point). Such misfits can produce artefacts

during interpolation and consequently, erroneous inter pretations if no suitable corrections have been applied.

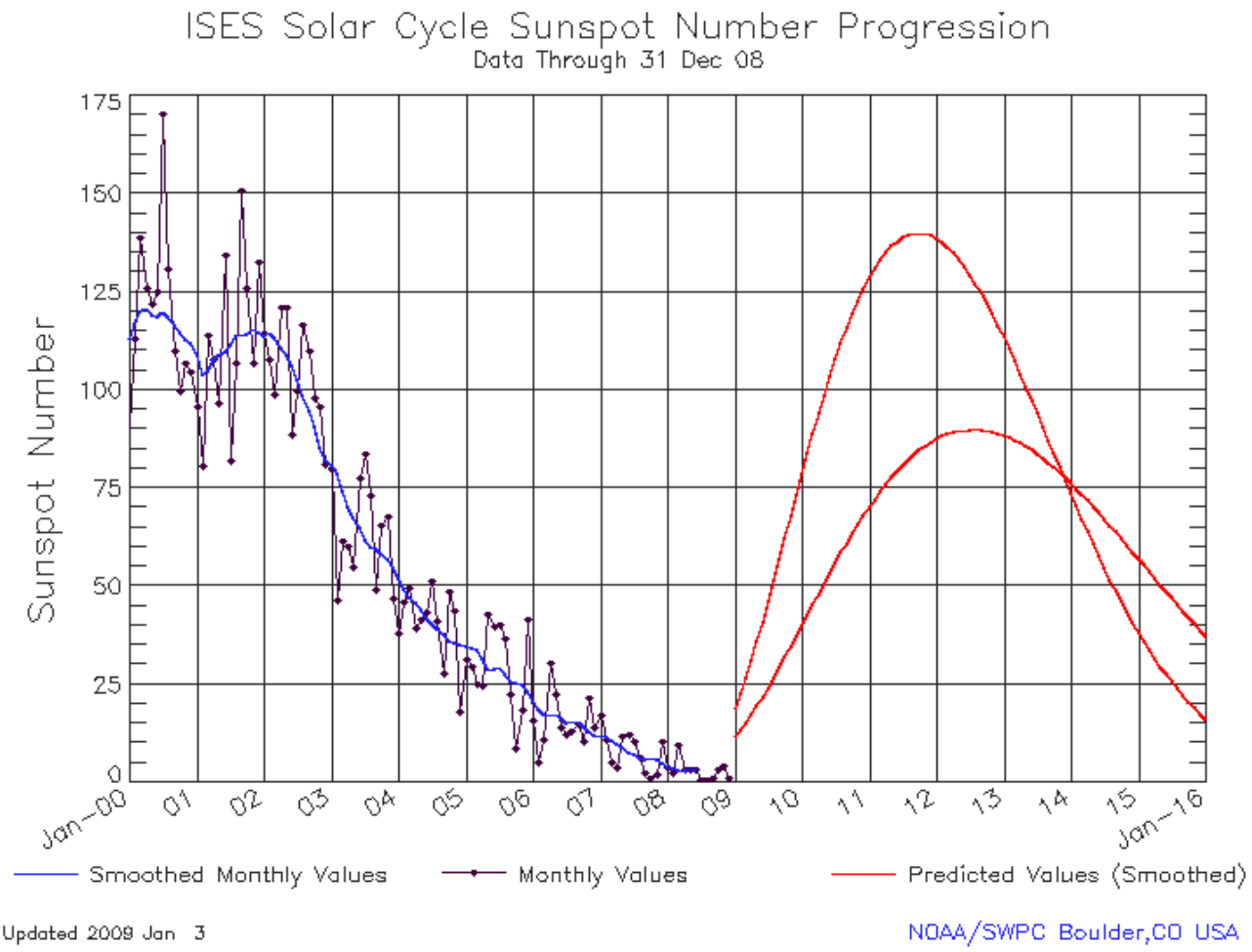

Figure 2.5 Observations and prediction models of sunspot numbers from the US National Oceanic and Atmospheric Administration (NOAA)(Hathaway et al. 1999). Monthly averages (updated monthly) of the sunspot numbers show that the number of sunspots visible on the sun waxes and wanes with an approximate 11-year mega cycle. The BASAR-08 survey was carried out during a period of extremely low solar activity, which presented excellent conditions for the aeromagnetic acquisition.

If the survey is located close to a base station site, the lines can be directly corrected for diurnal variation. However, most of the offshore acquisition extends far away from land stations and is then liable to experience different diurnal variations. Efficient statistical algorithms and filtering are usually required to solve this issue and to 'level' in an acceptable way all the magnetic profiles (see Chapter 3). The sunspot cycles strongly influence the geomagnetic field and dirunals. The BASAR-08 was acquired during a relatively quiet period. Solar cycle predictions suggest that 2008 was in or at least close to a minimum of sunspot activity (Figs. 2.5, 2.6), thus providing relatively good magnetic conditions at the time of acquisition. Nevertheless, due to the high latitude of the survey area, magnetic data can be locally strongly influenced by

variations in the Earth's magnetic field. Therefore, we applied several steps of quality control to minimize the amount of data affected by these variations:

- The daily flight-plan was made under consideration of the recorded Earth's magnetic field variations from base-stations in the area, e.g. Nordkappand on Bjørnøya and Sørøya (Recordings in realtime provided by the University of Tromsø: http://flux.phys.uit.no/).
- Data QC of every flight-day was carried out using NGU base-mag data to classify the data quality and to plan possible repeat flights (Tab. 2.3)
- Tie-line levelling was carried out in conjunction with the recorded variations in the Earth's magnetic field.

The diurnals for all flights are included in the database file delivered on the BASAR-08 archive CD. These plots ease the quality control of the acquired profiles. The data were classified into two quality groups according to the magnetic diurnals:

Class	Criteria	Profile length
1	< 10 nT/10 min. Linear	57,340 km
2	10 – 30 nT/10 min. Linear	620 km
Total		57,960 km

Table 2.3 Results from data QC and the re-fly programme of BASAR-08.

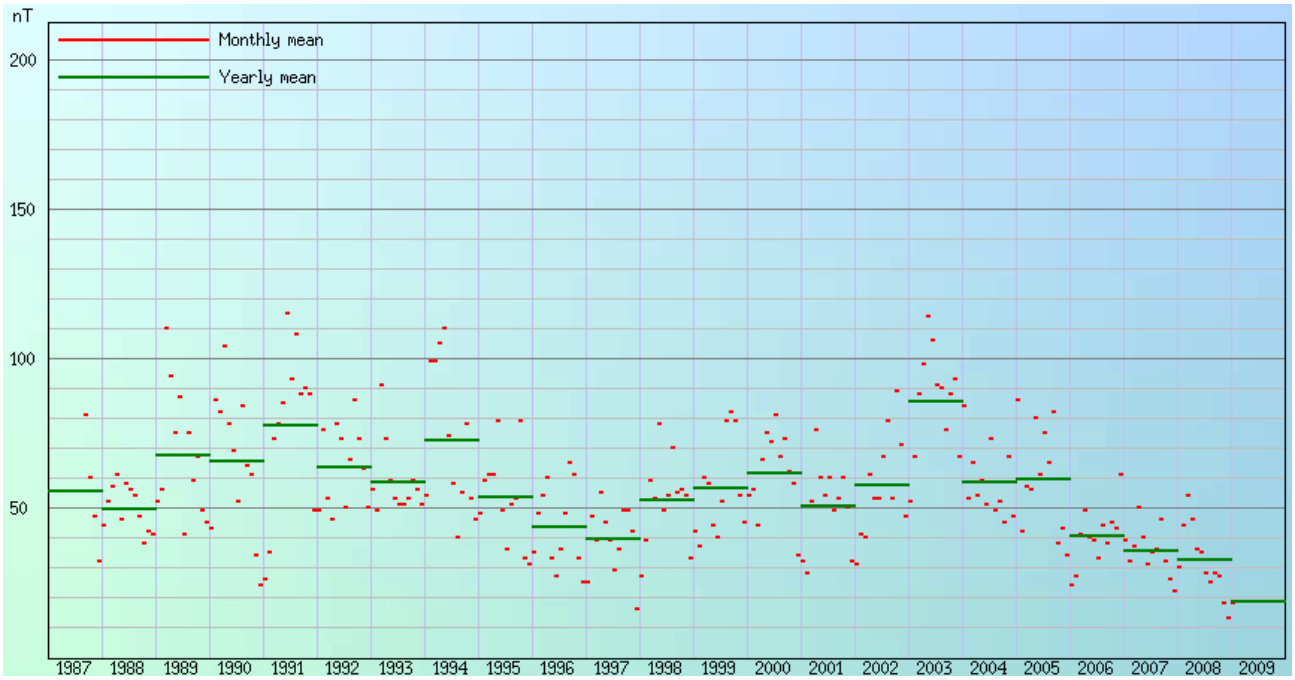

Figure 2.6 Diagram of the monthly mean values of the horizontal intensity of the geomagnetic field (H) observed at the Tromsø Observatory from 1987 to 2009. This graph illustrates the good correlation between the periodic and semi-periodic evolution of the field and sunspot activity. A similar variation between the polynomial average of H and its running average illustrates the average good magnetic conditions for aeromagnetic surveying during the period May-September 2008. Geomagnetic Data derive from Tromsø Geophysical Observatory (http://www.tgo.uit.no/aix).

A total of c. 620 line km was of intermediate quality (Fig. 2.8) and reflown at the end of the acquisition. During the levelling process, all remaining effects from the background magnetic field variations were further removed or reduced to a minimum.

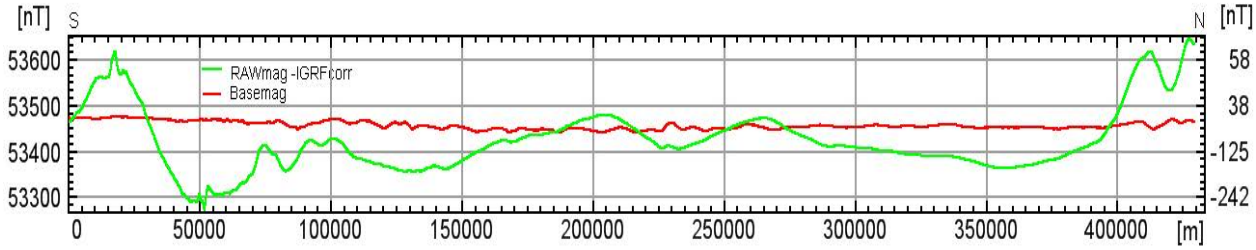

Figure 2.7 Magnetic diurnal and unlevelled IGRF corrected TMI data along profile 640. The base magnetometer reading (red) was used to estimate the diurnal influence on the recorded field (green). For the most of the time the recorded diurnal field was rather quite, which is an important factor for the data quality.

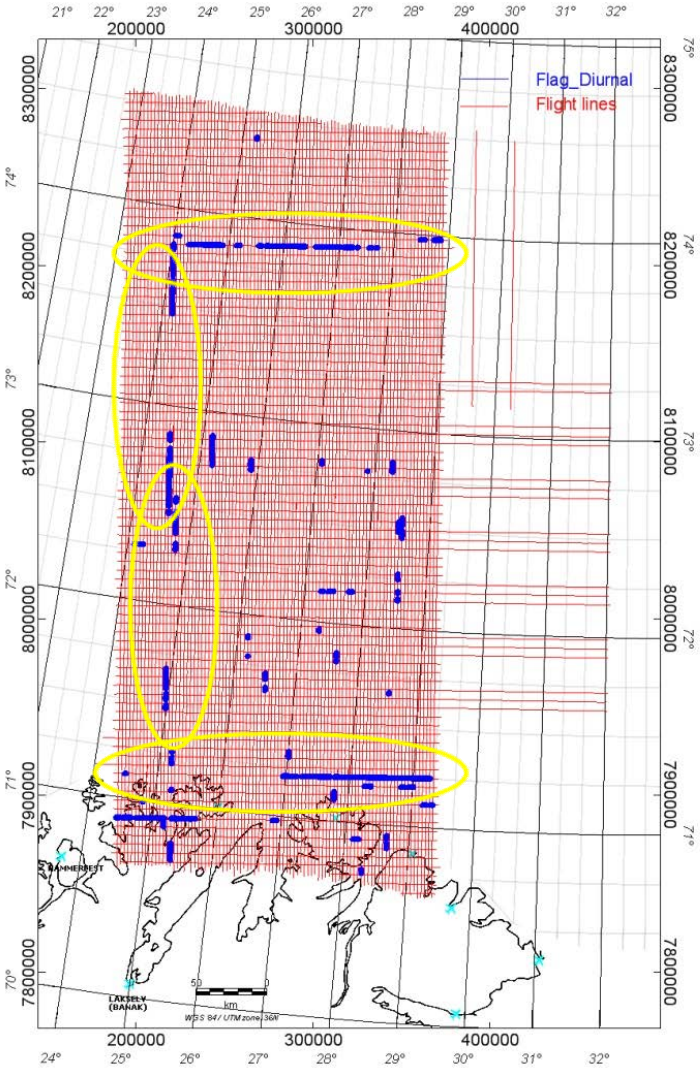

Figure 2.8 Profiles of intermediate quality (i.e. diurnal variation between 10 and 30 nT per 10 minutes) marked as blue lines. The total length of intermediate quality data is 620 km (i.e. 0.78 % of the total survey). The yellow ellipses mark the profiles which were decided to be reflown. The remaining locations were corrected during theprocess of levelling.

To estimate the influence of the magnetic signature of the aeroplane, a magnetic heading test (clover-leaf test) was carried out in October 2006 in the Hammerfest region for the SNAS-06 and BAS-06 projects. The magnetic signature of the aeroplane also includes 1) its permanent magnetisation induced by its motion through the Earth's magnetic field, 2) a component due to the flow of electric current within the plane, and 3) the orientation of the magnetic sensor inside the bird. The permanent magnetisation of the plane varies as the plane changes its orientation, thus leading to heading errors. The maximum difference of magnetometer readings in the four different directions as it turned out from this test, was small: 1.2 nT. We decided not to carry out another new clover-leaf test in 2008 and considered the effect as negligible.

2.6 Gridding, map production, projection and archive CD

The Oasis Montaj software (Geosoft 2004) was used throughout for the map production. This software package has become a standard for many potential field experts in the mineral and petroleum industry. All databases and grids in Geosoft format are provided on the BASAR-08 archive CD. The grids are usually presented with a shaded relief technique (illumination from the northeast) and a non-linear colour scale. Gridding was performed using the minimum curvature technique with a grid cell size of 500 x 500 m (¼ of the inline profile distance). Minimum curvature produces a smooth grid while attempting to honour the data as closely as possible (Press et al. 2002). However, for elongated, very narrow and high-amplitude anomalies which are not parallel to the profiles, the interpolation is insufficient and the anomalies appear scattered (e.g. onshore-offshore Mehamn town and Varanger Peninsula). Here other techniques such as bi-directional gridding achieve a more accurate result. Presentation of the maps with the shaded relief technique enhances lineaments that trend oblique to the illumination direction. Colour scale and colour distribution for the datasets have been computed using a histogram equalisation technique. These maps have been produced in the Universal Transverse Mercator projection (UTM zone 36) using the WGS 84 datum. We also used the UTM 36 projection for the regional interpretation.

On the CD we provide an Oasis Montaj Viewer and its tutorial for companies that do not use Oasis Montaj specifically. Oasis Montaj Viewer is a free and easy-to-use software that allows anyone to view, share and print published Geosoft grid (.grd) and database (.gdb) files. The viewer can also be used to convert grids and images to a variety of supported data formats, including AutoCAD, ArcView, ER Mapper, TIF and many more. The free software can also be shared and downloaded from http://www.geosoft.com/pinfo/oasismontaj/free/montajviewer.asp.

For specific questions on special needs please do not hesitate to contact NGU (either Marco.Bronner@ngu.no or Odleiv.Olesen@ngu.no).

3 DATA PROCESSING AND PROFILE LEVELLING

Marco Brönner

RAW-magnetic data (Fig. 3.1) cannot be used directly for gridding and requires a number of processing steps before the production of the final aeromagnetic grid and the map of the total magnetic intensity (TMI) for interpretation use. Noise filtering and statistical levelling processing were carried out using the professional OASIS Montaj software (Geosoft 2005b). Micro levelling was performed using the MAGMAP FFT package from OASIS Montaj (Geosoft 2005a). The raw data have been processed using standard procedures and methodologies used in many other geological surveys (Luyendyk 1997). Apart from covering the BASAR-08 area with aeromagnetic data, the BAS-06 area and database were supplemented with additional tie-lines and in-lines and were reprocessed together with the BASAR-08 data. At this juncture, previously noise-filtered and lag-corrected BAS-06 data were merged with the new BASAR-08 and processed jointly. The various processing steps and standard procedures are outlined below.

3.1 Preliminary noise filtering and basic corrections

3.1.1 Noise filtering

High-frequency noise is usually created as the aeroplane is manoeuvring. After acquisition, initial raw data were imported directly into an Oasis Montaj database and subsequently interpolated to a regular grid of 500 x 500 m cells, to check the quality of lines and tie-lines (Fig. 3.1). Spikes due to minor noise and artefacts were first removed by non-linear (Naudy) filtering and subsequently smoothed with a light low-pass filter (10 fiducials=500 m) in order to keep the signal intact.

3.1.2 Systematic lag corrections

A systematic lag correction for the BASAR-08 data was tested but not applied as it did not affect the data quality. For BAS-06 lag-corrected data were adopted from the previous processing (NGU Report 2007.035, Gernigon et al. 2007b). Here original magnetic profiles were lag-corrected, utilizing the Oasis Montaj processing package (Geosoft 2005a) with 5 fiducials (=250 m), but did not change the data significantly due to minor variations in values as a function of flight direction.

After noise filtering and lag correction of BASAR-08, the RAW data were merged with BAS-06 and are presented in figure 3.1. RAW data reflect the recorded magnetic field, including the Earth's geomagnetic main field and all disturbances.

The data are dominated by the Earth's geomagnetic field, observable by the increasing magnetics to the northeast. The BASAR-08 data have a higher niveau compared to the BAS-06 data, due to the long-term time variation of the Earth's geomagnetic field.

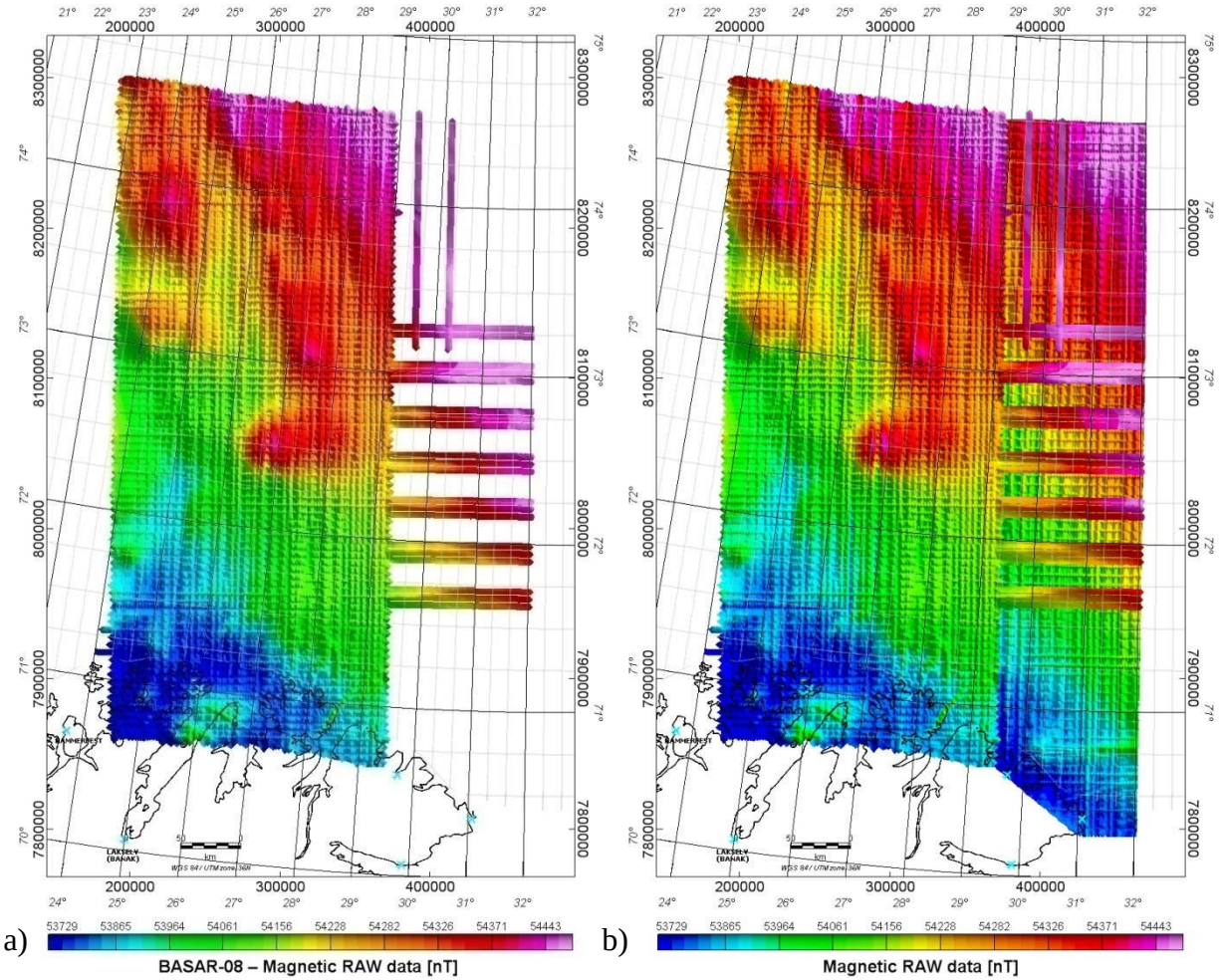

Figure 3.1 RAW magnetic profiles (without levelling) gridded by means of the minimum curvature algorithm (grid cell size at 500 x 500 m), a) of BASAR-08, b) both BASAR-08 and BAS-06 RAW data. Note that the artefacts are mostly parallel to the line profiles due to diurnals. Projection UTM 36, WGS 84.

3.1.3 International Geomagnetic Reference Field (IGRF correction)

As part of the processing, the total magnetic intensity (TMI) field is computed from the recorded magnetic field after subtraction of the International Geomagnetic Reference Field (IGRF) model (Fig. 3.2). The IGRF is a mathematical representation of the undisturbed Earth's geomagnetic field. The change of the IGRF field in the BASAR-08 survey area is about +57 nT per year, on average.

The International Geomagnetic Reference Fields for 2008 (IGRF-2008) and 2006 (IGRF-2006) were calculated using the Oasis Montaj IGRF tool (Geosoft 2005b). The result of this

subtraction isolates the component of the magnetic total field, which is dominated by the magnetic effects from the underlying crustal rocks.

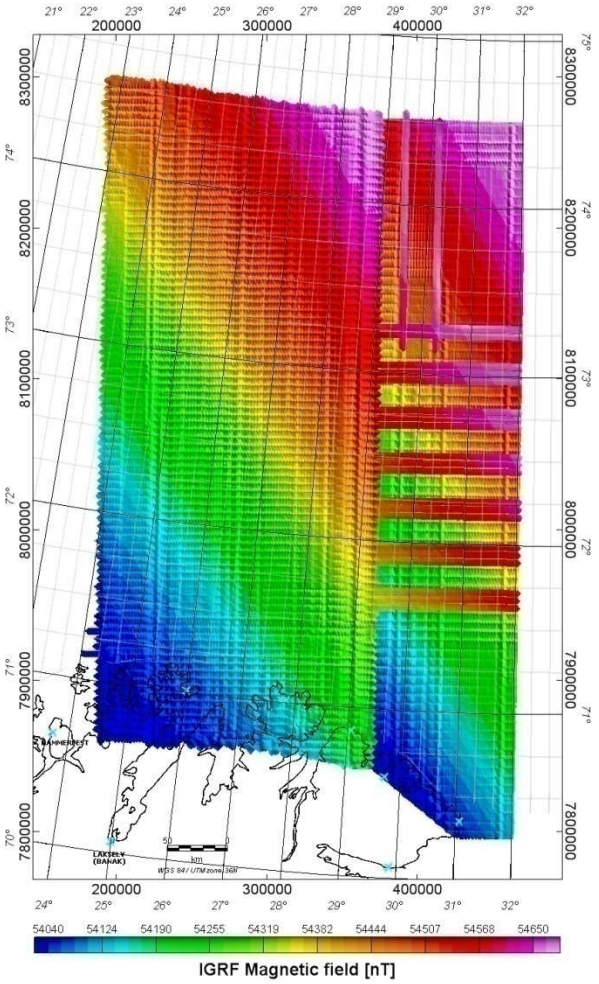

Figure 3.2 The IGRF-2008 / IGRF-2006 (formally 2005) model along the BASAR-08 and BAS-06 surveys.

After the IGRF correction a shift between both surveys remained. To evaluate the shift, the differences between the overlapping lines and conjunction points from both surveys were calculated. Although this evaluation is still influenced by diurnal effects, as an important outcome the difference, as it appears along these lines, was rather constant; no long-wavelength trend could be observed. Calculating an average value reduces the diurnal influences and the resulting map, where magnetic anomalies can be traced across both surveys, proves that the correction was right. In comparison with BASAR-08, for the BAS-06 data a higher niveau of, on average, 50 nT was observed. Accordingly, for the further processing a constant shift of 50 nT was subtracted from the BAS-06 data. Meanwhile, the reason for such a constant shift remains unclear. In the following, the term 'BASAR-08' is referring to the combined area of the BASAR-08 and BAS-06 surveys, if BAS-06 is not explicitly mentioned.

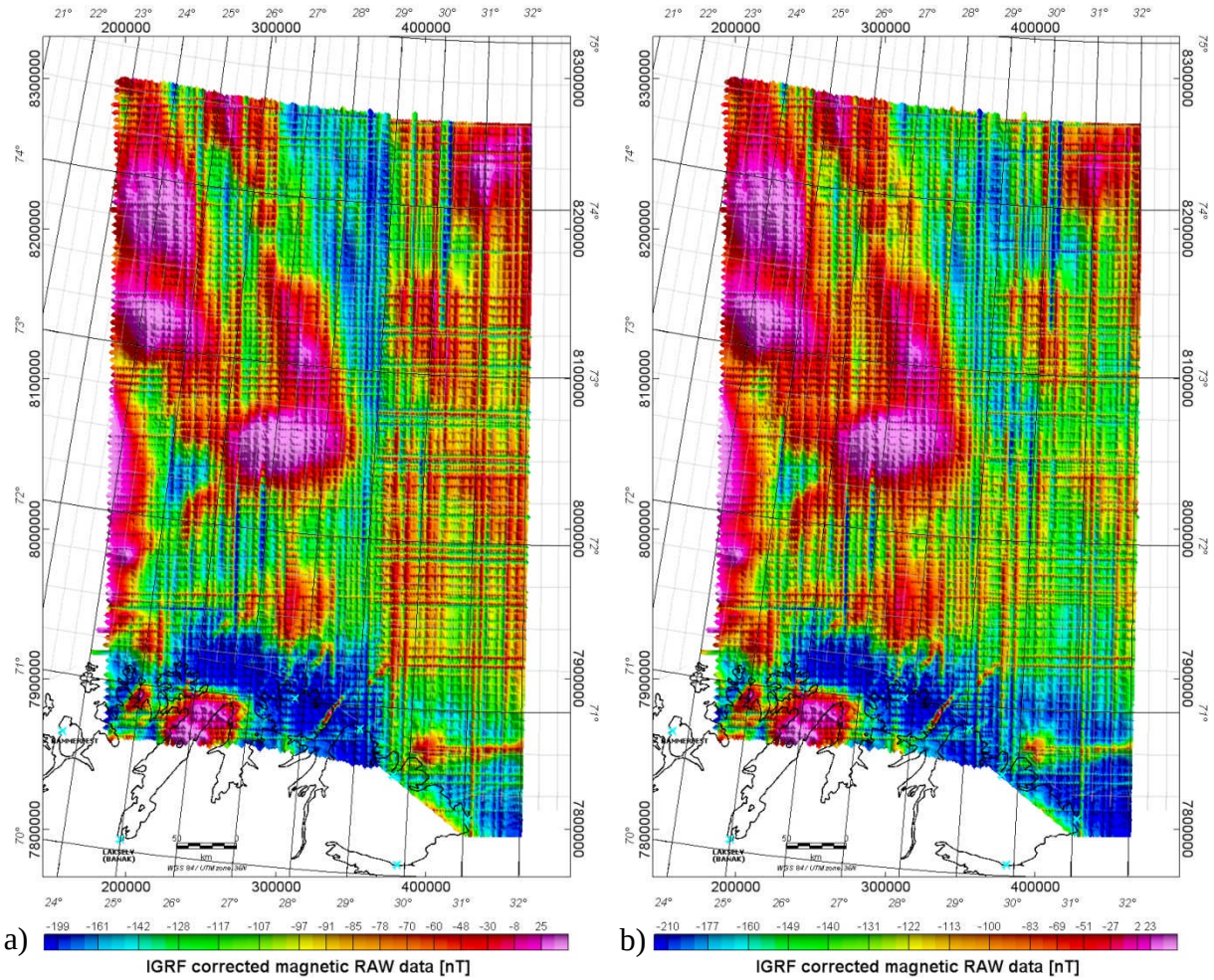

Figure 3.3 Combined BASAR-08 / BAS-06 IGRF-corrected total magnetic field RAW data with (a) and without (b) applied constant shift to BAS-06.

3.2 Levelling and micro-levelling of the magnetic profiles

3.2.1 Diurnal variation and use of base magnetometer readings

As shown in figures 3.1 and 3.3, a variety of external, time-varying, field factors usually influences and causes errors during aeromagnetic acquisition. This includes time variation in the magnetic field, ground clearance variation, altitude variation, magnetic effects of seawater swells and diurnal effects. These factors are usually sufficient to explain the errors at crossover points between line and tie-lines. The most complex and significant problem is probably the diurnal variation of the Earth's magnetic field influenced by the solar wind (Fig. 2.6). At polar latitudes, the most famous and spectacular expression of these diurnal effects is the aurora borealis, known to be caused by the collision of charged particles (e.g. electrons), in the magnetosphere with atoms in the Earth's upper atmosphere. Diurnal variations in the magnetic field can cause tie-lines and regular survey lines to have different readings at the intersections. Even if they are small, these long-wavelength effects can be visually distracting, particularly on

image-enhanced displays. Such misfits can produce artefacts during interpolation and consequently erroneous interpretation if no suitable corrections have been applied.

The most important reason for this is the time shift in the Earth's magnetic field variations between the large survey area and the onshore base station. There is normally a spatial difference in amplitude and frequency of these diurnals. Data from the base magnetometer have therefore only been used to assess the quality of individual lines and to make decisions on which lines should eventually be re-flown (see Chapter 2.5, Fig. 2.8).

3.2.2 Statistical levelling

The purpose of levelling is to minimise the residual differences in a coherent way by proportioning them between lines and tie lines. Proper levelling or micro-levelling algorithms usually require close and proper line spacing, and the quality of the final result is generally a function of this crucial parameter. The large line spacing of previous surveys did not allow proper levelling and interpolation of raw data produced erroneous or factitious anomalies.

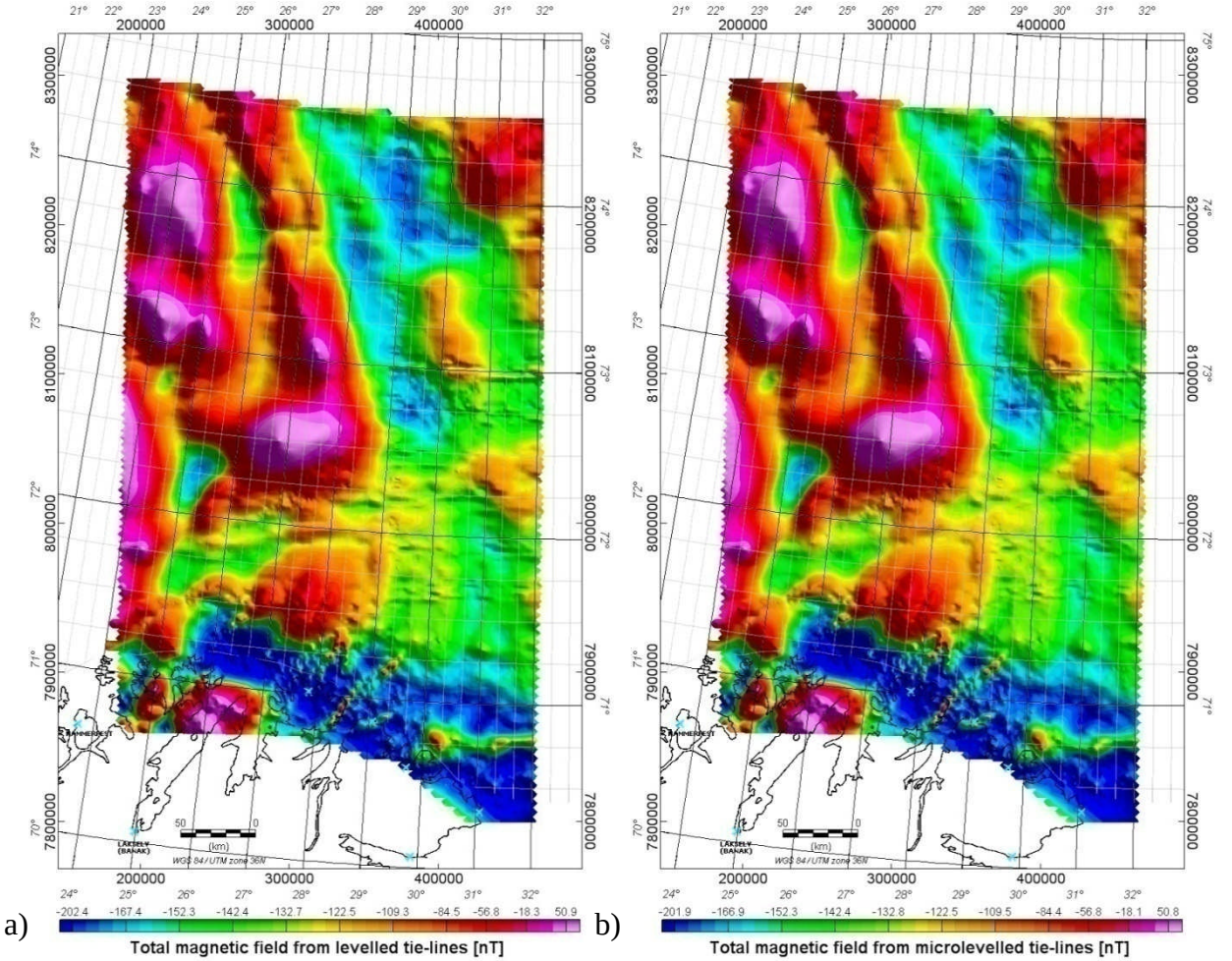

Figure 3.4 a) Statistical tie levelling of the magnetic profiles and b) micro-levelled TMI field from the levelled tie-lines. Gridding of the tie profiles used the minimum curvature algorithm (grid resolution: 500 x 500 m).

For this project, levelling was undertaken using a standard statistical levelling method of the tie-lines and survey lines, provided as part of the Geosoft Oasis montaj package (Geosoft 2005a). The new aeromagnetic survey was processed using a statistical levelling method by which the discrepancies between the readings at each crossover point were reduced by systematically proportioning them between the tie and line profiles. 'Suspicious' cross-over differences (outliers) were first removed manually before levelling and full-levelling of the tie-lines and line profiles. We used first a first-order (linear) trend removal in the levelling of the tie-lines, but a tension spline (b-spline) correction was finally adopted for the tie-line levelling after several preliminary tests. After a micro-levelling (see Ch. 3.2.3 for details) the detrended tie-line profiles were then used for full statistical levelling of the survey lines (Fig. 3.6a). Extreme mis-tie values (outliers) were checked and removed again manually before calculating the next full-levelling correction, until convergence was achieved.

The final result has to be considered as the best compromise between the removal of levelling errors and anomaly preservation.

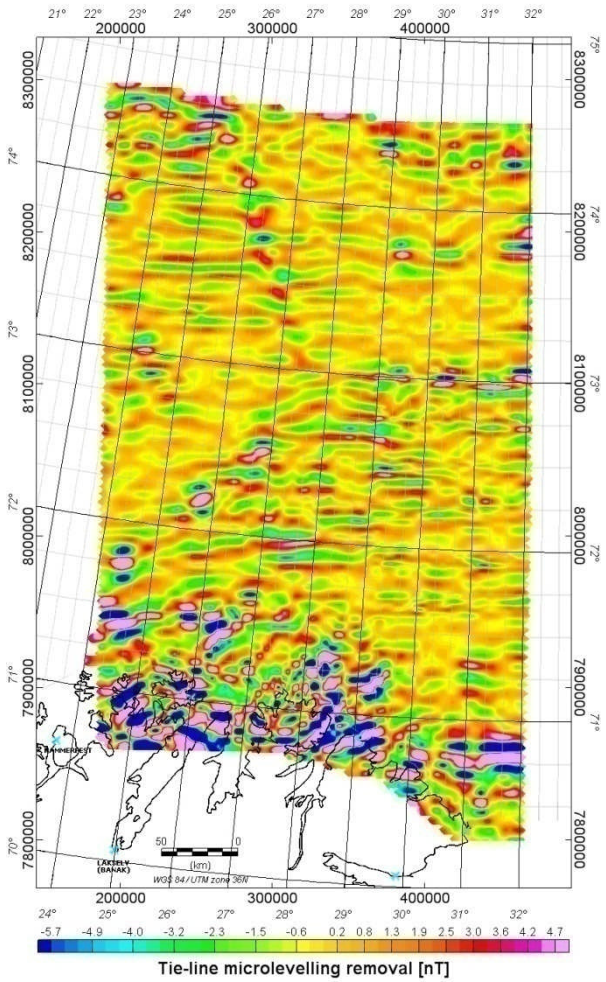

Figure 3.5 Full levelling magnetic grid of the magnetic profiles, lag corrected and referred to IGRF-2006. The levelling represents the second step of the levelling approach based on the least-square technique. Gridding of the line profiles used the minimum curvature algorithm (grid resolution: 500 x 500 m).

3.2.3 Micro-levelling

For both, tie-line levelling and full-levelling we performed micro-levelling to remove minor ('micro') levelling errors still remaining along parts of some profiles after the statistical levelling. Here two different techniques were used. To improve the tie-line levelling, the Geosoft micro-levelling approach using the PGW GX System of the available MAGMAP processing package (Geosoft 2005a) was used. It proved to be better adapted to preserve geological information for this specific case where the remaining levelling errors are irregularly distributed. The PGW GX System applies a decorrugation process in the frequency domain to isolate the levelling corrections before applying them to the original data (Figs. 3.4a and b). The BASAR-08 data have been decorrugated to reduce line-to-line levelling errors, which are visible as linear magnetic features parallel to the flight lines (Fig. 3.5). Decorrugation is simply a frequency domain procedure based on a directional cosine filter. This filter retains anomalies, from gridded data, in the flight line direction only.

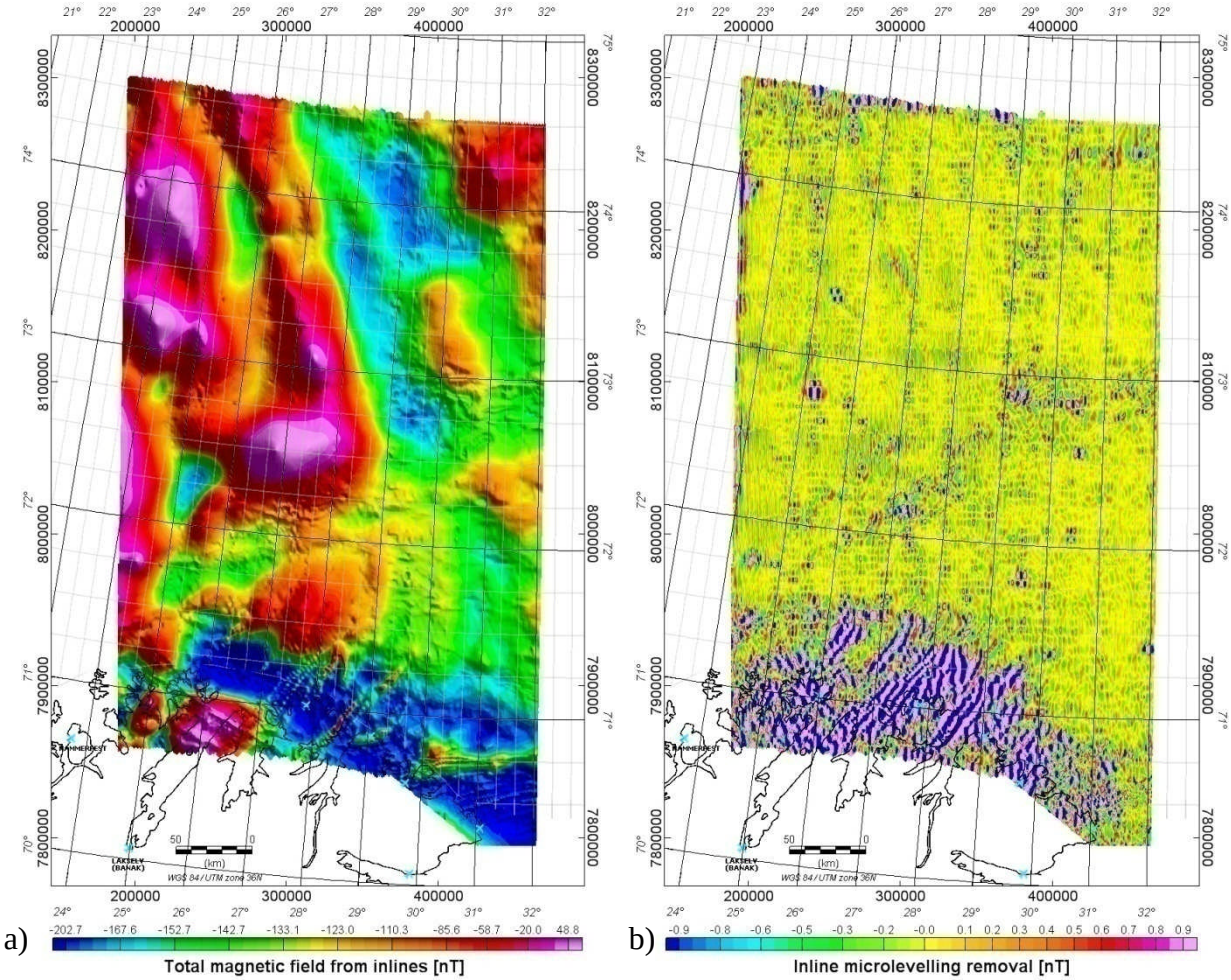

Figure 3.6 a) TMI field without micro-levelling and b) magnetic residual after micro-levelling by decorrugation and subtraction of the total field obtained by statistical levelling (500 x 500 m grid cell spacing).

First, a Butterworth high-pass filter is set to four times the line spacing to pass wavelengths on the order of two to four line separations. Such a process results from a line-to-line levelling error. In a second step, a directional cosine filter is set to pass wavelengths only in the direction of the lines. Afterwards, a line-based filter was used to separate the high frequency geological signal from the longer wavelength levelling errors. A low-pass non-linear filter was finally applied to clean the levelling error channel with a Naudy filter. The micro-levelling result was obtained by subtraction of the magnetic residual levelling grid (Fig. 3.5) from the original dataset (Fig. 3.4a). The subtracted field is mostly rather small in a range of appr. ±5 nT. Only locally and in the onshore regions, where the amplitudes are much higher, were larger values subtracted from the original field.

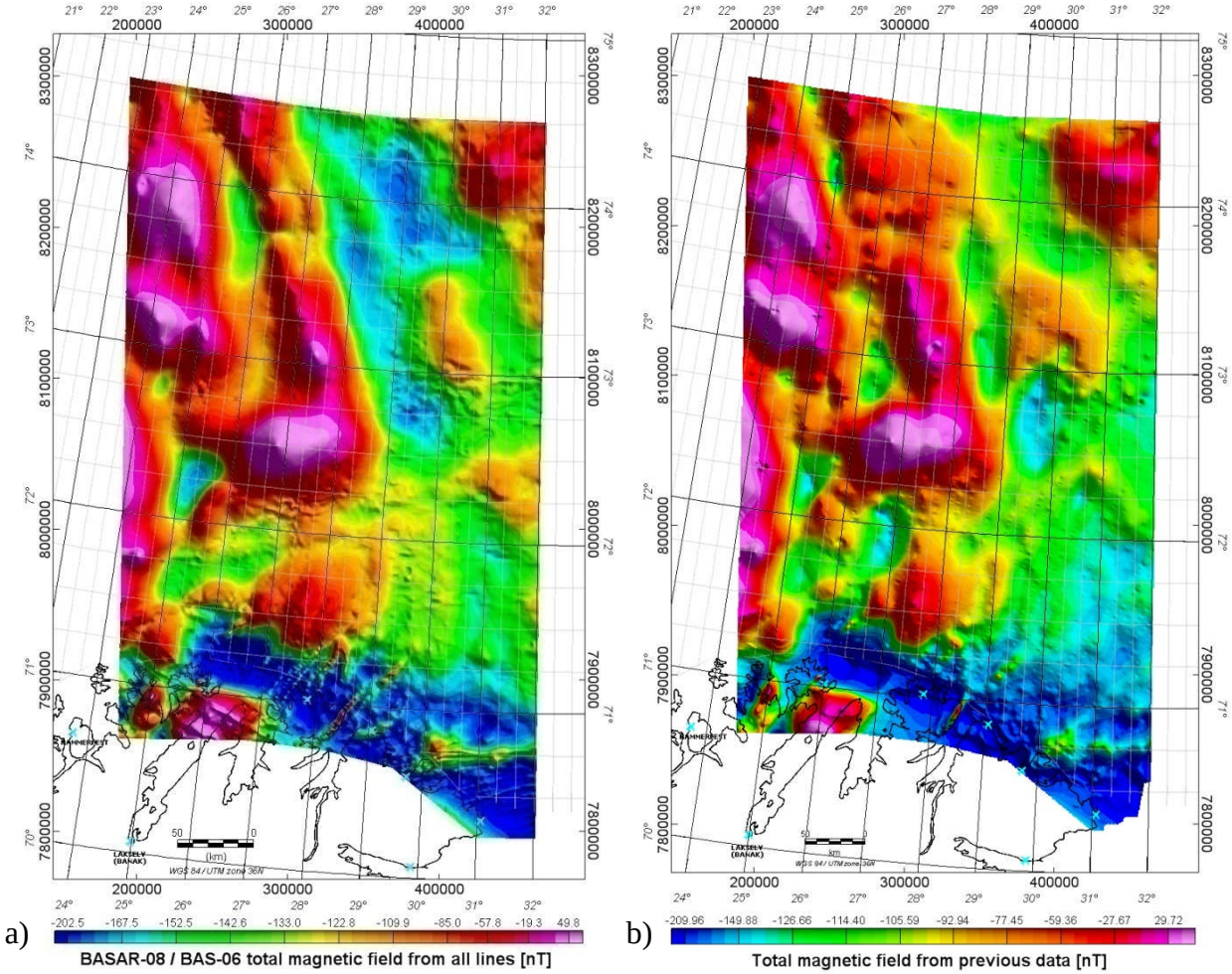

Figure 3.7 a) BASAR-08 total magnetic field from both tie-lines and in-lines after micro-levelling. Results from the FFT decorrugation technique of Geosoft. 500 x 500 m grid cell spacing using the minimum curvature gridding algorithm. b) vintage NGU-70 and BAMS-85 data.

After the full levelling of the in-lines a micro-levelling was carried out, mainly to reduce some very local levelling problems. Here, a simple decorrugation filtering was applied as described above. The subtracted field is accordingly small in a range of ±1 nT (Fig. 3.6b). In a last step, a full levelling with all lines, in-lines and tie-lines, was conducted to further improve the resolution of the grid and to present a high-resolution aeromagnetic dataset with the maximum of available resolution (Fig. 3.7).

4 FINAL MERGER AND COMPARISON WITH PREVIOUS COMPILATION

Marco Brönner & Odleiv Olesen

4.1 Merger of the BASAR-08 grid with the former regional grid

The BASAR-08 grid has been merged with the pre-existing NGU magnetic compilation of the Norwegian Barents Sea (Olesen et al. 2007). The suturing method of the Oasis montaj GridKnit module was used to merge the geophysical grids (Geosoft 2005d). The suturing method enables us to automatically or manually define a suture path for applying a proprietary and multi-frequency correction along the path. A mismatch in the data values of the grids along the line is corrected by adjusting the grids on either side of the path. However, this technique locally 'forces' the magnetic trend envelope of the BASAR-08 to be adjusted with the surrounding dataset.

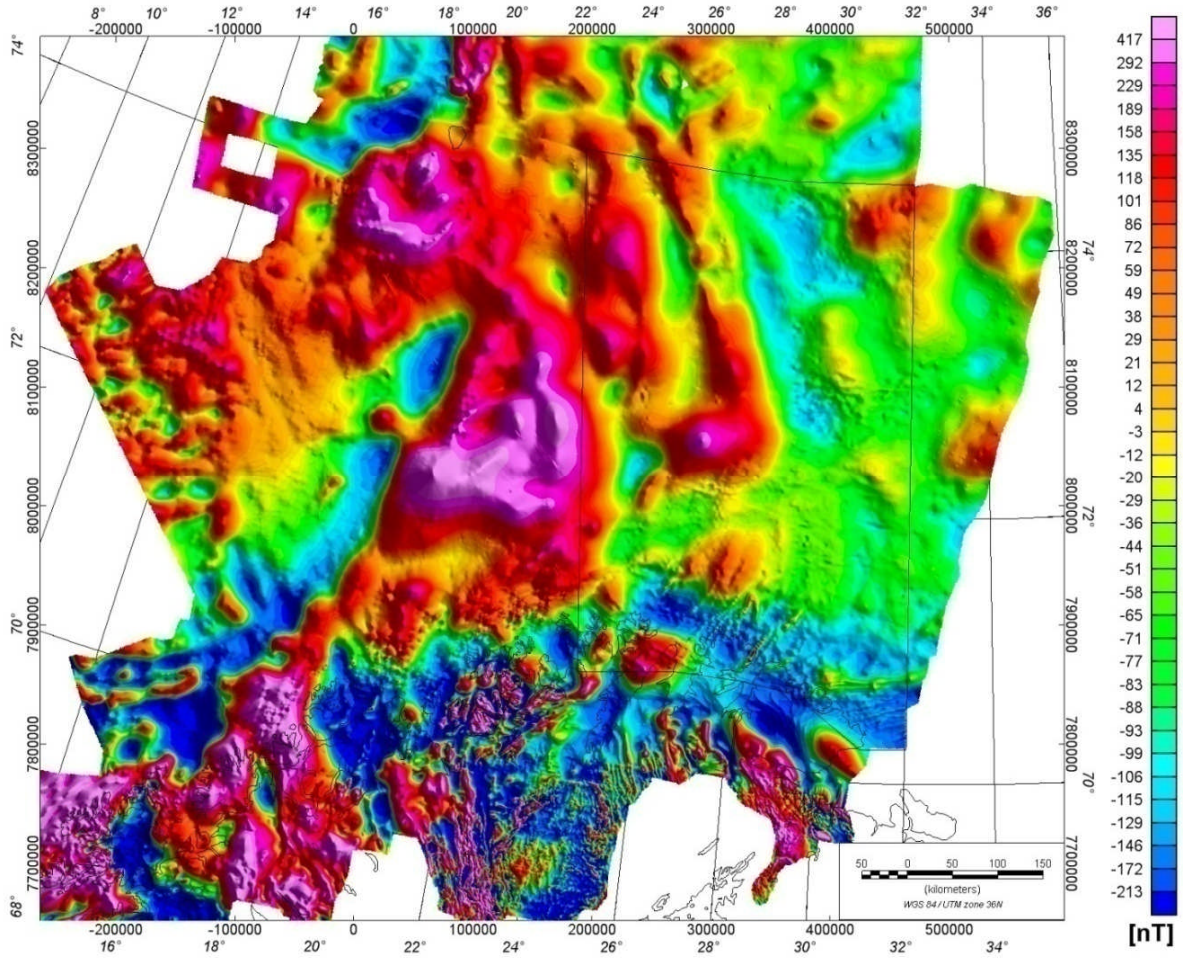

Figure 4.1 Updated regional compilation with BASAR-08 and previous BAMS-85, NGU-69 and -70 data (Åm 1975, Skilbrei et al. 1990, Skilbrei 1991, 1992, 1993, Olesen et al. 2006, 2007).

Since the surrounding magnetic datasets are partly old (NGU-70 survey to the east and BAMS-85 to the west), have low resolution and are less reliable, the merging process could adversely influence the initial high quality of the BASAR-08. For local interpretation and modelling, we consequently recommend using the original BASAR-08 grid. The final grid can only be provided to the partners that also purchased the vintage NGU magnetic datasets.

4.2 Comparison with the previous compilation

A comparison of the updated compilation from the present study with the vintage dataset reveals a significant improvement in data quality and resolution (Figs. 3.7a, b and 4.1 and 4.2). Some principal anomalies, such as the Norsel High, Mercurius High and the Western Varanger Graben, remain similar but in the new dataset they show additional small-amplitude features and the principal structures appear much more differentiated. In the BASAR-08 area, and even moreso in the BAS-06, area other magnetic lows and some smaller magnetic highs are much more pronounced.

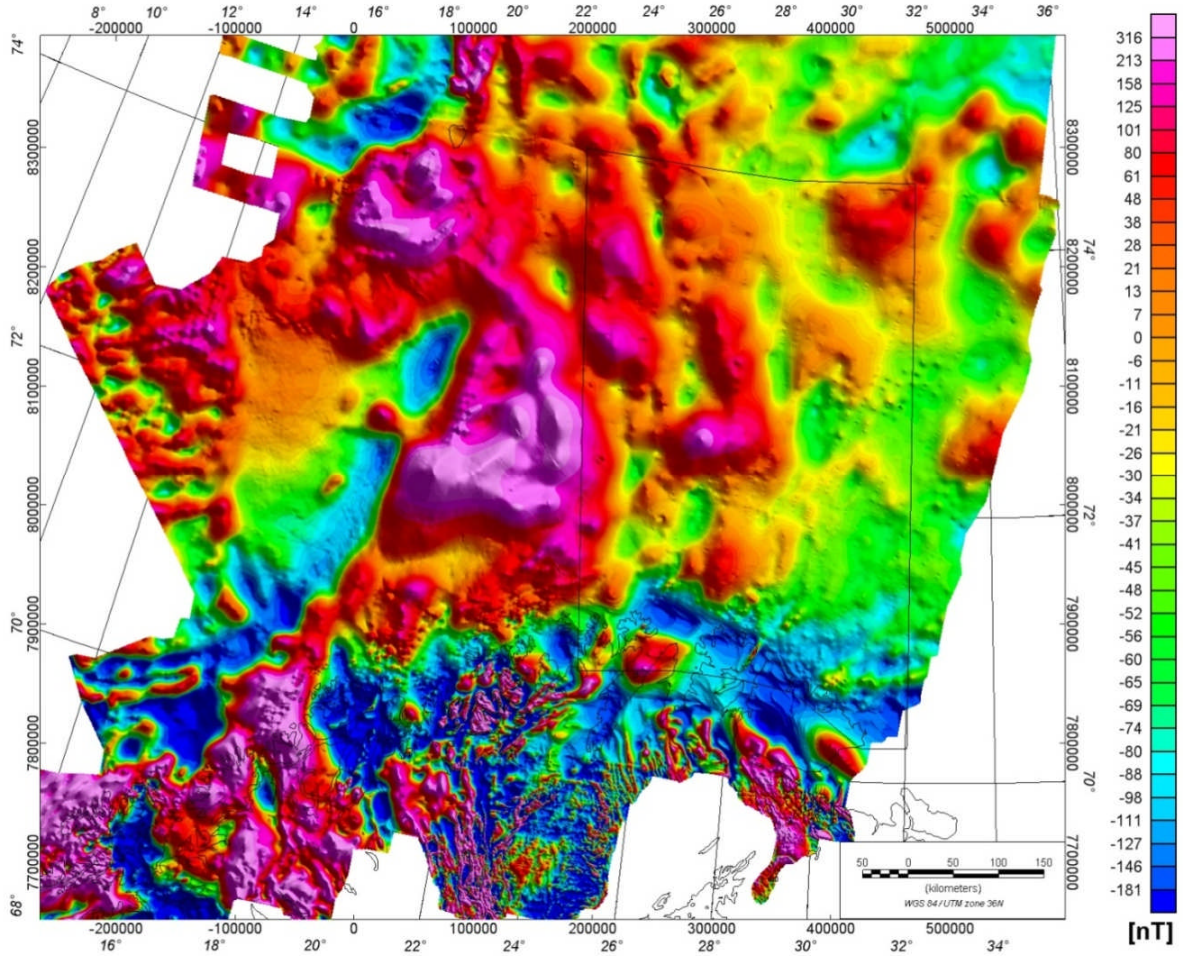

Figure 4.2 Regional compilation using vintage NGU data (Åm 1975, Skilbrei et al. 1990, Skilbrei, 1991, 1992, 1993, Olesen et al. 2006, 2007).

The longish, tail-like, magnetic high running north–northwest from the Norsel High appears to be narrower and more continuous and isolated from the adjacent areas than before. Just to the east a distinct magnetic low runs almost parallel to this structure continuously into the central Nordkapp Basin. Moreover, the previously undifferentiated magnetic high south of the southern Nordkapp Basin shows lineament features and a possible trisection. Furthermore, the new dataset reveals quite a number of completely new and interesting small-amplitude features associated with the salt structures, but there are also lineaments through and around the Nordkapp Basin which are likely to be fault and/or dyke related. Some of these lineaments were already mapped from other datasets like seismic or gravity, and here the new magnetic data can be helpful to complete or refine the picture of their geometry. Other structures are completely new, as e.g. a lineament trending in WSW-ENE direction and crossing almost the entire survey area.

In the southernmost part of the area there are some additional linear features, which can be linked with structures observed onshore, thus allowing a more detailed onshore-offshore correlation and providing a better basis for the interpretation of particular features.

5 OTHER DATASETS

Marco Brönner

5.1 Bathymetry

The bathymetric grid used in the present study is a NGU compilation and gridding of several ship-track bathymetric profiles available along the study area (Fig. 3.8). All the profiles have been levelled using the moving median filtering method (Mauring et al. 2002, Mauring & Kihle 2006).

5.2 Gravity

The gravity grid was compiled from gravity stations on mainland Norway with the addition of marine gravity data from the Geological Survey of Norway, the Norwegian Mapping Authority, the Norwegian Petroleum Directorate, and Norwegian and foreign universities and commercial companies (Skilbrei et al. 2000) (Fig. 5.1). The compiled Free-air dataset has been interpolated to a square grid of 2 km x 2 km using the minimum curvature method (Geosoft 2005a). The simple Bouguer correction at sea (Mathisen 1976) was carried out using the bathymetry data in Fig. 3.8 and a density of 2670 kg/m^3. The International Standardization Net 1971 (I.G.S.N. 71) and the Gravity Formula 1980 for normal gravity have been used to level the surveys.

5.3 Seismic data

Seismic reflection profiles provided by the Norwegian Petroleum Directorate were combined with gravity and magnetic data for interpretation and modelling. The seismic data were only available in two-way travel times. For the potential field modelling, a depth conversion was necessary and carried out by NGU using EasyDepth^{TM} from Beicip Franlab (Beicip-Franlab 2002). The resulting depth models were directly imported into the GM-SYS package and used for potential field modelling.

The interpretation of 3 regional transects, expanding the original survey area, has been realised during this work. We used key horizons presented in the previously published reports and papers and also used well information provided by NPD to constrain the geological model. A detailed description of the depth conversion and potential field modelling is presented in chapter 10.

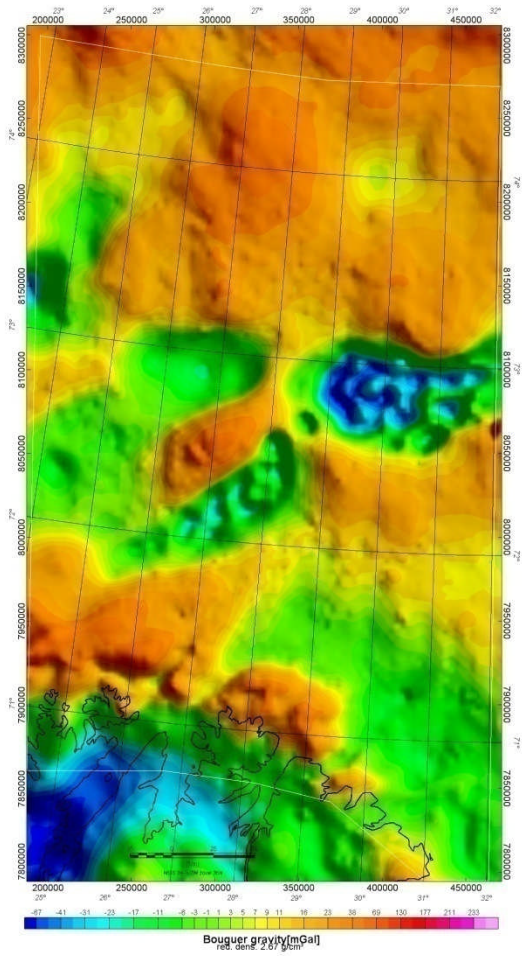

Figure 5.1 Bouguer gravity of the BASAR-08 survey area (reduction density 2.67 g/cm³).

6 CONVENTIONAL FILTERING TECHNIQUES

Marco Brönner & Laurent Gernigon

Affirmed development of the interpretation theory is usually associated with many case studies of successful application of seismic methods combined with filtered gravity and magnetic data in solving problems in exploration and structural geology. During the interpretation of the BASAR-08 survey, potential field techniques have been used intensively as complementary tools for the interpretation of the survey area. It was also a good way to test the validity of other geophysical models and was extremely beneficial for the seismic interpretation. Relevant filtering has been carried out in order to enhance the main structural changes and linear features observed within the BASAR-08 study area.

The aim of this section is to briefly present and discuss the different processing techniques used to enhance and model the magnetic data across the BASAR-08 survey area. Specific and preliminary interpretation based on these grids will be presented in another part of the present report (Chapters 9, 10 and 11).

6.1 Wavelength filtering, RTP and derivatives

Magnetic (and gravity) anomalies whose wavelengths are long relative to the dimensions of the geological objectives of a particular investigation are called regional anomalies. Because shallow geological features can have large lateral dimensions, one has to be careful, but regional anomalies are usually considered to reflect the effects of relatively deep features. Anomalies whose wavelengths are similar to the dimensions of the geological objectives of a particular investigation are called local anomalies. In the processing of magnetic data, it is beneficial to separate the regional and local anomalies prior to interpretation. Magnetic anomalies observed within the BASAR-08 survey area show the superposition of various sources reflecting the regional field, noise and lateral magnetic variations within the crust and upper mantle (e.g. Blakely 1995). Measured gravity anomalies, therefore, represent the combination of wavelengths associated with the spatially distributed sources.

During the BASAR-08 project, a number of transformation methods were used after data levelling in order to enhance the main structural and magnetic features. These techniques, used to separate regional from local gravity anomalies, take many forms and can all be considered as filtering in a general sense (Blakely 1995). Many of these techniques are the same as those employed in enhancing traditional remote sensing imagery, seismic data or processing digital elevation data (Milligan 1998, Mari et al. 2001).

Filters have been applied to the BASAR-08 gridded anomalies which enable us to isolate, interpret or/and enhance the wavelengths of greatest interest, therefore facilitating geological interpretations (e.g. Blakely 1995). The magnetic (and/or gravity) gridded datasets can be transformed from the space domain into the spectral domain and vice-versa using the Fast Fourier Transform (FFT). Transformation of the gridded data into the frequency domain is completed by application of a discrete 2D Fourier transform (DFT) (Bhattacharya 1966; Blakely et al. 1995).

For spectral analysis we used the Geosoft MAGMAP Discrete Fourier Transform algorithm (Geosoft 2005c), which applies the method of Bhattacharyya (1966). The DFT algorithm works fast by exploiting symmetries that are present for images of certain dimensions. The algorithm implemented by Geosoft in Oasis montaj is explicitly the Winograd DFT (Winograd 1978, Geosoft 2005c). This FFT transformation requires that the image fills an entire rectangle, a condition not met by the BASAR-08. Therefore, any survey gaps or irregular edges will also need to be filled with synthetic data. The edge matching and the gap filling were achieved using the maximum entropy algorithm (Burg 1975).

6.2 Reduction to the pole (RTP)

The magnetic data were reduced to the pole to properly register and locate the magnetic anomalies spatially above the magnetic bodies within the crust. The RTP is a process involving

a phase transformation of the magnetic anomaly, within the Fourier domain. The measured total field anomaly is transformed into the vertical component of the field (Arkani-Hamed 1988, Blakely 1995). The assumption following this transformation is that the magnetic anomalies had been magnetised vertically at the pole and that the anomalies are observed from the pole. Key assumptions are that the magnetisation of the source is entirely due to induced magnetisation. Therefore, the phase of the anomaly is transformed into simpler symmetrical shapes that are assumed to lie directly over the magnetic sources (Blakely 1995).

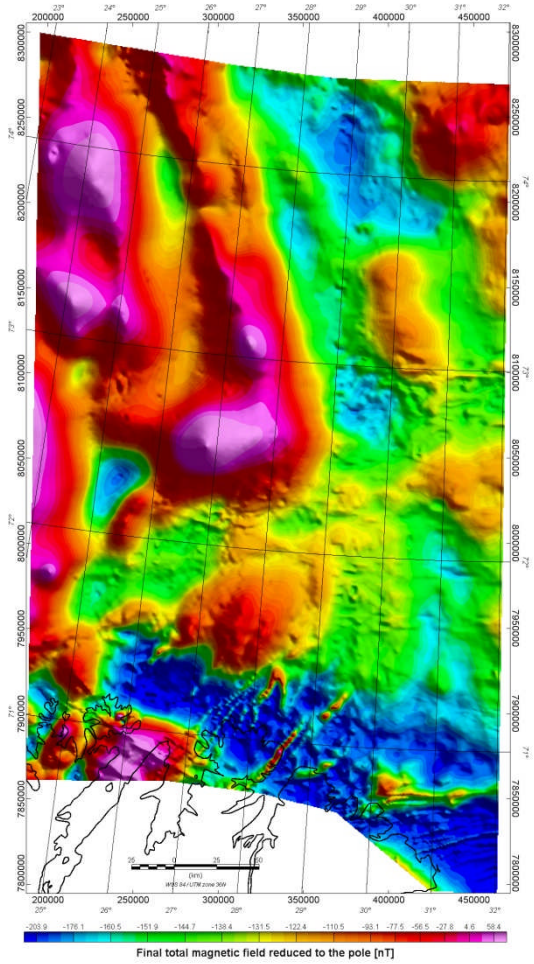

Figure 6.1 Gridded anomaly map of the total magnetic field reduced to the pole (Inc: 79.76; Dec: 12.8). The RTP was carried out using a 2D-FFT filtering along the microlevelled grid (500x500 m). The RTP transforms the anomaly into the one that would be observed with vertical magnetisation and with a vertical Earth's field, i.e. the anomaly that would be observed if the sources were located at the Earth's magnetic north pole. As a result, reduction to the pole removes asymmetries caused by the non-vertical inducing field and places the anomalies more directly over their causative bodies, thus facilitating the interpretation of the magnetic dataset. For the Barents Sea latitude these changes are relatively small.

This assumption is essential for future mapping and analysis of the magnetic anomalies because it is assumed, when applying edge enhancement, that the causative field is vertical. Consequently, some workers agree that the RTP correction should be carefully considered. Moreover, it is assumed that both the magnetic field and the magnetisation of the crust have constant directions within the study area (Arkani-Hamed 2007). The RTP filtering is also

limited for large surveys because each RTP equation does not consider the synchronous variation of both inclination and declination. Each transformation only considers one value for inclinations and declinations. Even if only minor changes can be observed in the BASAR-08 at the Barents Sea latitude, the process is usually recommended for the application of magnetic data, and makes magnetic maps more reliable for geological interpretation by removing some of the inherent complexity (Blakely 1995). For BASAR-08 the RTP correction was carried out using an average value for inclination and declination within the study area, derived from the IGRF model (Fig. 6.1).

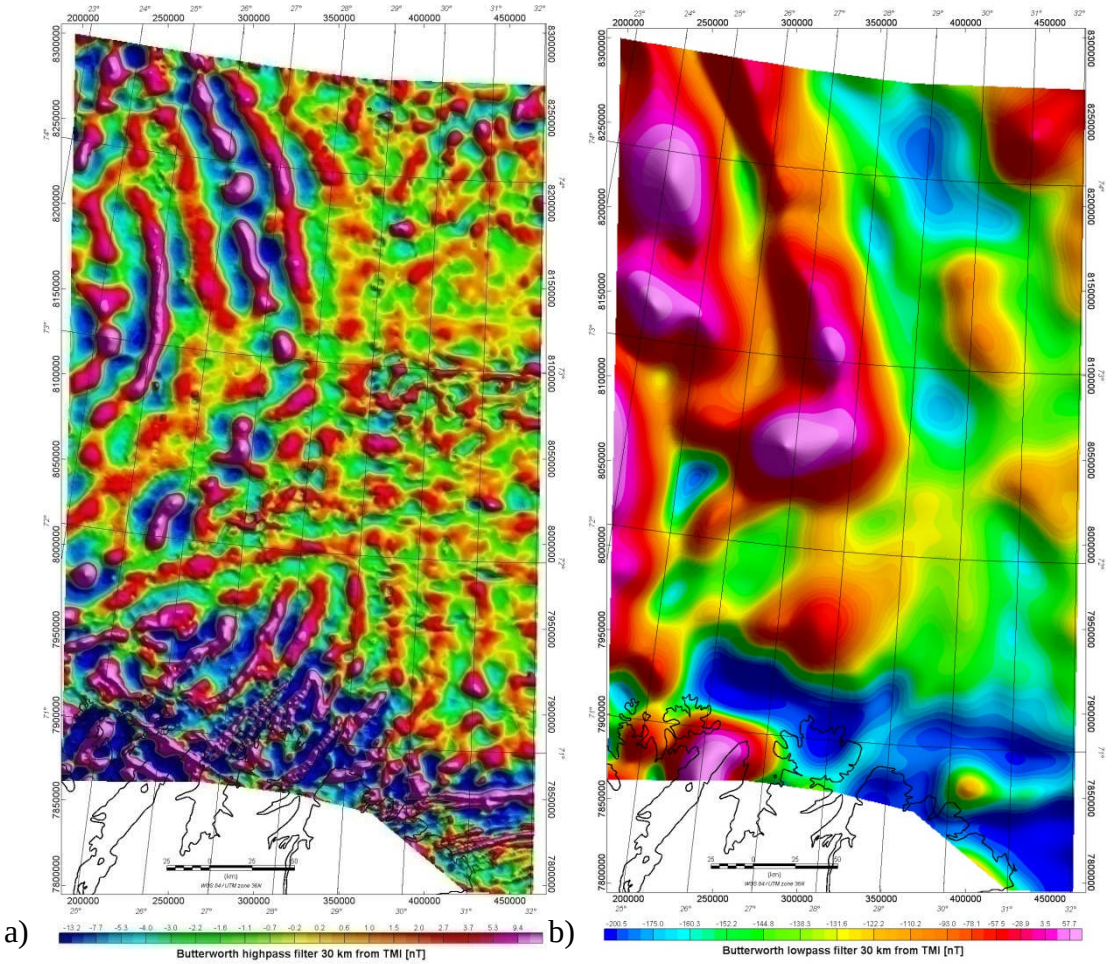

Figure 6.2 a) High-pass filtering (30 km) of the magnetic total field, RTP. This filter underlines the distribution of the short wavelengths. B) Low-pass filter (30 km) showing the corresponding residual field. Grid cell size is 500 x 500 m.

6.3 Wavelength and continuation filtering

Wavelength filters are a common tool to delineate shallow crustal features of shorter wavelengths from the regional field and supports a more accurate interpretation of sedimentary rock tectonics and basement structures.

The regional anomalies can be estimated employing a variety of analytical techniques, including high-pass and low-pass filters (Fig. 6.2). The magnetic data were most useful for determining

the presence, trends and depth of intrusions, faults and basement structures. High-pass filtering of the data at 30 km was used to highlight fault structures, salt diapirs and lineaments, which are likely related to basement variations and/or intruded material in the upper basement and overlying sedimentary strata (Fig. 6.2a). Figure 6.2b shows the corresponding 30 km low-pass filter, which represents predominant basement variations, as well as faults with a more regional impact.

Upward continuation is a low-pass filtering process simulating the result of the survey as if it had been carried out at a higher elevation (Fig. 6.3). This process is based on the physical fact that the further the observation is from the body causing the anomaly, the broader is the anomaly. The technique provides an excellent integrated view of the deeper magnetic settings undistorted by the local, high-amplitude, high-gradient anomalies of the magnetic sources in the shallow portion of the underground.

Upward continuations to 5 and 15 km have been used for the BASAR-08 survey to provide indications about the main magnetic and tectonic units in the area.

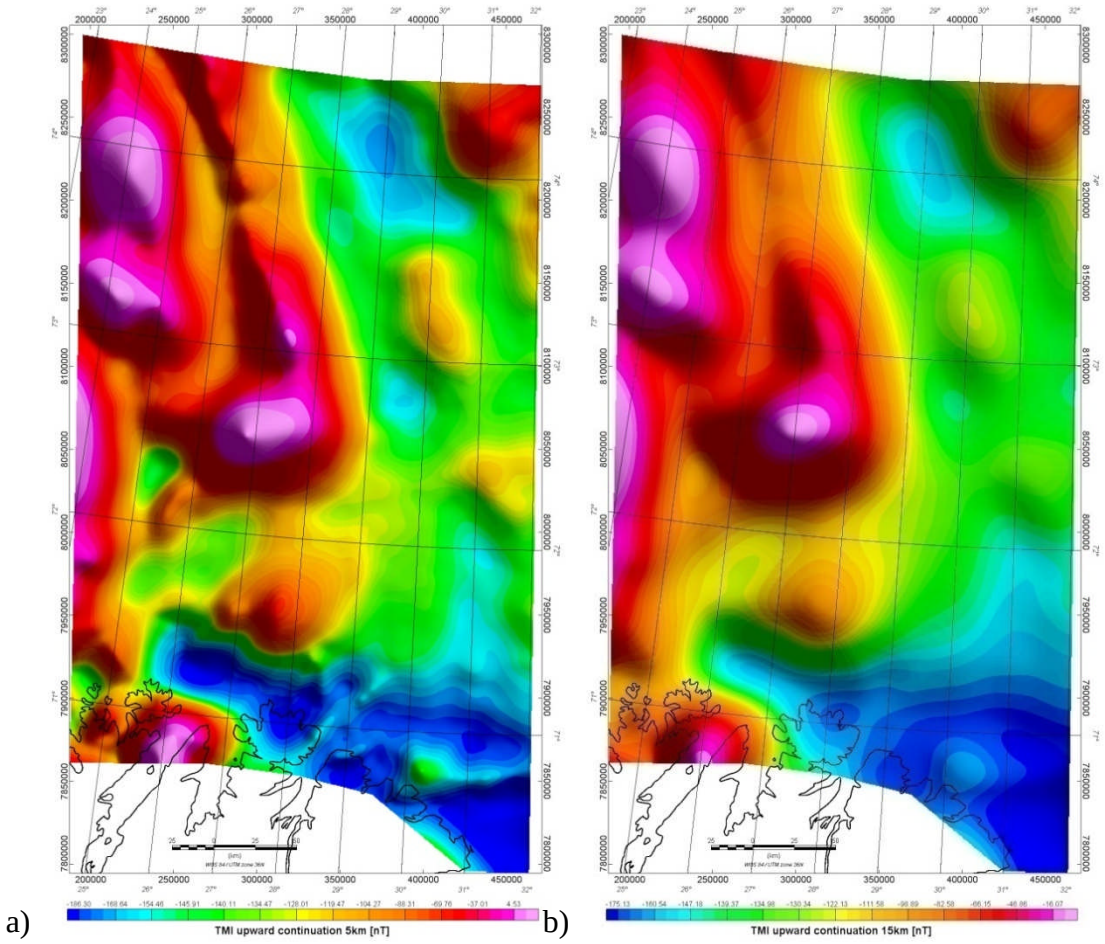

Figure 6.3 Upward continuations of the magnetic total field to a) 5 km and b) 15 km, respectively. Upward continuation uses wavelength filtering to simulate the appearance of potential-field maps as if the data had been recorded at a higher altitude. Large-scale regional anomalies and the main crustal patterns are revealed by this process.

7 ENHANCEMENT OF TREND USING STRUCTURAL FILTERS

Marco Brönner

The purposes of this chapter are 1) to show the benefit of derivative and normalised filters in investigation of the structural setting in the survey area; 2) to evaluate the images produced by several enhancement techniques for lineament mapping; and 3) to prepare structural and depth to magnetic basement estimation maps (lineament) based on magnetic data interpretation. Some newly discovered lineaments and features might be subsequently used as a reference for future geological mapping, interpretation or re-interpretation.

7.1 Automatic gain control (AGC)

The automatic gain control filtering (AGC) was used to convert waveforms of variable amplitude to a grid that gives an equal emphasis to signals with both low and high amplitudes (Mudge 1991).

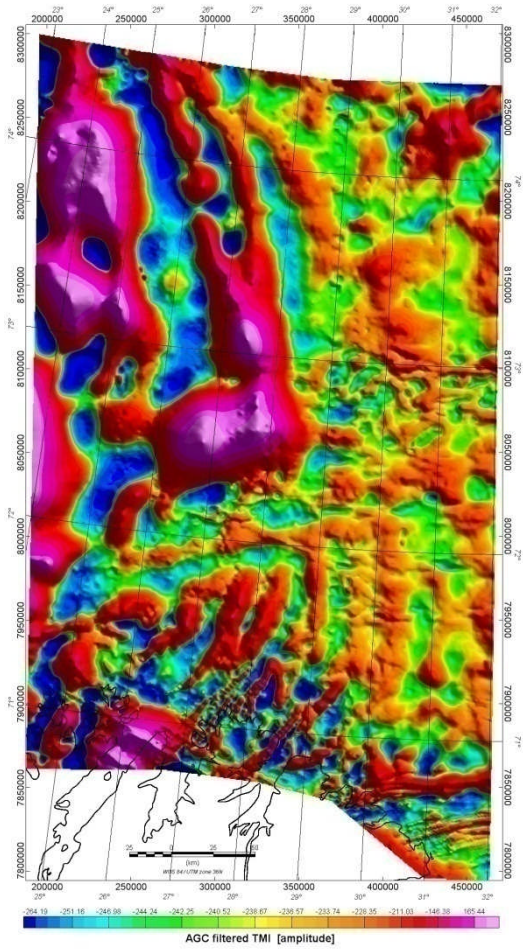

Figure 7.1 Automatic gain control filtering (AGC) of the BASAR-08 survey. To highlight the local anomaly details, automatic gain control (AGC) boosts amplitudes in areas with smooth anomalies, without sacrificing the long-wavelength information. Gain is estimated with a sliding square filter window, centred on each grid node.

Like derivative filters, the AGC filter is useful to underline structural features because it highlights trends with coherent alignments that are not always apparent in true amplitude data (Fig. 7.1). The AGC filter, in contradiction to the high-pass and derivative filters, emphasizes small-amplitude and short-wavelength features without masking the regional elements. This can be beneficial in identifying additional interplays and interferences among different magnetic structures.

7.2 Derivative filters

Derivatives of the magnetic total field and its analytic signal have been computed within this study to enhance short-wavelength features and the main lineations. Computation of the three orthogonal derivatives, (x, y, z) within potential field modelling is considered as a universally applicable and basic processing step (Thurston & Brown 1994, Blakely et al. 1995, Nabighian et al. 2005).

7.2.1 Vertical derivatives

Vertical derivatives (VDR) were used to enhance localised near-surface sources and trends, and to improve source resolution, assuming high-quality data (Figs. 7.2 and 7.3).

Transformation of potential-field data into a derivative map enhances edges or contacts by placing anomaly maxima at the point of the maximum horizontal gradient identified within the x- and y-orientations of the grid. The key assumptions made when transforming gravity and magnetic field data into the three orthogonal derivatives are that: (1) the potential field measured at the surface is the vertical component of the field; (2) the lithological contacts giving rise to the anomalies are abrupt, near-vertical and isolated from other sources. The first assumption is essentially true for gravity and for magnetic data reduced to the pole (Blakely 1995). In reality, however, geological contacts are rarely vertical and density and magnetisation can vary in all directions in a geological unit. Computation of the first vertical derivative (FVD) has been referred to as a pre-processing step, particularly before the interpretation of the Euler and analytic signals (see Chapter 8).

Moreover, it is also highly beneficial to map and interpret magnetic lineaments and structural elements as it highlights the edges of lateral changes in the observed magnetic field. From the FVD (Fig. 7.2) the high-amplitude lineaments in the south, for example are better pronounced as well as a slightly curved lineament in the central part of the survey area, trending NNW-SSE north of the Norsel High.

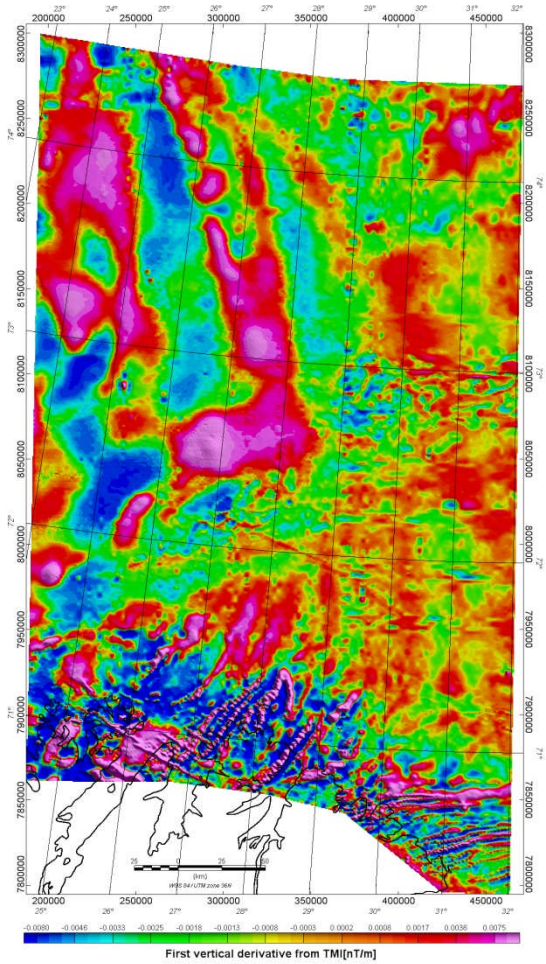

Figure 7.2 First vertical derivative obtained by convolution along the magnetic total field, reduced to the pole and gridded with a cell size of 500 m using minimum curvature. The vertical derivative of an anomaly is related to the depth and geometry of the causative body. The gradient operator attenuates broad, more regional anomalies and enhances local, more subtle, magnetic responses and, as such, is sensitive to shallow magnetic source bodies and contacts.

Computation of the second vertical derivative (Fig. 7.3) as described by Blakely (1995) can be unstable. The second vertical derivative, or rate of change of the fall-off rate of an anomaly, may be considered equivalent to a residualization of the data and is a common tool delineating source bodies. To stabilize the calculation and to suppress high-frequency noise and emphasizing contact features of various wavelengths, different low-pass filters were applied during the calculation. Figure 7.3 shows the SVD of the TMI data low-pass filtered with 4 km (a) and 8 km (b). Figure 7.3a is significantly affected by high-frequency noise due to the line character of the data acquisition, but nevertheless it emphasizes the different magnetisations of the shallower sources such as quite a few lineaments in the onshore-offshore region and the salt structures in the Nordkapp Basin.

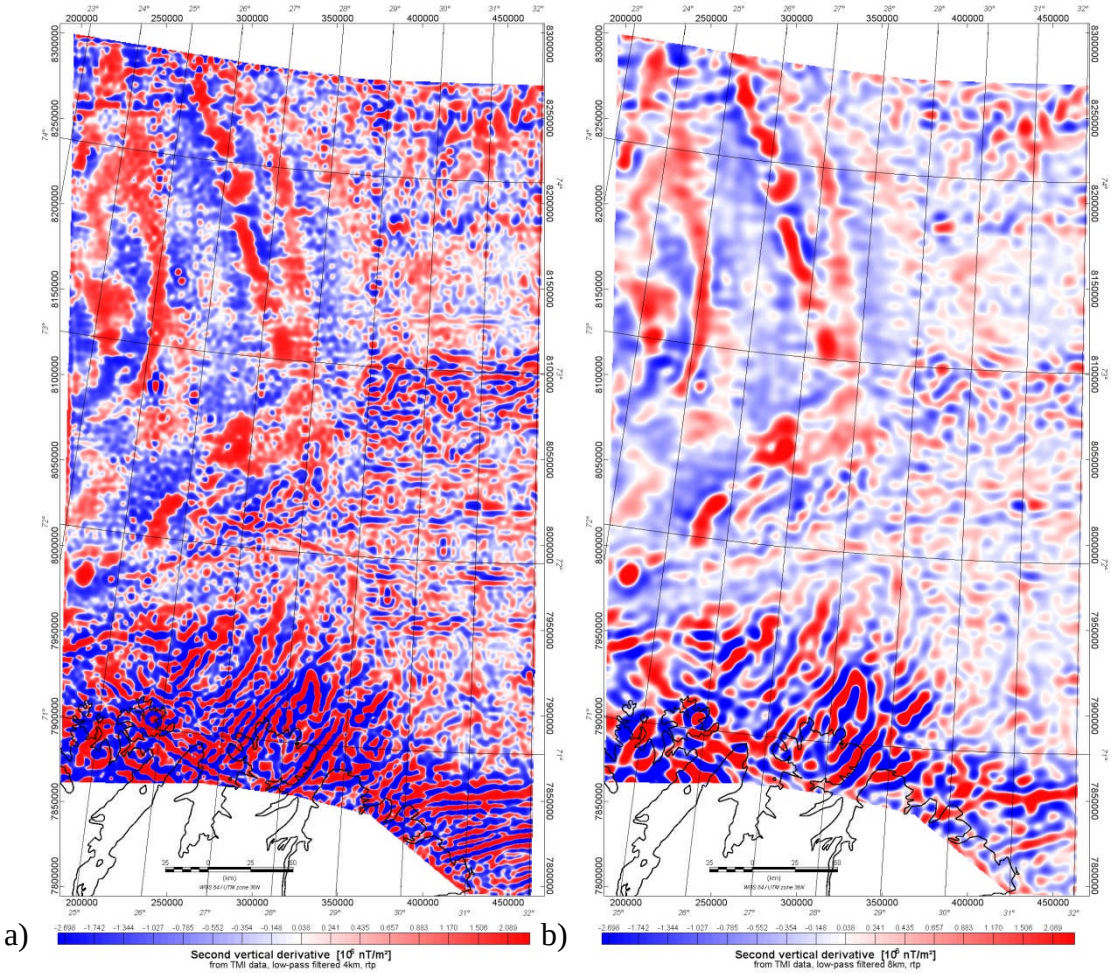

Figure 7.3 Second vertical derivative obtained by convolution along the magnetic total field reduced to the pole. The data were low-pass filtered with a) 4 km and b) 8 km to suppress high frequency noise and to highlight contact features of different wavelengths.

The SVD allows for example to define the lateral extension of the Nordkapp Basin from the magnetic data due to a significant change in the amplitude and frequency content. Applying an 8 km low-pass (Fig. 5.3b), many of these features are suppressed and longer wavelength trends from deeper levels or deeper-developed origins are more pronounced, e.g. a lineament striking NE-SW partly coinciding with the southern rim of the Nordkapp Basin, and a well developed lineament trending NNW-SSE, which appears more differentiated in the SVDs. Applying different low-pass filters can also provide hints of the development of different structures with depth.

7.2.2 The horizontal derivatives

The horizontal derivatives (HDR) can be used to predict the locations of major basement structures or sedimentary rock tectonics, igneous bodies and changes in basement grain (Grauch & Cordell 1987, Gunn 1997). Figure 7.4 shows the horizontal derivatives calculated in a) the E-W and b) the N-S directions.

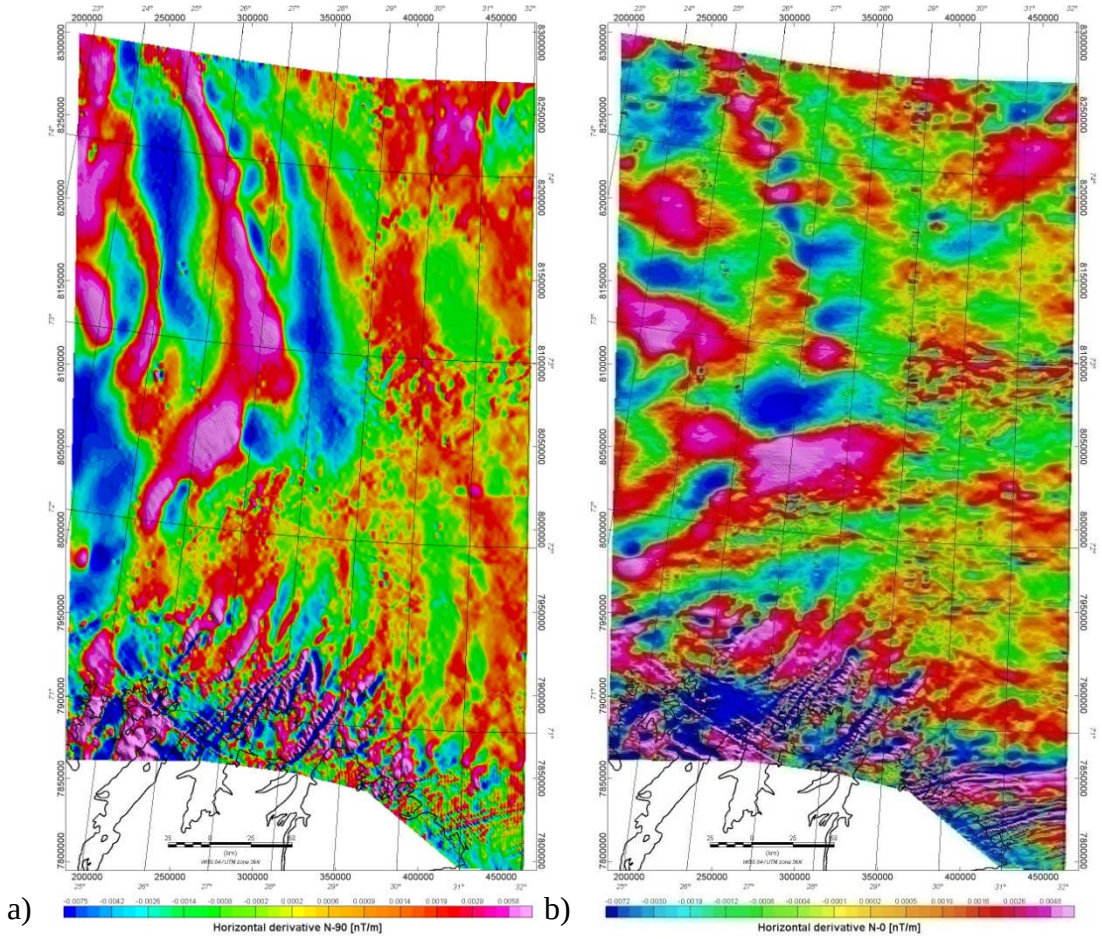

Figure 7.4 Directional horizontal derivatives in the BASAR-08 area. The filter enhances the high frequencies along the E-W (a) and N-S (b) trends.

7.2.3 The terrain slope or horizontal gradient magnitude (HGM)

Similar to the way the first directional derivative defines the slope at any point on the surface, the terrain slope filter has been applied to calculate the slope at any grid node of the BASAR-08 dataset (Fig 7.5). Grid files of the terrain slope can produce contour maps that show isolines of constant steepest magnetic slope. For any particular point on the surface, the HGM is based on the direction of steepest descent or ascent of the magnetic field at that point. This means that across the surface, the gradient direction can change. This operation is similar to the way the first directional derivative filter defines the slope at any point on the surface, but is more powerful as it automatically defines the gradient direction at each point on the map.

The HGM aided in defining the location of linear features which, in turn, are related to the trends of the lineaments in the area. It produces maximum ridges over edges of magnetic basement blocks and faults or other magnetic bodies.

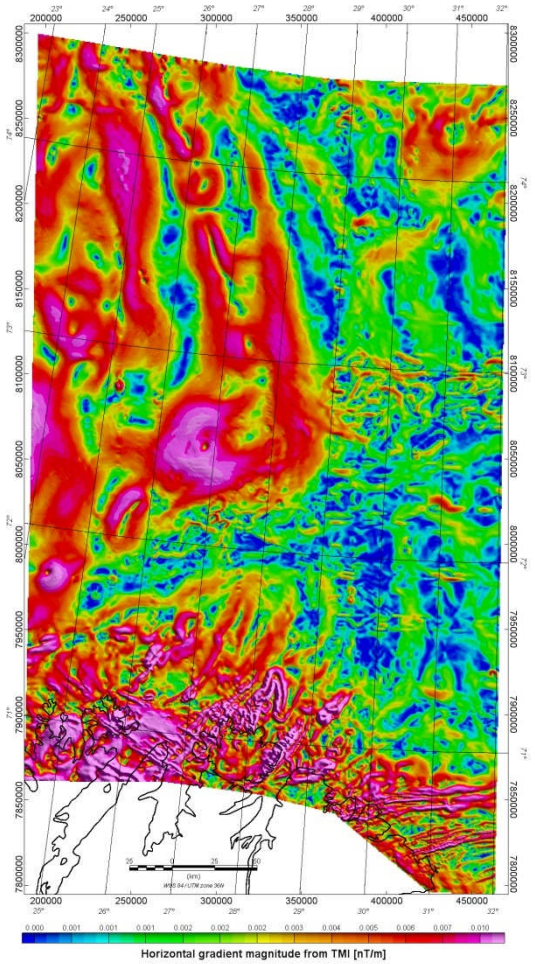

Figure 7.5 Horizontal gradient magnitude of the BASAR-08 dataset, reduced to the pole. After the reduction-to-pole correction, a magnetic body is spatially more directly associated with the related magnetic response. The horizontal gradient magnitude of the anomaly slope is then located near or over the body edge; i.e., the horizontal gradient operator in map form produces maximum ridges over edges of magnetic basement blocks and faults or other magnetic bodies. In addition, the horizontal gradient highlights linear and round-shaped features, related to magnetic contacts, in the dataset.

7.3 Analytic signal

The analytical signal combines calculated first derivatives in the x, y and z directions. The technique creates peaks over the edges of wide magnetic bodies and the centres of small bodies. The concept of analytic signal applied to magnetic anomalies was developed in two dimensions by Nabighian (1972) based on a concept initially proposed by the Frenchman Ville in 1948.

A common theme of the normalised derivatives is the concept of mapping angles (or functions of angles) derived from the gradients of the magnetic intensity.

The resulting shape of the analytic signal is expected to be centred above the magnetic body (Fig. 7.6). This has the effect of transforming the shape of the magnetic anomaly from any magnetic inclination to one, positive, body-centred anomaly at least in 2D (Nabighian 1972).

Analytic signal has been utilised widely for the mapping of structures and for determining the depth of sources (Pilkington et al. 2000, Florio et al. 2006).

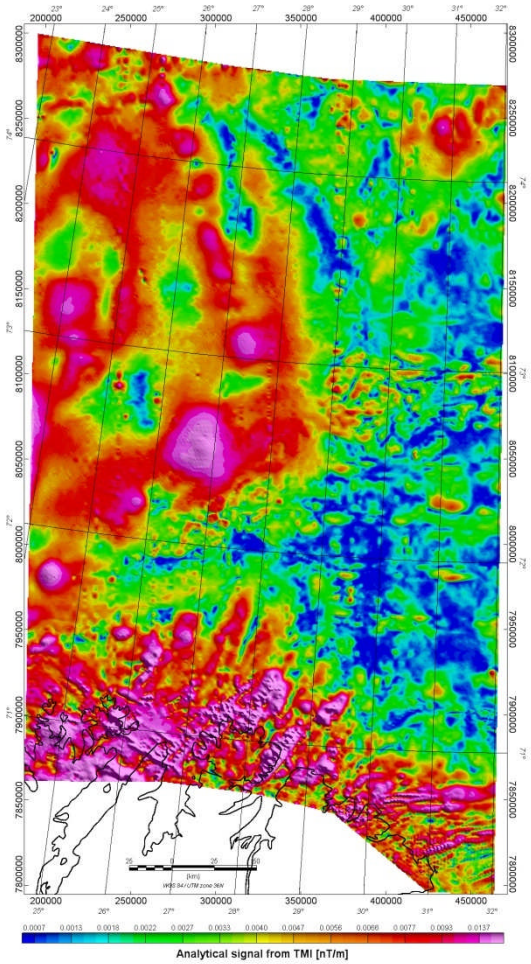

Figure 7.6 Analytic signal of the magnetic total field grid, reduced to the pole (500 x 500 m cell size).

The main advantage of the total gradient over the maximum horizontal gradient is its lack of dependence on dip and magnetisation direction, at least in 2D. When interpreting the analytic signal it is assumed that the causative sources are simple near-vertical or step-like geological structures (Roest et al. 1992, Roest & Pilkington 1993). Therefore, the 2D analytic signal has significant advantages over the simple derivatives and this application was utilised to map changes in basement structure, fabric and trends. Synthetic modelling has proved that the maxima of the analytic signal are located over the edges of anomalous sources (Roest et al. 1992). This simplification of the potential field, however, results in the compromise whereby during computation the sign of the original gravity and magnetic field is lost. Therefore, it cannot be determined whether the analytic signal anomaly represents a positive or a negative density or magnetic susceptibility contrast compared to its surroundings.

For large-scale magnetic surveys like the BASAR-08 or for shallower depths of causative bodies, the analytic signal method provides a useful and fast way of delineating magnetic boundaries in the subsurface (Fig. 7.6).

7.4 Tilt derivative (TDR)

The tilt derivative filter (TDR) is another powerful and normalised derivatives tool for shape and edge detection (Figs. 7.7). The result is strongly peaked along the maxima of the horizontal gradient. It gives a much sharper definition of the magnetic contacts than the horizontal gradient map.

For the BASAR-08 interpretation, this filter is particularly useful in identifying dykes or dyke swarms in the Barents Sea and Finnmark area, lineaments of shallow origins and also highlights the edges of the salt structures in the Nordkapp Basin. The TDR is defined in terms of the ratio between the first vertical derivative of the potential field and its total horizontal gradient of the field (Miller & Singh 1994, Verduzco et al. 2004, Cooper & Cowan 2006).

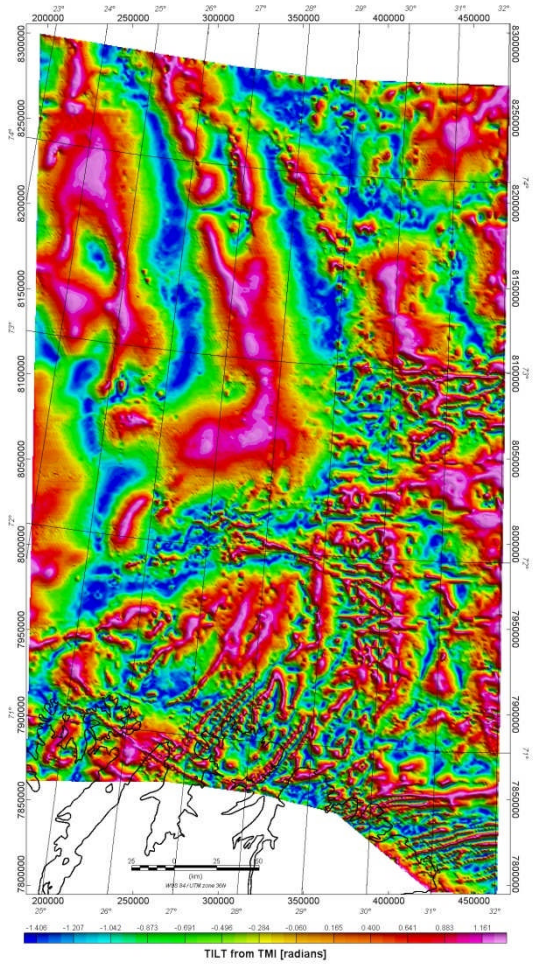

Figure 7.7 Tilt derivative of the magnetic total field RTP. The tilt derivative (TDR) is an alternative method for deriving the maximum gradient anomalies associated with magnetic contacts.

The TDR is restricted to values in the range $+\pi/2 > \text{Tilt} > -\pi/2$, and can be considered as an expression of the vertical derivative normalized by the total horizontal derivative. This measure has the property of being positive over a source and negative elsewhere (Fig. 7.7). The tilt filter

technique tends to enhance mapping of the subtle magnetic anomalies and maximises the geometrical contrast of the internal basin structure (partly constrained by seismics). The tilt angle was compared with other edge detection measures such as the horizontal gradient, the second vertical derivative and the analytic signal and has been found to have the added advantage of responding well to both shallow and deep sources within the BASAR-08 area. Combined with the 30 km high-pass wavelength filter, results were particularly useful for the structural interpretation of the BASAR-08 dataset.

8 ESTIMATION OF MAGNETIC DEPTHS

Marco Brönner

8.1 Implications

Depth to magnetic source calculation is a challenging and important task in magnetic interpretation. A complete and quantitative interpretation of potential field data aims at estimating information about the depth, dimension and contrast of the relevant geological units. Magnetic depth estimates are often a reasonable approximation to depth to the magnetic basement (i.e., metamorphic, igneous, oceanic), and the crystalline basement depth (or alternatively, the sedimentary thickness) is a primary exploration risk parameter. Furthermore, estimating basement depths are directly applicable to thermo-kinematical modelling and thermal maturity applications (e.g., heat-flow estimation, source-rock burial depth, distribution and volume).

However, it is noticeable that such an interpretation of depth to basement suffers from inherent ambiguity. As a matter of fact, it is not possible to obtain all three types of information simultaneously without other a priori information (e.g., the geological context or seismic data). These methods usually work for simplified source geometries (dimensions) and are most of the time independent of the susceptibility contrast. The depths estimated by some methods can be used as the final, quantitative solution in some ideal situations (i.e., where the anomaly is well isolated and the noise is insignificant or removed).

In this chapter, we present the results obtained using the 3D-located Euler deconvolution of the magnetic total field.

8.2 Euler deconvolution

The Euler method uses Euler's homogeneity equation to construct a system of linear equations, and then determines through a least-squares inversion for one window the (vertical and horizontal) position of a single source for a given source geometry (Reid et al. 1990). Euler deconvolution was first presented by Thompson (1982) for profile data and by Reid et al. (1990) for gridded data.

The method requires the use of the calculated horizontal and vertical derivatives of the magnetic field if they are not actually observed. Thompson (1982) called the fall-off rate (i.e., the negative of the degree of homogeneity) the structural index (N). Synthetic tests (Silva & Barbosa 2003, Keating & Pilkington 2004, Stavrev & Reid 2007) indicate (1) that the Euler method can locate

the outline and depth of a variety of simple geometrical shapes; and 2) that the structural indices will cluster and determine the best structural interpretation. Although detailed as vertical

Structural Index	Magnetic field	Gravity field
0	contact	sill/dyke/step
0.5	thick step	ribbon
1	sill/dyke	pipe
2	pipe	sphere
3	sphere	

Table 8.1 Summary of the structural indices for simple geometric models from a magnetic anomaly or gravity anomalies (Reid et al. 1990, Marson & Klingele 1993, Bainbridge et al. 2002).

contacts, faults with a large throw may be best displayed with a structural index of zero (Table 8.1).
Euler's homogeneity equation is valid for bodies of arbitrary shape, characterised by these indices. In practice, the Euler method assumes idealised structures such as contacts, thin sheets (dykes), vertical or horizontal cylinders and a 3D sphere. This section therefore briefly describes the theory, advantages and limitations behind the technique and presents its applications for the BASAR-08 survey.

Euler 3-D deconvolution is a semi-automated technique enabling rapid qualitative interpretation and depth estimation of source depths from large gridded gravity and magnetic datasets (Reid et al. 1990, Barbosa et al. 2000, Pilkington et al. 2000, Hsu 2002, Mushayandebvu et al. 2004, Florio et al. 2006). The technique has considerable advantages. 1) It can operate on large datasets extremely quickly; 2) provide a qualitative interpretation of geological structures; 3) provide depth estimates for the sources of the anomalies; 4) magnetic data do not need to be reduced to the pole (Reid et al. 1990); and 5) it is also insensitive to magnetic inclination, declination and remanence since these become part of the constant in the anomaly function of a given model.

8.3 Interpretation of the structural indices

Careful consideration of the distribution and clustering of Euler solutions is, however, required to discriminate which solution best represents the causative source at depth within the crust. Although in theory, interpretation of the Euler solutions requires no pre-geological knowledge, Reid et al. (1990) acknowledged that this can be significantly beneficial. Reid et al. (1990) claimed that the choice of structural index remains the prime limitation of the traditional Euler technique. This and other limitations arise as a product of some of the simplifying assumptions of the technique, which assume that the source is (1) equivalent to a simplified geometrical

feature, (2) spatially homogeneous, (3) independent of neighbouring magnetic sources and (4) has a heterogeneous magnetisation or density.
In the BASAR-08 survey, geological structures are most likely arbitrarily shaped sources, and are therefore not simply modelled or defined by the structural index. The fact that the sources may not be internally or spatially homogeneous (i.e. the magnetisation and shape of the source change with depth or along strike), or the source-to-observation distance increases (thus, the anomaly shape changes with depth) or other sources impinge on each other's spatial positions are inherent sources of scatter (Reid et al. 1990, Keating & Pilkington 2004). Consequently, it is necessary to examine a number of structural indices to compare results and clustering of solutions for several individual features. Alternatively, in such situations, geological constraints from external data sources would be beneficial to the interpretation of the BASAR-08 dataset in the future.

Complexities also arise with respect to the depth of burial of the source. Ravat (1996) noted that there was a strong inter-dependency between the choice of the structural index and the distance of the source-to-observation, and that with increased distance the results were biased towards the higher structural indices, explained by the exponential decay of a source anomaly with depth. It can be predicted that with increasing depth the attenuation rate of the anomaly is less; deeper sources may therefore only be represented by higher values (Ravat 1996). The relationships between the source type and the observation level are considerably altered following upward continuation of the observation level, thus increasing the possibility of mis-identification of the true structural index (Ravat 1996).

For BASAR-08 we found some correlation with the main trends. Lineaments associated with faults and mafic intrusions revealed both shallow and deep Euler solutions, which could give indications of the angle of dip, depth and the geotectonic impact of the different structures. Contacts with salt diapirs yielded a magnetic anomaly marking the outline of the salt structures and produced Euler solutions of rather shallow depth. Some major features, which are likely to be related to basement structures, produced a stabile distribution of Euler solutions. A final comparison with three wells, where basement was penetrated at depth, show similar or greater depths from the Euler deconvolution.
A detailed presentation of the results is given in Chapter 8.4.

8.4 Located 3D Euler method

Euler deconvolution usually assumes a 'moving window' technique (Reid et al. 1990). This standard technique produces a mathematical solution for each position of the window, estimating the unknowns after each sequential movement. The minimum and maximum depths that can be resolved are related to the grid cell size and the window size selected, highlighting the importance of the quality of the dataset and the nature of the investigations.

For this report, we preferred the ‘Located 3D Euler method’, which is a modified version of the standard Euler deconvolution (Bainbridge et al. 2002). The located 3D Euler method refines the standard method by first running a peak-finding routine (Blakely & Simpson 1986), which locates peaks and estimates an appropriate window size before the deconvolution. This method produces far fewer solutions because only a small subset of the grid will be at the centre of peaks in the dataset. Combined with discrimination techniques, we can obtain more reliable Euler solutions. Only upper crustal sources (<15 km) have been selected in the following examples. Peak detection was automatically obtained using the Blakely grid peak-picking algorithm of Blakely & Simpson (1986).

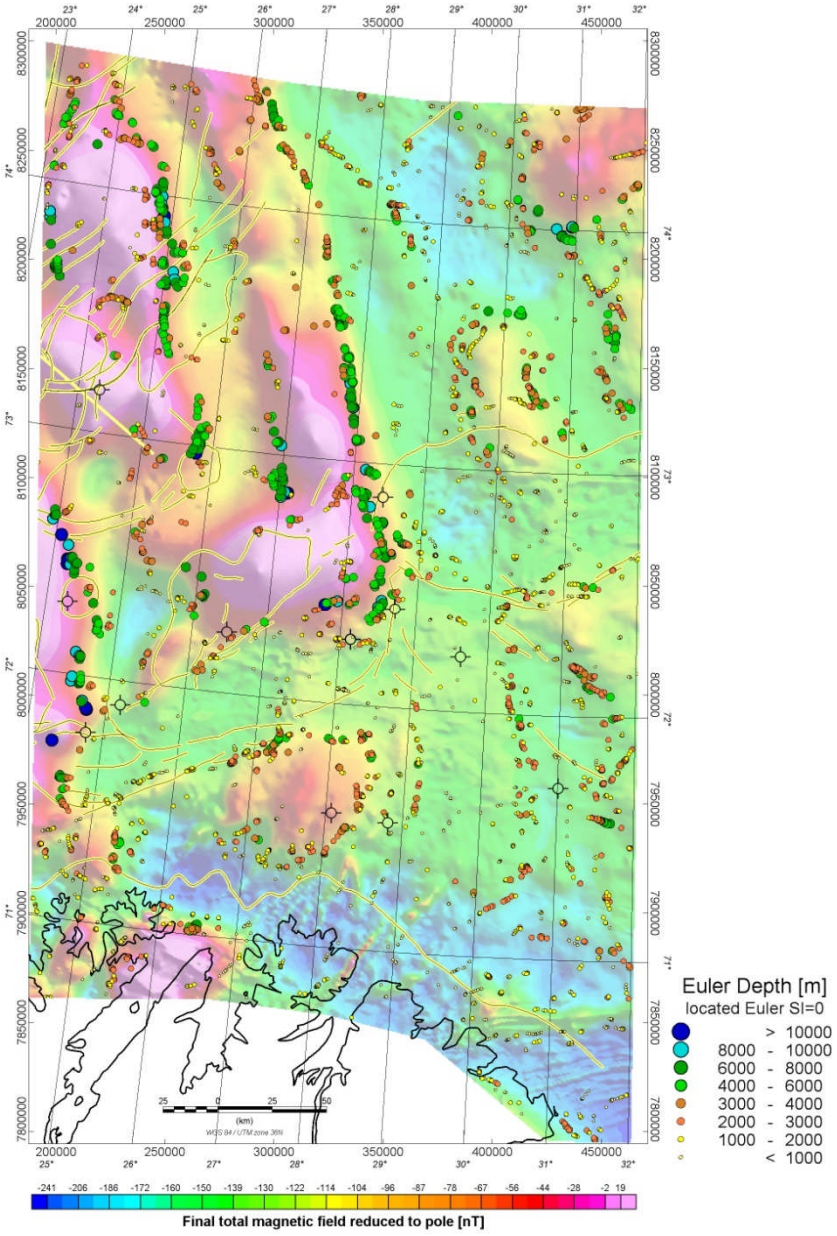

Figure 8.1 Result from located Euler deconvolution of the BASAR-08 data. Results using a structural index of 0.

A pre-processing of the dataset used the analytic signal as the primary grid for Euler deconvolution. However, such procedures may increase the ratio of noise to signal within the grid; therefore, such pre-processing is limited by the initial quality of the dataset, because noise will contribute to the scattering of solutions. In the present project, we tried different upward continuations to remove some remaining noise within the BASAR-08 data. We finally dispensed with this smoothing for two reasons:

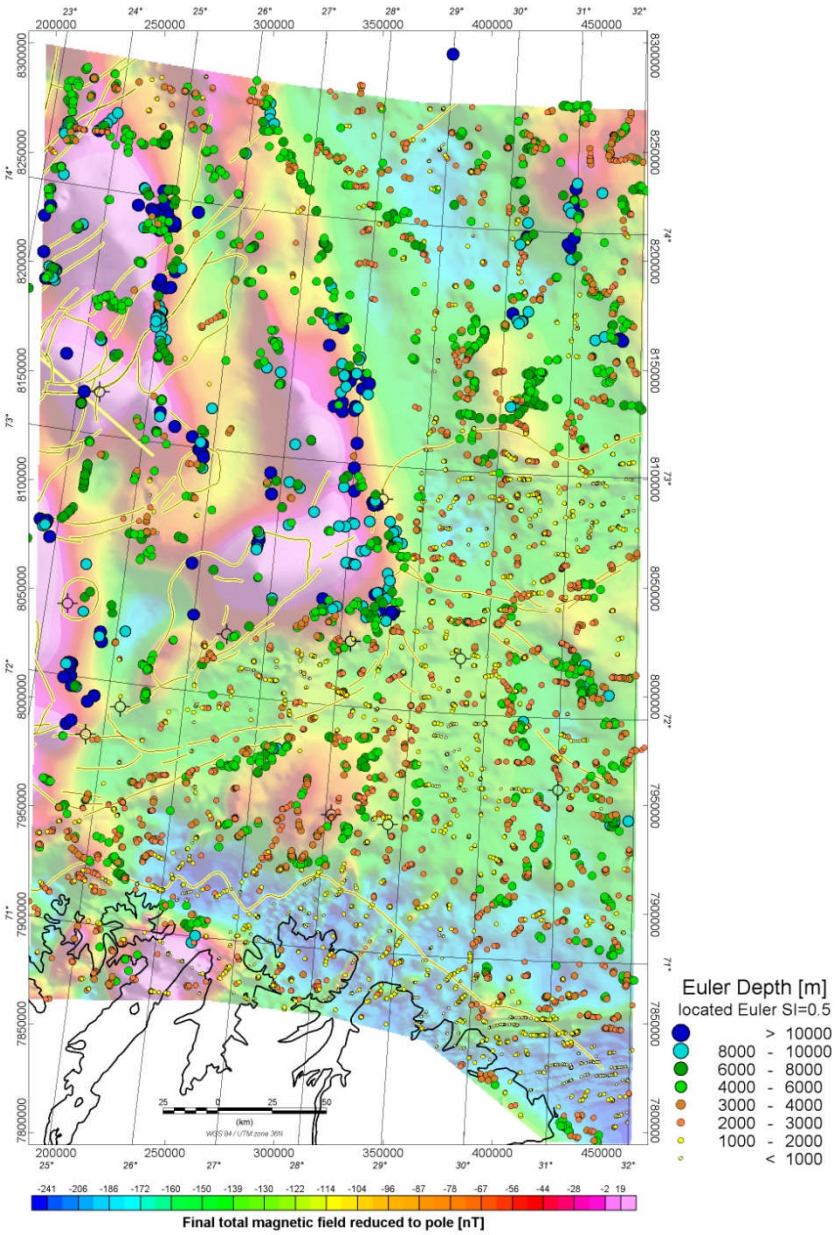

Figure 8.2 Result from located Euler deconvolution of the BASAR-08 data. Results using a structural index of 0.5

1) this could have significant consequences for the determination of the source-to-window ratio and would complicate the depth interpretation of the deconvolution (Ravat et al. 2002), and 2) the BASAR-08 dataset shows quite a number of interesting high-frequency and low-amplitude

anomalies which would be suppressed by upward continuation. Instead we decided to clip the results and eliminate depth solutions shallower than 500 m, which suppress at least some of the noise.
During the BASAR-08 modelling, a series of maps, encompassing all the different structural indices, was required to accurately assess the different geological structures present within a study area particularly within complex regions. Best results for BASAR-08 have been obtained using located Euler solution using indices of 0, 0.5 and 1, and are displayed in figures. 8.1, 8.2 and 8.3.
Figure 8.1 shows located Euler solutions using the structural index 0, which is supposed to reflect 'infinitive steps' and highlights geological contacts. Apart from some sparsely distributed irregular locations, the Euler solutions for this index show edges of the principal features in the BASAR-08 survey area, such as the almost N-S-striking curved lineaments already obvious from some of the filtering (e.g. Fig. 6.2) and a NE-SW-striking lineament south of the Nordkapp Basin.

Calculating Euler solutions for the structural indices SI=0.5 and SI=1 (Figs. 8.2 and 8.3), which are more adapted to discover 'thick steps' and 'sheet edges', the pictures become more complex as Euler solutions for more of the shallower features are calculated. Nevertheless, apart from some scattered noise-related solutions, most of the depth estimations can be correlated with geological structures and reveal some interesting insights into geological settings.

In general, the northwestern part of the survey area with the Norsel High, Mercurius High and the easternmost edge of the Loppa High appears as a kind of compact block with predominantly deep Euler solutions. Shallower features are rare here or magnetically invisible, and underline a different feature of this area in comparison with the areas to the east and south. For these areas, the deeper Euler solutions likely mark the principal geotectonic units as seen from figure 8.1, possibly related to basement structures, but a multiplicity of magnetic features is obviously of shallower and intra-sedimentary origin. For the Nordkapp Basin, for example, solutions along the outline of the salt diapirs are prominent and probably conceal a proper depth-to-basement calculation by using the Euler deconvolution. A lineament running across the southern Nordkapp Basin towards the southeast shows Euler solutions of maximum 3,500 m, and is definitely of intra-sedimentary origin. Other lineaments to the south of the area with NW-SE and NE-SW trends also show a rather shallow origin (<3,000 m) and can be correlated with onshore features such as faults and dykes or high-magnetic sedimentary rocks. Depth solutions show intermediate depths of c. 5,000-10,000 m along the linear structures in the northwest, with some maximum solutions of ~15,000 m in the westernmost part of the survey area and shallower depths of c. 1,000 - 6,000 m, locally up to 8,000 – 10,000 m in the areas east and southeast of the Norsel High.

To estimate the reliability of the method the depth-to-basement results from Euler deconvolution were compared with observed basement depths from well logs and depth-converted seismics. Basement was reached in three wells, 7226/11-1 at c. 5140 m, 7128/4-1 and 7128/6-1 both at c.

2500 m, and we could achieve similar results from Euler deconvolution and a SI=0.5.

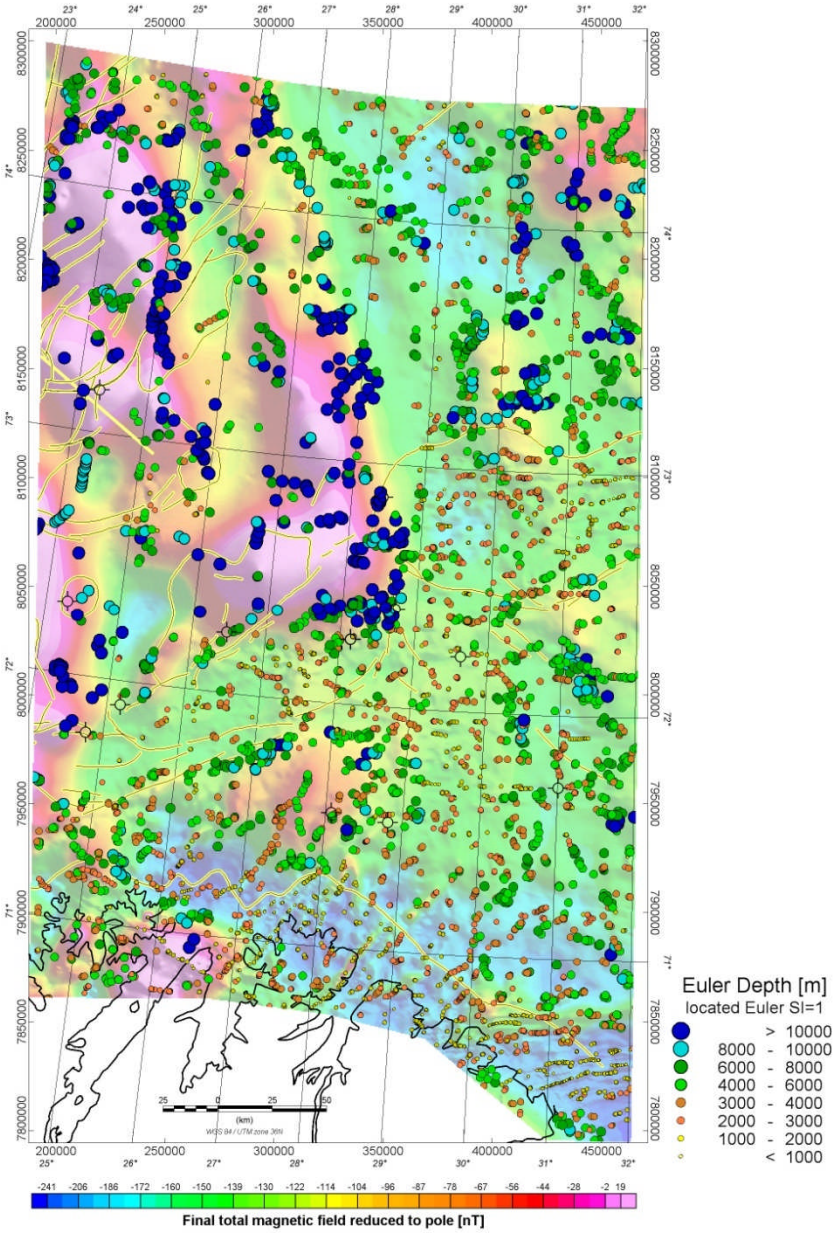

Figure 8.3 Result from located Euler deconvolution of the BASAR-08 data. Results using a structural index of 1.

Along the provided three seismic lines, additional correlations with basement depth could be made. A 6 km depth of the Ottar Basin, for example, fits rather well with the top basement observed on seismic data. Nevertheless, we consider the study area to be not so perfectly adapted for the Euler techniques. Thick piles of sediment (5-10 km or more) and probably a small magnetic sediment-basement contrast over wide areas of the survey blur the magnetic signature from the basement and reduce the applicability of the Euler deconvolution in terms of a depth-to-magnetic basement calculation. Here, modelling rather than Euler techniques is definitely the method of choice to get a better hand on the depth-to-basement.

8.5 Werner deconvolution

The Werner deconvolution method (Werner 1953, Gunn 1997) was applied to the new magnetic dataset along the three seismic lines to support the modelling and interpretation in 2D. It has been used to estimate and/or underline the potential depth of magnetic sources along these specific transects (see Chapter 10). The basic assumption of the Werner deconvolution is that all magnetic anomalies are the result of either a sequence of dykes or edge interfaces. The strike lengths and depths of the source bodies are also assumed to be infinite, whereas the width of each body is assumed to be either: (1) finite, representing a dyke; or (2) approaching zero, such that it represents an interface between two bodies of differing magnetic susceptibility. The robustness of the technique is such that no reduction to the pole is required and it works effectively with both induced and remnant magnetisations. The results were compared with the Euler solutions computed in the previous part of the chapter.

Werner (1953) recognised that analysing magnetic anomalies could be complicated because of the interference from adjacent anomalies and the effect of noise (e.g. diurnal variations, non-two-dimensionality and induced versus remnant magnetism). For this reason, the Werner deconvolution algorithm uses simple models for the sources and a quadratic form for the source/noise interference to determine the magnetisation properties of the causative bodies. To reduce the noise we applied first an upward continuation filter to smooth the BASAR-08 magnetic grid. If the deconvolution is successful in defining a ‘real’ source, then depth estimates should define either the edges of the causative body or the depth range of an interface or the upper boundary of an intrusion.

9 INTERPRETATION

Marco Brönner, Laurent Gernigon & David Roberts

9.1 Introduction

The BASAR-08 survey covers a significant part of the southwestern Barents Sea including the entire Nordkapp Basin and northernmost Finnmark. The magnetic patterns are directly linked to the geological evolution and tectonic history of the area and we therefore here provide a short summary of the tectonostratigraphic evolution of the study area in order to set the scene for the structural interpretation of the new magnetic and modelling data. For further information and references about the geodynamic and Palaeogeographic framework of the Barents Sea we refer particularly to Gabrielsen et al. (1990, 1992), Johansen et al. (1993), Doré (1995), Gudlaugsson et al. (1998), Larssen et al. (2005), Worsley (2006), Barrère et al. (2009a).

The Barents Sea consists of complex structural elements with platform areas, basement highs and sedimentary basins (Fig. 1.3 and 9.1). It has been affected by a long and complicated tectonic history involving the entire crust, and has been affected by major continental collisions and a complex rift history that ultimately led to continental breakup in Cenozoic time (Gudlaugsson et al. 1998, Faleide et al. 1993).

9.2 Finnmark Geology

The geology of the northern Finnmark region at the southern limit of the BASAR-08 survey area is characterised mainly by Mesoproterozoic to Early Palaeozoic sedimentary successions. With the exception of rocks on the island of Magerøya, these successions are generally inferred to have been deposited along the northern and northwestern margin of the Fennoscandian Shield and later folded and thrusted during the Caledonian orogeny (Fig. 9.1). The Scandinavian Caledonides as a whole have been divided tectonostratigraphically into an Autochthon, Parautochthon, and Lower, Middle, Upper and Uppermost Allochthons (Roberts & Gee 1985). All these units, perhaps with the exception of the Uppermost Allochthon, are represented in Finnmark. The Lower and Middle Allochthons are considered to consist of shelf and continental rise units deposited along the Baltoscandian margin, which faced the Iapetus Ocean in Early Palaeozoic time (Stephens & Gee 1985, Siedlecka 1987, Roberts 2003). The Upper Allochthon in Finnmark is represented solely by the Magerøy Nappe. This is an exotic, Iapetan element which has recently been interpreted to have Laurentian affinities (Corfu et al. 2006). This may imply that the Magerøy Nappe could form a part of the Uppermost Allochthon, rather than the Upper Allochthon, but this question does not concern us directly here.

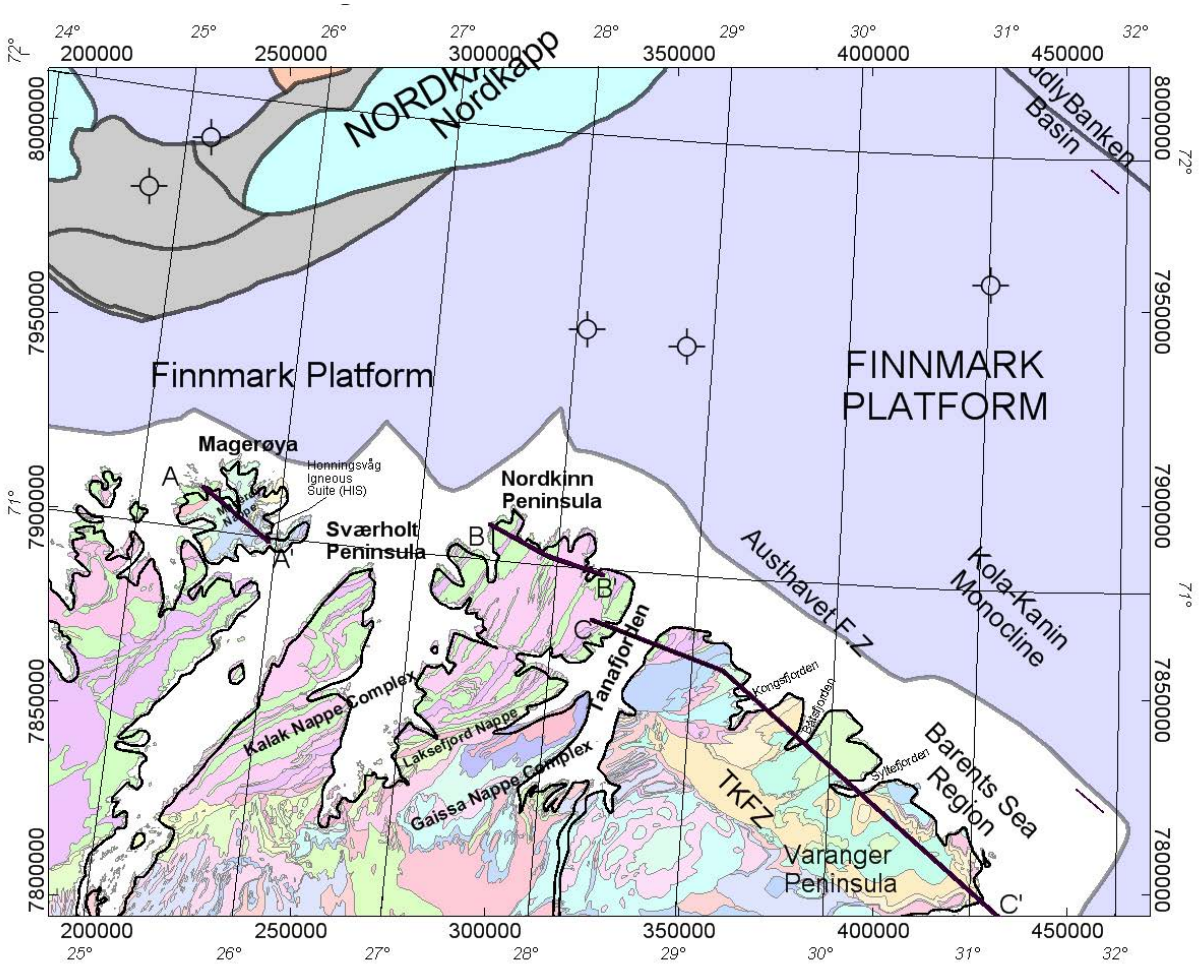

Figure 9.1 Finnmark geology from 1:500,0000 map (Siedlecka & Roberts 1996)and main structural elements of the southern Finnmark Platform with survey outline (blue) and location of geological sections in this report (black).

The Caledonian tectonostratigraphy in Finnmark (Ramsay et al. 1985, Rice et al. 1989a, Siedlecka & Roberts 1996) above the level of the Parautochthon is divided into four major nappe units (Fig. 9.1), in ascending structural order: (1) the Gaissa Nappe Complex, (2) Laksefjord Nappe Complex, (3) Kalak Nappe Complex and (4) Magerøy Nappe. The Gaissa Nappe Complex is a part of the Lower Allochthon and comprises low-grade, Neoproterozoic to Early Ordovician sedimentary rocks. The Laksefjord Nappe Complex, which includes a basal thrust sheet of Precambrian crystalline basement rocks (Rice 2001), constitutes the lowermost unit of the Middle Allochthon in the Laksefjorden area. The metasediments in the Laksefjord Nappe Complex are considered to be of Neoproterozoic age (Sundvoll & Roberts 2003). The Kalak Nappe Complex constitutes the main part of the Middle Allochthon (Roberts 1985, Rice & Frank 2003) and consists largely of Meso- to Neoproterozoic metasedimentary rocks in the BASAR-08 survey area. The Magerøy Nappe comprises metasedimentary rocks of Early Silurian age that are intruded by a Silurian, mafic-ultramafic, plutonic complex (Robins 1998, Roberts et al. 2003, Corfu et al. 2006).

In many of the nappes the metasedimentary rocks are intruded by mafic dykes of Vendian (Ediacaran) or Devonian age, and at some levels of the tectonostratigraphy there are major plutonic complexes such as the 570-560 Ma, Seiland Igneous Province (Robins 1998, Roberts et al. 2006), which lies outside and to the southwest of the survey area, and the Early Silurian, Honningsvåg Igneous Suite on Magerøya (Robins 1998, Corfu et al. 2006). On Magerøya, there are also a few mafic dykes of Carboniferous age, dated to c. 337 Ma (Lippard & Prestvik 1997, Roberts et al. 2003). The dykes occur in several different places on the island and generally lie parallel to NW-SE-trending extensional faults. Accordingly, the dykes and faults have been interpreted as associated with the Late Palaeozoic extension and rifting in the Barents Sea (Roberts et al. 1991, Lippard & Prestvik 1997).

East of Tanafjorden, in the northwestern part of Varanger Peninsula, mid greenschist-facies, turbiditic metasedimentary rocks of the Berlevåg Formation (Levell & Roberts 1977) occur within the Tanahorn Nappe, which is generally considered to form the lowest part of the Kalak Nappe Complex on this peninsula (Levell & Roberts 1977, Rice & Frank 2003, Roberts 2009). The base of the Tanahorn Nappe is a steep, NW-dipping, thrust fault that separates the Berlevåg Formation from what has been termed the Barents Sea Caledonides (Gayer et al. 1987) (Fig. 9.10c), part of the Lower Allochthon, coinciding with a drop in metamorphic grade from mid greenschist-facies to epizone (Rice et al. 1989b). Below the basal Tanahorn thrust fault, the rocks of the Lower Allochthon comprise the Løkvikfjellet Group, a 5.8 km-thick, terrigenous sandstone sequence of assumed Vendian age that unconformably overlies turbidites and deltaic rocks of the 9 km-thick, Riphean to Lower Vendian, Barents Sea Group (Siedlecka & Siedlecki 1971, Siedlecka 1987, Gernigon et al. 2007b).

The Varanger Peninsula is divided into two regions separated by the major, c. NW-SE-trending, Trollfjorden-Komagelva Fault Zone (TKFZ), which marks a clear metamorphic and structural boundary (Siedlecka & Roberts 1992) (Fig. 9.9). The Barents Sea Region (BSR) lies to the north of the TKFZ and the Tanafjorden-Varangerfjorden Region (TVR) represents the southern part of the peninsula. The TVR consists of up to 3.8 km of Late Riphean to Early Cambrian successions lying unconformably upon the Neoarchaean basement complex of the Fennoscandian Shield (Siedlecka & Roberts 1992).

The regional significance, structure and evolution of the TKFZ has been discussed in several publications (e.g., Siedlecka 1975, Rice et al. 1989a, Siedlecka & Roberts 1992, Karpuz et al. 1993a, b, 1995). The fault zone is almost parallel to the axis of the Kola-Kanin Monocline (Fig. 9.1) and extends southeastwards onto the Rybachi and Sredni peninsulas along the northern coast of the Kola Peninsula in Russia (Roberts 1995). A northwestern extension of the TKFZ into the Southwest Barents Sea has also been proposed by Gabrielsen & Færseth (1989).

Previous, integrated, remote sensing and aeromagnetic studies of the Varanger Peninsula have indicated that major, penetrative, NW-SE, NNW-SSE to NNE-SSW and NE-SW lineaments were inherited from Archaean to Palaeoproterozoic, crystalline basement features (Karpuz et al.

1993a, b, 1995). The NW-SE-trending lineament zones are particularly prominent and significant in both remote sensing and potential field datasets and, by comparison with the structural history of Kola Peninsula, probably represent the oldest weakness zones in this part of the Fennoscandian Shield (Karpuz et al. 1995). Structural investigations have suggested that many of these lineaments have been reactivated at several stages in their history from Archaean to Mesozoic time (Siedlecka & Roberts 1992, Karpuz et al. 1993b, 1995).

The metasedimentary succession of the Barents Sea Group was deposited in a basin bounded to the south by a precursor fault to the TKFZ. During most of the Neoproterozoic this structure was a major, extensional, border fault separating a platformal domain to the southwest from a basin deepening to the northeast (Siedlecka 1985, Siedlecka & Roberts 1992). In Vendian time, during the Timanian orogeny, basinal inversion along the fault led to SW-directed thrusting. Subsequently, dextral strike-slip deformation occurred along the TKFZ during the Caledonian orogeny, with later dip-slip or oblique-slip movements in the Late Palaeozoic and Mesozoic (Lippard & Roberts 1987). Several estimates of the amount of Caledonian, dextral strike-slip displacement along the TKFZ have been proposed, but an offset of just 50-100 km would seem to be most reasonable (Rice 1994). Jensen & Sørensen (1992) also considered a post-Caledonian dextral movement along the TKFZ of less than 5 km associated with a Late Palaeozoic rifting phase in the southwestern Barents Sea.

From east to west, the BSR shows a complex structural setting influenced by both the Timanian and the Caledonian orogenies. To the east, the low-grade rocks of the Barents Sea Group in the Vardø district show a fold axial trend and associated, steep cleavage oriented between NW-SE and NNW-SSE near the eastern coastline, swinging gradually towards c. N-S farther to the west (Karpuz et al. 1993a, b, Roberts 1996). In earlier interpretations a Scandian (Silurian) age was assumed for the NNW-SSE structural grain in this part of the BSR, the folds arising either through buffering in front of a rigid basement block (Roberts 1972) or as tip-folds that developed by late-Caledonian back-thrusting (Rice et al. 1989a). Comparative field studies on th Rybachi Peninsula just 50 km to the southeast in Russia provided convincing evidence that the main folds and cleavage in the eastern part of the BSR formed during the Vendian-age Timanian orogeny.

This inferred Timanian structural grain in the eastern BSR, however, is interrupted by cross-folds and a weak cleavage of ENE-WSW to NE-SW trend, interpreted by Roberts (1996) to be Caledonian in age. Only one attempt at dating the penetrative cleavage in this area has been made, providing an imprecise Rb-Sr whole-rock isochron date of 520 ± 47 Ma (Taylor & Pickering 1981). Recalculations of these analytical data have tended to favour an older, Vendian age (B.Sundvoll, pers. comm., in Roberts & Olovyanishnikov 2004).

In western Varanger Peninsula the principal structures are of Caledonian age (Roberts 1972, Karpuz et al. 1995, Rice & Frank 2003). In the BSR there is a general decrease in intensity of deformation from northwest to southeast. Structural features are mostly NE-SW to ENE-WSW

trending and represent SE-verging folds and thrusts as shown in Figures 9.9(?) and 9.10c (?). In the footwall of the Tanahorn Nappe, the Lower Allochthon is represented by the Rákkočearru thrust sheet (Roberts 2009). Similar structures occur southwest of the TKFZ in the western TVR, in the Gaissa Nappe Complex (Rice et al. 1989a, Siedlecka & Roberts 1996), where there are also indications of possible Finnmarkian, low-grade metamorphism (Sundvoll & Roberts 2003), here of post-Early Tremadoc age.

In the central parts of the BSR, there is a zone of transition where the Caledonian structures appear to die out eastwards against, but also overprint, the Timanian folds. However, a basal thrust sheet of the Lower Allochthon appears to enter the sea in Syltefjorden (D.Roberts, pers. comm. 2007). Earlier, the precise age of the Caledonian deformation in the BSR was not well constrained, but in a ^{40}Ar-^{39}Ar study Rice & Frank (2003) have shown that the pervasive cleavage in the Tanahorn Nappe and subjacent rocks is of Early to Mid Ordovician age. This was also the time of the major, dextral strike-slip movement along the TKFZ.

A feature of the northwestern and central parts of the BSR is that metadolerite dykes are profuse and locally attain swarm proportions (Roberts 1972), but no maps showing all the dykes have so far been published. Most of the mafic dykes are of Vendian age and thus pre-date the Caledonian folding (Rice et al. 2004), but there is also a later set of more sporadic dolerite dykes of Late Devonian age (Guise & Roberts 2002).

The Nordkinn Peninsula, west of Tanafjorden, also lies within the onshore area covered by the BASAR-08 survey. There, the upper greenschist-facies succession forms part of the Kalak Nappe Complex and consists of diverse metasandstones and phyllites with garnet appearing as an index mineral in western areas (Roberts & Andersen 1985). The arkosic sandstone formations on Nordkinn are invariably cross-bedded and locally enriched in heavy-mineral layers. Palaeocurrent data indicate that the source areas for the detritus were situated to the south and southeast (Roberts 2007).

9.3 Geodynamic and geological background of the Barents Sea

The tectonic and 'basement' history of the Barents Sea is strongly influenced by the Palaeoproterozoic (Karelian) orogeny, which established the stable Russian-European platform adjacent to the Archaean Fennoscandian Shield (Alsgaard 1993, Gee et al. 2008). Subsequently, a latest Neoproterozoic Timanian orogeny (previously called Baikalian) developed as a fold-and-thrust belt in the eastern part of the Barents Sea region during Ediacarian (Vendian) time. The Timanide orogen resulted from the accretion and assemblage of diverse magmatosedimentary terranes including intra-oceanic subduction systems, islands arcs and isolated micro-blocks. The main NW-SE Timanian orogenic trends are exemplified by the Kanin-Timan Ridge and the Kola-Kanin Monocline southwest of the Timan-Pechora and Barents provinces (Roberts & Siedlecka 2002, Gee & Pease 2004). In the Timan–Kanin–

Pechora region, major NW–SE structural trends also reflect the reactivation of known Palaeoproterozoic and older lineaments during the Meso- to Neoproterozoic (Mid to Late Riphean) crustal extension which characterised the Timanian margin of proto-Baltica. Field evidence of Timanian deformation in Russia, as described in detail later in this report, is also documented in the eastern part of the Varanger Peninsula (Roberts 1995, 1996, Roberts & Olovyanishnikov 2004) as noted earlier.

In the West Barents Sea area the main collisional events mostly refer to the Caledonide orogen, which is recorded in northern Norway and ascribed to two major tectonic phases:
1) the Finnmarkian (Late Cambrian to Early Ordovician) and
2) the Scandian phase (Mid-Silurian-Devonian) (Roberts 2003).
The Scandian orogen culminated approximately 400 million years ago and resulted in the consolidation of the Laurentian and Baltican plates into the Laurasian supercontinent (Fig. 9.2) after the closure of the Iapetus Ocean, a major seaway occupying a position more or less similar to the modern northeast Atlantic (Breivik et al. 1998, Roberts 2003, Gee et al. 2006). The eastern side of the Barentsian Caledonides is flanked by the remnants of the Late Neoproterozoic Timanian fold belt, recognised up to the Timan-Pechora and Novaya Zemlya regions (Gudlaugsson et al. 1998, Roberts & Siedlecka 2002).

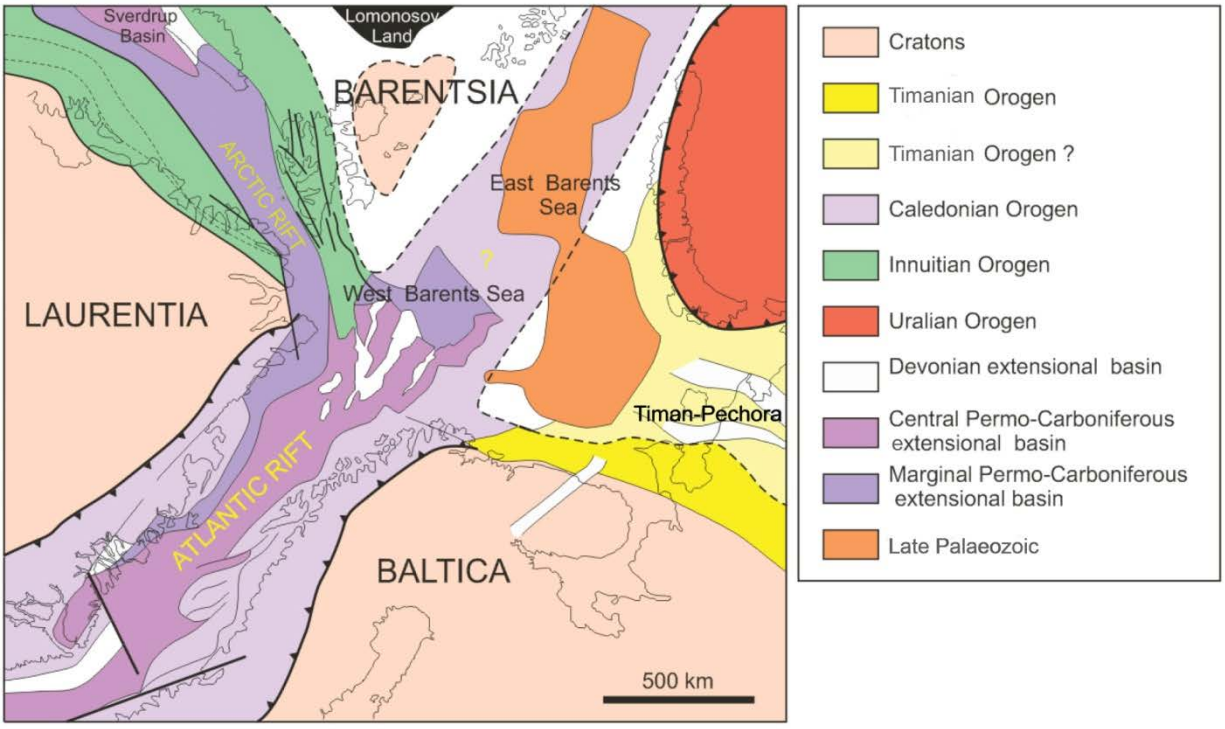

Figure 9.2 Regional palaeotectonics and main orogens and rift zones of the Barents Sea area. Reconstruction at end-Permian time (modified after Gudlaugsson et al. 1998).

The eastern part of the Barents Sea was subsequently affected by a younger collision phase between the Laurasian continent and western Siberia, which culminated in latest Permian to

earliest Triassic time. The Urals mountain chain and its northern extension, Novaya Zemlya, mark the suture zone of this closure, which appears younger to be in the latter region.
The Late Palaeozoic and Mesozoic tectonic history of the Barents Sea was mostly dominated by extensional tectonics which followed the collapse of the Caledonian and Uralian orogenic belts. Rift episodes have been documented in the Early-Middle Devonian, Carboniferous, Permian, Triassic and Late Jurassic-Early Cretaceous (Johansen et al. 1993). These events created the major rift basins on the Barents Shelf. While deposition of a continental nature took place locally during Late Palaeozoic and Early Mesozoic time in the syn- and post-orogenic collapse basins, marine sedimentation was by far the dominant factor from the Late Palaeozoic to the present day (Worsley 2006). A significant magmatic event, which affected the northern part of the Barents Sea, is also recognised in Early Cretaceous time and was most likely part of a Large Igneous Province linking Greenland, Svalbard, Franz-Joseph Land and adjacent shelf areas before the continental break-up and ocean basin formation occured (Grogan et al. 1998, Maher 2001).

The transition to a passive continental drifting between North Greenland and the Barents margin, and the initiation of the Arctic-Atlantic oceanic connection probably took place in Mid-Cenozoic (Oligocene) times. The opening of the Nansen Basin with the separation of the Lomonosov Ridge, a continental slice from the Barents margin, probably began in the latest Cretaceous. Subsequent break-up and spreading into the Norwegian Sea between Norway and Greenland is presumed to have commenced in Late Palaeocene - Early Eocene time. Later serious uplift and erosion is documented in most of the Barents Sea area. During the Late Neogene several kilometres of sedimentary rocks were probably removed from this area (Nyland et al. 1992, Faleide et al. 1996). Erosion and redeposition are thought to have been particularly intense during Plio-Pleistocene time.

9.4 Main regional trends and potential field interpretation

With the new magnetic data and the integration with gravity data (Figs. 9.3, 9.4 and 9.5) a number of structural elements could be observed and utilised for a detailed and more accurate interpretation than had been possible from the previous dataset. The high quality and resolution of the BASAR-08 magnetic data allow new insights into the main regional trends and basement settings of the study area.

Both magnetic and gravity measurements are usually sensitive to variations in the structure and composition of the crystalline basement. The comparison of main magnetic and gravity anomalies is used to discover the distribution of different basement types and basement faulting, which gives a direct indication of the geological development of the area (Fig.9.5). Most of the bodies within the basement have distinctive magnetic signatures, characterised by their anomaly magnitudes, heterogeneity and magnetic fabric. By calibrating noticeable features from gravity

and/or magnetic maps with known onshore geology these structures can be linked directly together and thus support a more detailed and reliable interpretation.

The main boundaries that delineate units of the first structural order within a basin can generally be identified from correlating aeromagnetic and gravity maps. Major basement domains are expected to have pronounced expressions in both aeromagnetic and gravity data. Figure 9.5 illustrates the correlation between gravity highs and magnetic lows. However, for the BASAR-08 survey area, such a correlation cannot be found for all the principal anomalies. The Norsel High and the NNW-SSE-striking magnetic high M-BH2 have rather good analogues in both the magnetic and the gravity maps. Also the Kola-Kanin Monocline and at least the central Nordkapp Basin show extended magnetic and gravity lows. On the other hand for the most of the area the correlation is poor and appears to be accidental. One possible explanation, as pointed out earlier, can be a less well developed magnetic sediment-basement contrast, but a c. 5-10 km thick succession of sedimentary rocks could also blur basement signatures in the magnetic data.

Nevertheless, a comparison of the gravity and magnetic data leads to an enhanced interpretation of the regional geological setting in the study area. The Bouguer gravity highlights the locations and extensions of the sedimentary basins like the Nordkapp, Ottar and Maud Basins and assists in explaining several linear features and structural changes observed in the magnetic data. Furthermore, the opposite conclusion based on our assumption of a blured magnetic basement signature, can imply the presence of uplifted and possibly rotated basement blocks on the Norsel High and the magnetic high M-BH5.

Another interesting feature to point out is that the magnetic signature can often be associated with both deep and shallow structures, as suggested by the combination of seismic observations with the potential field data (Figs. 10.5, 10.6 and 10.8). Since the earliest basement configuration and evolution is probably the first-order factor for subsequent fault reactivation and subsidence patterns, it appears that several magnetic domains are associated with more than one structural level.

Previous studies have shown that subcropping tilted sedimentary strata or folded sedimentary units have generally low magnetic susceptibilities but might also generate measurable magnetic anomalies (Gibson & Millegan 1998). Faults, carbonate units or other irregularities in the sedimentary strata do influence mainly the short-wavelength magnetic signature and can be distinguished from basement structures by appropriate filter techniques. In our approach we extracted and interpreted such small-wavelength attributes by mostly using the tilt derivative (TDR) (Verduzco et al. 2004) and a 30 km high-pass filter.

The various magnetic and gravity attribute maps interpreted in this report (Fig. 9.3, 9.4 and 9.5) describe the features and patterns of the basement blocks relative to their surroundings. The structural pattern of the basement as revealed from magnetic interpretations combined with

gravity was characterised by a hierarchy of structural elements involving 1) large structural zones, 2) tectonic domains and 3) sub-domains and internal magnetic lineaments (Fig. 9.6, 9.7 and 9.8). For each domain there are also additional extended features that overprint some of these structures and are potentially related to the deposition of basin sediments and salt tectonics.

Caledonian trends clearly dominate the basement architecture in the survey area, but towards the east and especially in the southeast, Timanian trends are more and more noticeable and are most likely to have influenced the rift and basin configuration particularly in the central Nordkapp Basin. Old inherited structures usually appear to be the first-order crustal parameters that control the rift or basin architecture (e.g. Doré et al. 1997, Roberts & Lippard 2005). Caledonian influences are usually recognised by the N-S structural grain of the western Barents margin and Svalbard, and the NE-SW grain of the southwestern Barents Sea and Finnmark (e.g. Doré 1991, Doré 1995, Fichler et al. 1997 Roberts & Lippard 2005,).

The BASAR-08 magnetic data confirm this general interpretation, showing these trends quite clearly (Fig. 9.6). Prominent, almost N–S-trending and eastward-curved lineaments are interpreted as different settings or stages in a most likely Caledonian basement and reveal a clear bisection of the survey area (Bjarmeland and Finnmark platforms) with the Norsel High, the Nordkapp Basin and a distinct fault complex in between. The penultimate identified curved lineament to the east on the Finnmark Platform can even be linked directly to the base of the Middle Allochthon (Tanahorn Nappe) in northwestern Varanger Peninsula. WNW-ESE-striking, high-amplitude magnetic lineaments, however, cross-cut and superpose signatures from deeper origins and complicate the tracing of more of these N-S lineaments across the Austhavet Fault Zone. Nevertheless, the strike of the geological units on the Nordkinn and Sværholt peninsulas are clearly parallel to the lineaments observed and interpreted offshore.

From a comparison with the Bouguer gravity, we notice a connection of the distribution of the basins in the area with the disruption of the N-S-trending lineaments. Not only in the Nordkapp Basin but also in the Ottar Basin and potentially in the Maud Basin there are similar disturbances of the basement signatures, which are in line with the seismically proven, post-Caledonian, rifting phases and basin development in the Barents Sea (e.g. Faleide et al. 1993, Breivik et al. 1995, Gudlaugsson et al. 1998).

Two systems of principal and probably deep faults could be observed from the new magnetic dataset (Fig. 9.6). The first one is north of the Nordkapp Basin striking NW-SE, and located at the northern flank and within the Ottar Basin. The fault to the south of the basin separates the Swaen Graben from the Norvarg Dome and runs into the Norsel High to the southwest. It is located at the southern edge of a gravity minimum (G-BL3) and with regard to the Ottar Basin configuration defined by Gudlaugsson (1994) and Breivik et al. (1995) it might possibly coincide with the edge of an intra-basin high but not with the actual boundary of the basin.

Two lineaments are observed at the northern rim of the Ottar basin, and might link to two major rifting phases and a gently dipping basin flank. There is weak evidence for a south-westward continuation of the southerly located lineament into the central Nordkapp Basin which, in fact, partly coincides with an intra-basin fault observed on seismics.The second system coincides with the mapped fault complex south of the Nordkapp Basin (Måsøy and Thor Iversen fault complexes). The main feature of this complex is a distinct linear structure that is obvious from the 30 km high-pass filter and striks NE-SW across the entire survey area (Fig. 9.6b). The structure is disturbed by a NNW-SSE-oriented, dextral strike-slip fault in the central part of the fault zone just south of the narrow part of the Nordkapp Basin, and provides evidence of an additional NNW-SSE stress component in the eastern part of the survey area. The western part of this same lineament transects the southern Nordkapp Basin and probably marks the northern flank of the Mårøy Fault Complex, whereas to the east the width of the fault complex is less well defined. Here, there are no additional sharp linear features to be seen except for the lineament and the coinciding Thor Iversen Fault Complex. The N-S-trending curved characteristics of the magnetic data fade out towards the lineament instead of ending abruptly as they do further west. This, however, might indicate that it is either a less distinct fault system or a superposition of magnetic signatures from other origins in this particular area.

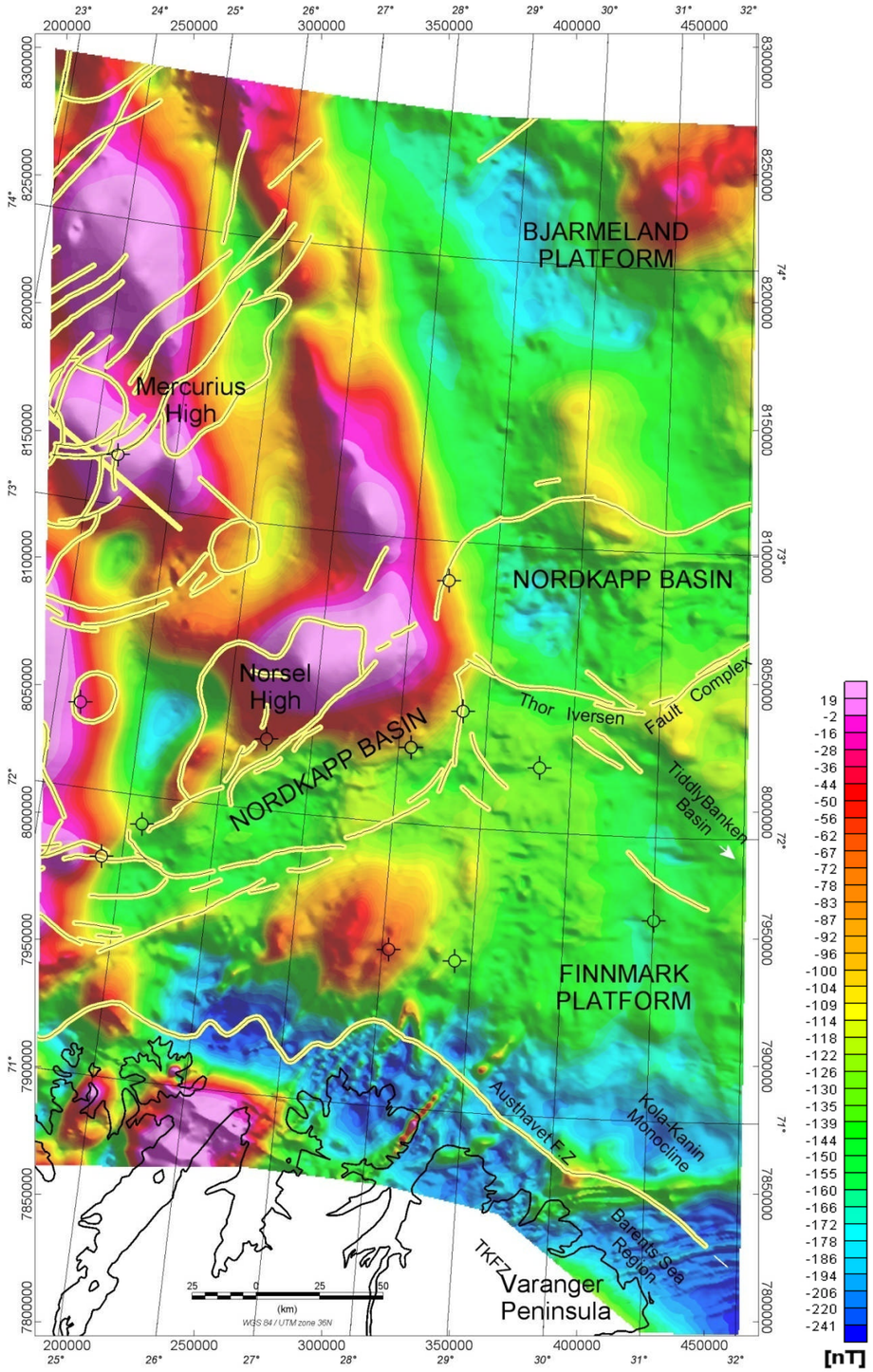

a)

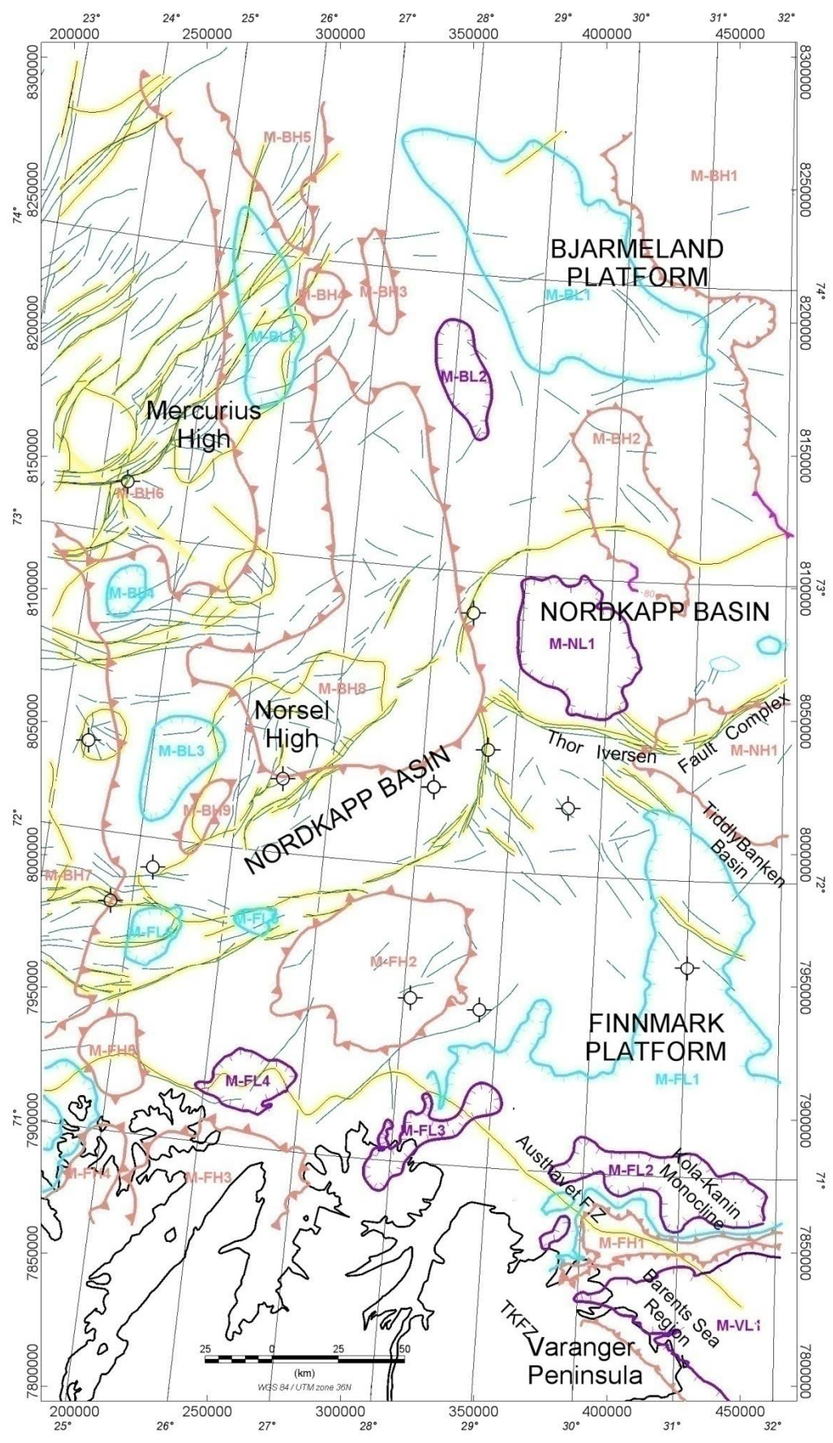

b)

Figure 9.3 Magnetic total field (left) and outline of the main anomalies (right). Black and yellow lines underline the main structural features of the area (Gabrielsen et al. 1990). Grey lines represent the faults mapped at base Cretaceous level (Gabrielsen et al. 1990).

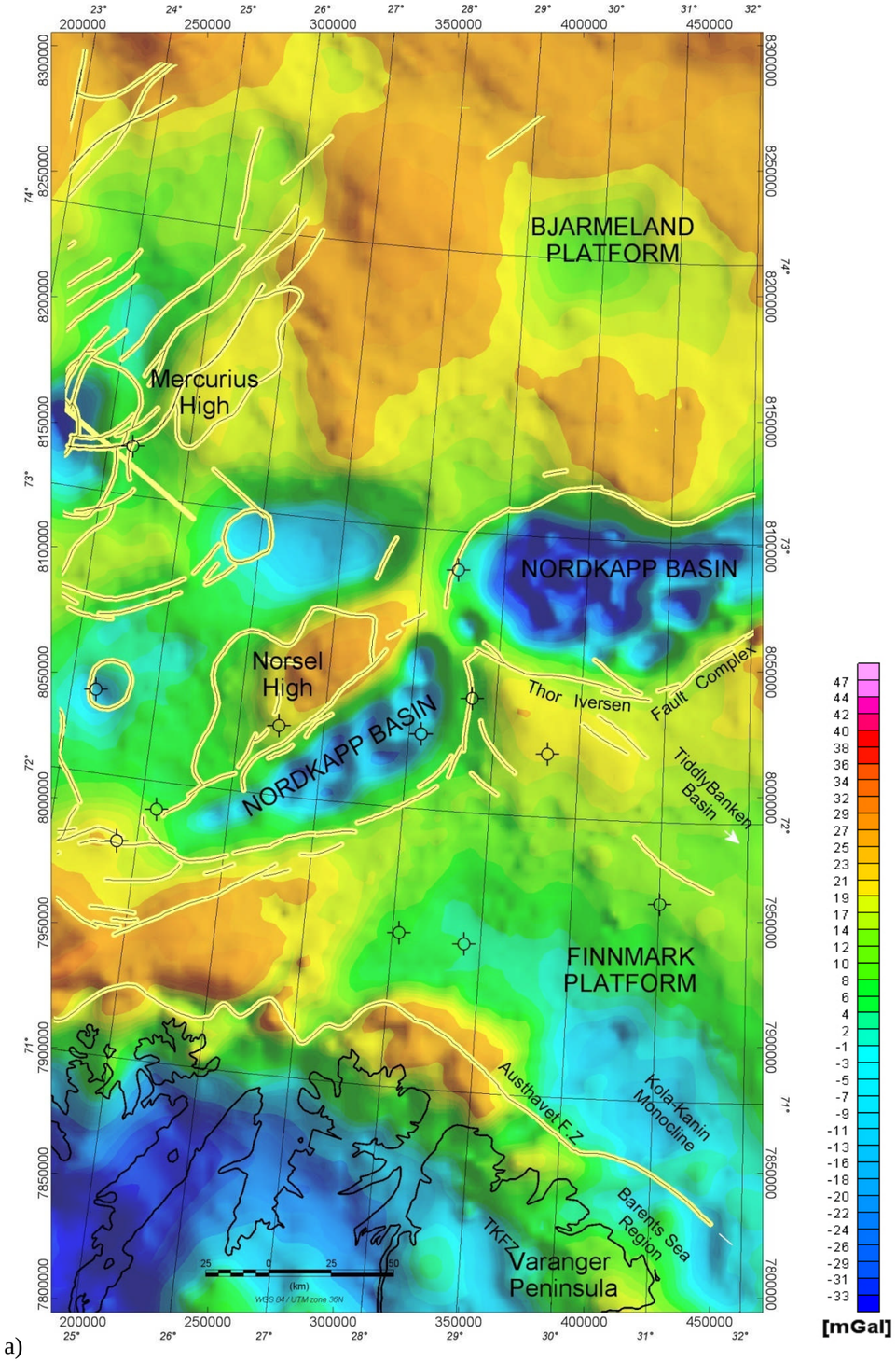

a)

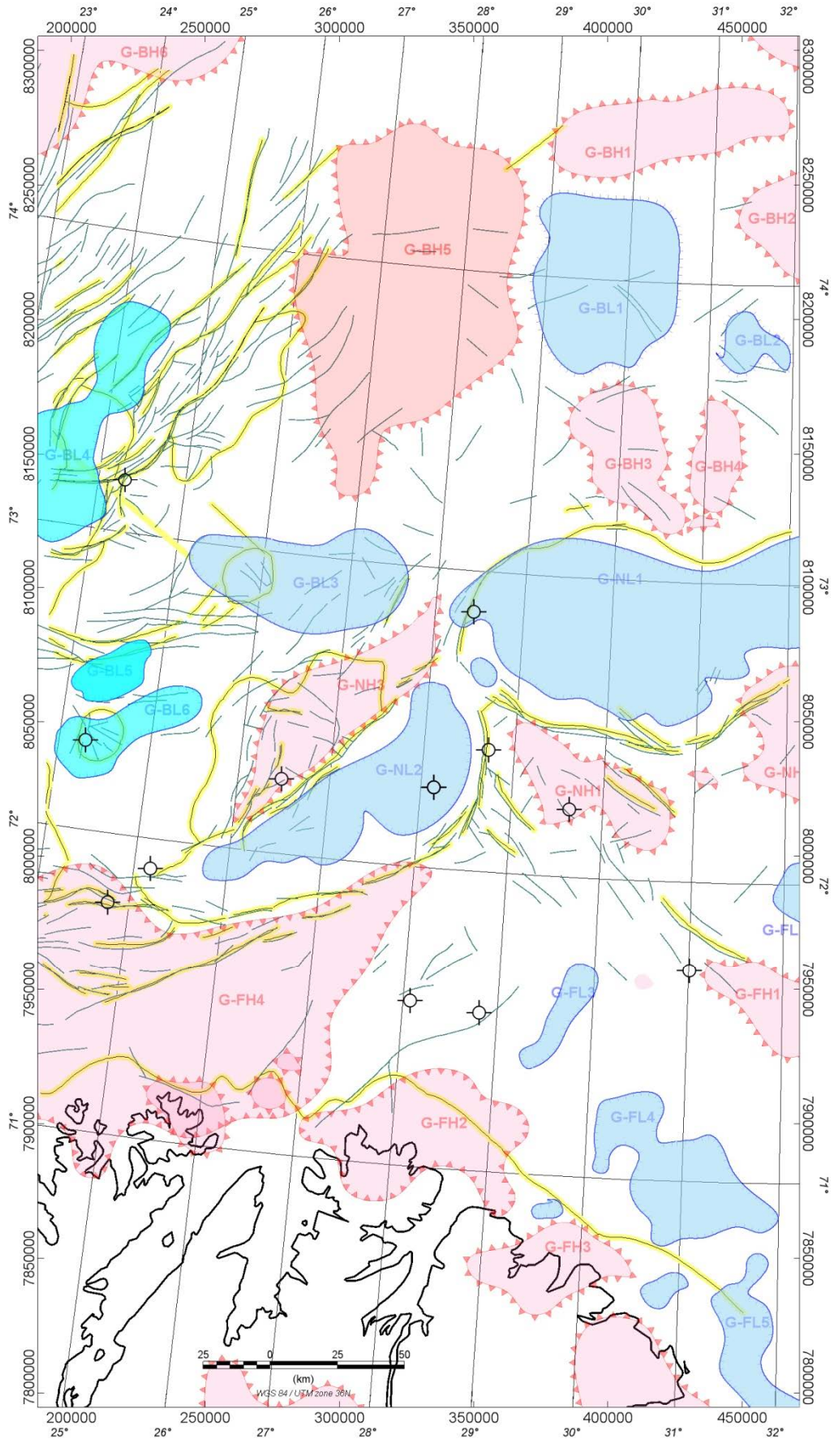

b)

Figure 9.4 Bouguer anomalies along the BASAR-08 survey area and interpretation of the main anomaly highs and lows. Black and yellow lines underline the main structural features of the area (Gabrielsen et al. 1990). Grey lines represent the faults mapped at base Cretaceous level (Gabrielsen et al. 1990).

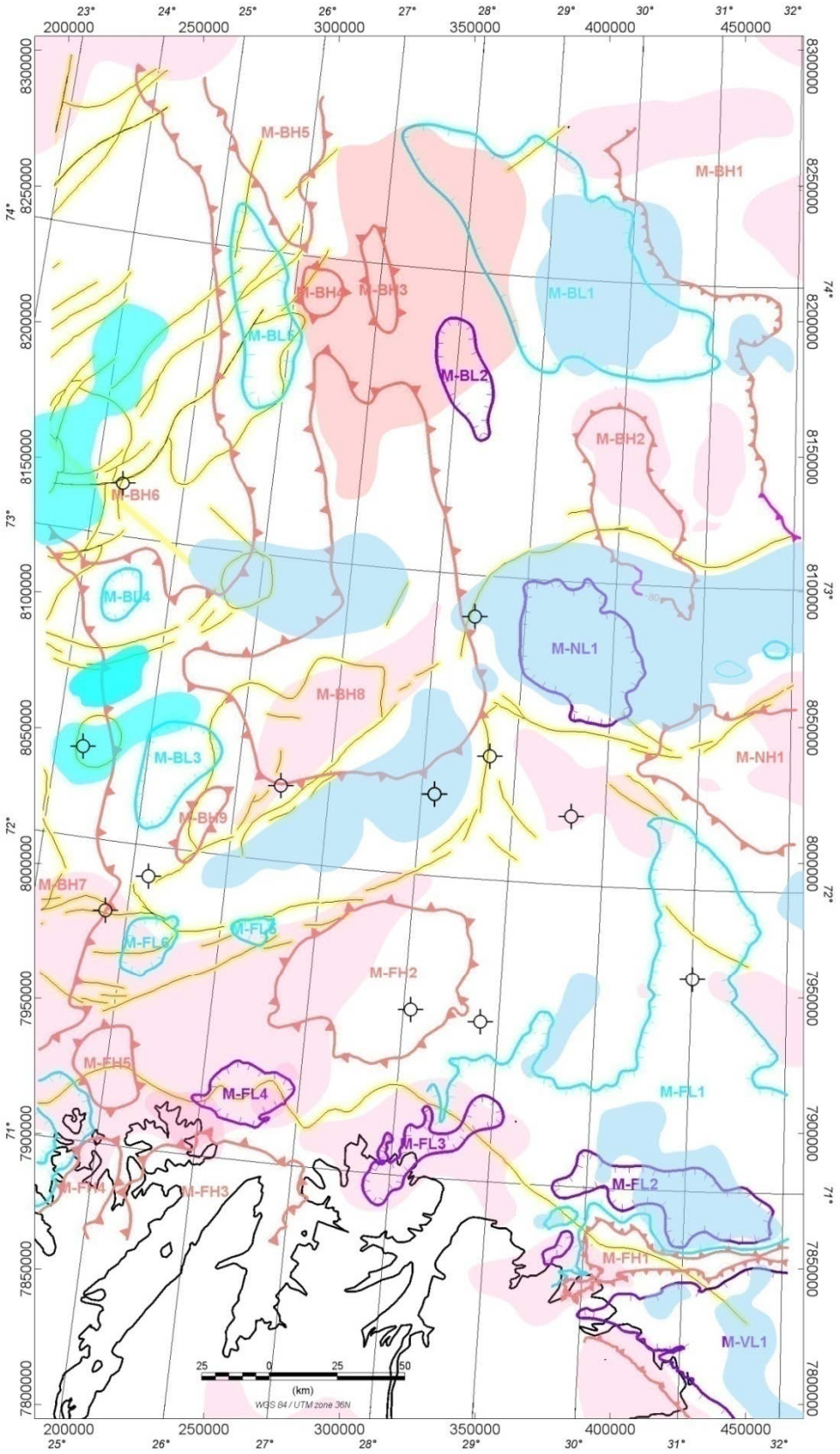

Figure 9.5 Interpretation of the main anomaly highs and lows from Bouguer (filled) and TMI (outlines) maps. Black and yellow lines underline the main structural features of the area (Gabrielsen et al. 1990). Grey lines represent the faults mapped at base Cretaceous level (Gabrielsen et al. 1990).

Together with the distribution of the basins (Fig. 9.6b) and the correlations with the Bouguer gravity (Fig. 9.4), the first-order lineaments already provide new insights into the basement structure and different basement domains within the study area (Fig. 9.8c).

In addition we have mapped second-order structures using TILT derivatives and high-pass frequency filtering. Such features are likely to be of shallower origin, deriving from somewhere within the sedimentary succession, and in fact there are a number of obvious similarities between the existing BCU map (Gabrielsen et al. 1990) and observable features from the high-pass filtering (Figs. 9.6c and 9.7b). We used the new magnetic dataset to supplement the existing BCU map, even though the origin is not compulsively the BCU, but intrasedimentary. A comprehensive overview of the observable short wavelength lineaments can be interpreted and directly linked with diverse structures within the sedimentary successions. The resulting map expresses the different structural development of the Bjarmeland and Finnmark platforms with opposed strike orientations, a feature probably deriving from the time of the initial rifting phase in the Late Palaeozoic. Nevertheless, both platforms also show some lineaments orientated along the principal strike of its neighbours, which gradually decrease from west to east on the Finnmark Platform and from east to west on the Bjarmeland Platform. A detailed description and interpretation for each area is presented below.
While the observed structures on the platforms are probably associated with reactivation along Early Palaeozoic and Precambrian basement structures, the lineaments within the Nordkapp Basin are different and reflect rather the different rifting phases in Mesozoic and Ceneozoic times. We should point out that the salt signature made it difficult to establish a clear differentiation between salt-related features and faults. Nevertheless, based on the mapped lineaments there is strong evidence that the southern and central parts of the Nordkapp Basin show different developments.

9.4.1 The Bjarmeland Platform

The Bjarmeland Platform includes the extensive platformal areas east of the Loppa High and north of the Nordkapp Basin. The platform was established in the Permian but subsequent uplift and erosion tilted the Palaeozoic and Mesozoic sequences southwards, with unconsolidated Quaternary sediments overlying successively older rocks towards the north. Five exploration wells have been drilled on the Bjarmeland Platform, exclusively in the southern part. Two of the wells were drilled into the transitional area between the platform and the Nordkapp and Hammerfest Basins. Both wells reached the Upper Palaeozoic succession (7226/11-1 and 7124/3-1), and the former demonstrated a mid-Carboniferous onlap of the basement (Larssen et al. 2005).

The central part of the Bjarmeland Platform is dominated by the magnetic high centred on the Norsel High (Fig.9.3b) and its NNW-SSE-striking tail-like structure (M-BH8) that extends all the way to the north of the survey area with extended magnetic lows to the west and east (M-BL2 and M-BL5). A marked magnetic high (M-BH6, M-BH7) appears in the westernmost part

of the platform with smaller but noticeably round magnetic minima southwards between the Norsel High and the easternmost extension of the Loppa High (M-BL3 and M-BL4). The area to the east is characterised by regional NNW-SSE-striking (M-BH2 and M-BH1) anomaly highs. The structures reflect the predominantly Caledonian character of the basement of the Bjarmeland Platform. Nevertheless, a noticeable change in the amplitude is visible east of the Norsel High and M-BH8, and from Euler deconvolution deep Euler solutions indicate that a major structural change is probably present in the basement at this location. The magnetic data to the east appear smoother with smaller anomalies and gentler slopes. Filtered magnetic data reveal the absence of the characteristic N-S-oriented and curved lineaments in this part of the platform. From wavelength filtering and derivatives, the magnetic field shows mainly second-order NE-SW-oriented lineaments, which are prominent in the western Bjarmeland Platform and are of Caledonian origin. To the east the NE-SW trend progressively interferes with the NW-SE-striking features (Figs. 9.7c and 9.8a). These magnetic patterns could be inherited from the Timanian structural grain or even date back to Archaean time, as recognised mainly along the Kola-Kanin Monocline structure, and probably extend as far as to the Timan-Pechora Basin on the Russian side. The NW-SE regional and crustal trends are particularly prominent in the area of the Finnmark Platform but are also seen on the Bjarmeland Platform and have probably been reactivated during the different rifting events.

The Norsel High and the broad NNW-SSE positive anomaly (M-BH2) are prominent magnetic highs on the platform and coincide with gravity highs. This confidence usually reflects old tectonic features most likely associated with basement units. Indeed, M-BH2 could fit with high-amplitude seismic reflections observed on the northern flank of the Nordkapp Basin, but the seismic imaging is still too poor to pursue this idea at the present stage. As NE-SW seismic lines were not available to us during this project, we could not execute an accurate structural investigation. For the Norsel High, the basement was drilled at c. 5150 m, showing what was interpreted to be a 'Pre-Devonian Basement'. Basement rock samples from the Finnmark Platform generally show only rather low magnetisation of the interfered Caledonian basement, which raises the question as to whether the two highs in the survey area represent basement blocks of Precambrian age or at least a partial Precambrian basement in an uplifted position. Precambrian basement usually shows higher magnetisation and could therefore explain the high amplitude of the magnetic anomalies. Simple inversion results from 3D modelling (Ch. 11) support this idea, but the 2D modelling (Ch. 10) and actually also from a comparison with the gravity reveals, however, a more complex picture involving intruded and highly magnetic mafic rocks at a shallow level. This would seem to better explain the gravity and magnetic observations, and in particular the significantly different shape of the Norsel High anomaly on both datasets.

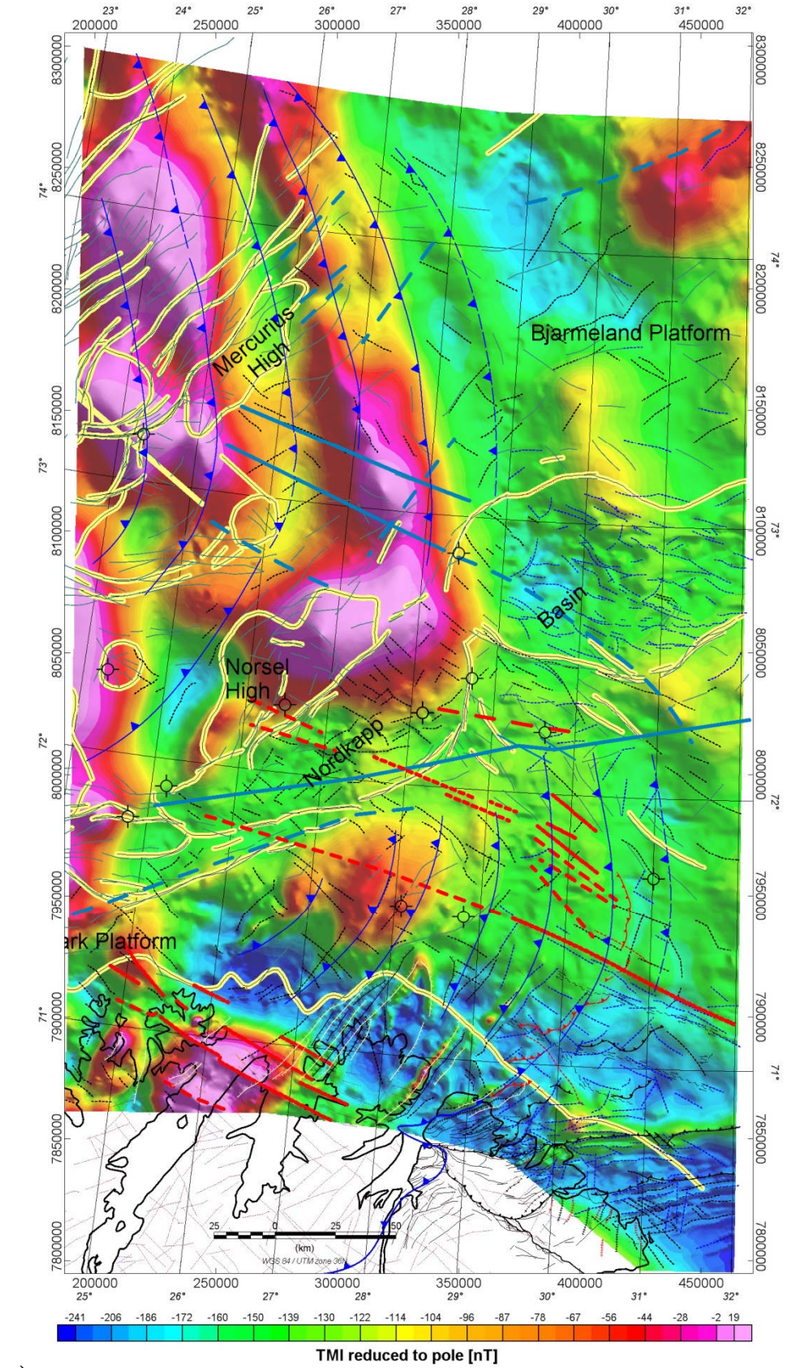

a)

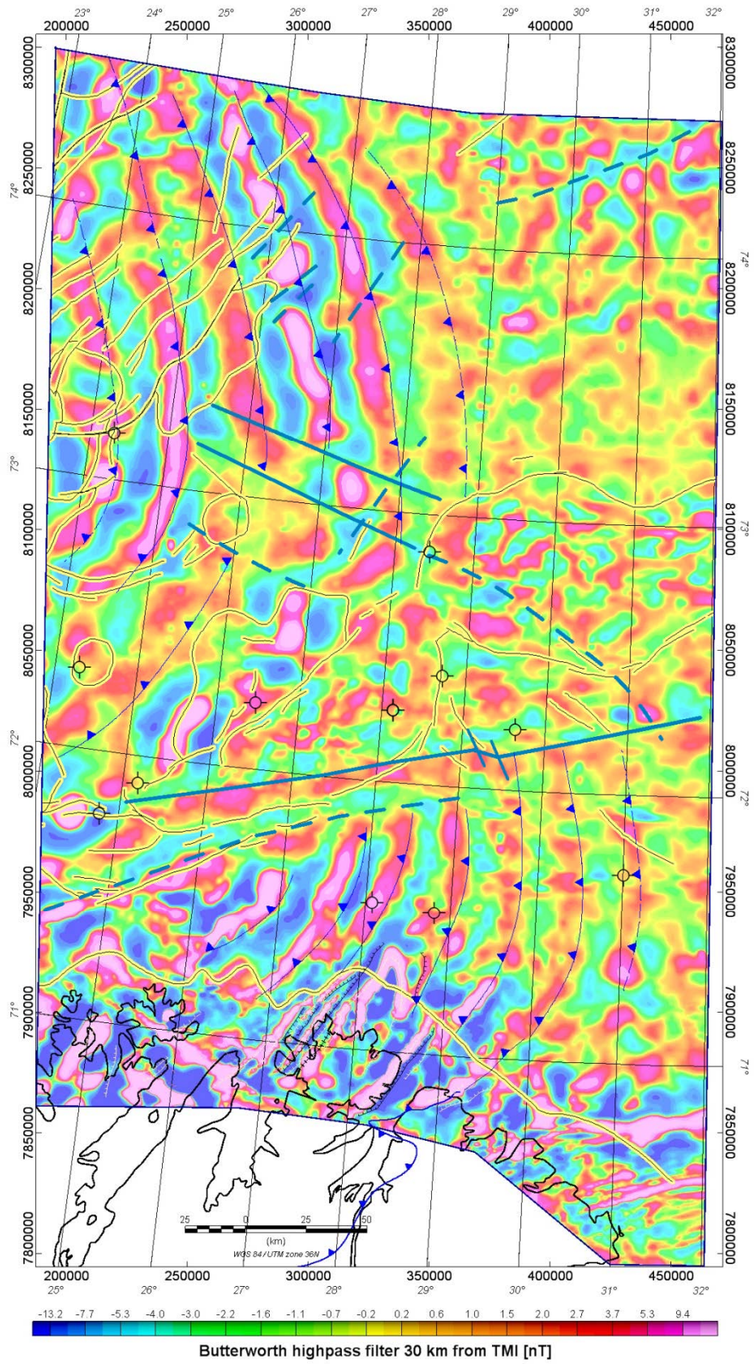

b)

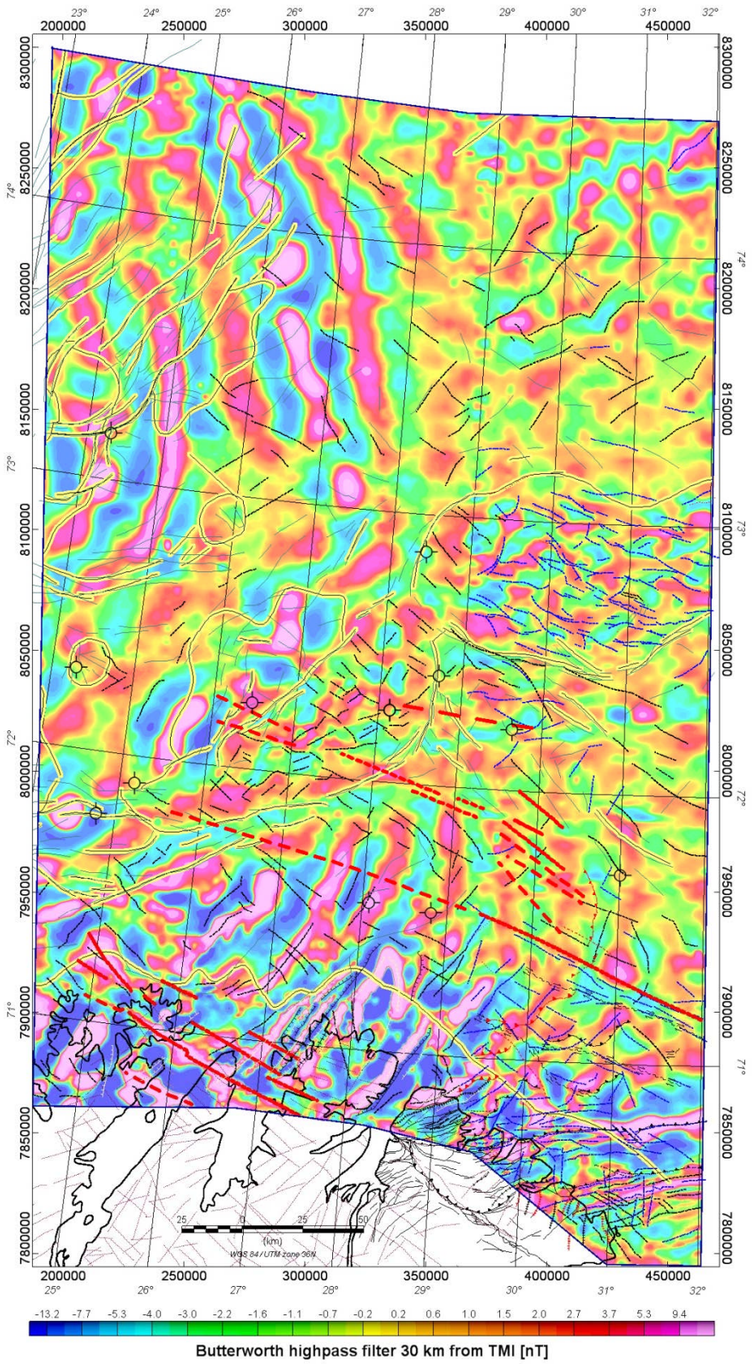

c)

Figure 9.6 a) TMI grid with complete structural interpretation, b) 30 km high-pass filter with first-order tectonic elements and c) 30 km high-pass with complete structural interpretation. Blue curved lines are observed lineaments from the magnetic map and are most likely associated with Caledonian nappes, dark blue lines are major faults. Red lines show fault-related lineaments probably associated with high-magnetic material such as dykes (see text). Black and yellow lines underline the main structural features of the area (Gabrielsen et al. 1990). Grey lines represent the faults mapped at base Cretaceous level (Gabrielsen et al. 1990), black (BASAR-08) and blue (BAS-06) dotted lines represent second class lineaments with a more shallow origin, based on magnetic interpretation.

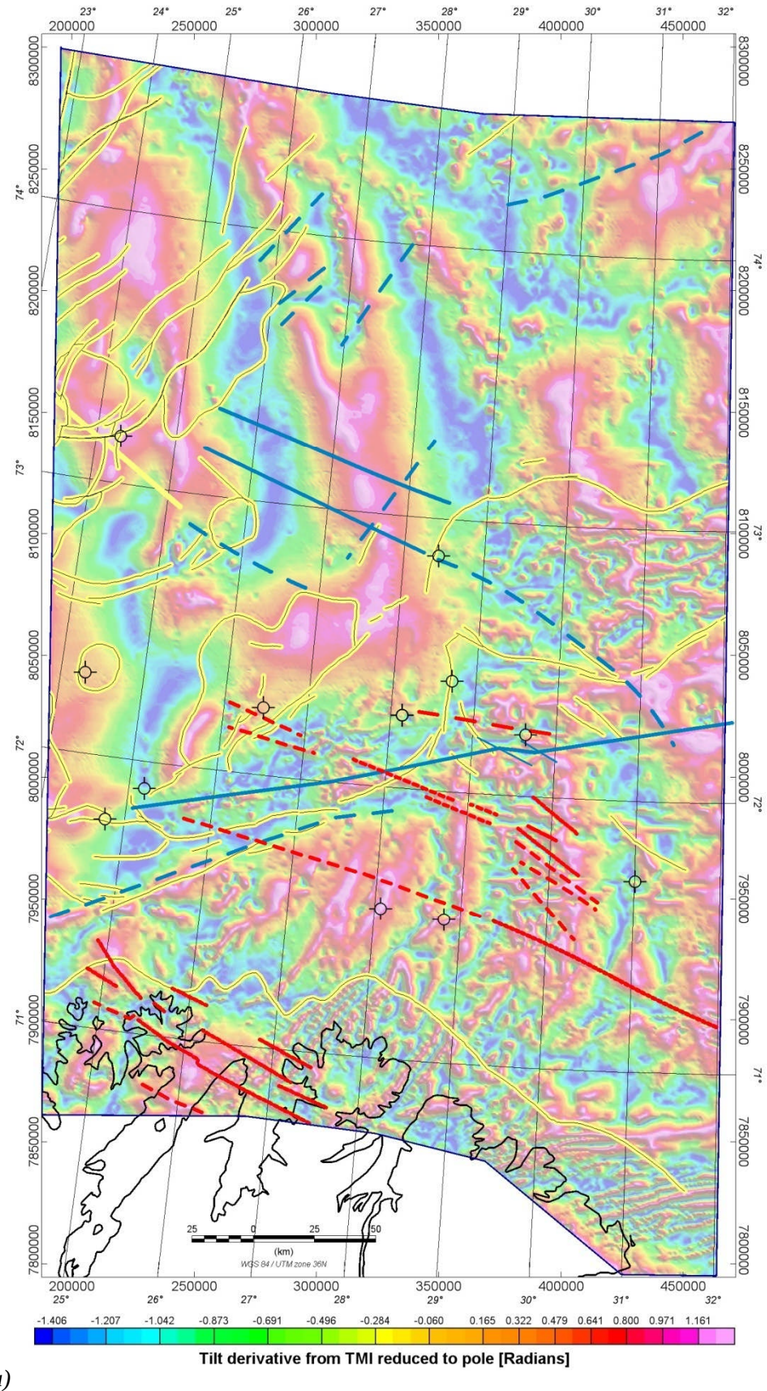

a)

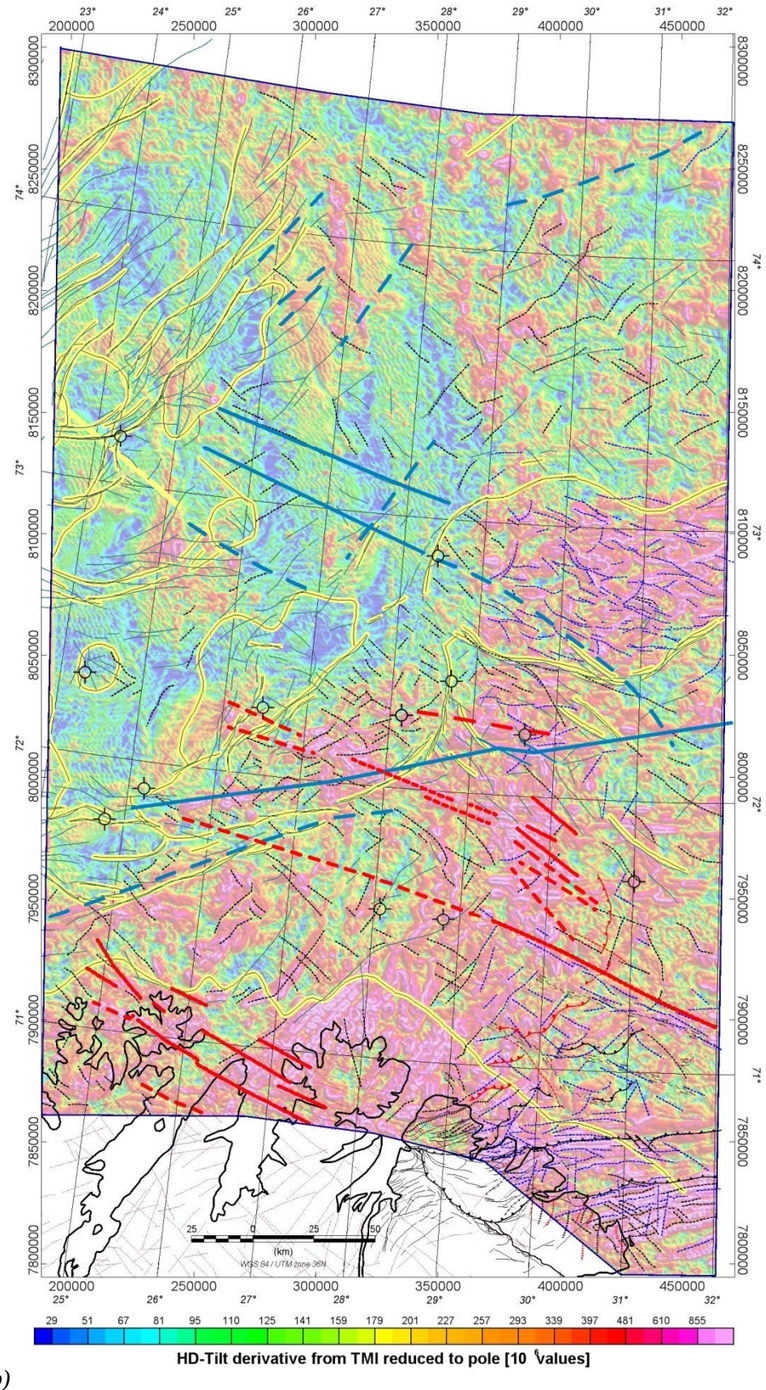

b)

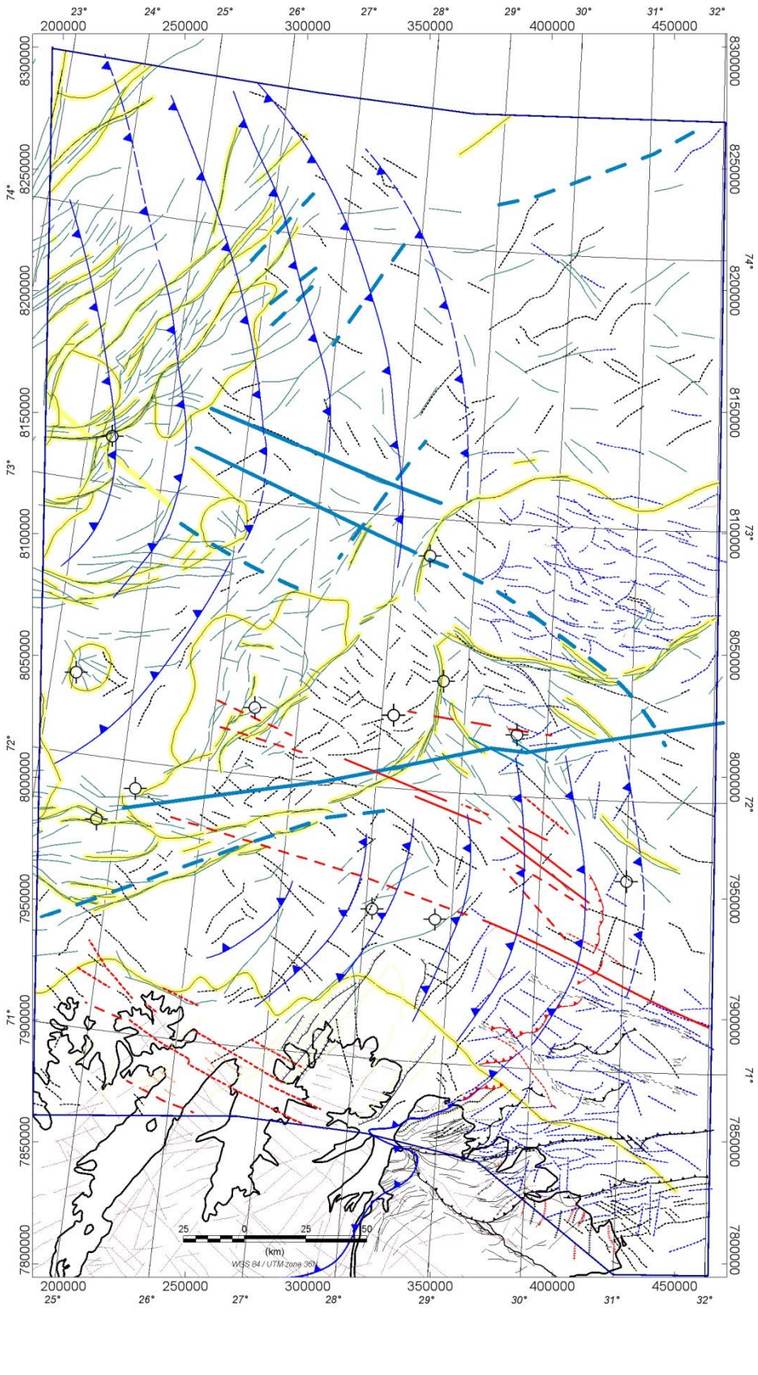

c)

Figure 9.7 a) TILT derivative from TMI grid with principal possibly intruded faults, b) HD-TILT from TMI with complete structural interpretation and c) the complete structural interpretation. Blue curved lines are observed lineaments from the magnetic map and are most likely associated with Caledonian nappes, dark blue lines are major faults. Red lines show fault-related lineaments probably associated with high-magnetic material such as dykes (see text). Black and yellow lines underline the main structural features of the area (Gabrielsen et al. 1990). Grey lines represent the faults mapped at base Cretaceous level (Gabrielsen et al. 1990), black (BASAR-08) and blue (BAS-06) dashed lines represent second-order lineaments with a more shallow origin based on magnetic interpretation.

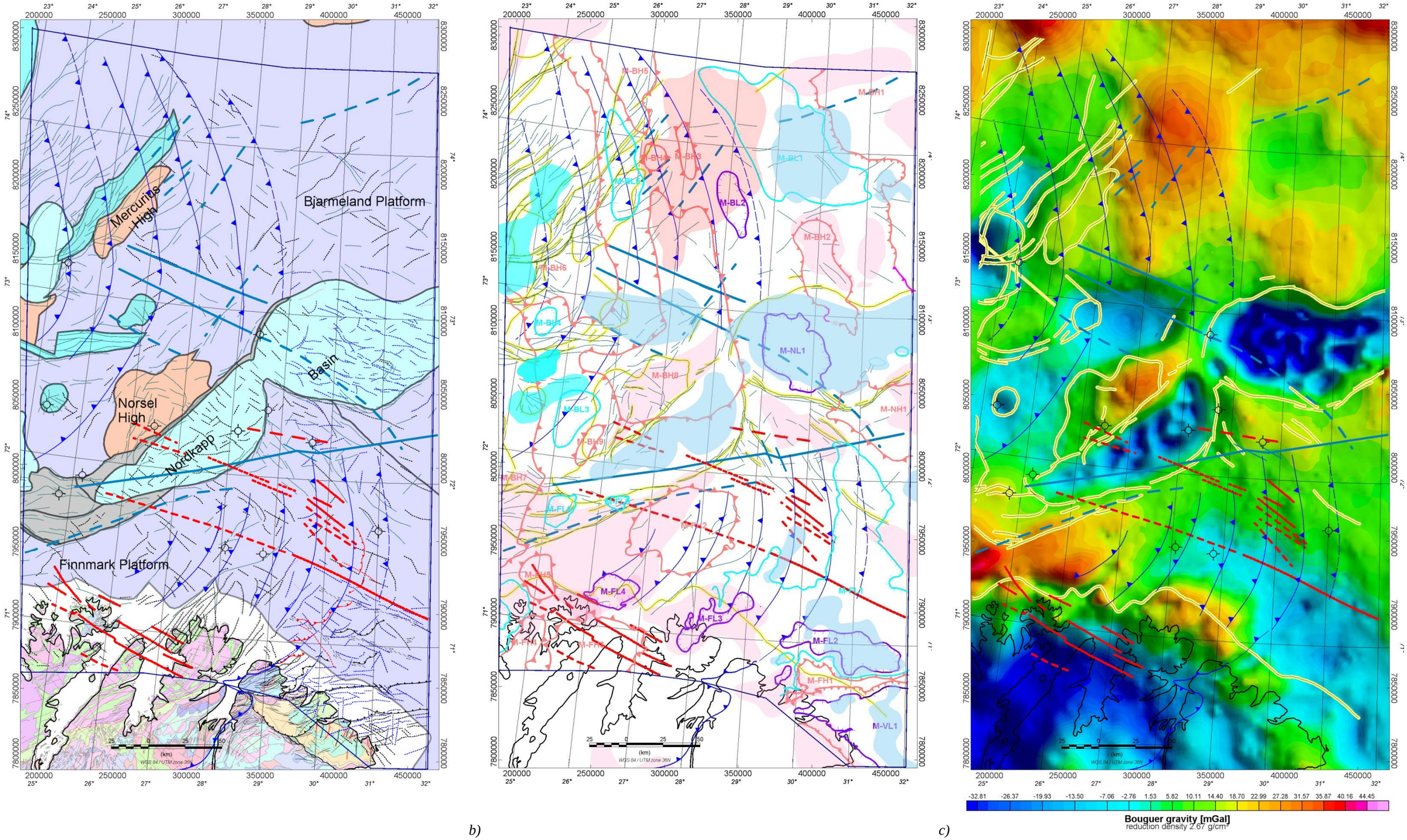

a) *b)* *c)*

Figure 9.8 a) Structural elements with complete structural interpretation, b) Interpretation of the main anomaly highs and lows from Bouguer (filled) and TMI (outlines) maps with complete structural interpretation and c) Bouguer gravity with first-order tectonic elements and possibly intruded faults. Blue curved lines are observed lineaments from the magnetic map and are most likely associated with Caledonian nappes, dark blue are major faults. Red lines show fault-related lineaments probably associated with high-magnetic material such as dykes (see texte). Black and yellow lines underline the main structural features of the area (Gabrielsen et al. 1990). Grey lines represent the faults mapped at base Cretaceous level (Gabrielsen et al. 1990), black (BASAR-08) and blue (BAS-06) dashed lines represent second-order lineaments with a more shallow origin, based on magnetic interpretation.

9.4.2 The Nordkapp Basin and surrounding margins

Both the SNAS-06 and the BAS-06 surveys have already provided a new, reliable and almost complete magnetic coverage of the Nordkapp Basin. With the reprocessed and merged dataset from BAS-06 and BASAR-08, a comprehensive overview of the magnetic settings in the Nordkapp Basin can now be presented, covering the entire Nordkapp Basin in the undisputed Norwegian part of the Barents Sea.

A comparison of the old and new magnetic data reveals quite a number of new details such as salt structures and fault systems (Fig. 9.9). Furthermore, the outline and the shape of the anomalies in the basin give new and important evidence for the depth-to-basement structure, and the presence of possible sub-basins and intra-basin highs, which results in a more accurate and sophisticated interpretation of the Nordkapp Basin and its development. New trends are now observed from the magnetic surveys and suggest a more complex crustal and basin architecture of the Nordkapp Basin, which is clearly divided into sub-magnetic segments.

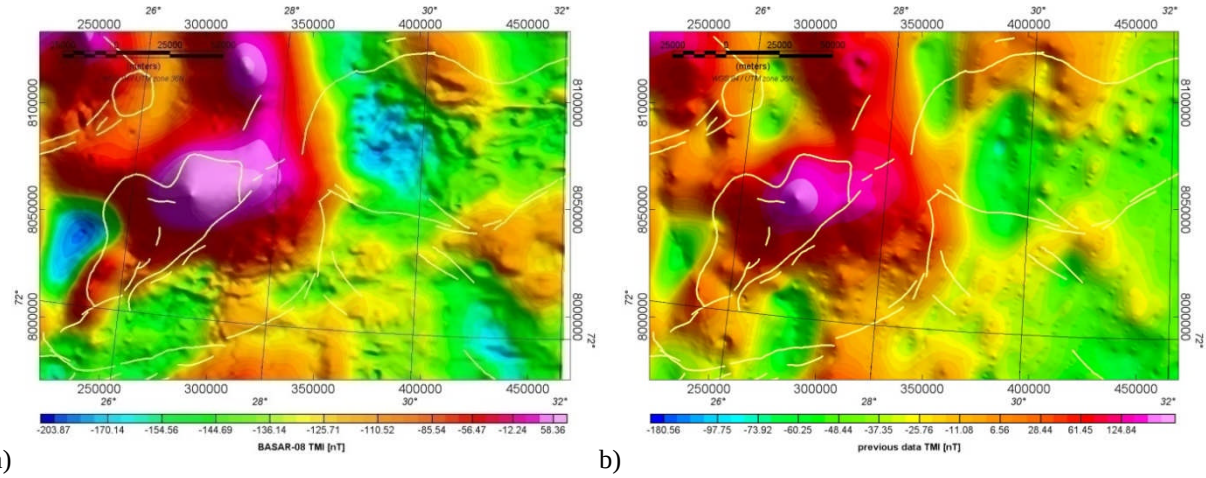

a) b)

Figure 9.9 Comparison between (a) the new and (b) the vintage magnetic data for the Nordkapp Basin. The BASAR-08 data (left) have a significantly higher resolution, showing various features such as salt structures and faults in much more details.

The Nordkapp Basin is a fault-controlled graben located along the NE-SW-trending rift system that extends eastwards from the Hammerfest Basin to the disputed area between Russia and Norway (Gabrielsen et al. 1990, Nilsen et al. 1995). The basin was initiated during Late Palaeozoic extension and, like the Russian basins, constituted a major sink for Triassic sedimentary deposition (Roberts & Lippard 2005). The lateral extension of the basin is well constrained by the gravity data (Figs. 9.4a). The SVD of the new magnetic data highlights the positions of the shallow salt structures and also allows an estimation of the basin outline, whereas especially in the southern part of the Nordkapp Basin long-wavelength effects from the Norsel High conceal the real basin extension (Figs. 7.2 and 9.3a). The main regional orientation of the Nordkapp Basin, also expressed by the Måsøy and Thor Iversen fault complexes, is

mostly N°100-110 to N°70-80 oriented and coincides with local low- to medium-wavelength magnetic trends (Figs. 9.6c and 9.7).

The Thor Iversen Fault Complex is a prolongation of the Troms-Finnmark and Måsøy fault complexes and represents a regional deformation zone in the Barents Sea. These principal fault trends were characterised by peak faulting activity at specific times, and many can be linked fairly confidently with known faults on the Finnmark mainland (Gabrielsen et al. 1992, Jensen & Sørensen 1992). The NE-SW offshore fault trend is known to have been operative in Devonian-Carboniferous time exploiting the Caledonian structural heritage (Faleide et al. 1984, Gabrielsen et al. 1992, Bugge et al. 1995). Basin-bordering movements continued through the Permo-Triassic interval and appear to have extended into the Late Mesozoic. Many such NE-SW-trending faults can be traced onshore, in Finnmark (Gabrielsen 1984, Lippard & Roberts 1987). The existing faults in Finnmark, especially those in western areas, were subjected to successive reactivations in Permo-Triassic and notably in Jurassic-Late Cretaceous (Roberts & Lippard 2005).

From the new dataset, some evidence was found for a NE-SW structural trend both north and south of the Thor Iversen Fault Complex, possibly indicating a prolongation of one of the regional trends which define the Tiddlybanken Basin and West Kola Graben described by Ivanova (2001). A feature of some dispute is the narrow part of the Nordkapp Basin and its geotectonic significance. A strike-slip pattern along the NE-SW-striking lineament and the irregular and slightly rotated magnetic lineaments possibly suggest the presence of an almost N-S-trending shear zone, which might then be related to the reactivation and superposition of old Caledonian and Timanian patterns or a rifting event in the central Nordkapp Basin, partly decoupled from the southern basin (Gernigon et al. 2007b).

The Nordkapp Basin is bounded in the north by the Bjarmeland Platform and in the south by the Finnmark Platform, and is divided into a northeastern and a southwestern segment. Caledonian basement structures, detected in the new magnetic data, are disrupted in the vicinity of the basin, but at least in the western part of the survey area can be traced both north and south of the basin. The assumed sedimentary thickness of c. 10-16 km allows only an ambiguous interpretation of this feature. Either the thick pile of sedimentary rocks masks the magnetic basement signature or the basement was at least strongly deformed during the rifting process. In fact from 2D modelling an involvement of the Caledonian basement in the rifting process is evident with different stages from thinning (Fig. 10.8) to break up (Fig.10.5).
Both the southern and the central part of the Nordkapp Basin are characterised by two regional gravity lows (G-NL1 and G-NL2) surrounded by broad gravity highs (G-BH3, G-BH4, G-NH1, G-NH2, G-NH3and G-FH4). The magnetics, however, do not reflect the presence of such a dominant sedimentary basin, but the western part of the central Nordkapp Basin does show a magnetic domain (M-NL1), flanked to the northeast and southeast by two magnetic highs (M-BH2 and M-NH1), which both extend into the sedimentary basin. Even though the origin of these highs remains unclear, as pointed out earlier we consider them as an old basement

structure of probable Precambrian age. Before rifting was iniciated, this was likely one NW-SE-striking unit perhaps associated with old Timanian trends. From the TDR of the new magnetic data, we deduce a difference in basement depth probably associated with a NW-SE-striking fault system at the eastern rim of the magnetic low and separating the wider western part from the narrower and shallower eastern part of the central Nordkapp Basin. Gernigon et al. (2007) explained the changing structural style of the Nordkapp Basin from west to east by an interaction between rift deformation affected by pre-existing oblique, deep features and/or pre-existing grabens. We agree with this interpretation and want to set the observed NW-SE-trending lineament in the southwestern part of the central Nordkapp Basin in the same context and link it with the fault system observed in the Ottar Basin. The trend is subparallel to the Trollfjord-Komagelva Fault Zone, which dates to Meso/Neoproterozoic or even Archaean times, before being reactivated during the Timanian and Caledonian orogenies and the rifting phases in the Late Palaeozoic and later times.

The southern Nordkapp Basin is even less obvious from the magnetic data. No distinct magnetic low is observed and the dominant magnetic high associated with the Norsel High (M-BH8) reaches far into the basin with a long-wavelength anomaly and covers the northeastern part of the southern Nordkapp Basin, concealing the basinal characteristics and large depth to basement depth in this area (Fig. 9.4). Although a relative high is observed in both the gravity and the magnetic data, the lateral extension of the magnetic anomaly far exceeds the one seen in the gravity map. The correlation in itself suggests an old, probably uplifted basement block of high density and magnetisation. As discussed earlier, the different shapes of the anomalies and the much wider magnetic anomaly indicate the presence of additional high-magnetic to intermediate dense material, e.g. mafic rocks. It is likely that some mafic material intruded into the basement and the sedimentary succession during the various rifting phases and that volcanic rocks accumulated on top of the paleo-surface. From 2D modelling, magma infiltration along detachment faults is also suggested (Ch. 10). Carboniferous dolerite dykes are for example exposed on Magerøya and Late Devonian dykes on the Varanger Peninsula (Robins 1998, Guise & Roberts 2002). Although the presence of volcanic material in the southern Nordkapp Basin has to our knowledge not been confirmed so far, we propose this model to explain the contradictory expressions of the gravity and magnetic data. Furthermore, there is definitely more evidence for the presence of high-magnetic material in the vicinity of the Nordkapp Basin. Two noticeable lineaments are crossing the southern Nordkapp Basin, trending NE-SW and NW-SE: The NE-SW-trending structures was discussed earlier as a first-order lineament, probably associated with the northern boundary of the Måsøy Fault Complex and a reactivation of old Caledonian faults during the opening of the Nordkapp Basin. The NW-SE striking lineament runs through the central southern Nordkapp Basin and can be traced far into the Finnmark Platform. Because of its orientation it can be of Precambrian age similar to the lineaments observed farther north, north of the Norsel High and in the southeastern central Nordkapp Basin.

In contrast to the other magnetic patterns this NW-SE striking lineament shows an apparently sharper and symmetrical signal, which indicates the presence of dykes or fault-intruded high-magnetic material (Grauch et al. 2001, Grauch & Hudson 2007). In this case, we suggest a fault intruded by mafic material. Based on Euler deconvolution, the depth to the source is rather shallow and definitely intra-sedimentary (up to ~3500 m). Unfortunately, none of the three seismic lines crosses this feature. Even so, depending on the dip angle and thickness of, intrusions, such bodies may be difficult to see on seismic sections. However, as shown before, volcanism and mafic intrusions are rather common in the basement. For the southern Nordkapp Basin and parts of the Finnmark Platform, we suggest a discrete volcanic event, possibly associated with the rifting of the Nordkapp Basin and a likely uplift of the basement block of the Norsel High. Mafic material was most likely emplaced into the southern Nordkapp Basin mainly southeast of the Norsel High and intruded along reactivated, Caledonian or older basement faults.

Shallow magnetic patterns in the Nordkapp Basin show both NE-SW and NW-SE-striking lineaments, indicating the likely pre-existense of Precambrian and Caledonian faults. We have, however, observed a gradual decrease in the NE-SW-trending magnetic patterns within the Nordkapp Basin towards the east. Although the densely distributed salt diapirs within the basin might blur many of the fault patterns, this can be considered as an additional indication for the gradual thinning of the Caledonian nappes towards the east.

9.4.3 The Ottar Basin

The Ottar Basin situated between the Loppa High and the Mercurius High in the northwest and the Norsel High in the southeast. According to Breivik et al. (1995) the basin is c. 170 km long and 50-80 km wide with a predominant NE-SW striking direction. Two large salt domes are present within the basin, the Samson Dome and the Norvarg Dome. The domes were apparently created by non-penetrative movements of deeply buried, Upper Palaeozoic salt (Gabrielsen et al. 1990, Gudlaugsson et al. 1998). From the gravity and magnetic data it appears rather inconspicuous; two gravity lows are visible to the north and east of the Norsel High, separated by a NW-SE-oriented narrow bar with relatively higher gravity. For the magnetics, the signature of this basin is even smaller; two minima are visible, slightly displaced compared to the gravity anomalies. The southern one appears better developed. In comparison with the Nordkapp Basin the long-wavelength content in this area is rather high. No indications of salt diapirism have been be observed. Magnetic or gravity patterns of shallower origin are almost absent and points to a different evolutionary history. From the magnetic, undisturbed Caledonian nappe anomalies can be observed in the southern part of the basin. Fault-related structures are observed in the north around the Norvarg Dome and were discussed previously in chapter 9.3.1.

Surprisingly little is published on the Ottar Basin. Identified as late as 1988 by Jensen & Broks (1988), Breivik et al. (1995) subsequently carried out an intensive study on the deep-seated, immobilised salt in the basin and estimated the basin's depth. They provided evidence for a wider and deeper basin than had been reported from previous studies (Dengo & Røssland 1992, Jensen & Sørensen 1992) and concluded that the Ottar Basin is a much more important structure than previously thought, comparable in dimensions and depth to the Nordkapp Basin. From gravity modelling across the Norvarg Dome, Breivik et al. (1995) estimated a basin depth of about. 9.5 km and an average salt thickness of 2.4 km. Across the Samson Dome, salt was observed below the near base Permian reflector and the salt thickness was estimated to 3.5 km (Breivik et al. 1995). Gudlaugsson et al. (1998), however, assumed an even greater salt thickness of 4-6 km and interpreted the Ottar Basin as a major Late Palaeozoic rift basin. Based on the new magnetic data we propose that the basindeveloped possibly during only one major rifting phase in the Palaeozoic. The absence of almost any magnetic pattern suggests that there was only a minimal reactivation, if any at all, in later times. Later rift phases might also have led to a mobilisation of the salt similar and comparable to that in the Nordkapp Basin.

9.4.4 The Finnmark Platform - Kola Kanin Monocline

The Finnmark Platform formed a relatively stable and slowly subsiding block during the Late Carboniferous and Permian, influenced only by movements along NE–SW (Caledonian) and NW–SE (Timanian) trending structures (Gabrielsen et al. 1990, Alsgaard 1993, Gee & Pease, 2004, Gee & Teben´kov, 2004, Rafaelsen et al. 2008). It is bounded to the northwest by the deep Harstad and Tromsø basins and to the north by the Hammerfest and Nordkapp basins. From the mid-Carboniferous and throughout the Permian, the platform formed a northerly dipping, distally steepening carbonate ramp with buildups (Samuelsberg et al. 2003). In the surveys of BASAR-08 and BAS-06 the Finnmark Platform occupies the southern parts of the survey areas.

In the southeasternmost part of the new survey, a broad, NW-SE-elongated gravity low (G-FL4 and G-FL5) is observed. The minimum has an analogue in the magnetic data (M-FL2 and M-VL1), but a more distinct magnetic pattern is also visible and probably disturbs a response from a deep and old structure. It is situated to the north of the Varanger Peninsula and coincides with a northwestern prolongation of the Kola-Kanin Monocline (Fig. 9.3b). The NW-SE regional trends also coincide with well-known onshore Archaean and Proterozoic megastructures (Karpuz et al. 1995) that are further discussed in the next chapter dealing specifically with onshore-offshore relationships. To the west, the gravity map is dominated by relative gravity highs (G-FH3 and G-FH3), in an area where the magnetics show a contradictory picture with local but significant lows (M-FL3 and M-FL4). A correlation with gravity is observed only for the magnetic high in the central part of the Finnmark Platform (M-FH2), at least for the western part. Except for the Kola-Kanin Monocline, where gravity and magnetic correlate, the identified gravity highs and lows appear to be of a more regional character. The magnetics, however,

seem to spot rather local and probably shallower features, except for the M-FH2. This structure is most likely basement-related and shows a clear linear trend associated with the development and eastward propagation of the Caledonian nappes.

The magnetic signature of the Finnmark Platform is complex and involves both shallow and deep magnetic sources. Due to the natural ambiguity of potential field data it is difficult to distinguish between all the factors especially because they interact. The subsidence patterns, bathymetry and shapes of the sedimentary basins are commonly controlled by the deep basement architecture of the platform and, similar to the Bjarmeland Platform, some correlation also exists between deep structures and subcropping units. Nevertheless, the deep-seated contributions are certainly most important to explain the amplitude of the gravity and the magnetic total field. Short-wavelength features highlighted by filtering (high-pass or tilt derivative) may represent the lithological contrasts of shallow faults rooted or controlled by deeper crustal faults or shear zones (Figs. 9.6 and 9.7).

While the Caledonian trends are dominating on the Bjarmeland Platform, we observe on the Finnmark Platfrom a similar influence of both trends, Caledonian and the earlier Timanian. The Timanian trend is clearly expressed in major and deep-seated fault structures such as the Austhavet and the Trollfjorden-Komagelva fault zones. The orientations of the Kola-Kanin Monocline and the Tiddlybanken Basin are also parallel to the NW-SE trend. Second-order magnetic lineaments observed offshore and fault systems mapped onshore in northern Finnmark (e.g. Lippard & Roberts 1987) actually show both NW-SE and NE-SW trends, but the Timanian trend is definitely dominating and towards the east the NE-SW trends are almost no longer visible. Roberts & Siedlecka (2002) considered that the Timanide orogen, centered in the Russian southern Barents Sea, the Pechora Basin and the Timans, had a major influence on the basement configuration of the eastern Finnmark Platform whereas the Caledonian and Innuitian orogenies were more active in the western and northern parts of the Barents Sea (Rønnevik et al. 1981).

On the other hand, the characteristic, curved and eastward-convex, magnetic signature of the Caledonian propagation is clearly visible on the Finnmark Platform and even farther to the east than on the Bjarmeland Platform. With the Måsøy and Thor Iversen fault complexes and the observed NE-SW-trending complex on the Finnmark Platform, another pattern from Caledonian times is observed. The entire impact of this fault complex zone, however, is not clear yet. Especially in the area south of the narrowest part of the Nordkapp Basin, with an apparent strike-slip component noted along the lineaments, the more chaotic magnetic pattern remains suspicious and unclear. Based on observed kinks in some of the lineaments to the south of the complex zone, we suspect the presence of an approximately 30 km wide and apparently N-S-oriented belt that may have acted as a transpression zone, perhaps limited to the sedimentary units and with no basement structures involved.

From the new magnetic data, the northeastward propagation of the Caledonides shows a rather clear magnetic signature, obviously related to the different nappes, which is curved and convex to the east in the offshore regions. We assume a similar nappe-like structure to that observed in the onshore regions of Finnmark with varying thicknesses of the allochthons. The boundary of these different nappes possibly associated with fault generation and/or block rotation generates this characteristic magnetic signature. The significant high-magnetic amplitudes also suggest an involvement of the Precambrian basement in the Caledonian deformation at least in the northwestern part of the survey area. Analogues for such a deformation can be found on the mainland in West Finnmark (Olesen et al. 1990). The Precambrian rocks within the Alta-Kvænangen and Repparfjord-Komagfjord tectonic windows were for instance partly deformed and thrusted during the Caledonian nappe emplacement (Roberts 1985, Gayer et al. 1987).

The region at and around the Nordkapp Basin is heavily disturbed due to the rifting and basin development, but a correlation of the different lineaments south and north of the southern Nordkapp Basin can be made by amplitude analysis. A marked high-amplitude lineament in the central part of the survey area is running NNW-SSE into the Norsel High anomaly, disappearing at the Nordkapp Basin and continuing farther south on the Finnmark Platform, north of the Nordkinn Peninsula. To the east, the amplitude of this pattern is fading out and on the Bjarmeland Platform north of the central Nordkapp Basin it is already absent. An explanation for this could be a reduced magnetic contrast between the different nappes to the east, probably combined with reduced folding and thrusting of the involved Precambrian basement and/or an increased thickness of the overlying sedimentary rocks, which are likely to conceal the magnetic signature from the basement. In our opinon it is a bit of both: the folding and faulting of the basement is diminishing to the east, as can also be observed onshore on Varanger Peninsula for the Lower Allochthon for example (Siedlecki 1980, Gernigon et al. 2007b). To the north, the younger sedimentary succession is considered to thicken and this can explain the absence of the magnetic signature in this part of the survey area.

In the southernmost part of the survey area the new aeromagnetic data highlight new positive trends and structures. The southwestern Finnmark Platform, as shown by the new aeromagnetic data, is dominated by NW-SE and NE-SW-striking lineaments, which can partly be traced across the Austhavet Fault Zone. In the southeastern part of the platform, WNW-ESE-striking lineaments are observed northeast of the Varanger Peninsula (e.g. Fig. 9.8a). They coincide with discrete gravity changes in the Finnmark Platform and can be correlated with thrusted and folded structures onshore described in some detail in the following chapter. A prominent N°80-trending high-amplitude and elongated magnetic anomaly (M-FH1) is particularly noticeable here and clearly delimits two magnetic domains in the southern part of the Finnmark Platform and also coincides with discrete trends in the gravity signature.

The new magnetic data also refine the magnetic picture of the hinge zone located between the Finnmark Platform and the Kola-Kanin Monocline. North of Varanger Peninsula, the deeper part of the Finnmark Platform is characterised by an underlying rift topography with fault

blocks containing siliciclastic sedimentary rocks of Early Carboniferous age. These rocks were onlapped in the Mid-Carboniferous in certain intervals by minor carbonate evaporites (Bugge et al. 1995). Exploration wells have been drilled on the Finnmark Platform, all reaching the Upper Palaeozoic (7120/12-4 on the western platform and 7229/11-1, 7128/4-1, 7128/6-1 and 7228/9-1 in the east, Larssen et al. 2005). The Palaeozoic is overlapped by Triassic and Cretaceous units, tilted to the north and truncated in the southern part of the platform (e.g. Bugge et al. 1995).

The Kola-Kanin Monocline represents a thick complex of Riphean to Vendian age, which extends into the southern part of the BAS-06 survey area. The regional gravity low could roughly represent the potential field expression of the West Varanger Graben, which is part of the Kola-Kanin Monocline. The thickness of the Riphean metasediments may be as much as 10 km on the Kola Shelf but is probably less north of Varanger Peninsula. These formations underlie the Palaeozoic and Mesozoic sediments that pinch-out on the southern flank of the monocline. A more detailed description of the eastern provinces and their interrelationships can be found in Gernigon et al. (2007b).

9.4.5 Finnmark Region and near-shore domain: Onshore-offshore relationships

The BASAR-08/BAS-06 surveys overlap onto the northern onshore parts of the Finnmark region (Fig. 9.10). This overlap allows us to constrain and understand the meaning of the magnetic anomalies, which extend offshore (e.g. Gernigon et al., 2007b). A good understanding of the onshore geology was essential for a better evaluation of the onshore-offshore relationships.

The principal features of the bedrock geology of the Finnmark region are described on the NGU 1: 500,000 bedrock geology map by Siedlecka & Roberts (1996) (Fig. 9.11), and are described in many of the published papers cited in chapter 9, section 2. The previous aeromagnetic magnetic compilation of the Finnmark Region (Olesen et al. 1990) has also been merged with the BASAR-08 data to provide a better onshore coverage of the new survey (Fig. 9.10). Susceptibility measurements from onshore northern Finnmark, collected by NGU, were utilized to link correlations of sampled rock types and observed anomalies.

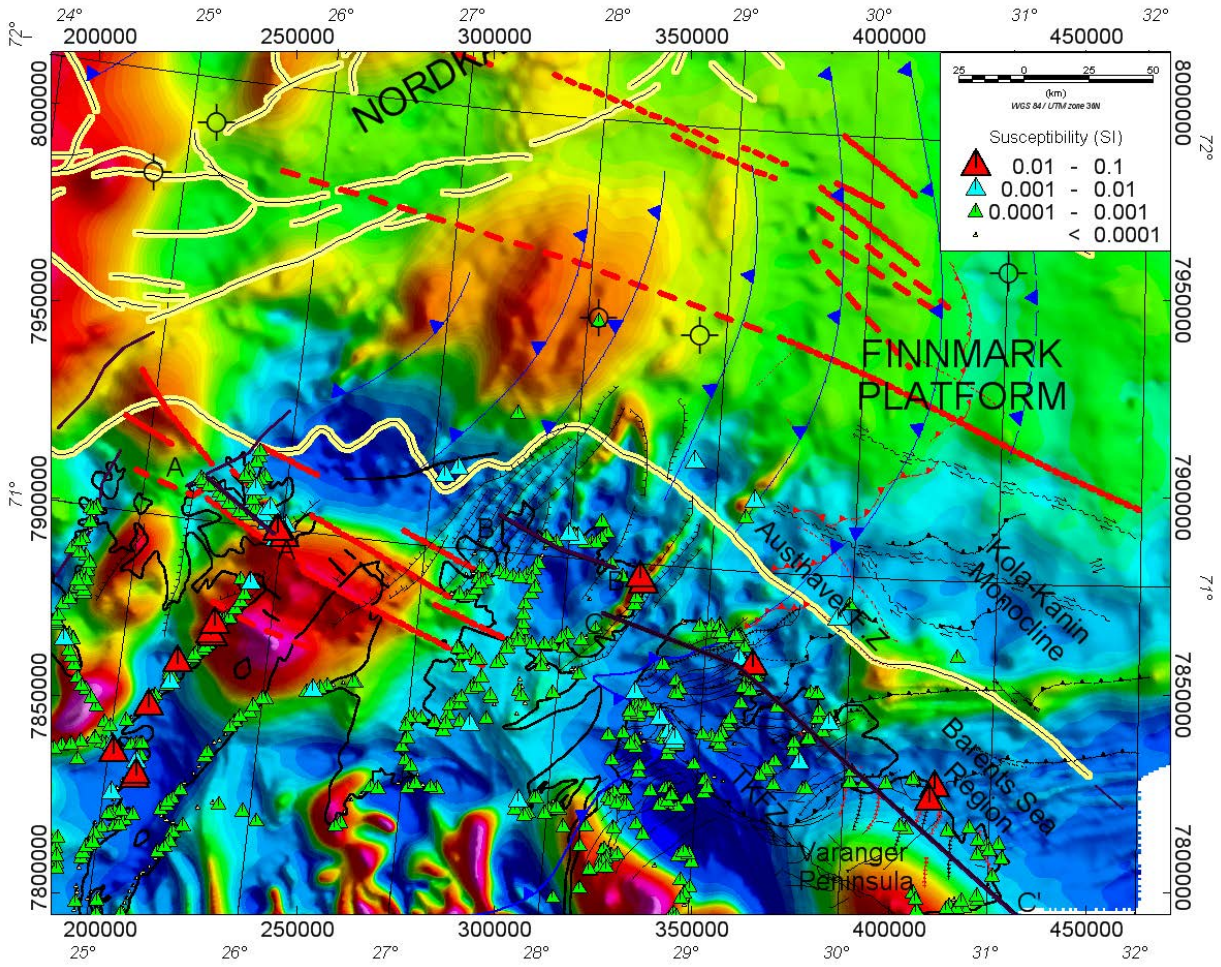

Figure 9.10 Onshore-offshore correlation utilising the TMI data from the new regional compilation with the main structural interpretations and susceptibility measurements from onshore northern Finnmark.

The new aeromagnetic data from BASAR-08 and BAS-06, however, improved the resolution of the magnetic field in both the offshore and the onshore areas in northern Finnmark as well as on the Finnmark Platform. The higher resolution revealed a lot of interesting onshore-offshore relationships which, for Varanger Peninsula, have already been discussed in the BAS-06 report (Gernigon et al. 2007b). For the sake of completeness, this interpretation is summarised here, slightly updated and complemented by the new magnetic data and the observations to the west. The new survey confirms these previous regional hypotheses and better constrains the geology farther to the west.

West of the Nordkinn Peninsula, NW-SE-oriented lineaments are observed (Fig. 9.10) in the onshore–offshore region, parallel to the TKFZ and obviously correlating with the dominant Timanide-related fault patterns onshore northern Finnmark and on the Finnmark Platform (see above). These faults were active during Late Palaeozoic extension (Roberts and Lippard 2005), probably with coeval dyke intrusions, which would explain the high and sharp magnetic signal along these faults. In fact, we can observe additional NW-SE-striking features offshore on the Finnmark Platform and in the southern Nordkapp Basin with a similar amplitude pattern,

emphasising the Late Palaeozoic rifting as the major rift event in this area, coupled with mafic intrusions and possibly sills. The seismic sections on hand unfortunately do not cross these features and we are therefore unable to investigate these relationships further.

NNE-SSW to NE-SW-trending faults represent the second group of faults observed in northern Finnmark (Lippard & Roberts 1987) and these are also well known from the offshore regions. The NE-SW offshore faults are known to have been active in Devono-Carboniferous time (Gabrielsen 1984, Bugge et al. 1995) in this southwestern Barents Shelf domain, presumably reflecting the Caledonian structure (e.g. Faleide et al. 1984, Gabrielsen 1984), and are also well expressed in the surface geology (Fig. 9.11). The magnetic signature of these patterns is observable in the new data, but for Magerøya and the Porsanger and Sværholt peninsulas the magnetic anomalies are rather small. Susceptibility measurements on samples reveal a relatively uniform and low magnetic basement in this region (Fig. 9.10) with some local examples of highly induced magnetisation e.g. in the Honningsvåg Igneous Suite (HIS) (Torsvik et al. 1992).

A geological profile across Magerøya with the corresponding gravity and magnetic data (Fig. 9.12a) plotted on top expresses the small but existing correlation of faults and contacts in the potential field data. The profile strikes NW-SE and shows the contact between the Kalak Nappe Complex (KNC) and Magerøy Nappe in the north, and the Magerøy Nappe and the HIS in the south, where both contacts are observable from the magnetic and gravity data. The Magerøy Nappe is the uppermost unit in the Caledonian tectonostratigraphy of Finnmark (Roberts & Andersen 1985), and was deformed by large-scale, north-plunging folds during the nappe emplacement. The sedimentary rocks are intruded by the HIS, which has been modelled by Lønne & Sellevoll (1975) and Torsvik et al. (1992) to a depth of approximately 6 km.

On the Nordkinn Peninsula, however, the magnetic signatures change significantly. Although NW-SE trending structures are still observed west and southwest of Nordkinn, NE-SW-striking, high-amplitude lineaments that flank the peninsula to the east and west become predominant. This high magnetisation was observed already on the NGU-70 aeromagnetic dataset on eastern Nordkinn Peninsula (Åm 1975), and its origin was ascribed to the profusion of thinbeds and foresets composed almost exclusively of high-magnetic minerals (magnetite, hematite and ilmenite) in fluvial metasandstones (Siedlecka & Siedlecki 1970, Siedlecka & Roberts 1992, Siedlecka & Roberts 1996, Roberts 2007, Fig. 9.10). The distribution of this unit, shown on the geological map (Fig. 9.11) reveals a remarkably good correlation with the distribution of magnetic anomalies in the onshore domain, which can be traced offshore towards the northeast and across the Austhavet Fault Zone. The magnetic lineaments show a converging trend, suggesting a the presence of a major anticlinal fold, plunging towards north-northeast. A geological profile (Fig. 9.12b) across a part of this structure reveals, however, a series of upright folds rather than a single anticline, with many steep faults and contacts which are also expressed in the potential field data. This, of course, explains even better the set of almost parallel lineaments in the magnetic map, which probably is a visible expression of the KNC.

The shape of the anomaly offshore and the north-northeast plunge of the main fold suggest that this part of the KNC may be overrun by a younger thrust sheet just to the north.

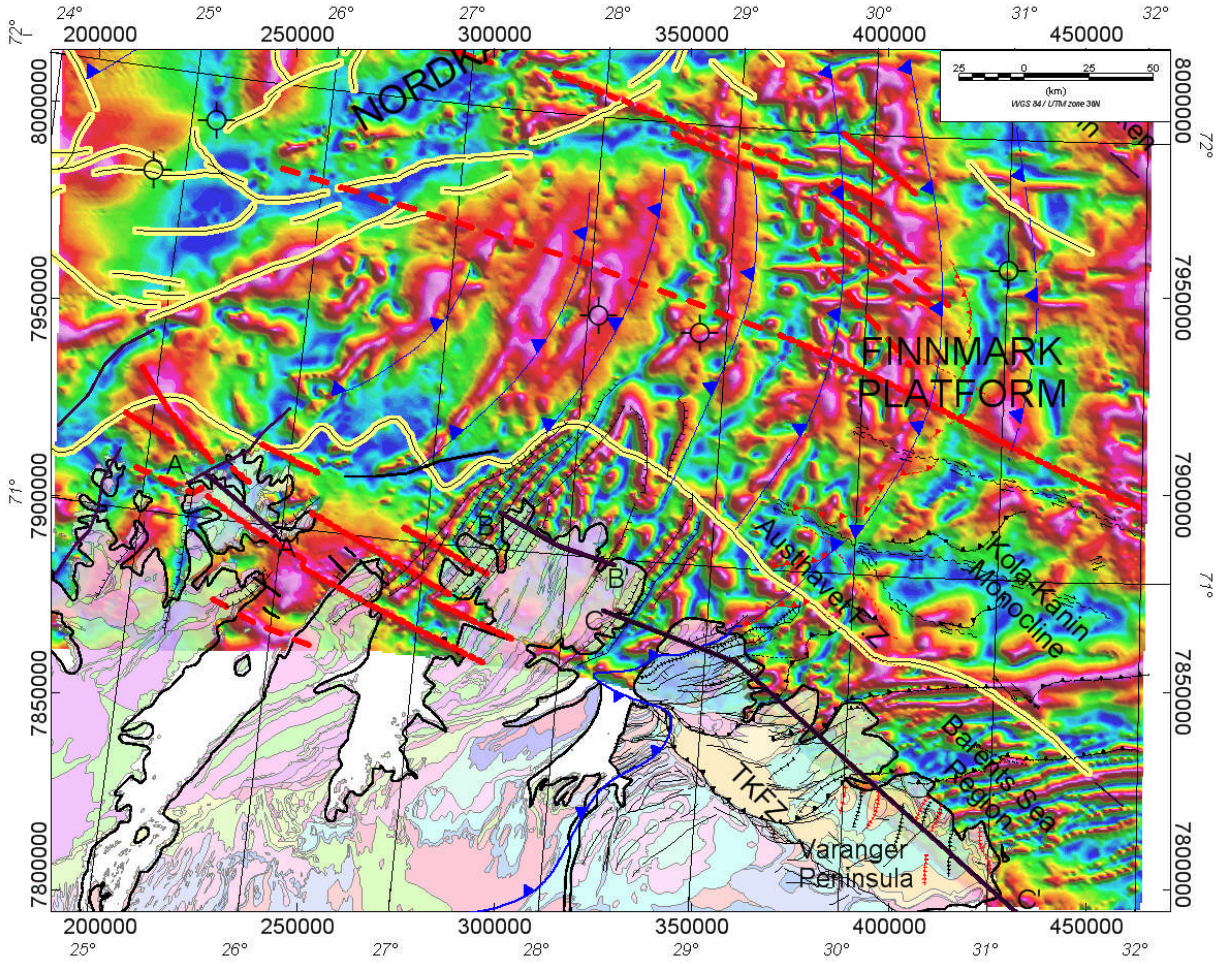

Figure 9.11 Onshore-offshore correlation: TILT derivative with main structural interpretations and onshore geology map (Siedlecka & Roberts, 1996).

Along the profile, there are three different meta-sandstone formations. At the northwestern end of the section there is a major, steep magnetic high which correlates with the metasandstones from the same geological unit (22) sampled in the eastern part of the peninsula with high-susceptibility minerals (Fig. 9.10). The distribution of the high-magnetic minerals within the sandstone unit is obviously not homogeneous, as a second block of the same unit induces a significantly smaller magnetic anomaly, but the distribution of the relative magnetic highs along this line does correlate with the exposures of this unit. It is interesting that the gravity shows an almost identical pattern as that of the magnetic data, indicating that high-magnetic Caledonian units have a low density and vice versa. In fact, the rock samples confirm this observation with the high-magnetic metasandstones showing a lower density than the adjacent units.

Large magnetic and gravity anomalies coincide with the major structural domains present along the geological transects (Fig. 9.12). A third transect runs from eastern Nordkinn towards the southeast and across the entire Barents Sea Region of the Varanger Peninsula (Fig. 9.12c). The primary structural boundary along this profile coincides with the base of the Tanahorn Nappe (Middle Allochthon), which is a steeply northwest-dipping thrust fault that separates the Berlevåg Formation (covered to the west by the BASAR-08 survey) from the Lower Allochthon of the Barents Sea Caledonides (mostly covered to the east by the BAS-06 survey). To the west, northewest of Tanafjorden, the profile coincides with the high-magnetic unit already discussed for profile BB'. The magnetic signal shows accordingly a steep and high-amplitude magnetic anomaly which on the new dataset can be traced far into the Barents Sea to just south of the Nordkapp Basin, underlining the impact of this boundary for the structural framework of the Barents Sea. Near the base of the Tanahorn Nappe, which is in effect a 'metamorphic front', the magnetic anomalies coincide with fault-propagation folds and thrusts that gradually steepen towards the southeast (Karpuz et al. 1995, Gernigon et al. 2007b).

East of the base of the Tanahorn Nappe the magnetic trends vary mainly from NW-SE close to the Berlevåg to N°70-N°80 farther to the east, defining a distinct magnetic region within the Lower Allochthon. The main N°70 magnetic anomaly trend observed in this northern part of the BSR correlates with the formations and overthrusts observed between Kongsfjorden and Syltefjorden (Fig. 9.11). It represents a set of thrust faults with probably a strike-slip (dextral) component within the Rákkocearru thrust sheet and a lower, unnamed thrust unit (Roberts 2009 and pers. comm. 2007). Inland from Syltefjorden it could be connected with a deeper shear zone. Offshore in its central part, the zone of N°70 striking anomalies is affected by minor dextral strike-slip offsets along the N°110-trending Austhavet Fault Zone.

A marked magnetic positive anomaly runs in the prolongation of the overthrusted structures and faults observed onshore (Rákkocearru thrust sheet) between Kongsfjorden and Båtsfjorden. The amplitude of this anomaly is relatively high compared to similar NW-SE magnetic features also related to major faults and was consequently puzzling. An explanation for the higher amplitude was found on the 1:50.000 geological map-sheet of the Syltefjord region (Siedlecka 1984) where the southwestern end of the NW-SE anomaly overlaps the coastline between Makkaursandfjorden and Båtsfjorden. The geological map-sheet indicates that this particular area is heavily intruded by a swarm of dolerite dykes. The dykes trend between E-W and NW-SE and the dyke spacing is usually less than 300 m (Siedlecka 1984) with a decreasing intensity towards Båtsfjorden. The atypical concentration of dykes in this area could explain the high magnetic response.

A second and major structural and magnetic change is observed between Syltefjorden and Persfjorden. It also coincides with a clear gravity contrast within the BSR, which may divide the BSR into distinct crustal blocks. It could possibly represent a deep Proterozoic fault or shear zone, likely reactivated during the Caledonian event. On the surface, a dip-slip reactivated thrust-fault is inferred to mark the base of the Lower Allochthon (D. Roberts, pers. comm.

2007). This boundary can be extrapolated offshore and seems to coincide with a discrete subdivision in the well-layered magnetic pattern. Euler solutions for these areas (Gernigon et al. 2007b) suggested that the N°70-80 magnetic lineations observed in the southern part of the BAS-06 lie at depths deeper than 2 to 3 km and increasing to the southeast.

In that magnetic domain, the magnetic trends are still N°70 but several N-S lineations were underlined by enhancement filtering. They slightly disrupt the N°70-80 layering pattern. Southwest of this striped zone, deformation in the onshore part is less intense and mostly affected by anticlines and synclines, instead of the reverse faults and thrustthat are prominent in the northwestern part of the peninsula. The trends of the onshore structures also change between Syltefjorden and Vardø with a dominant N-S to NNW-SSE orientation of fold-axes structures (Fig. 9.10).

On a regional scale, the eastern part of the BSR shows a significant magnetic change with a prominent magnetic anomaly not observed in the northwestern part of the Varanger Peninsula (Fig. 9.10). The correlation between potential field data and the structurally contrasting style observed onshore is suggestive of a major crustal boundary. The significance of this anomaly was already discussed by Karpuz et al. (1995). The anomaly coincides with the southeastern segment of the TKFZ and according to Åm (1975) could originate at a depth of 5 km. With the new survey, we also got some clusters of Euler solutions at a similar depth of 3.5-5 km (Fig. 8.2). According to Karpuz et al. (1995), the spatial coincidence with gravity anomaly G-FH4 may suggest the presence of a possible basement high or intrusion at depth in this part of the Varanger Peninsula.

Compared to the contrasting NE-SW structures described from the Gaissa Nappe Complex in the southwestern part of Varanger Peninsula, the main dominant magnetic trends in the eastern offshore area still remain N°70 and even though the N-S to NW-SE fold trend dominates onshore (Figs. 9.11). This could possibly be explained by a late Caledonian dislocation and rotation of fault blocks. Although some folds with a reversed facing polarity may also suggest a possible backthrusting process, which could explain the trend differences between the magnetic lineations and the N-S axis of the folds, structural studies have shown that a c. NE-SW-trending, Caledonian, secondary cleavage overprints the penetrative NNW-SSE-trending (Timanian) cleavage in this area (Gjelsvik 1998, Herrevold et al. in press). A deeper thrust system involving a trailing imbricate fan above a deeper detachment could also influence such a conjugate, orthogonal faulting and folding. A deeper blind-thrust hypothesis is suggested in our transect C (Fig. 9.12).

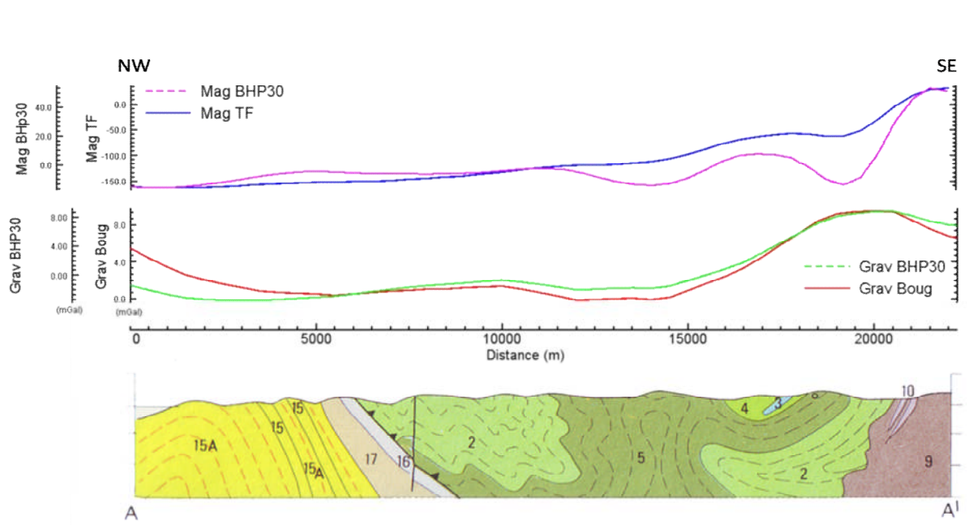

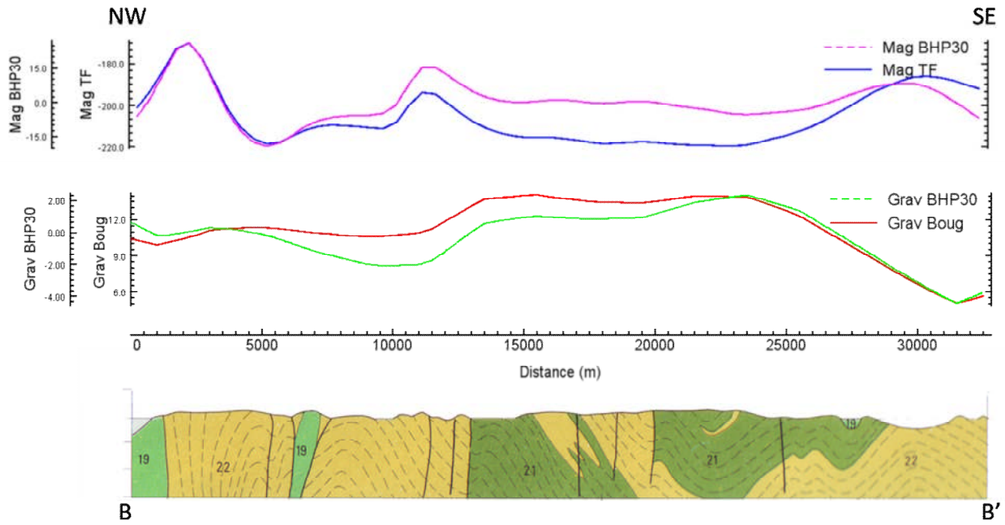

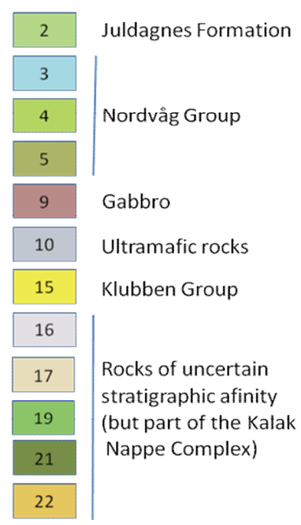

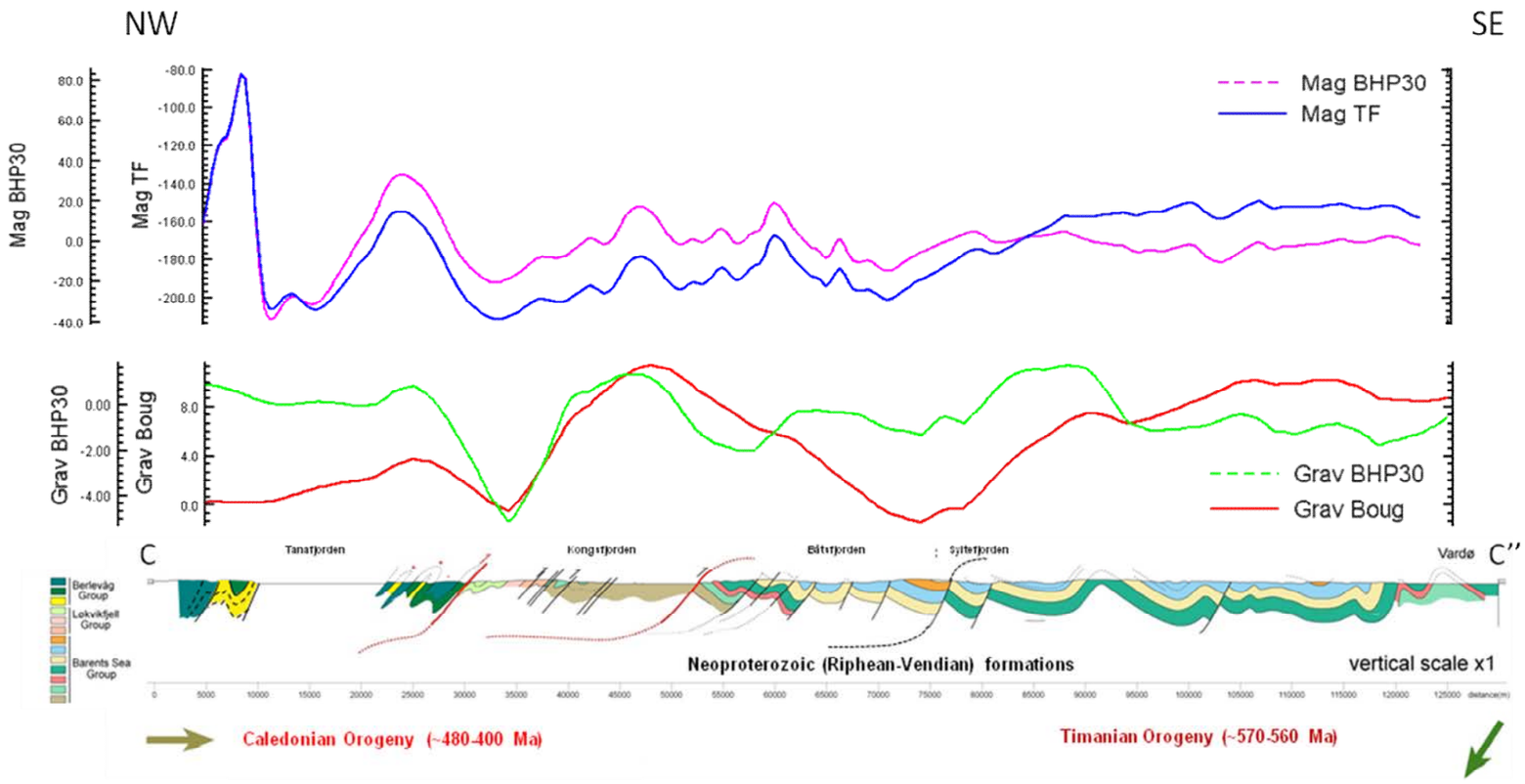

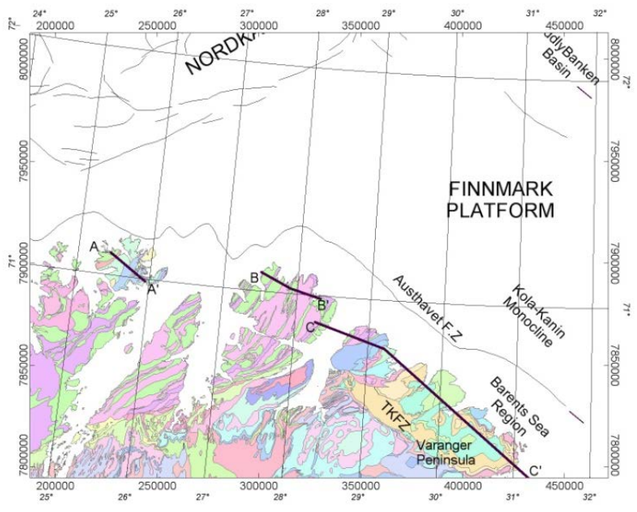

Figure 9.12 Geological profiles with corresponding Bouguer gravity and magnetic total field plotted on top across a) Magerøya, b) northern Nordkinn Peninsula and c) the BSR of the Varanger Peninsula . Large magnetic and gravity amplitudes coincide with major structural domains underlined by the geological transect. Geological sections are by Roberts (1981) (a and b) and Gernigon (2007b) (c), Overview with profile locations and simplified geological map (Siedlecka & Roberts, 1996).

10 GRAVITY AND MAGNETIC MODELLING

Laurent Gernigon

10.1 Modelling methods and assumptions

10.1.1 Forward modelling approach

The modelling and interpretation process described here was designed and carried out to quantitatively validate the interpretation of the MN89-202, D9 and D11 seismic lines selected to illustrate the new BASAR-08 survey (Fig. 10.1). The new magnetic anomalies highlighted by the new magnetic compilation do not necessarily coincide with the Mesozoic sub-basin geometry and the regional gravity pattern and most likely reflect magnetic basement features. Despite the large uncertainties about the basement depth in most of the survey area, forward modelling allowed us to refine and adjust its geometry to some degree. The basin geometry is generally well constrained by the reflection seismic data down to at least Permian depths, but the main unknowns remain the importance and distribution in depth of the pre-Permian Palaeozoic basins. Both gravity and magnetic anomalies (Figs. 10.2 & 10.3) provide relevant information about the nature and distribution of the main magnetic basement units; combined with seismics, the anomalies provide an interesting combination to analyse the basin architecture. Using 2¾D forward modelling, we can better constrain the depth to basement, identify several characteristics in the distinct petrophysical properties and better assess the crustal architecture along the three regional transects.

10.1.2 Methods

The 2¾D forward modelling has been carried out using the commercial software GM-SYS (Northwest-Geophysical-Associates-Incorporation 2006). GM-SYS is an interactive gravity and magnetic modelling program applying a method of summing the effects of irregular polygons modified after Talwani (1973). The method also uses the divergence theorem (Blakely 1995) for the magnetic modelling. With the 2¾D approach structures (bodies) of varying and limited extent, both laterally and perpendicularly to the line and in front of and behind the plane of the profile, may be defined and their effects included in the calculated anomaly.

The shallow geometry of the models is based on the interpretation of major seismic reflectors interpreted on the 3 seismic sections provided by NPD (Fig. 10.4). Apart from the sea bottom, the main horizons include 1) base Quaternary, 2) base Upper Cretaceous 3) near base Cretaceous, 4) base of Upper Jurassic, 6) Intra-Middle Triassic, 7) near top Lower Triassic, 8) intra Early Triassic, 9) near top Permian and 10) near top basement reflectors (Devonian-Carboniferous ?).

Our modelling procedure includes a direct interaction with the seismic data and the magnetic field. The SEGY files have first been depth-converted for this specific project and the depth-converted SEG-Y files have been imported as background and guide in the GM-SYS. The mean regional velocity values used for the depth conversion are indicated in Table 10.1. When available, check shot values from wells were included in order to refine locally the initial velocity model, by dynamic readjustment of the velocity grid using the Themis-Easydepth^{TM} software (Beicip-Franlab 2002).

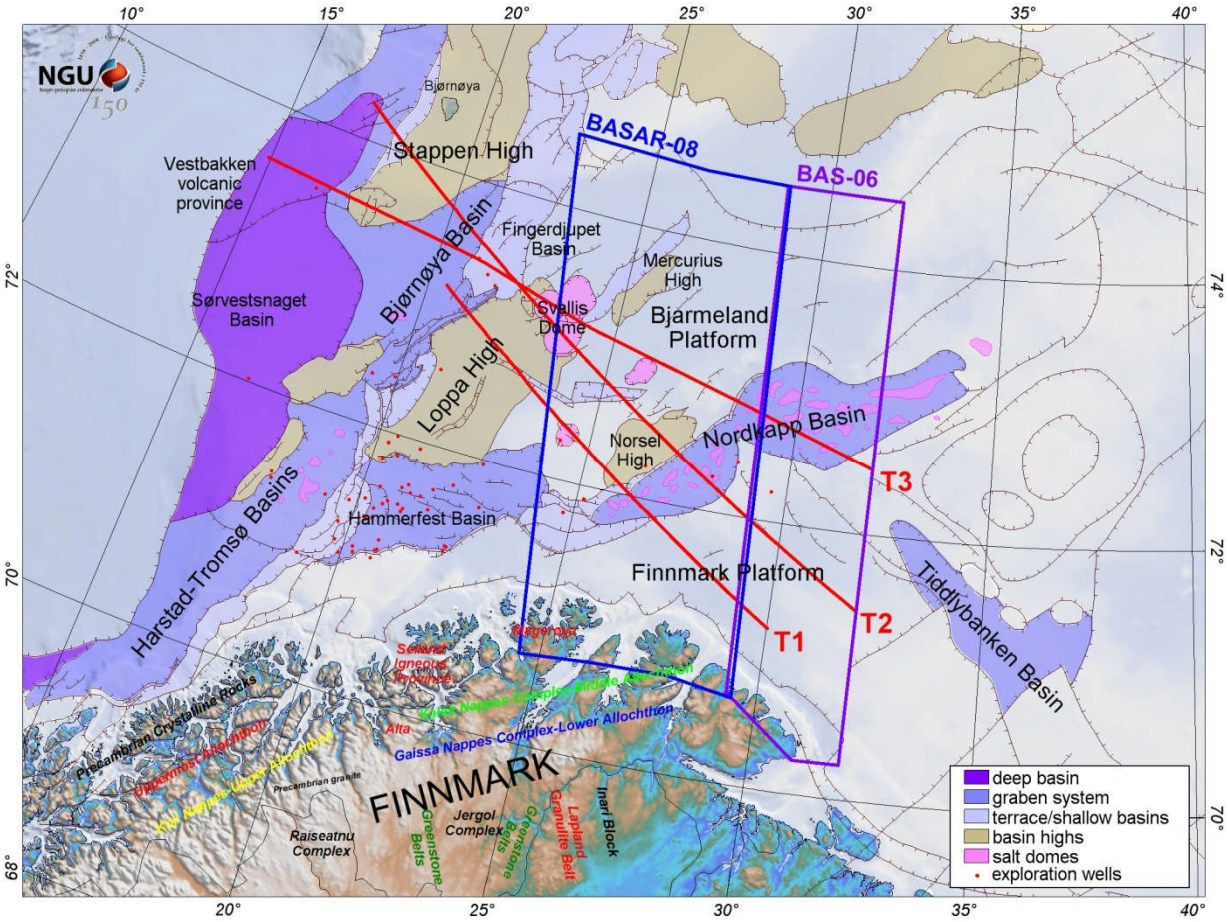

Figure 10.1 Location of the regional transects and outline of the main structural elements of the western Barents Sea. The main structural elements are modified from NPD (Gabrielsen et al. 1990). The map also shows the onshore topography of Finnmark and some of the main geological units.

Wherever possible, features interpreted on the seismic data have been used to constrain the geometries of the basins and various geo-bodies (e.g. salt diapirs) were included in the modelling, where indicated. The modelled layer geometries in the top 10 km below seafloor are comparatively well constrained by the seismic interpretation. Furthermore, along the three lines top basement was identified over long distances, typically expressed as strong-amplitude reflections. For areas where such a reflector was missing, we mostly rely on early top magnetic basement estimation from Skilbrei (1993). Below this, the seismic data quality is locally relatively poor owing to noise, multiples and poor sub-salt imaging, and no seismic interpretation was attempted. Farther west, the qualities of the seismic data used in this project were relatively bad in the vicinity of the Stappen High and did not allow a reliable horizon picking.

Along the different transects, the middle crust boundary and the Moho have only been modelled in order to fit the overall gross shapes of the potential fields and to be consistent with the limited crustal information including, for example, the IKU transects (Gudlaugsson 1987, Barrère 2009) and recent regional compilations (Ritzmann et al. 2007). To constrain the initial Moho depth, we used a recent Moho compilation of the European plate (Grad et al. 2009) which provides an updated version of the Barents50 model (Ritzmann et al. 2007).

The model was constructed in different steps including: 1) the definition of the 2D initial crustal geometry, 2) the lateral and perpendicular extension of the main seismic horizons to infinity in order to reduce the edge effects when necessary; 3) the definition of the appropriate density values and 4) the forward modelling interaction.

For every sedimentary interval of velocities we attributed a density using appropriate velocity-density functions based on appropriate estimation of the geological setting and their uncertainties (Nafe & Drake 1957, Gardner et al. 1984, Carlson 1990, Larsen 1994, Christensen & Mooney 1995, Christensen 1995, Birch 1996, Godfrey 1997). The average density for each polygon can then be calculated from the interval velocities. Top basement and Moho usually coincide with the main density contrasts in the lithosphere. Furthermore, petrophysical constraints were adopted from the literature (Barrère, 2009, Table 10.1).

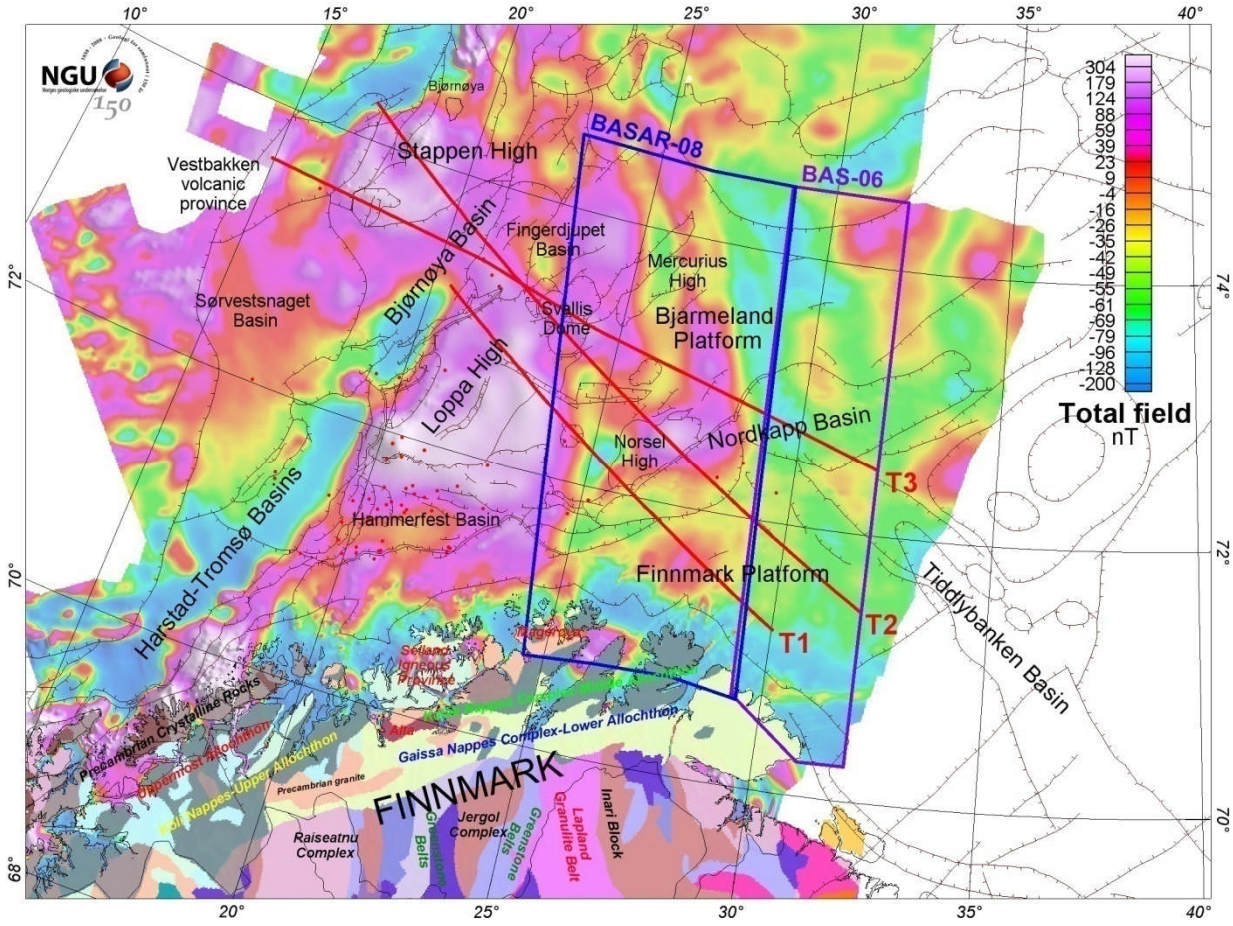

Figure 10.2 Location of the regional transects and magnetic total field anomaly map of the western Barents Sea.

Density, magnetic susceptibility and remanence values from onshore samples measured at NGU (Troms and Finnmark regions) (Olesen et al. 1990) were chosen as starting values in the models (Table 10.1). Average density values were applied to all layers (Table 10.1). The densities of the sedimentary layers are based on a review of the available well data (Tsikalas et al. 1992, Gernigon et al. 2007b). Tables published by Breivik (1995), Breivik (1998) and Ritzmann et al. (2007) based on velocity–density relationships for the deepest sedimentary units obtained from the seismic refraction and reflection/gravity studies have also been considered. In our model we set an average density of 2750 kg/m³ for the upper crust, 2950-3100 kg/m³ for the lower crust and 3300 kg/m³ for the upper mantle (Table 10.1).

The petrophysically attributed geometrical models were subsequently iteratively modified using forward modelling and inversion techniques and adjusted to the observed gravity and magnetic fields.

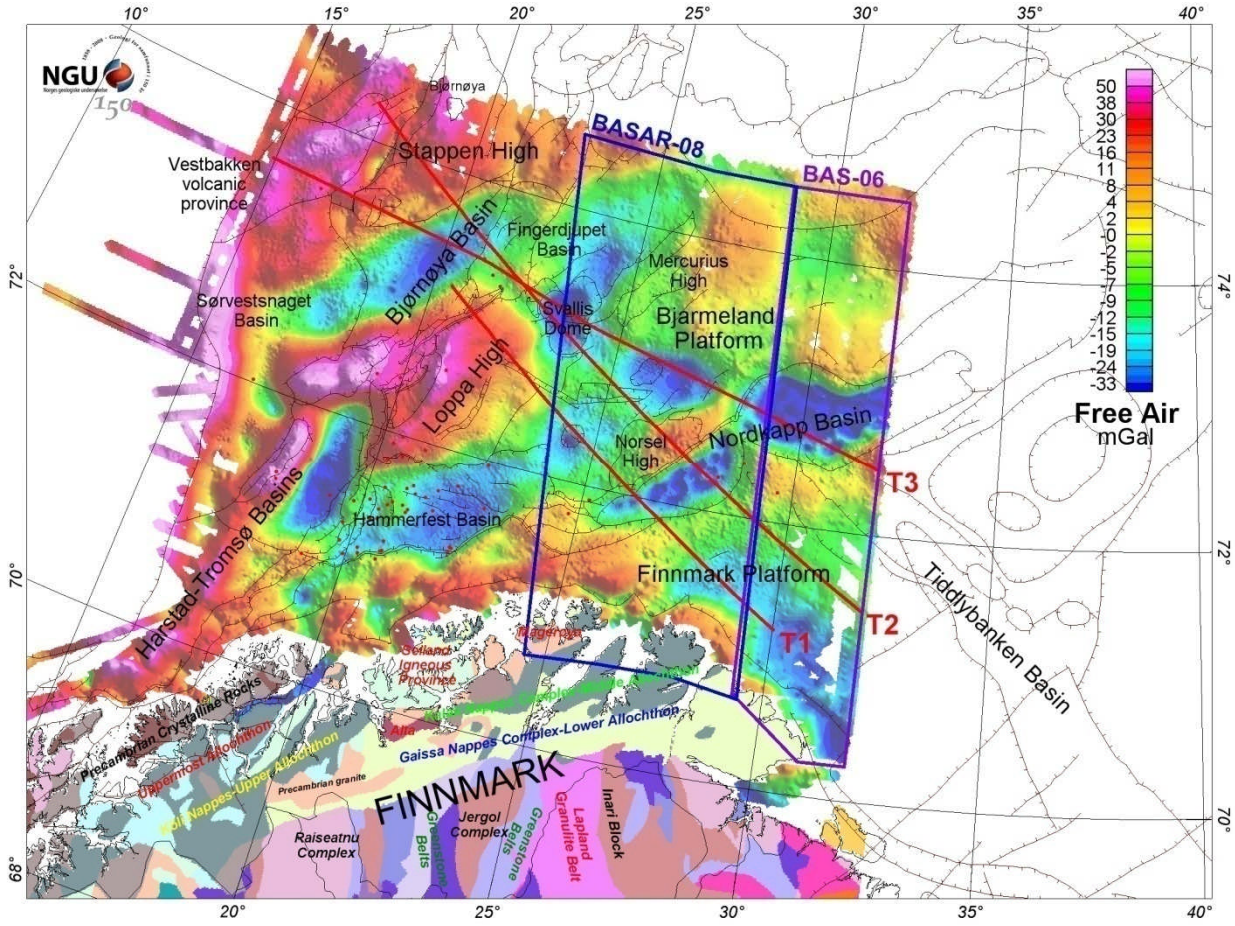

Figure 10.3 Location of the regional transects and free-air gravity map of the western Barents Sea. The map also shows the main onshore geological units.

The body responses were modelled in their correct x, y and z locations not projected into a plane. The calculations do not take into account the spherical and curvature effect of the Earth over the distance of the baseline. Induced errors due to this assumption, based on comparison of similar modelling and spherical 3D models by Wienecke et al. (2007) are of the order of 10%. Given the

noise envelope of approximately 1-3×10^{-5} m/s^2, the uncertainties in our geological model and the dynamic range of the data (c. 100×10^{-5} m/s^2), these errors are not considered as significant.

10.2 Magnetic modelling

Interpretation and modelling of magnetic data are usually more complex and tricky as compared with gravity data. The magnetic susceptibilities of the different rock types can differ by 2 to 3 orders of magnitude, in contrast to gravity data where crustal densities differ only by 30%. Our model considers reasonable geological assumptions but the reader should be aware that magnetic modelling always has to apply simplifications due to uncertainties, the lack of direct measurements and method limitations. The combined interpretation of seismic, gravity and magnetic data and a relative understanding of the tectonic setting generally reduces these uncertainties and ambiguities.

Magnetic modelling helped to split and identify the crust into blocks of contrasting magnetic properties (see Table 10.1). Onshore-offshore relationships (Fig. 9.9) also help us to understand the meaning of the main gravity and magnetic provinces. For modelling, magnetic induction (J_I) is assumed to be the principal method of generating magnetic anomalies in continental crust; in these bodies the dimensionless apparent Königsberger ratio (Q), the ratio of the remanent field to the inducing field, is set to zero. Some inferred igneous bodies and terrains could have non-zero Q values, implying a local contribution from magnetic remanence (J_R) to fit the observed magnetic anomalies.

In the absence of detailed magnetic measurements on drillcores from the Barents Sea basement, the magnetic properties of the crust along the BASAR-08 survey remain the least-constrained part of our validation process. Magnetic data are normalised to the current magnetic field, but this field was frequently reversed in the Earth's geological past, resulting in strong negative magnetisations in the dataset. The true values of Q might be significantly different to those modelled if there is a high angle between real remanent vectors and the current inducing field vector.

Inclination and declination have been aligned to the present-day geomagnetic field (average inclination I= 79°, average declination D=4.3°). The induced magnetisation (H) is proportional to the strength of the, present-day induced, geomagnetic field (B) (B=54,000 nT ~42.97 A/m). Aligning the induced magnetisation and the remanence magnetisation corresponds to adding their respective vectors. This simplification tends to give maximum magnetisation values and we consider the direction of the remanent field to be the same as for the induced field. The ratio of remanent magnetisation (Jr) to induced magnetisation (Ji) is expressed by the Königsberger ratio (Q-ratio).

The remanent magnetisation of the Archaean to Palaeoproterozoic and Caledonian rocks is related to the abundance of magnetic minerals within the rocks and the thermo-mechanical history and geomagnetic field when the rocks formed. In order to compute the Q-ratio, both magnetic

susceptibility and remanence were considered for each unit (Table 10.1). The Q-ratio was estimated for each block and geologically interpreted with respect to published values.

From the values published by Olesen et al. (1990), Barrère et al. (2009a), a mean remanence of 0.2-0.3 A/m for the older Archaean to Palaeoproterozoic rocks and mafic complexes and a remanence value of 0.0001 to 0.01 A/m for the Caledonian rocks were originally selected (Barrère et al. 2009a), tested and adjusted when necessary. The Curie temperature for magnetite is 580° C, and therefore we limit the extension of potential magnetic sources to the older Precambrian basement and lower crustal blocks. Sedimentary rocks below the Moho are assumed to be non-magnetic.

10.3 Werner deconvolution

Before forward modelling using GMS-SYS, a Werner deconvolution technique, as described in chapter 8.6, has been applied along the 3 transects to get a first and quick overview of the main distribution of magnetic sources and major magnetic contrasts. The method locally creates nice clusters of magnetic solutions which likely represent a major magnetic contact (Fig. 10.4). Reliable solutions were particularly expected locally near or on the Loppa High and Norsel High, and the contact between the Stappen High and the Vestbakken Volcanic Province was clearly highlighted by the deconvolution. After different tests on the window sizes, most of the solutions seem to have originated in the upper crust.

Breivik et al. (1995)		Mjelde et al. (2002)	Ritzmann et al. 2007 (Barents50)		Breivik et al. (2003)	Breivik et al. (1998)	Clark et al. 2008	Barrère et al. (2008)		Modified after Gernigon et al. (2007) SW Barents Sea-BASAR-08 study		
SEDIMENTARY ROCKS												
Density (kg/m³)	Velocity (m/s)	Density (kg/m³)	Density(kg/m³)	Velocity(m/s)	Velocity (m/s)	Velocity (m/s)	Velocity (m/s)	Density (kg/m³)	Magnetic properties (Ji, Jr, Q)	Density (kg/m³)	Magnetic properties (Ji, Jr, Q)	Velocity (m/s)
1800-2050	1800-2360	2050	1.8-2.05	1800-2250	1800-2250	-	2000	2300	0	1800-2000	0.00056 SI, 0 A/m	1800-2100
2050	2360	2200	2.05-2.28	2250-3260	2250-3500	-	2000-3000	2300	0	2000	0.00056 SI, 0 A/m	2000-2350
2140	2750	2300	2240	2750-3600	3500-3600	3200-3360	3000-4500	2550	0	2100	0.0005 SI, 0 A/m	2400
			2370							2150	0.0005 SI, 0 A/m	2400-2500
		2400	2590		3800-5000	3300-4050						
2340	3700	2480	2380-2590	4000-5450	4000	4800	4500-5000	2550	0	2350	0.0006 SI, 0 A/m	3500-4500
2390	4000		2470-2590		4600-5450	4000-4800				2400	0.0006 SI, 0 A/m	4000-4500
2430	4200		2520-2590		4600-5450	4000-4800				2450	0.0006 SI, 0 A/m	4000-4600
2500	4600		2520-2590		5100-5450	4500-4950				2500	0.0006 SI, 0 A/m	
2610	5200	2620	2640	4500-5900	5650-5900	5100-5520	5000	2600	0	2600	0.0002 SI, 0 A/m	5000-5200
2660	5500		5.50	5500-6000	5920-5950	5800-6000	-	-	0	2650-2680	0.0009 SI, 0 A/m	5500
2200	4500	2150	-		-	-	-	-	0	2150	-0.0001 SI, 0 A/m	4500
2660	5500		2710						0	2700	0.0009 SI, 0 A/m	5500
Ottar Basin Nordkapp Basin 2770	6000	(Sørvestsnaget Basin) 2750	Average Barents Sea 2770	6200-6600	S. Svalbard 6200-6500	SE Svalbard 6200-6500	SW Barents Sea Loppa High 6000-6500	Caledonian Nappes 2750	(0.0001 to 0.01 SI, 0.01 A/m, Q>1)	Caledonian Nappes: 2750 Finnmark Platform	(0.0001 to 0.01 SI, 0.01 A/m, Q>1)	6000
										Central unit >:2750	**(0.07 SI, 0 A/m)**	6000
										Central unit <:2750	(0.005 SI, 0 A/m)	6000
								Magerøya: 3000	**(0.005 to 0.05 SI, 0.2 A/m, Q>1)**	Loppa High block >: 2750	**(0.03 SI, 0.5 A/m)**	6000
								Seiland Igneous Province:2850		Loppa High block:< 2760	**(0.085 SI, 0.5 A/m)**	
-	-	-	-	-	-	-	-	-	-	Stappen High block >: 2700-2750	**(0.09 SI, 0 A/m)**	6000
										Stappen High block <: 2750	**(0.025 SI, 0 A/m)**	
2930	>6600	2820	2980-3050	7100-7600	2890-2990	-	6500-7000	Archaean to Proterozoic rocks 2750-2850	(0.01-0.1 SI, 0.2 A/m, Q<1)	Lower crust West: 2950	(0.0001 SI, 0 A/m, Q=0)	-
								Lower crust: 2950	(0.0001 SI, 0 A/m, Q=0)	Lower crust East: 2950	(0.0001 SI, 0.3-1.5A/m, Q=0)	
		2950-3050	2980-3050				3.1	3000				
		2800-2850					3.0	3000				
		2950			2900-2950							
3330	>8000	3220	3300	>8000	>8000	3.33-3.34	>8000	3300		3300		

Table 10.1 Initial values used for the modelling, velocity, density, magnetic susceptibility, magnetic remanence and Q-ratios for all basinal and crustal units were compiled from previously published papers and NGU reports. The different formation ages are presented in the following transect interpretation using the CGMW International colour code (see figure 10.5).

10.4 2D transect interpretation

10.4.1 Transect 1: section D9 from the Finnmark Platform to the north of Loppa High

Transect 1 runs NW-SE from the northern Loppa High to the Finnmark Platform (Fig. 10.1). The eastern end of the transect coincides closely with the northern prolongation of the base of the Middle Allochton (Tanahorn Nappe) interpreted in the BAS-06 report (Gernigon et al. 2007b). The transect also crosses the southern Nordkapp Basin and the Ottar Basin as defined by Breivik et al. 1995).
Along the transect D9, the Loppa High represents a clear and distinct crustal block with a deep Moho (> 30 km) compared to the surrounding terranes (e.g. Barrère et al. 2009a). The basement is characterised in most areas by bands of high-amplitude reflectors indicating internal layering dipping steeply towards the east. A wedge of Upper Palaeozoic sedimentary strata dipping and thickening eastwards overlies the eastern flank of the basement block. The seismic profile crossing the western boundary of the Loppa High shows clear evidence of syntectonic sedimentation in response to down-to-the-west normal faulting towards the Bjørnøya Basin (Fig. 10.5). The faulting occured mostly in the Mesozoic (Jurassic-Cretaceous), while due to difficulties in establishing reliable stratigraphic correlations, earlier movements are only documented from Permian to the Early Triassic. An angular unconformity at the crest of the Loppa High was either partly caused by footwall uplift and erosion in response to tectonic 'unroofing' in the Carboniferous rifting phase (Gudlaugsson et al. 1998) or could have initiated earlier in Devonian time (Barrère et al. 2009a) during the inferred post-orogenic collapse.

In addition to the main N-S-striking fault zones confining the Loppa High in the west, a 50-70 km-long, pre-Permian terrace is observed on the southeastern flank of the main high (Fig. 10.5). Precise pre-Permian interpretation along our transect was not possible due to the lack of calibration and poor seismic quality. However, in conjunction with a nearby borehole seismic data show that Mid Carboniferous faulting most likely occurs to the south with the development of half-graben features (Gudlaugsson et al. 1998).

The Loppa High is characterised by a noticeable gravity high (0-30 mGal) and the highest magnetic total field amplitude (150-330 nT) and both potential field data show two different provinces within this high (Figs. 10.2 & 10.3). The western part of the Loppa High is characterised by a pronounced free air anomaly (15-30 mGal) and a moderate magnetic anomaly (50-160 nT). In contrast, the eastern part is marked by a gradual decrease in free air anomalies to the east from 15 to -10 mGal, but an increase in magnetic anomalies up to 250-350 nT is observed.

The basement block has been modelled in this study as a trapezoidal shape with a steeply west-dipping fault complex to the west and a smooth east-dipping boundary to the east. The shallow basement modelled by gravity (top of the 2750 kg/m^3 unit) was set at ~4 km depth on the main high, and at ~6 km in the eastern terrace. The top basement deepens to 10 km towards the Bjørnøya

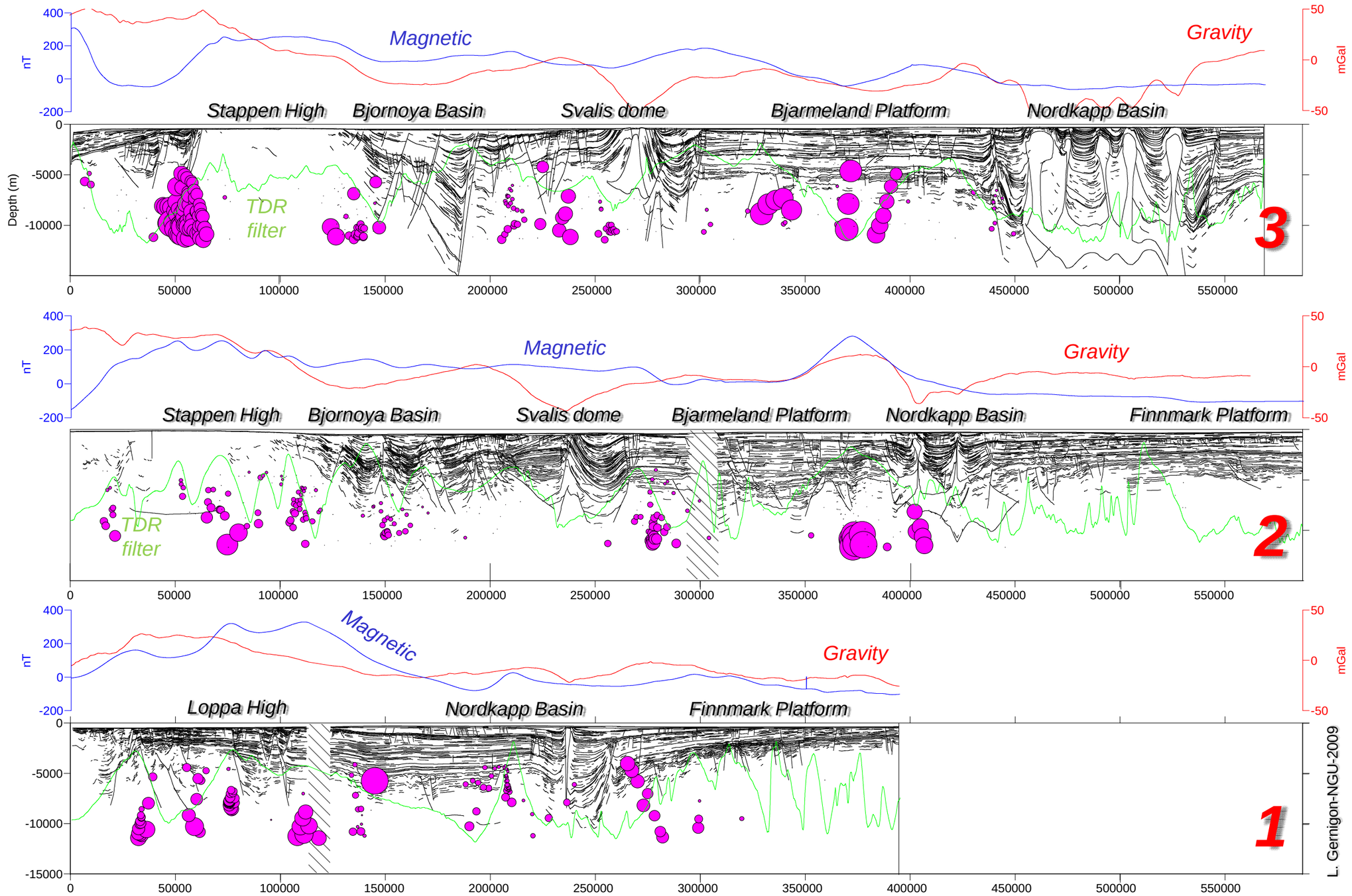

Figure 10.4 Line drawings of the three regional transects with free air gravity (red curve), TILT derivative filter (green curve) and the magnetic total field (blue curve) The figure also shows the solution plots of the Werner deconvolution applied along the magnetic anomalies, displayed along the three regional transects. The main clusters in pink colours are expected to indicate major magnetic contacts.

Fault Complex. On the Loppa High, we considered an upper crust/lower crust boundary (contrast between 2750 and 2950 kg/m³) at 15-16 km. Low-susceptibility values in the sediments cannot explain the dominant amplitude observed in the Loppa High region. The magnetic sources appear to be pre-Permian and are most likely part of the crystalline upper crust or near top basement. The magnetic signature requires high susceptibility values in the upper part of the basement. The long-wavelength magnetic anomaly in the vicinity of the Loppa High was modelled assuming two magnetic bodies in the upper crystalline crust beneath low-susceptibility sedimentary units (usually lower than 0.0001 SI).

After various tests, our modelling suggests that the 250–350 nT strong anomaly is induced by an upper crustal magnetic body with an average susceptibility of 0.085 SI and a remanence value of 0.5 A/m. At the current modelling stage, we simply assume that the induced magnetisation is dominant. The top of the magnetic body is situated at ~6 km depth underneath the eastern terrace and reveals a steep flank to the northwest. The western anomalies of the magnetic anomaly could be fitted with a magnetic body of relatively high susceptibility of 0.035 SI, which thickens to the west. The top of this magnetic block almost follows the shape of the magnetic anomaly at depths of 6–20 km and has a gentle slope in the southeast. Werner solutions also suggest cluster sources at around 6-10 km depth at the Loppa High and also suggest a lateral contact between the two main magnetic units (Fig. 10.4). The westernmost part of the Loppa High coincides with a thickening of the sedimentary section towards the Bjørnøya Basin which is almost non-magnetic. Carboniferous shallow intrusions of magmatic rocks, near top basement could partly explain some of the short-wavelength anomalies. Carboniferous mafic dykes are known from the island of Magerøya (Lippard & Prestvik 1997, Roberts et al. 2003) but these do not reflect a significant intrusive event and cannot easily explain such a regional magnetic feature. The pronounced magnetic signature and high susceptibility values of the magnetic units proposed in our model rather indicate massive and relatively thick, magnetic, crystalline and metasedimentary basement units. Near the coastline, the Fennoscandian Shield in that region is partly covered by Caledonian nappes, of which the Kalak, Laksefjord and Gaissa nappe complexes (Fig. 10.1) locally reach up to 5 km in thickness. In many of the nappes, the metasedimentary rocks are intruded by mafic dykes of Vendian and/or Late Devonian age. Major, mafic–ultramafic, plutonic complexes such as the Vendian-age Seiland Igneous Province (Roberts et al. 2006) are characterised by high susceptibility values (Olesen et al. 1990). A similar complex could most likely explain part of the magnetic signal. The regional magnetic feature produced by the Loppa High is also quite similar in size and amplitude to the signature produced by Precambrian crystalline complexes (e.g. Lofoten) and/or older basement such as the broad Transcandinavian Igneous Belt (TIB) along the western margin of the Svecofennian domain (Olesen et al. 1990, Skilbrei et al. 1992, Juhojuntti et al. 2001). In the Finnmark area the combination of Caledonian nappes overlying Archaen and Palaeoproterozoic terranes also locally produces broad and high-amplitude anomalies.

Between the Loppa High and the Nordkapp Basin, the 170 km long and 50-80 km wide Ottar Basin is striking NE-SW in the central part of the D9 transect. On conventional seismics it represents a relatively uniform platform (the Bjarmeland Platform), developed since Permian time (Fig. 10.5). The seismic data have limited pre-Permian penetration in this area, but there are several indications

that the basin may be deeper beneath the ~4-5 km-thick Permo-Cenozoic units. Breivik et al. (1995) also suggested the presence of a deeper Palaeozoic basin, as has already been discussed in Chapter 9.4.3. Our potential field modelling can confirm this idea and suggests the presence of relatively thick basins west of Norsel High. Major, regional, Late Carboniferous to Early Permian salt deposits are well known from the adjacent Nordkapp Basin and surrounding areas. In the Ottar Basin, a thick accumulation of evaporites is clearly suggested by the local domes and the highly reflective and chaotic seismic patterns observed underneath the Permian. Salt features in the Ottar Basin are particularly observed near the Norvarg Dome and the Samson Dome imaged by the D9 section (Fig. 10.5). The Samson Dome was apparently created by non-penetrative movements of deeply buried Upper Palaeozoic salt that do not pierce the Mesozoic units (Gabrielsen et al. 1990, Breivik et al. 1995).

The regional negative anomaly observed between the Loppa and the Norsel highs may be explained by a thick basin lying underneath the Permian unit. From seismic observation, further sedimentary successions underlying the Permian are to be expected (Gudlaugsson et al. 1998) but we do not know precisely the depth-to-basement or the nature of the basin infill. The main limitations are the lack of deep seismic imaging, proper velocity estimation and uncertainties about the average rock density to apply to the Upper Palaeozoic units where thick salt layers are present and exercise an influence on the average density values. Therefore, it is definitely reasonable to assume that there exist major evaporite deposits in the Ottar Basin, as proposed by Breivik et al. (1995). Modelling some medium gravity wavelengths should locally require low density polygons (between 2500 and 2600 kg/m³) even at depths of more than 5 km below sea level. Local negative anomalies of more than -15 mGal, with short wavelengths (15-30 km) could reflect shallow, sub-Permian, density variations inside the Ottar Basin (Fig. 10.5).

This is particularly obvious over the Samson Dome, which cannot easily be explained by sources deeper than 6-7 km. This might also correlate with Carboniferous salt layers. Earlier gravity modelling of the anomaly at the Norvarg Dome, north of D9, has already suggested the presence of a large mass deficiency due to salt below the Permian level (Breivik et al. 1995). Assuming the thickness of Permo-Cenozoic units at the present day (5-5.5 km) and the Cenozoic denudation in the western Barents Sea (> 1000 m) (Riis 1992), clastic and carbonate sediments should reach higher degrees of compaction and densities of approximately. 2700 kg/m³ (without the salt). Salt can, however, maintain a constant density of 2150-2200 kg/m³ even at such depths (Jackson & Talbot 1986). After it loses its effective porosity by 100-200 m of burial, the density of halite of 2.2 remains constant throughout the diagenetic realm and should be almost incompressible at depths of 6-8 km. Therefore, it can have much lower densities than carbonate or clastic sedimentary rocks expected at such depths. This could possibly be an explanation for the mass deficiency in the Ottar Basin. However, other observations suggest that salt could also have a slightly higher density of 2450-2500 kg/m³ if we agree with recent but controversial density versus depth estimations for salt in the Gulf of Mexico (Hudec et al. 2009).

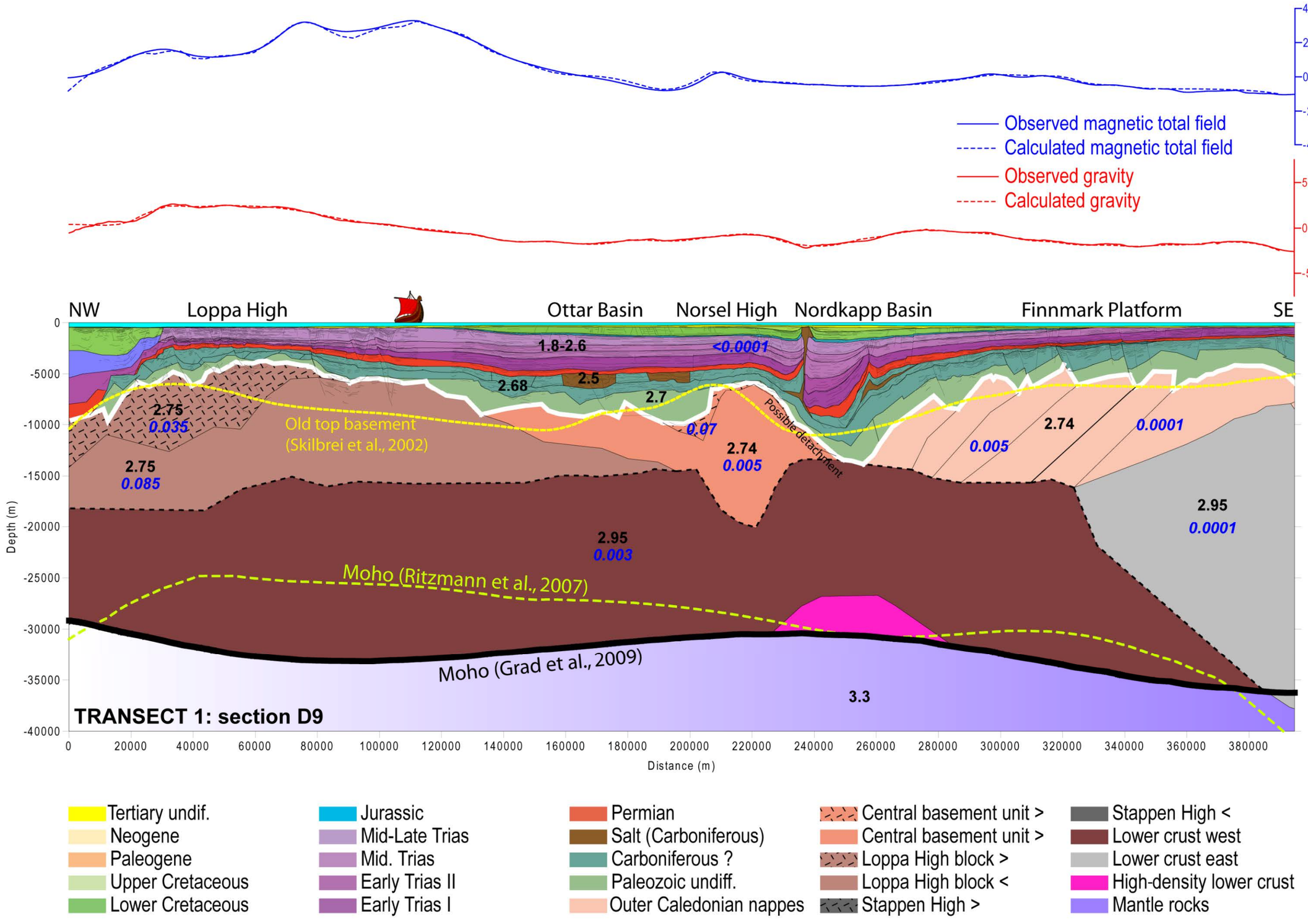

Figure 10.5 Interpretation and potential field modelling along transect 1.

It was not possible for us to acquire access to a similar density versus depth estimation for the Barents Sea, but if densities of the evaporite formations in the Ottar Basin are higher then we should think about deeper basement to fit the gravity signal. We tested all possible values between 2200 and 2500 kg/m^3. First, it was not possible to reproduce the shape of each anomaly using a simple low-density polygon between the top basement and the base Permian. If the density of the Upper Palaeozoic section was increased to 2600-2700 kg/m³ the depth of the basin became unrealistically large and the shape and amplitude of the gravity anomalies could no longer be well reproduced. The same problem was discussed by Breivik et al. (1995). They also tested different densities from 2450 to 2700 kg/m³ for the pre-Permian salt formations and showed that different depth variations of the saliferous basin can be proposed to model the same gravity response with uncertainties and differences of, in some cases, up to 3-5 km.

The new BASAR-08 survey provides, however, additional magnetic information tat has been used to better constrain and refine the basement depth estimation and consequently the maximum thickness of the pre-Permian deposits expected in the Ottar Basin. The Ottar Basin is bounded to the east by the Norsel High. The distinct magnetic anomalies at the level of the Norsel High require a shallow source. They have been modelled at a depth of 8 km by using upper magnetic basement units with a susceptibility of 0.06 SI overlying a crustal block with a susceptibility expected to be lower (0.005 SI) (Fig. 10.5). The main magnetic source at the Norsel High is assumed to be located close to the top crystalline basement and possibly developed on both flanks of the Norsel High as suggested by our modelling. It could represent either a thin, upper crystalline, magnetic unit or a magmatic intrusion emplaced close to a pre-existing top basement. The modelling suggests that the depth of the northeastern part of the Ottar Basin is not much greater than in the Samson Dome area, but it must be wider to accommodate the significant amounts of salt. For the Ottar Basin, we assume a lateral density variation from 2500 to 2650 kg/m³ in the upper pre-Permian layer. Our favoured result from modelling shows that the magnetic anomalies which are developed between the Samson Dome and the Norsel High require a magnetic basement at 5 to 9 km depth close to the Samson Dome. After various tests, we estimate that the Ottar Basin does not exceed 15 km in depth and we propose a top magnetic basement at an average depth of 8-9 km along the D9 profile. Nevertheless, we expect a maximum uncertainty of ± 2 km for this estimation.

We conclude and agree that the Ottar Basin represents a major Late Palaeozoic basin, comparable in dimensions and depth to the Nordkapp Basin. It is, however, slightly shallower along D9 and was negligibly reactivated during Mesozoic time. The dome and the low density expected at such a depth suggest a broad distribution of evaporites. However, deeper seismic and 3D modelling will be required to fit properly the gravity and magnetic signals and obtain a better approximation.

In the western part of the D9 transect, the Nordkapp Basin is one of the most notable Late Palaeozoic-Mesozoic rift structures in the West Barents Sea. Although the rift basin is several kilometres deep, in some places it is difficult to define the top basement exactly because of poor penetration of the seismic data and an overprint by salt diapirs. The clearest and most easily mappable boundary criterion is a marked increase in the dip of the top Permian reflector as it goes deeper into the basin. Evidence of a pre-Permian extensional tectonic phase is observed in many

locations in the Finnmark Platform and indicates the presence of half-graben features, probably situated above major Caledonian fault contacts. Locally, unconformities related to the onset of faulting are clearly observed. It has not been possible for us to correlate these unconformities between the different basin segments and obtain a precise age dating for this event (Carboniferous-older?). Taking into account the lack of stratigraphic control and the limited resolution of the seismic data, it is possible that the basin developed in more than one phase through repeated reactivation of the same fault systems (Gudlaugsson et al. 1998).

The thickening of Lower and Middle Triassic (Smithian-Ladinian) strata into the basin is clearly related to the diapiric rise of salt from the deeper parts of the basin (Nilsen et al. 1995). The salt layer was deposited in the platform areas surrounding the Nordkapp Basin near the Carboniferous-Permian transition and may have contributed to the formation of the marginal salt pillows (Nilsen et al. 1995). The diapirs developed, however, mainly from a much thicker salt layer in the central part of the basin itself.

Between the Norsel High and the south Nordkapp Basin, the Nysleppen Fault Complex consists of normal faults with large downthrows to the southeast. The southern Nordkapp Basin is characterised by a noticeable asymmetry along the seismic profile D9, which is also suggested by the modelling with an increasing thickness of Palaeozoic and Mesozoic sedimentary rocks towards the southeast (Fig 10.5). On the southeastern side, the Finnmark Platform basement dips into the basin from 4 km to an estimated maximum depth of 10-12 km and synthetic faults are observed.

Although the data quality is poor, the basin seems to be a large half-graben, developed by a north-westward rotation against a basin-bounding crustal detachment fault (e.g. the Nysleppen Fault Complex) with the deformation of the hanging wall being taken up by a set of NW-dipping, synthetic normal faults locally decoupled in the salt (Fig 10.5). Along the southeastern flank of the Nordkapp Basin, which has a pre-Permian origin, the entire Upper Palaeozoic sedimentary succession down to the basement is locally imaged in the seismic data and extrapolated by means of the potential field modelling. The Palaeozoic successions show a continuous increase in thickness towards the basin flanks and are probably present in the central part of the southern Nordkapp Basin.

Even if salt can seriously influence both the seismic and the gravity signatures, the regional gravity low in the southern Nordkapp Basin should require a crustal and/or mantle compensation at depth; otherwise the gravity low would be more pronounced. Assuming that the Moho of Grad et al. (2009) is correct, the modelling of the southern Nordkapp signature should require a high density lower crust (2950 kg/m^3) at a shallow level (11 km) underneath the main basin depocent. Consequently, our model considers thinner pre-Permian formations at the northeastern flank of the southern Nordkapp Basin. In such a case, the top lower crust would most likely coincide with the maximum depth of the crustal detachment also expected at that level. This model could explain the northwestern dip of the pre-Permian sequences observed on the Finnmark Platform. Alternatively, the gravity low could also coincide with a less dense upper crust and/or a narrow mantle upwelling (if we consider Airy isostasy) or all intermediate solutions. Breivik et al. (1995) proposed such a model but considered a calculated isostatic Moho assuming Airy conditions. At this stage of the

modelling, we only rely on the last seismic Moho compilation of Grad et al. (2009) which does not allow us to detect such a narrow mantle upwelling but instead a broad one, which coincides with the large sag system developed between the Finnmark Platform and the Loppa High. The uppermost Carboniferous to Lower Permian section refined by the modelling shows that the western Barents Sea has the character of a regional sag with major depocents in the Nordkapp and Ottar basins separated by the Norsel High to the east and the Loppa High to the west. The shape of this sag basin gives an indication of the magnitude and distribution of the underlying rift basins.

10.4.2 Transect 2: Profile D1 from the Finnmark Platform to the Vestbakken Volcanic Province

Transect 2 runs NW-SE from the Vestbakken Volcanic Province to the Finnmark Platform. This transect also illustrates major structural features of the West Barents Sea including, from west to east: the Stappen High, the northern Bjørnøya Basin, the Fingerdjupet Basin, the Svalis Dome, the Norsel High and the Southern Nordkapp Basin (Fig 10.1). The Moho depth along the transect was extracted from the regional grid of Grad et al. (2009). Transect 2 is sub-parallel to IKU Line A, which also provides information about the deep structures. Transect 2 runs almost parallel to transect 1 over a distance of approximately 50 km.

The southeastern part of transect 2 maps the offshore prolongation of the Caledonian nappes, also interpreted farther south on transect 1. The same properties have been used to model the Caledonian nappes. The Finnmark Platform is characterised as the lowest magnetic region compared to the northwestern magnetic province. To adjust the model response to this lowmagnetic province with long magnetic wavelengths, we considered different properties for the lower to middle crust. Compared to the northwestern magnetic province, higher remanence values (0.5-1 A/m) were proposed in the mid-lower crust to fit the magnetic signature. It may eventually represent different terranes affected by the Timanian orogeny and/or older Proterozoic events.

To the west, the southern Nordkapp Basin has been modelled in a similar manner to that of profile D9. We also considered a shallow, high-density, lower crust underneath the deep Palaeozoic basins, controlled by a major SE-dipping low-angle detachment. Because of its location along the Nysleppen Fault Complex, it is reasonable to explain the older and more significant tectonic phase as resulting from a footwall uplift of the Norsel High coevally with the development of the southern Nordkapp Basin in the hanging wall. The shallow lower-crustal exhumation could be associated with an early crustal exhumation phase (possibly a post-orogenic metamorphic core complex?) in Devonian-Carboniferous time, and later reactivated in the Late Paleozoic and Mesozoic.

The Norsel High has a characteristic high gravity and magnetic signature. It is associated with a positive gravity anomaly of more than 20×10^{-5} m/g^2 and a strong magnetic anomaly of 280-300 nT. A marked angular unconformity separates a thin cover of relatively flat-lying, Upper Palaeozoic, sedimentary strata from an underlying unit exhibiting internal layering dipping steeply towards the northwest. The unconformity is an erosion surface corresponding to the top basement, and has been confirmed by drilling (Gabrielsen et al.1990).

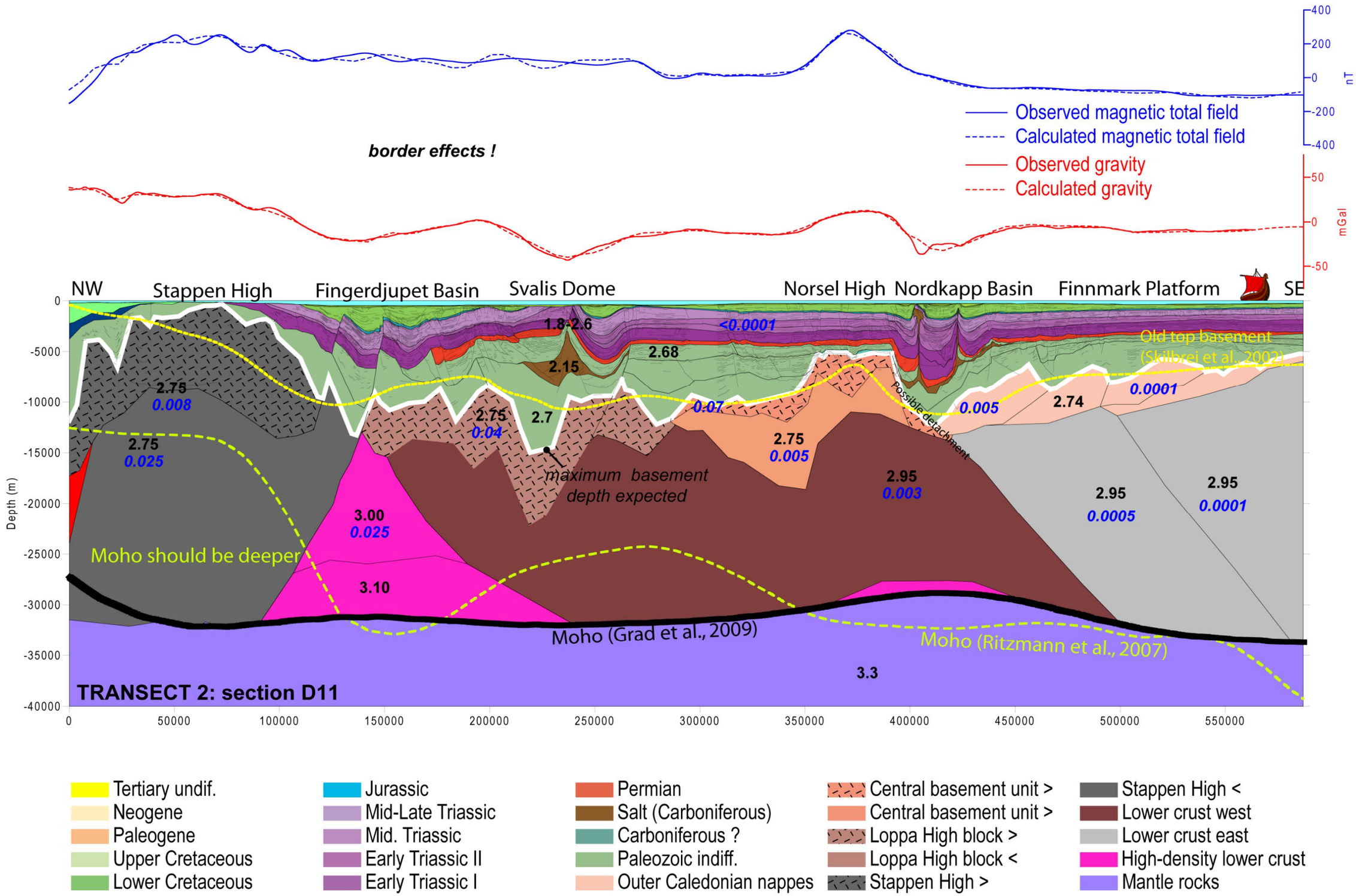

Figure 10.6 Interpretation and potential field modelling along transect 2.

The gravity anomaly which represents the outline of the Norsel High requires shallow, high-density material and the main anomaly has been obtained by setting the 2750 kg/m³ top layer at ~5 km depth along transect 2. Like transect 1, the Norsel High magnetic anomaly has been obtained by assuming a shallow magnetic unit (with a susceptibility of 0.07 SI) lying on top of the basement high. To some extents this magnetic unit could extend into the southern Nordkapp Basin and can explain the stronger magnetic signal observed in the northeastern part of the basin. This magnetic layer could represent a magnetic Caledonian unit or later intrusions possibly controlled by the pre-existing detachment, if we assume the presence of a metamorphic core complex.

The occurrence of salt diapirs in the Nordkapp, Ottar and Maud basins also proves the presence of several Late Palaeozoic, evaporitic sub-basins in the Barents Sea. The Svalis Dome in the southwestern part of the Maud Basins is crossed by transect 2 and is associated with a clear negative gravity anomaly of more than -40/-50 mGal. A less negative anomaly (-30 mGal) indicates that immobilised salt may be present farther north in the basin. The pronounced gravity low signature is partly explained by the thick salt formation with low density (set to 2150 kg/m³) but might also require deeper Palaeozoic sediments beneath. The basement depths could reach a maximum of 10-13 km if we assume a density of 2700 kg/m³ for the lower Palaeozoic sedimentary unit. The Svalis Dome consists mostly of pre-Permian salt originally deposited as a thick layer west of the Mercurius High (Bugge & Fanavoll 1995). The magnetic pattern also suggests that the Svalis dome was developed in a complex structural setting with the main Carboniferous depocent probably formed in a kind of pull-apart basin system which probably initiated north of the Loppa High. The magnetic pattern on the northern Loppa High and west of the Mercurius High is relatively similar and could suggest similar terranes displaced by a regional shear zone. This shear zone probably acted as a relay ramp during the Caledonian orogeny and possibly reactivated in a strike-slip system in Devonian-Carboniferous time as suggested by our tentative reconstruction of the magnetic pattern (Fig. 10.6).
According to our modelling, the prolongation of the Mercurius High coincides with a basement high located at 8-9 km depth. An eastward-dipping reflection pattern within the Mercurius High has been observed by Gudlaugsson et al. (1998). The geometric relationship with the Hoop Fault Complex, which marks the western boundary of the high, indicates that the high is cored by higher density material as suggested by our modelling.

Close to the Mercurius High, the Swaen Graben could also coincide with a change of magnetic basement. We also note that the Swaen Graben is developed along the NW-SE regional trend which likely represents a regional crustal contact. According to Gudlaugsson et al. (1998), the configuration of the Swaen Graben may indicate that it was caused by tensional forces in the post-Carboniferous sedimentary succession originally induced by the formation of the large salt domes. Alternatively, we think that the Swaen Graben could also have initiated by salt dissolution and collapse.

Northwest of the Svalis Dome most of the deformation is pre-Permian, but the thickening of the Permian, Triassic and Cretaceous sequences towards a fault system also indicates extensive deformation during those periods. Both Carboniferous and Permian fault movements occurred on

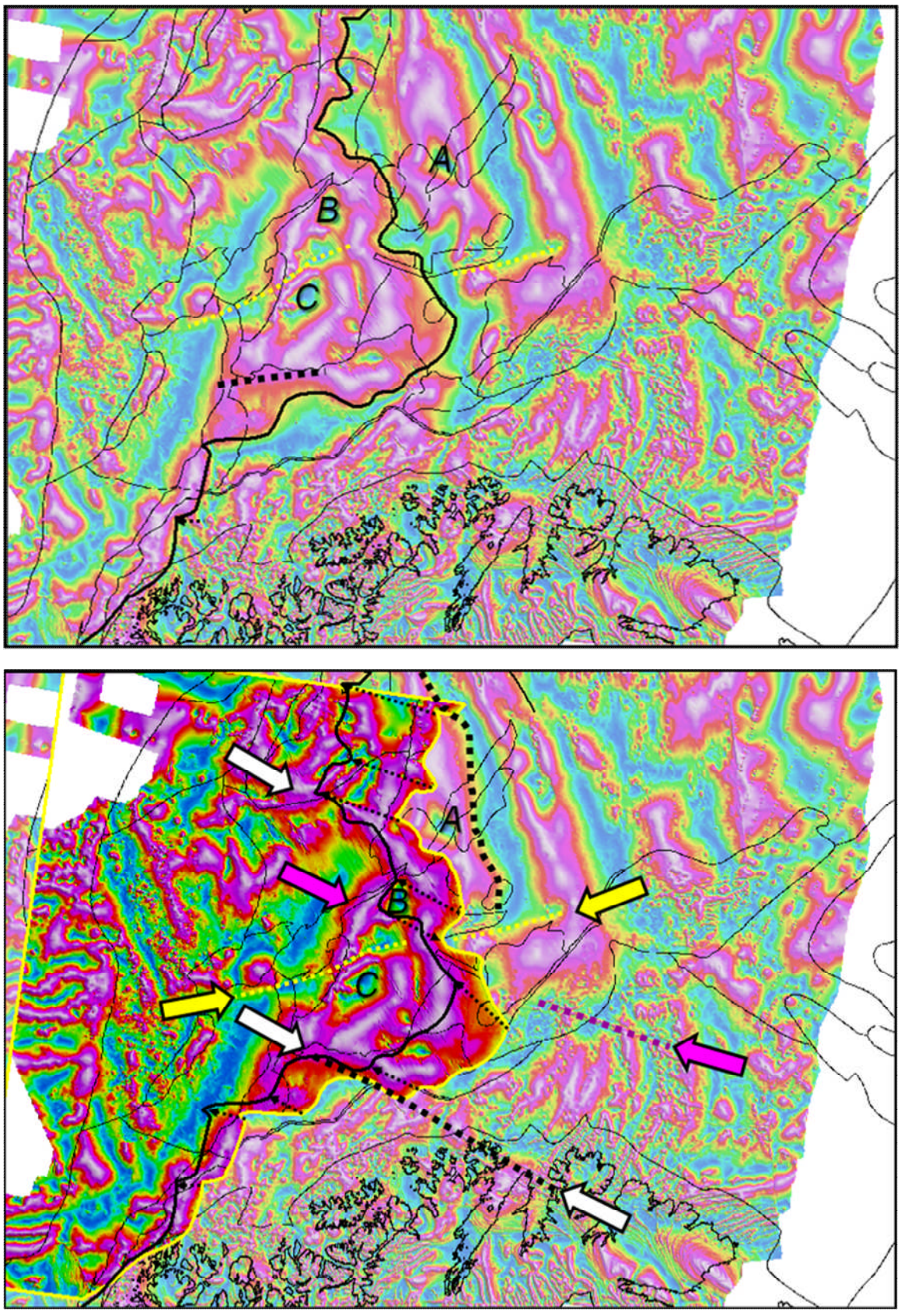

Figure 10.7 Tentative reconstruction of the tilt derivative (TDR) magnetic pattern if one considers a slight rotation of the Loppa High Block leading to a progressive (mostly Palaeozoic) extension from the Hammerfest Basin towards the Ottar Basin characterised by low TDR values. After reconstruction, the TDR pattern north of the Svalis Dome (A) seems to be similar to the northern Loppa High anomalies (B). A link between the Norsel High and south Loppa High could also be expected. The model also suggests that strike-slip deformation occured north of the Loppa High (between A and B).

Bjørnøya Island located to the east of the Stappen High (Worsley et al. 2001). Significant Late Palaeozoic and Mesozoic extension also occurred in the Fingerdjupet Basin, as shown by the seismic profile D11. Basement blocks on transect 2 indicate extension in the order of 10 - 15 km on basin-delimiting, listric normal faults with downthrows towards the northwest. The basin developed as a westward-tilted half-graben in the hanging wall of this fault and is bounded to the southwest by a intra-basinal horst. The position of the horst appears to be controlled at depth by an eastward-tilted basement block, marking a shift in the polarity and characterising the eastern flank of the main western rift basin farther south. This also confirms the presence of a major crustal boundary north of the Loppa High, as suggested by the magnetic pattern.

The main west-dipping fault in the Fingerdjupet Basin (the Leidjupet Fault) coincides with a major crustal boundary and limits the Stappen High domain to the west (Fig. 10.6). This limit coincides with a gravity low and requires higher density material at depth (3000-3100 kg/m^3), as also suggested in the Bjørnøya Basin (Fig 10.6). This high-density material could either represent pre-existing crustal material and/or anomalous crust or altered mantle rocks formed during the significant thinning phase of the Bjørnøya and Fingerdjupet Basin. To the west, the Stappen high is interpreted, like the Loppa High, as a thick, independent crustal block. Carboniferous and Permian fault movements occurred on Bjørnøya (Worsley et al. 2001) but the main thinning deformation at the crustal scale mostly developed in the eastern part of the Bjørnøya Basin and to the west along its sheared margin, leading to the final breakup in the Cenozoic. In such a context, the Loppa High is interpreted as a regional ribbon microcontinent poorly affected by crustal thinning.

Being aware that there are large Moho uncertainties in that area, the Stappen High is characterised by a lower density in the lower crust and the magnetic signature was obtained assuming two magnetic units: 1) an upper unit with higher induced magnetisation (0.09 SI) and 2) a lower unit with lower magnetisation (0.025 SI). If we consider the shallow Moho as proposed by the Barents50 model of Ritzmann et al. (2007), it is impossible to fit the gravity signal. The new version by Grad et al. (2009) appears to be more consistent with our potential field interpretation.

10.4.3 Transect 3: Profile MN89-202 from the outer Finnmark Platform to the Vestbakken Volcanic Province

The third transect MN89-202 runs WNW-ESE and is almost sub-parallel to the D11 transect. The transect MN89-202 illustrates the Vestbakken Volcanic Province, the Stappen High, the northern part of the Bjørnøya Basin, the Svalis Dome, the Bjarmeland Platform, the central Nordkapp Basin and the outer Finnmark Platform close to the disputed area between Norway and Russia (Fig.10.1).

Basically the same characteristics and concepts previously discussed for transect 2 can be applied to transect 3. Similar units and petrophysical properties have been proposed to fit the gravity and magnetic signal (Fig. 10.7). As previously, we also suggest different properties for the middle and lower crust between the western magnetic province and the eastern low-magnetic province. We consider a major crustal change at the level of the Nordkapp Basin where NW-SE magnetic trends swing towards the north. The meaning of the deep crustal change is unclear but could be related to

the old Precambrian geological evolution of the margin and/or represent the western extent of the Timanian terranes, which are well documented on the Russian side of the Barents Sea (Roberts & Siedlecka 2002, Roberts & Olovyanishnikov 2004, Gee et al. 2008). A magnetic kink is observed at the level of the northern Norsel High and suggests that the transition between the southern and central Nordkapp Basins represents a major NNW-SSE crustal boundary as previously suggested by Gernigon et al. (2007). New trends are now observed with the latest magnetic survey and suggest a more complex crustal and basinal architecture of the Nordkapp Basin, clearly divided into magnetic segments.

The western part of the central Nordkapp Basin is characterised by a lower magnetic domain compared to its eastern and southern parts, which correlates with the minimum of the negative Bouguer gravity anomaly in the central Nordkapp Basin (Fig. 10.8). However, the eastern part represents a narrower graben, where more linear and elongated magnetic trends are observed. The variable structural style of the Nordkapp Basin from southwest to northeast and the contrasting E-W magnetic pattern of the Nordkapp Basin can be explained by an interaction between rift deformation affected by oblique, pre-existing deep features and/or pre-existing grabens. NNW-SSE trending magnetic anomalies extend from the Bjarmeland Platform to the central Nordkapp Basin and probably characterise an old basement or Palaeozoic features, which influenced the graben architectural development during successive rifting episodes. The NNW-SSE magnetic trends may also coincide with the northwestern prolongation of similar trends observed on the Tiddlybanken Basin, possibly influenced by older Timanian structures. These trends are definitively perpendicular to the main gravity trend that characterises the whole of the Nordkapp Basin and its Mesozoic rift history.

The NNW-SSE-trending magnetic anomalies could represent the trends of old Palaeozoic basins influenced by the interaction of Caledonian and older Timanian trends before the subsequent rift-induced dislocation and segmentation in Mesozoic time (Gernigon et al. 2007b). Our modelling also suggests a deepening of the top basement from the eastern to the western part of the central Nordkapp Basin, confirming that the crustal architecture varies laterally in the Nordkapp Basin area (Fig. 10.8).

To the west, a northern prolongation of the Norsel High is suggested by a basement horst feature with a top observed at 8-9 km depth. Farther to the west of this horst, a NNW-SSE magnetic anomaly coincides with a thick Palaeozoic basin. The presence of the Norvarg Dome to the south and along the same trend also suggests the presence of non-mobilised salt in this area. We can therefore expect lateral density variations as previously discussed. Assuming a Palaeozoic rock density of 2680-2700 kg/m^3, the basin could reach significant depths (13-15 km). If massive salt is present, the basin could be even deeper.

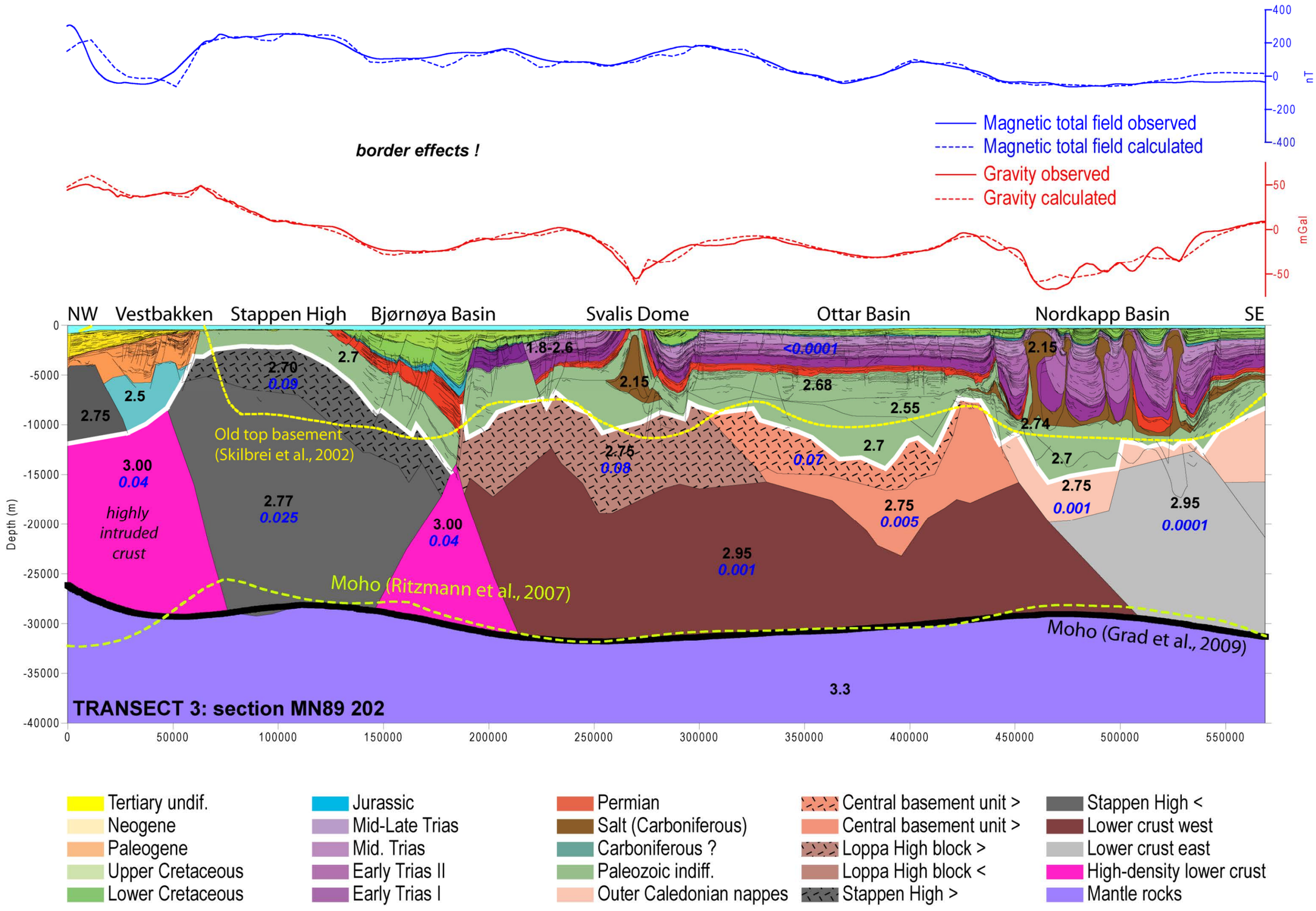

Figure 10.8 Interpretation and potential field modelling along transect 3.

11 3D DENSITY AND MAGNETIC CRUSTAL CHARACTERISATION

Jörg Ebbing & Cécile Barrère

11.1 Introduction

We evaluate and update the top basement geometry and crustal characterisation given by Barrère et al. (2009a) for the new BAS-06 and BASAR-08 survey data. We will do this by applying the geometry of the complete 3D model, which will be presented briefly as an introduction for the new data.

Barrère et al. (2009b) modified the top basement from Skilbrei (1991, 1995), making use of a significantly improved seismic coverage (e.g. Breivik et al. 2005) and an improved aeromagnetic and gravity database (e.g. Olesen et al. 2009). Barrère et al. (2009a) presented also a characterisation of the basement lithology. The structure of the western Barents Sea shelf has a complex history imprinted in the basement structure and lithology. Using the petrophysical data from onshore Norway and following magnetic lineations from onshore to the Barents Sea, a division into different basement blocks can be made (Barrère et al. 2009a, b) in the western Barents Sea.

11.2 Modelling Concept

The SW Barents Sea margin has been studied by 3D modelling integrating a wealth of geophysical data: seismic profiles, commercial and scientific drilling on the shelf and mainland Norway, petrophysical sampling and a dense coverage of gravity and aeromagnetic data. Magnetic depth estimates provide a good starting point for a genuine structural interpretation (e.g. an interactive modelling or a constrained inversion). Skilbrei et al. (1991) and Mørk et al. (2002) showed that the susceptibilities of the basement can range between 0.005 and 0.035 SI, whereas the susceptibilities of the overlying sedimentary rocks are only in the order of 0.0003 SI, some one to two orders of magnitude lower. The range of susceptibilities for the basement is depending on composition and varies from 0.005 to 0.01 SI for Caledonian basement, 0.01 to 0.035 SI for Precambrian basement, to even higher values for mafic intruded basement (e.g. Ebbing et al. 2009, Barrère et al. 2009a). Therefore, magnetic data are extremely useful for estimating the depth to top basement.

For the 3D modelling the IGMAS software (Götze and Lahmeyer, 1988) has been used. Within IGMAS the geometry is defined along parallel vertical cross-sections (white solid lines, Fig. 11.1). In our model, line spacing is ranging from 10 to 20 kilometres depending on the complexity of the modelled structures. The geometry is automatically triangulated between the sections defining the 3D geometry. The gravity and magnetic fields are then calculated and the resulting field compared with the observed potential field.

Magnetisation of crustal rocks is mainly related to the magnetite content in the bedrock, e.g. sedimentary rocks can be considered non-magnetic relative to basement rocks. The Curie temperature of magnetite is 580ºC and at this temperature rocks lose their ability to remain magnetised. Assuming a normal thermal gradient, the Curie temperature is located in the deep crust (e.g. Ebbing et al. 2009). Therefore, we can limit the extension of magnetic sources to the crust. Magnetic field calculations require the definition of an external magnetic field. We define the normal inducing magnetic field with a field-strength of 53,300 nT, an inclination of 79º and a declination of 4.3º. We can also use the true magnetic field over the study area, which improves the results slightly, but increases substantially the computation time. Therefore, we use a constant magnetic field and the remanent magnetisation is modelled parallel to the induced magnetic field.

To establish a 3D model, information about the geometry and density/magnetisation of the crustal rocks is needed. These parameters are described in the following section.

11.3 DATA

The Bouguer anomaly map (Fig. 11.1a) is calculated from the Free-air gravity compilation by Skilbrei et al. (2000). A simple Bouguer correction at sea was carried out using a bathymetric grid with a resolution of 2000 m and reduction densities of 2200 kg/m³ and 2670 kg/m³ for the offshore and onshore, respectively. The applied bathymetric data are based on the International Bathymetric Chart of the Arctic Ocean (IBCAO) (Jakobsson et al. 2000) combined with the GTOPO30 grid (onshore data) (http://edc.usgs.gov/products/elevation/gtopo30/dem_img.html), with resolutions of 2.5 and 1 km, respectively.

Aeromagnetic data are available from a magnetic compilation (Fig. 11.1b) of the western Barents Sea by Olesen et al. (2009). The dataset is compiled from reprocessed aeromagnetic surveys and line spacing ranges from 0.5 to 2.5 km over mainland Norway and from 3 to 10 km over the continental shelf.

11.3.1 Petrophysical data

Densities of the sedimentary layers are based on well data (Tsikalas, 1992) and tables published by Ritzmann et al. (2007) based on velocity-density relationships of sedimentary units obtained from the seismic refraction and reflection/gravity studies. Bedrock densities are based on direct onshore sampling and laboratory measurements (Olesen *et al.* 1990, Galitchanina *et al.* 1995).

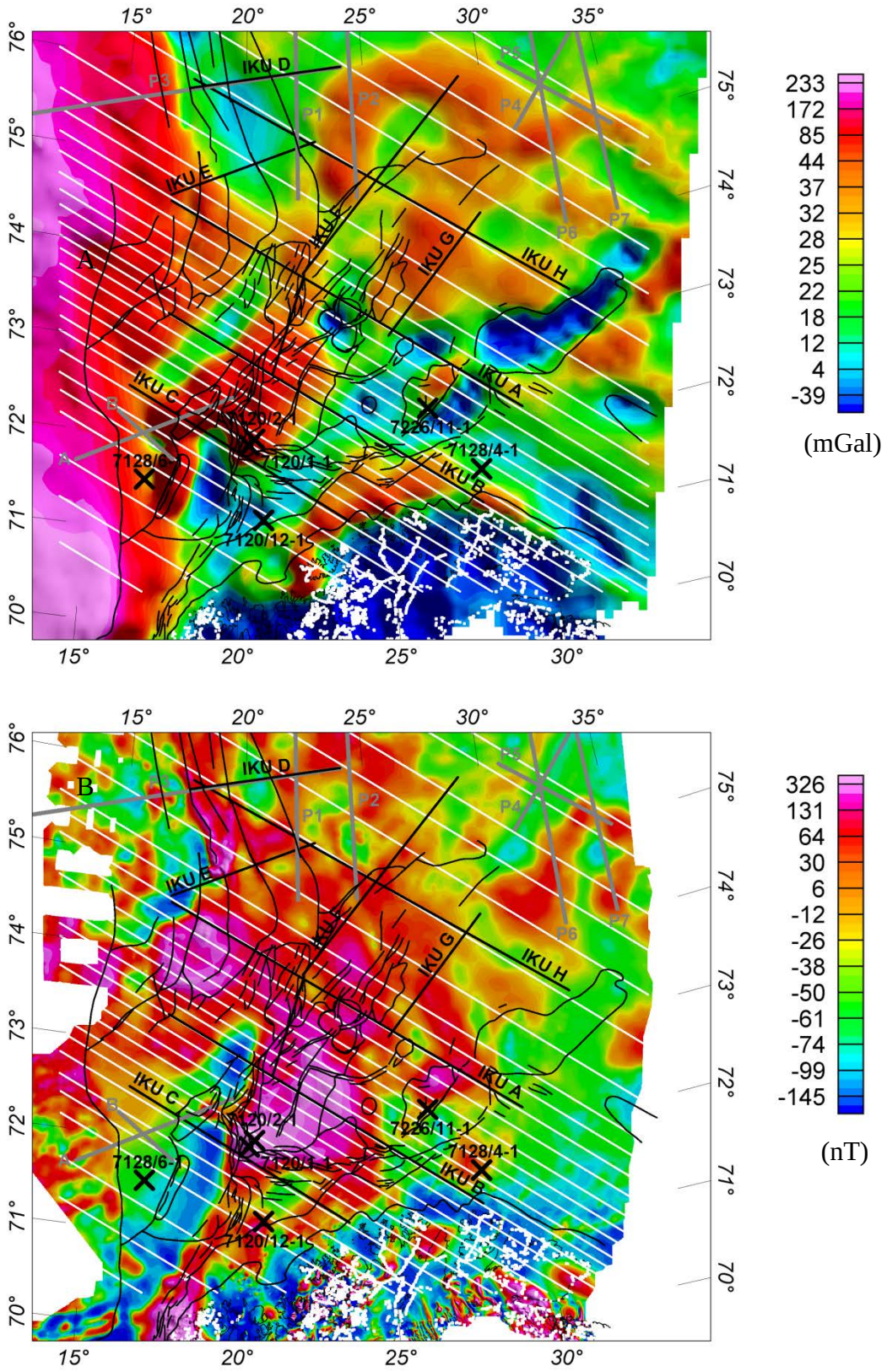

Figure 11.1 a) Bouguer anomaly map and b) original total magnetic field anomaly map used for the modelling (reduced to the pole). White lines indicate the vertical planes defining the 3D model, thick grey lines show wide-angle data, thick black lines the IKU deep-seismic reflection data, black crosses the wells reaching the top basement. Locations of petrophysical samples are given by white dots.

Deep crustal densities are based on published values from refraction models (Breivik *et al.* 1998, Breivik *et al.* 2002, Mjelde *et al.* 2002, Breivik *et al.* 2003, Breivik *et al.* 2005) inferred from velocity-density relationships and gravity modelling. The density errors from the velocity-density relations are in the order of ±50 kg/m³ and ±100 kg/m³ for the upper and deep crustal layers, respectively.

For the magnetic field, the magnetic susceptibility and remanence from the magnetic modelling along the deep IKU lines A, B and C by Barrère et al. (2009a) were used as initial parameters. Those values were derived from onshore and offshore samples from the Troms and Finnmark regions (Olesen et al. 1990; Slagstad et al. 2008). Q-ratios (the relationship between remanent and induced magnetisation) were adapted according to the petrophysical data and modified during the modelling. We set a homogeneous and low Q-ratio for the lower crust and mantle of Q=0.4 and a magnetic susceptibility of $1000 \cdot 10^{-5}$ (SI). Sedimentary rocks are set to 30×10^{-5} (SI) as they are very low-magnetic in comparison to the basement rocks.

11.3.2 Geometric constraints from seismics

To constrain the sedimentary layers we obtained access to three, industrial, depth-converted, seismic horizons: top Tertiary, base Cretaceous and top Permian. These horizons were produced by depth-conversion of seismic horizons using regional velocity laws calibrated by well data. The sedimentary rocks are thus subdivided into four sedimentary units: Cenozoic, Cretaceous/Jurassic, Triassic and Palaeozoic. Six wells (black crosses, Fig. 11.1) reach the top basement in the southwestern Barents Sea region; they were used to calibrate the modelled top basement and check the reliability of the depth-converted seismic horizons.

We set up our initial crustal structure using the Barents50 model (Ritzmann et al. 2007). The Barents50 model is a seismic-velocity model of the crust in the Barents Sea with a lateral resolution of 50 km (Fig. 11.2) which also provides information along all available regional seismic profiles with 25 km sampling. The Barents50 model is based on 2D wide-angle reflection and refraction lines, passive seismological stations and, to a limited extent, potential field data (Ritzmann et al. 2007). The Barents50 compilation also provides information on the deep structure of the crust. For the crust, this compilation includes an intra-crustal horizon inferred mainly on the basis of velocity models and 2D gravity modelling because crustal reflectivity does not allow clear imaging from seismic data alone (e.g. Breivik et al. 2005).

The IKU deep seismic reflection profiles and the seismic refraction data (Mjelde *et al.* 2002, Breivik *et al.* 2002, 2003, 2005) were used to constrain the crustal structure of our model. The upper-lower crustal boundary varies between 20 and 22 kilometres depending on the reflectivity along the IKU profiles and the seismic velocities from refraction seismic lines.

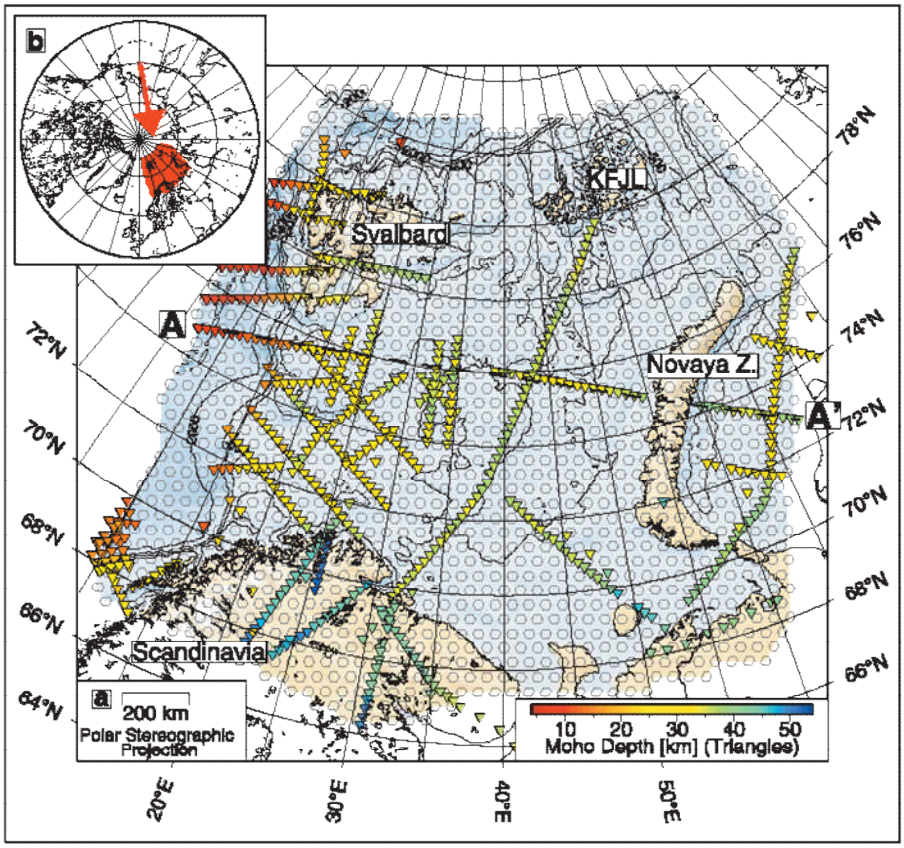

Figure 11.2 Presentation of the spatial resolution of the Barents50 and the utilised seismic profiles (in colour) (Ritzmann et al. 2007).

A recent OBS profile (Clark et al. 2009) has been used in the final step of the modelling. This profile is running along profile IKU-B, but is extended in the north-west and south-east, and includes stations located onshore Norway.

11.4 Modelling results

The final differences between the measured and modelled gravity anomalies have a standard deviation of less than ±6.8 mGal. This value is slightly higher than the accuracy for the gravity data, but the remaining mismatch can be explained largely as being related to local structures below the resolution of our model (e.g. salt domes). The short-wavelength anomalies (<10 km) onshore have not been modelled and subsequently create local deviations from the modelled Bouguer anomalies.

The general pattern is comparable between the observed and the modelled magnetic anomalies. The 100-200 km wavelength anomalies linked to basement topography are relatively well explained by the model compared to the short-wavelength (<100 km) anomalies linked to intra-basement magnetic sources and/or shallow magnetic sources. Because of our simplified settings, the magnetic modelling is representing the general magnetic gradients but not the absolute magnetic field amplitudes.

11.4.1 Modelled densities

The different crustal units in the model are presented in table 11.1 and figure 11.4a. To produce Moho depth compatible with the computed isostatic Moho and the seismic Moho (Ritzmann et al. 2007), a lower crustal body (LCB) had to be introduced over the central part of the SW Barents Shelf with a density of 3100 kg/m³ (compared with 2950 kg/m³ for the surroundings).

11.4.2 Modelled susceptibilities

The top of the magnetic sources is assumed to be the top basement and the top of the oceanic basalts obtained by density modelling, for the continental and oceanic crust, respectively. Due to the resolution of the model and lack of constraining data, no intra-basement magnetic sources are distinguished. The resulting magnetic modelling therefore highlights the main changes in magnetic properties of the upper crust.

The final model shows a variation of the upper crustal magnetic susceptibility values from $500 \cdot 10^{-5}$ to $5000 \cdot 10^{-5}$ SI.

			Density (kg/m³)	Magnetic properties	
				Q-ratio	Susceptibility (10^{-5} SI)
lower crust	standard lower crust		2950	0.4	1000
	LCB High-density body		3100	0.4	1000
oceanic crust	basalt		2950	1	2000
upper crust	onshore zone	BAS1 onshore Fennoscandian Shield	2700-2750	0.5	1000
		Caledonian nappes – CN	2750	1	500
	coastal zone	UCB high-density body	2810-2850	0.5	1000
	Loppa High zone	BAS1 Loppa High (south & west)	2750	0.6	4000
		BAS1 Loppa High (east & north)		0.5	3000
		Stappen High (south)	2850	0.5	3000
	COT zone	MB1 Hornsund area	2850	0.5	1000-5000 3000
		Sørvestsnaget Basin	2850	0.5	
		MB2 Harstad Basin	2860	0.5	4000
		MB2 Vestbakken Volcanic Province	2850	0.5	3000
	eastern zones	BAS2 North of Nordkapp Basin BAS2 South of Nordkapp Basin	2820 2820	0.5 0.5	2000 1000
		MI (Norsel High, N-E Loppa High)	2750	0.6	3000
	northern area	BAS2 Stappen High North	2750	0.5	3500
		BAS2 central area		0.7	1500

Table 11.1 Modelling parameters: different crustal units are defined by a combination of petrophysical values obtained by density and magnetic modelling. Figure 11.4a shows the location of the different basement units.

a) Bouguer anomaly and density distribution

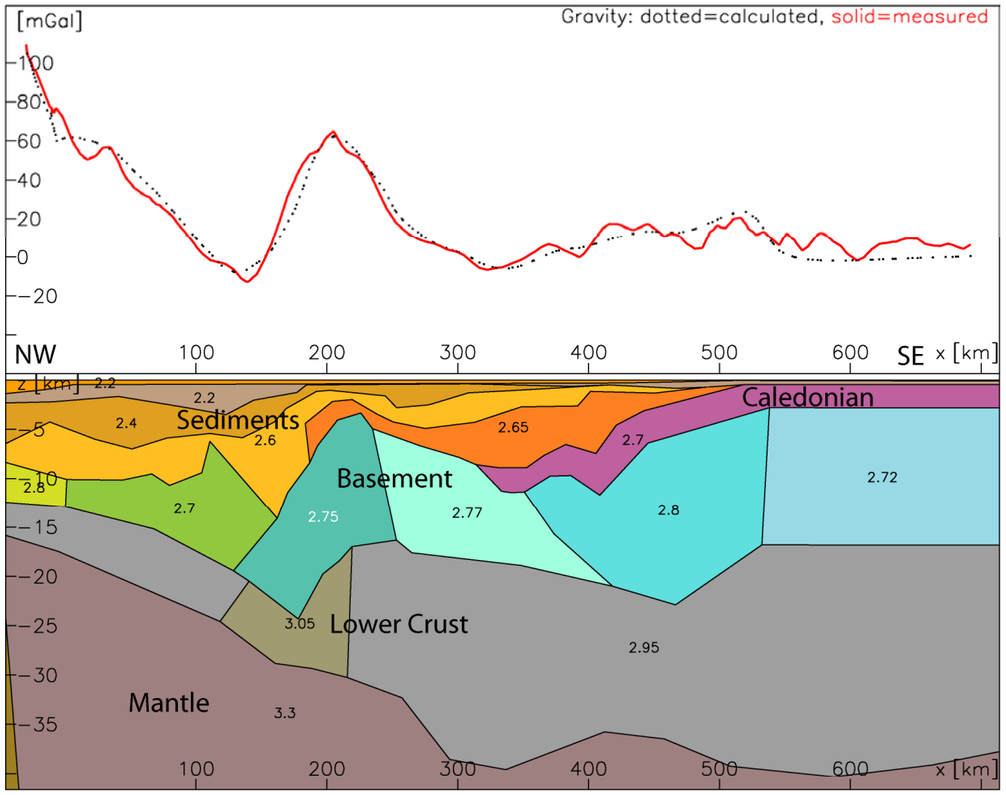

b) Line drawing of IKU-B

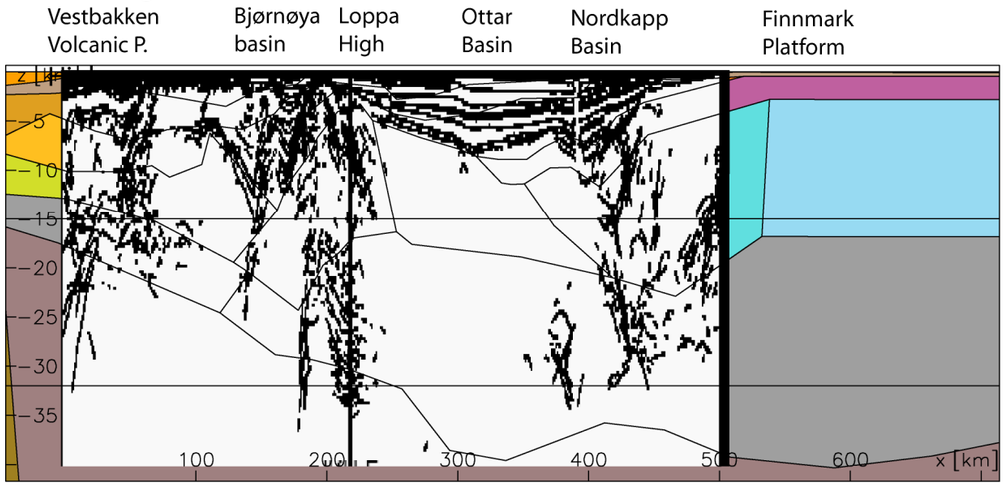

c) Induced magnetic field and sucseptibility distribution

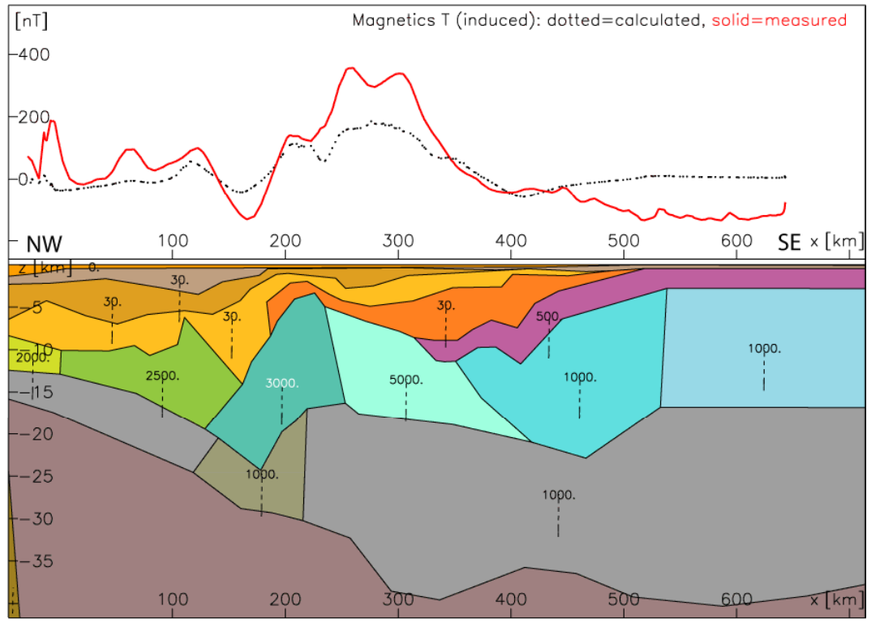

d) Induced and remnant magnetic field and Q-ratio distribution

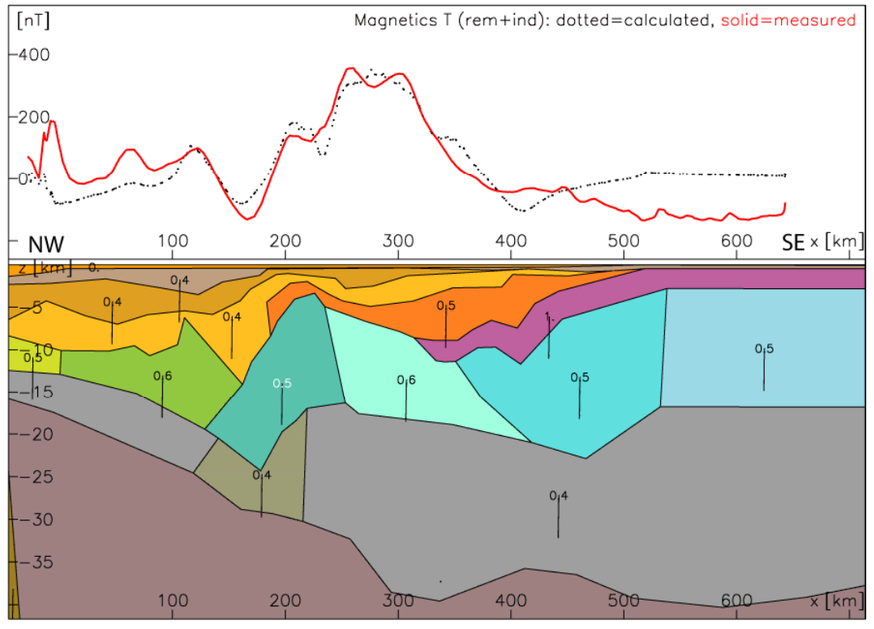

Figure 11.3 NW-SE orientated cross-section through the SW Barents Sea along profile IKU-B and Petrobar-07. a) Density structure and modelled Bouguer anomaly. Densities are given in kg/m³. b) Reflectivity of the seismic profile IKU-B for comparison, c) Modelled induced magnetic field and susceptibility distribution (10^{-5} SI), d) Modelled remanent and induced magnetic field and Q-ratio distribution for the model. Remanent magnetisation has to be included in the modelling to match the observed anomalies. The direction of the remanent magnetisation is parallel to the induced field (inclination: 79°, declination: 4.3°).

11.4.3 3D configuration

Our 3D model allows us to present key elements of the southwestern Barents Sea crustal architecture. Figures 11.4 and 11.5 show the top basement depth, distribution of basement units, Moho depth and crustal thickness as defined in the 3D model.

11.4.4 Depth to top basement

The extension of the top basement map is limited by the transition to the Norwegian-Greenland Sea, as indicated by the Senja Fracture Zone. To the east, the compilation ends at the transition between the Norwegian and Russian sectors of the Barents Sea, where seismic data are sparse and where the transition occurs from the Mesozoic rift basins of the western Barents Sea to the deep eastern Barents Seabasins.

The density contrast between the basement and Palaeozoic sedimentary rocks is at least 50 kg/m³ (Fig. 11.3, Table 11.1). The top basement (Fig. 11.4a) in our model is also the top of the magnetic sources, as sedimentary rocks are considered relatively non-magnetic. Over large parts of the shelf, the top basement is located at depths between 4 and 10 km. The shallowest basement (< 2 km) is mapped at the Gardarbanken High, north of the Stappen High and below Bjørnøya. Along the continental slope, the top basement deepens to more than 11 km in an area where a thick fan of Neogene sediments has been reported (Engen et al. 2006). With the depth to crystalline basement reaching 12 km the northern part of the Nordkapp Basin can therefore be classified as a deep basin. Much deeper basins to the west of the Loppa High and south of the Stappen High are modelled with a depth-to-basement locally reaching >15 km.

11.4.5 Depth to the crust-mantle boundary (Moho)

The Moho (Fig. 11.5a) is, in general, associated with a density contrast of 350 kg/m³ between the lower crust and the upper mantle. Only across the lower crustal body (LCB) is this contrast slightly smaller. The resulting Moho geometry reflects the Moho of the Barents50 model (Fig. 11.5b) at the continental margin and onshore. Over most of the margin the Moho is similar to the Barents50 model, but varies significantly in the anomaly trends. Along existing seismic profiles the depths are essentially the same with the exception of IKU-B, where the new OBS profile Petrobar-07 has recently been acquired and provided for the modelling (Clark et al. 2009).

The Moho undulates over the continental shelf between depths of 20 and 35 km. In the central study area, an E-W shallowing correlates with the locations of basins and highs. We also notice a steep deepening of the Moho, from 20 km to 30 km, between the COT and the Ringvassøy-Loppa and Bjørnøyrenna fault complexes.

Interestingly, Moho depth is in the order of 30-32.5 km below the Bjarmeland Platform and northwards and shows a gradual decrease from north to south.

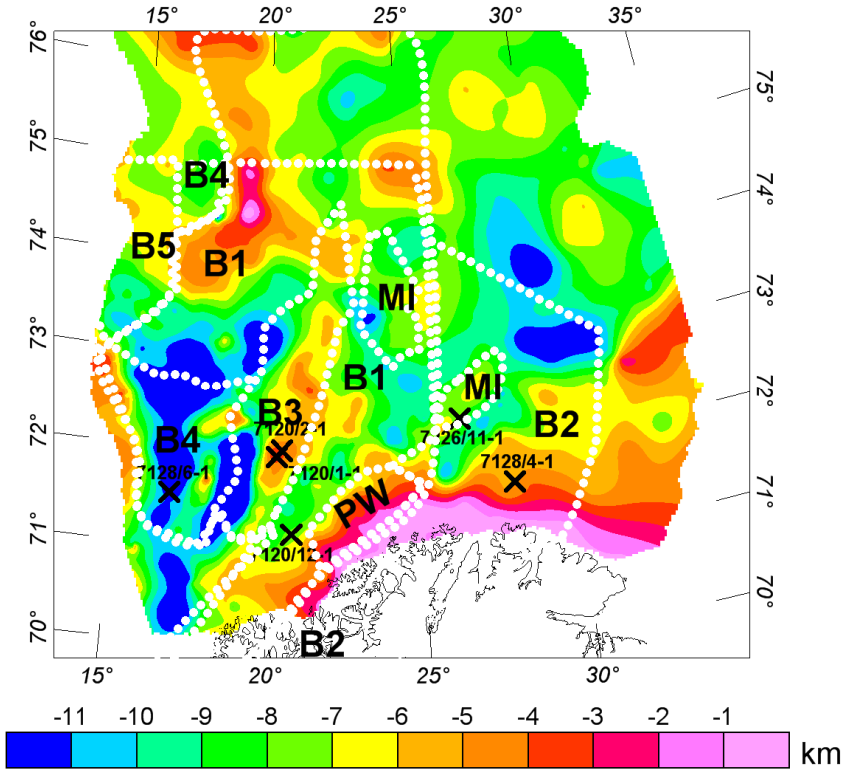

a)

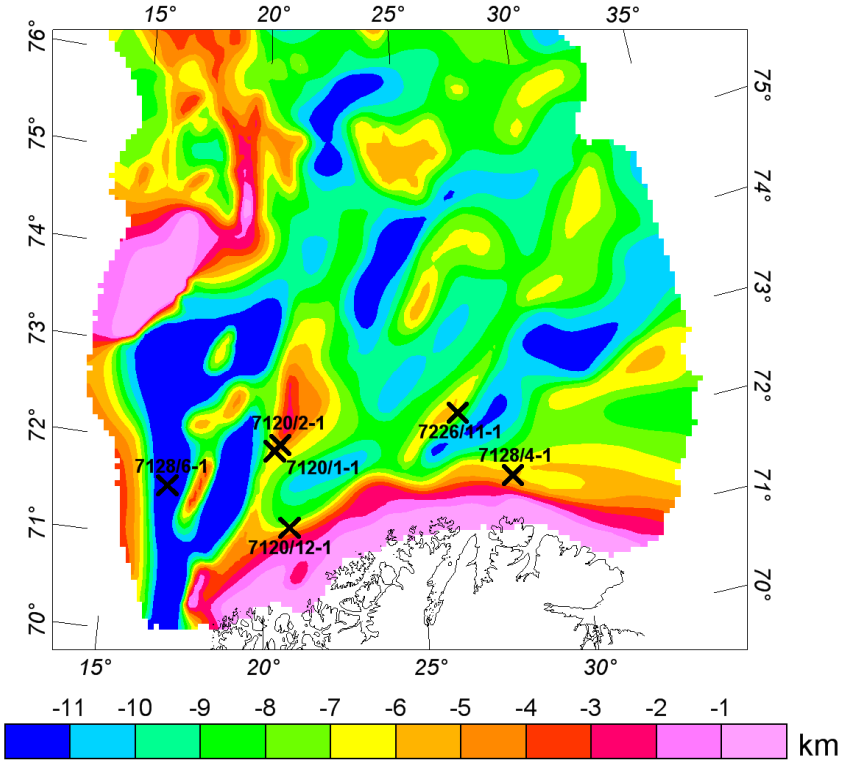

b)

Figure 11.4 a) Top basement as defined in the 3D model with different basement units on top (as defined in Table 11.1): b) Top basement map after Skilbrei et al. (1995) based mainly on magnetic depth estimates.

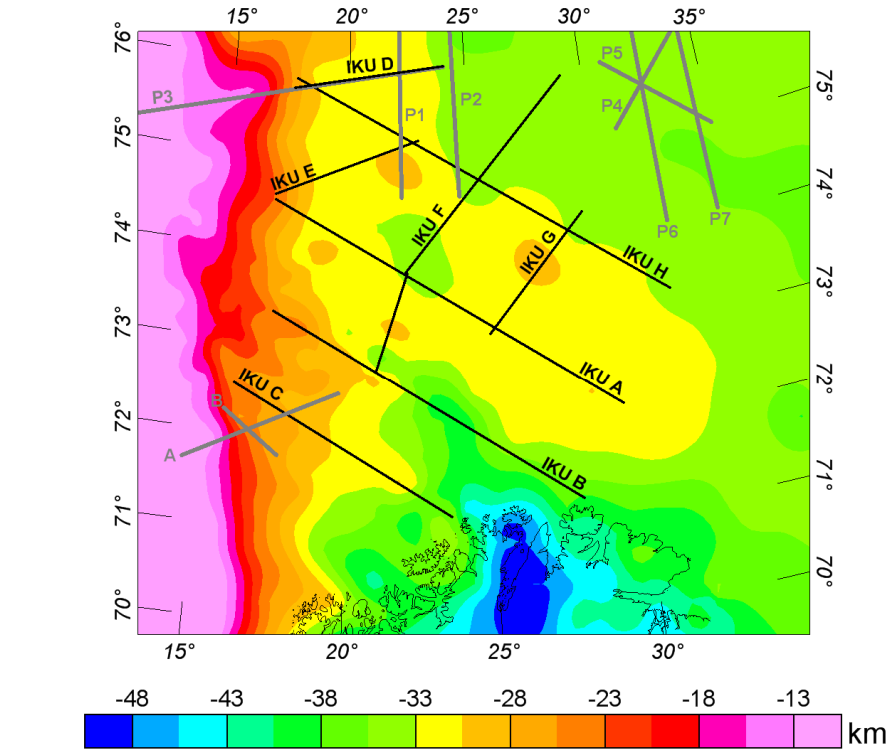

a)

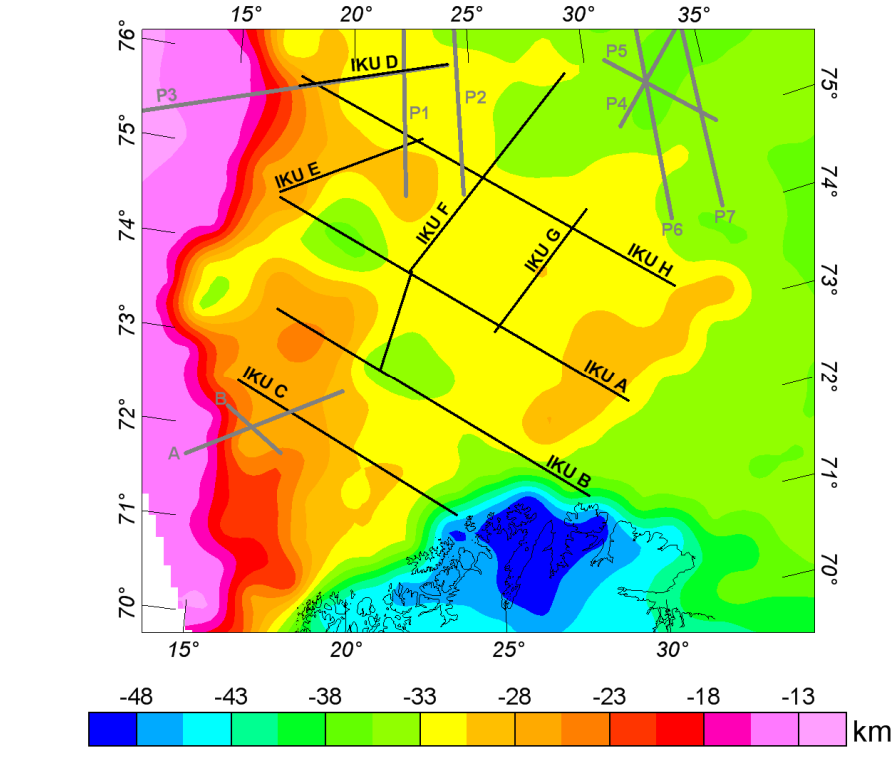

b)

Figure 11.5 a) Depth to Moho from the 3D model, b) depth to Moho from the Barents50 model. Black and grey lines show locations of seismic profiles.

11.5 Basement characterization and basin characteristics

The western and eastern Barents Sea contains a series of deep sedimentary basins of more than 10 km thickness with very different characteristics, when considering the wavelengths involved: the eastern Barents Sea basins are very large whereas the western Barents Sea basins are characterised by much smaller cross-wavelengths. This observation is an indication of a different history of formation of the basins which may correlate with different crustal properties. Figure 11.4a and Table 11.1 show the different crustal domains.

On the Bjarmeland Platform, the densities are slightly higher than the 2750 kg/m³ average values usually considered for the Fennoscandian Shield (Galitchanina et al. 1995). This slight increase between the crustal units BAS1 and BAS2 was required with respect to the constraints on the Moho depth, both from seismics and isostatic observations. Although the western boundary of the BAS2 crustal unit (Fig. 11.4a) is schematic in its definition of the geometry along the vertical sections, the seismics confirm the presence of both a major reflectivity change and a possible structural boundary coinciding with contrasting density/magnetisation values (Barrère et al. 2009a,b,c).

The densities and magnetic properties (Table 11.1) are used to distinguish different units, but resolve the Caledonian nappes only in a more general way. The Norwegian Caledonian nappes correspond to low-magnetic basement on top of an Archaean to Palaeoproterozoic basement of higher magnetisation (Olesen et al. 1990). The extension of the Caledonian nappes is based on the assumption of the offshore propagation of the different nappes mapped in Finnmark (Åm 1975, Olesen et al. 1990, Skilbrei 1991, Siedlecka & Roberts 1996, Drinkwater et al. 1996) and on the integrated analysis carried out by Barrère et al. (2009a). Estimation of the extensions and thicknesses from our model are difficult as the density and magnetisation contrasts between the nappes and the Archaean to Palaeoproterozoic basement are low.

However, fives crustal zones consisting of one or several units (B1-5 in Fig. 11.4a) are distinguished: (1) an onshore zone, (2) an offshore coastal zone, (3) a zone along the COT, (4) a central zone and (5) a last zone covering the eastern and northern areas.

11.6 Refinements with the BASAR-08 data

Figure 11.6 shows the magnetic residual of the original 3D model for the new BASAR-08 magnetic data compilation. Large differences can be observed, mostly related to the new data base. The anomalies were not as pronounced on the data available before the new surveys. The 3D model shows different basement units over the SW Barents Sea (Fig. 11.4a), and also for the survey area.

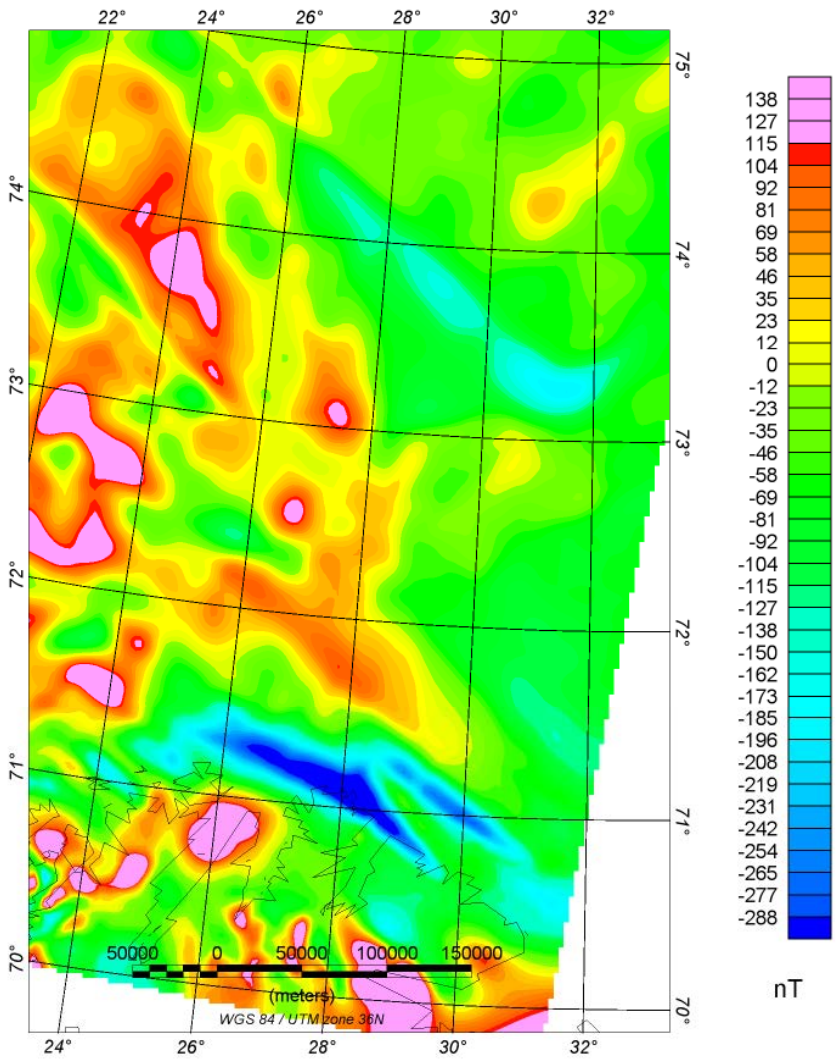

Figure 11.6 Magnetic residual of the 3D model by Barrère et al. (2009b) for the BAS-06/BASAR-08 survey compilation.

The resolution of the 3D model is around 10 km, and to evaluate the advantage of the new survey data, an inversion of the basement magnetisation was performed. The density of the basement is 2750 kg/m³ +/- 50 kg/m³ within the survey area, which means that no significant variations beyond the resolution of seismic velocities and density conversions can be expected. Therefore, we concentrated only on the new aeromagnetic data.

To study the distribution of different basement types in the survey area, we used the geometry of the model by Barrère et al. (2009b) for the top basement (Fig. 11.7a) and invert for its susceptibility distribution. Inversion of the well pre-defined 3D model allowed an evaluation of the distribution of the different basement lithologies, as presented previously.

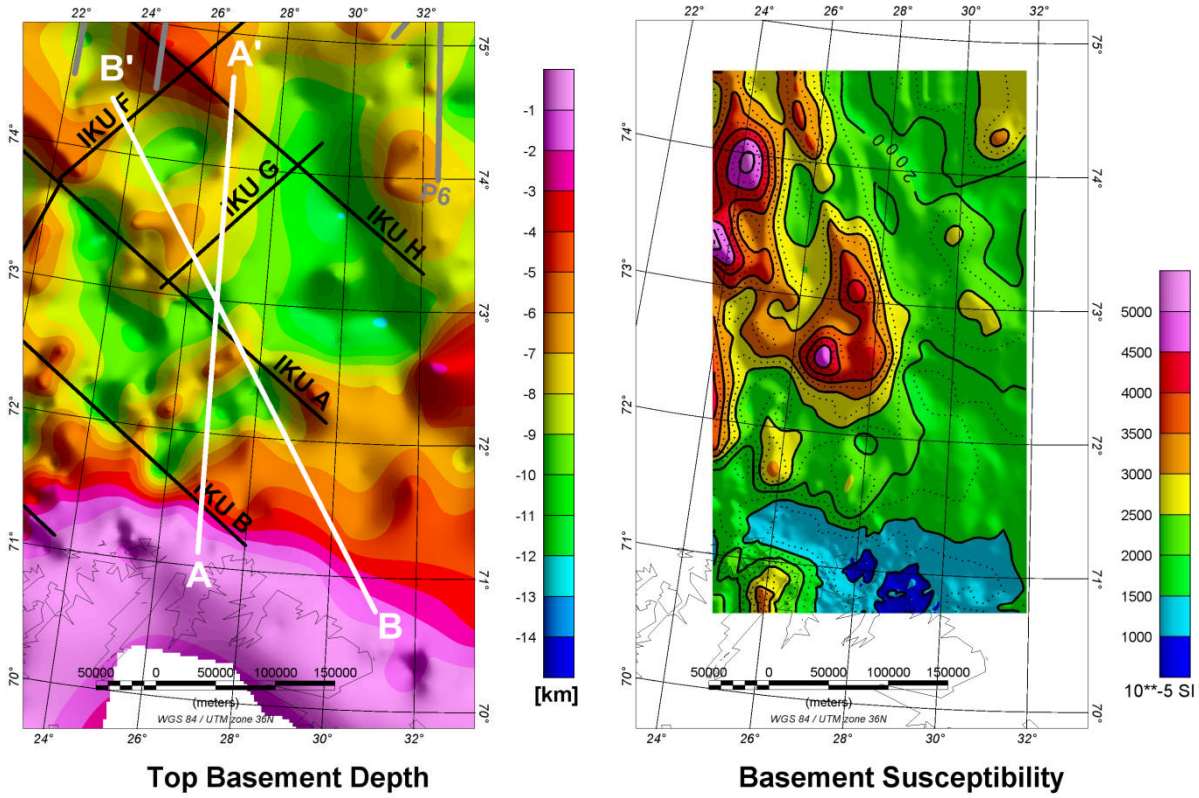

Figure 11.7 a) Top basement depth after Barrère et al. (2009b) and b) susceptibility distribution after the inversion. The regional seismic lines are shown with black lines; white lines show the location of the profiles in figures 11.8 and 11.9.

We used the GMSYS-3D software (Popowski et al. 2006) and built a three-layer model: water (non-magnetic), sedimentary rocks (apparent susceptibility: 50×10^{-5} SI), and basement (starting apparent susceptibility: 2500×10^{-5} SI). The base of the basement was chosen at 20 km depth as the lower crust is less magnetic than the basement. Furthermore, magnetic data are highly dependent on source distance and step contacts. A flat-lying base for the model is therefore only dependent on the susceptibility distribution within the model. We furthermore disregarded remanent magnetisation in our model, which of course has to be remembered when interpreting the susceptibility values. As the direction of the remanent field is regarded as parallel to the induced field, in the absence of better information, the real susceptibility is only 50 % (Q-ratio: 1) to 70 % (Q-ratio: 0.4) of the resulting apparent susceptibility. The initial model response is presented along two profiles in figures 11.8 and 11.9. As the main susceptibility contrast is at the top basement with a constant contrast, the amplitude of the modelled magnetic field is relatively small compared to the observed anomalies. However, the locations of the main anomalies are in agreement with the observed datea, which shows the first-order influence of the top basement on magnetic anomalies.

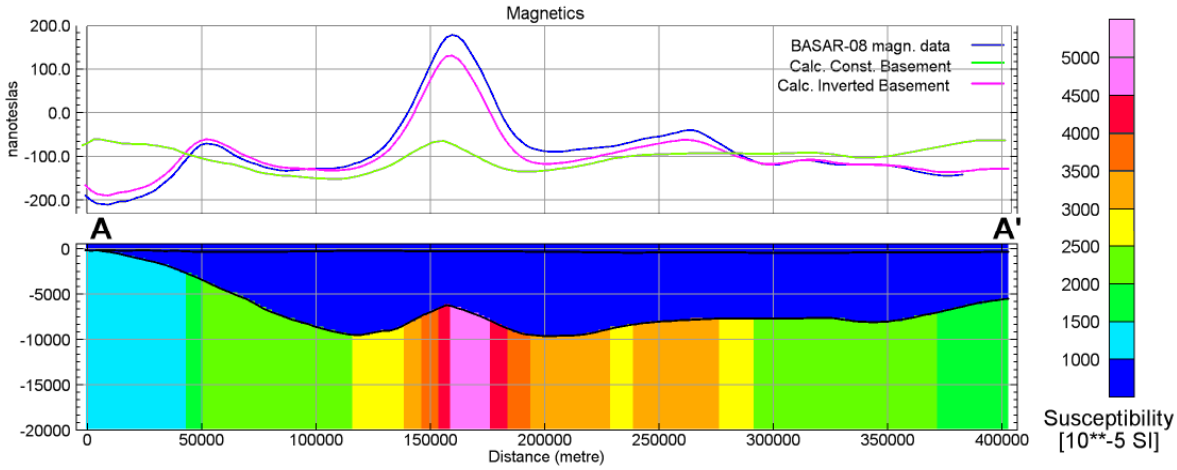

Figure 11.8 Model response along the south-north profile AA'. The lower panel shows the susceptibility distribution after the 1-step inversion for the basement susceptibility. The upper panel shows the observed magnetic anomaly, and the model response before (green line) and after the inversion (purple). For profile location, see figure 11.7.

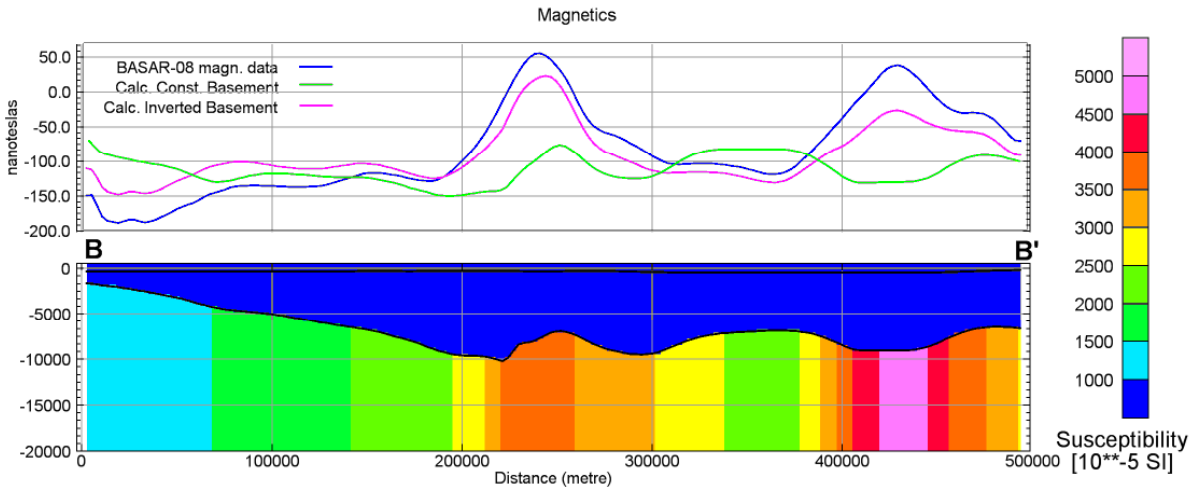

Figure 11.9 Model response along the south-north profile BB'. The lower panel shows the susceptibility distribution after the 1-step inversion for the basement susceptibility. The upper panel shows the observed magnetic anomaly, and the model response before (green line) and after the inversion (purple). For profile location, see figure 11.7.

The 3D model (Fig. 11.3) shows, however, that lateral contrasts in magnetisation have a large influence on the modelled magnetic anomalies. The inversion is performed by a 1-step inversion, which transforms the magnetic error grid to an apparent susceptibility grid and adds the result to the existing lateral susceptibility distribution grid. The resulting lateral susceptibility distribution is shown in figures 11.7 & 11.10 and along the profiles in figures 11.8 & 11.9. The lateral susceptibility grid leads to a close match with the observed magnetic field, as both lateral susceptibility contrasts and the contrast at the top basement influences the magnetic anomalies. A regional long-wavelength difference can be observed, which can be

attributed to the magnetisation in the lower crust and the geometry at the contact between lower and upper (basement) crust, and lower crust and upper mantle.

The resulting susceptibility distribution shows a correlation with the basement geometry (Figs. 11.8 &11.9), which indicates that the evolution of different basement units affects both the geometry and the magnetisation history, e.g. the Norsel High is clearly a basement high associated with high magnetisation. Most of the area can be linked to Caledonian-type basement with relative low magnetisation (<2500×10^{-5} SI). Towards the west, the magnetisation is increasing to >2500 ×10^{-5} SI and the transition is clearly observed in the top basement and the susceptibility distribution, similar to the basement distribution map in Figure 11.4a.

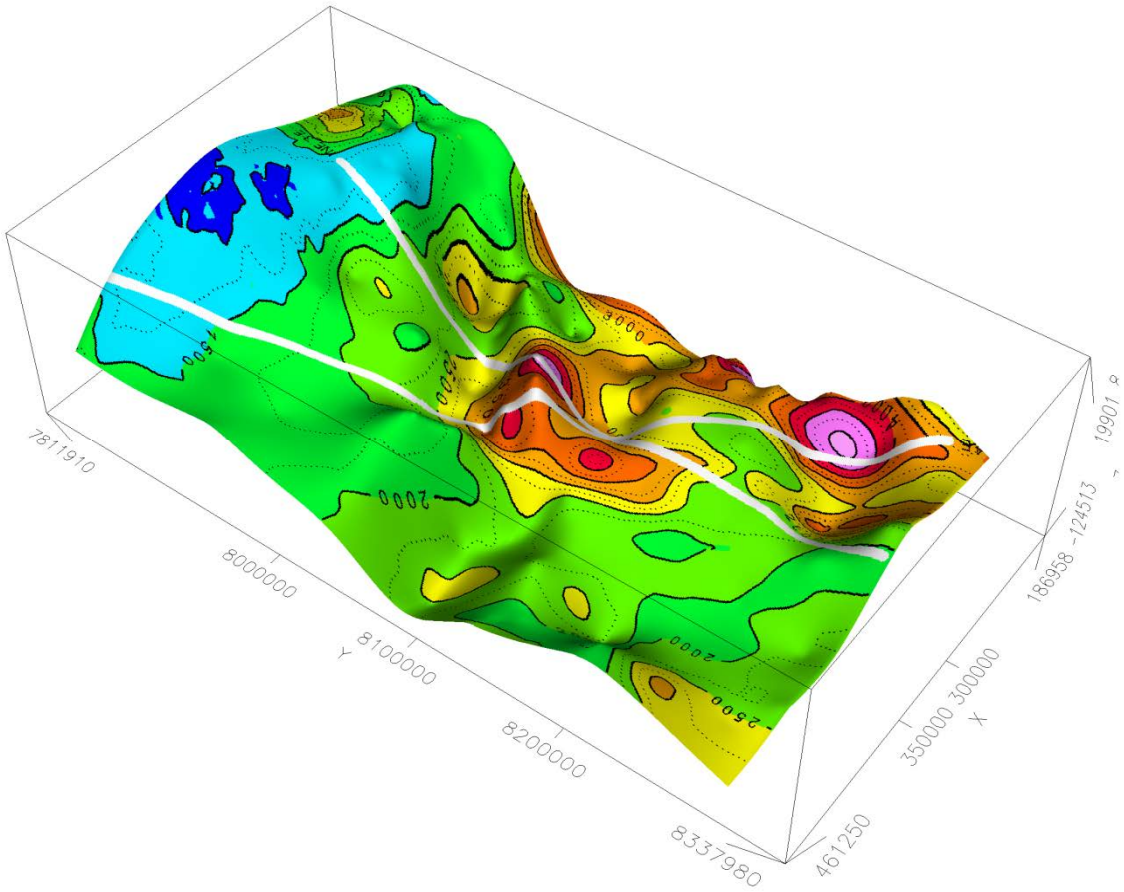

Figure 11.10 Top basement and susceptibility distribution in 3D. The figure shows the top basement horizons, with the susceptibility distribution draped on top in colour and with contour lines. White lines show the profile locations of figures 11.8 & 11.9.

A more refined model of the susceptibility distribution will be made with the interpretation of the new BASAR-09 data. A detailed analysis should carefully investigate the presence of short-wavelength anomalies, which must be related to intra-sedimentary sources, e.g. salt and the long-wavelength misfit in the model presented here, which might be related to deep-crustal structures, and which have a wavelength greater than our present study area.

12 CONCLUSIONS AND PERSPECTIVES

12.1 Main results

- The new high-resolution aeromagnetic survey BASAR-08 and the combined reprocessing of BAS-06 yielded a consistent and high-quality aeromagnetic map, identifying new and additional structures on local as well as regional scales. The data are of excellent quality and provide a new and more accurate magnetic picture for our geological understanding of the eastern Norwegian Barents Sea.

- Various filters and derivatives were applied to enhance different magnetic features and to support the structural interpretation. A number of different lineaments were observed and correlated with both Caledonian and Timanian structures, providing a better image of the interaction of these two major events and the ancient development of the Barents Sea continental shelf.

- Additional fault structures and most likely dykes were observed in the offshore domains, reactivated during the different rifting phases in the Barents Sea, providing new insights into the importance of rifting for the entire region.

- The Nordkapp and Ottar basins reveal a significantly different development as suggested by the new magnetic data. Whereas the Nordkapp Basin is characterised by extensive salt diapirism and obvious, repeated, fault reactivation and rifting, the Ottar Basin appears as a similarly deep sedimentary basin but did not undergo a comparable, complex extensional development.

- The southern Nordkapp Basin and the Norsel High have distinct gravity and magnetic properties which reflect the structure of a halfgraben system possibly controlled in depth by a major SE-dipping detachment and/or associated with lower crustal exhumation.

- Onshore-offshore correlations were capable of linking onshore geology with magnetic anomalies and extrapolating them into the offshore domains. They bear witness to complex tectonics involving the Caledonian deformation, superimposed on Timanian structures, and the extension of nappes into the offshore regions. The three presented sections show the differences and attributes of the Magerøy Nappe, part of the Kalak Nappe Complex and the Middle and Lower Allochtons of the BSR of Varanger Peninsula and highlight the sensitivity of magnetic data to assist in the mapping of diverse geology and fault structures.

- 2D grav/mag modelling along three regional seismic transects facilitates interpretation of the main structural elements highlighted by the BASAR-08 survey. The resulting models show the capability of integrated modelling to gain additional information on sedimentary basins, intra-sedimentary geo-bodies and crustal geometries, but also disclose the weakness of the method when not giving sifficient consideration to 3D effects. This might partly explain remaining discrepancies between calculated and observed data and/or significant differences in the 2D and 3D modelling results.

- The Stappen and the Loppa highs appear to be of a distinct and thick crustal terrane type obviously containing magnetic material. They may possibly have formed a ribbon microcontinent during the Palaeozoic and Mesozoic rifting episodes. The Loppa High is interpreted as a major continental rigid block that behaved as a 'buffer' region during Palaeozoic and subsequent Mesozoic rifting episodes and possibly earlier during the Caledonian orogeny.

- Gravity and magnetic modelling also demonstrated the presence of major sub-Permian rift basins (e.g. Ottar Basin) with large accumulations of mostly immobilised salt to the west. The models show that the Palaeozoic basins could be of significant depths even if we consider low (salt-influenced) density values for the Palaeozoic sedimentary rocks. The basin strikes NE-SW, parallel to the southwestern segment of the Nordkapp Basin, and is separated from it by the Norse1 High. Furthermore, we propose that some Palaeozoic depocentres (early stages?) could also have been controlled by pre-existing Caledonian trends which are mostly NNW-SSE in the Bjarmeland Platform area as suggested by the new magnetic picture. We conclude that the trends of the Late Palaeozoic basins, most likely influenced by the collapse of the Caledonian nappes and fault reactivation, are not necessarily sub-parallel to the NE-SW axes of Mesozoic basins as has often been suggested in the literature. This provides a new basis for discussion of a possible re-interpretation of the Devonian-Carboniferous paleogeographic setting of the West Barents Sea.

- The 3D model covers the entire southern Norwegian Barents Sea and reveals five crustal zones distinguished by integrated geophysical modelling. The Moho depth varies in a range from 20 km to 35 km. An inversion of the basement susceptibility shows some evidence for different basement types and their distribution.

12.2 Proposition for further work

- The structure of the Palaeozoic rift systems and underlying basement complexes in the western Barents Sea still remains unclear and more investigations need to be carried out to fully understand this system. The new magnetic survey suggests that the Palaeozoic system is more complex that we thought, and until now, poor imaging of the sub-

Permian units had not allowed us to map it properly. Further regional transects combined and extrapolated with the new magnetic survey should help us to get a first and quick 3D overview of this old system and its interaction with the Caledonian and older Timanian structures and the subsequent Mesozoic rift system. There is no unique solution in just potential field modelling, and the capabilities and reliability of an integrated modelling approach can be increased appreciably using higher quality seismic data as additional constraints. Similar modelling, but using better regional and long-offset seismic lines (e.g. Fugro NBR 2006-2008), could definitively help us toward an improved understanding of the deep basins and crustal architecture of the West Barents Sea.

- Gravity data were used intensively in this study for 2D and 3D modelling and to some extent for the structural interpretation. Nevertheless, and especially to gain a better knowledge of the deeper crustal structures the full potential of the gravity data was not tapped and some additional work might be worthwhile.

- The updated 3D model is partly in good correlation with the results from the 2D modelling, but does not have the same resolution as along the transects. Moreover the 3D model at its present stage barely considers local features such as mafic intrusions, as proposed at the Norsel High, or deep sedimentary basins with huge amounts of low-density salt. For a more accurate and detailed interpretation and for a better understanding of the Barents Sea settings, a higher resolution of the top basement is a major requirement. On the other hand, 2D modelling does not sufficiently consider 3D effects and might lead to erroneous interpretations. To understand the complex distribution of basins and basement highs in the Barents Sea, an update and further refinement of the current 3D model is highly recommended.

- The results of this study are definitely most useful to facilitate the further detailed geological mapping of the southwestern Barents Sea. Due to the sparse seismic coverage available for the preliminary interpretation, a full constraint on the meaning of each magnetic anomaly and the structures highlighted by the new survey was not always possible. Further studies combining seismic, gravity and the new magnetic data would be appropriate to refine the geological model in the future. NGU suggests a reinvestigation of the Norwegian Barents Sea and specific trends in greater detail using a more confined interaction between seismic data, the new magnetic grid and the high-resolution gravity DRAGON database (available only to specific partners). Such an integrated study combined with the petrophysical database and the geological knowledge available at NGU, would be useful to develop additional 2D and/or refine the existing 3D gravity modelling in the area. With the upcoming BASAR-09 project, NGU will complete the aeromagnetic remapping of the southern Norwegian Barents Sea. This state-of-the-art dataset, combined with additional geophysical and geological data will be extremely valuable for reconsidering the depth-to-basement map of the

region and for gaining a better knowledge of the overall geological evolution of the Barents Sea.

- We suggest that the BASAR-09 sponsors agree to the regional gravity compilation for the SW Barents Sea.

13 ACKNOWLEDGEMENTS

Det norske, Eni Norge, NGU, NPD, and StatoilHydro financed the BASAR-08 Survey. We express our thanks to these companies. We further wish to thank in particular Arne Gronlie, Kai Hogstad, Tom Bugge, Tore Hoy, Hans Konrad Johnsen, Peter Midbøe and Snorre Olaussen for giving valuable advice and assistance during the survey planning and interpretation.

14 REFERENCES

Alsgaard, P. 1993: Eastern Barents Sea late Palaeozoic setting and potential source rocks. *In* Vorren, T.O., Bergsager, E., Dahl-Stamnes, Ø.A., Holter, E., Johansen, B., Lie, E., Lund, T.B. (eds) Arctic Geology and Petroleum Potential. *Norwegian Petroleum Society, Special Publication 2, Elsevier, Amsterdam*, 405-418.

Åm, K., 1975: Aeromagnetic basement complex mapping north of latitude 62 N, Norway, *Norges geologiske undersøkelse* 316**,** 351-374.

Arkani Hamed, J. 1988: Differential reduction to the pole of regional magnetic anomalies. *Geophysics* 53, 1592-1600.

Arkani, H. J. 1988: Differential reduction to the pole of regional magnetic anomalies: Geophysics, 53, 1592-1600.

Arkani-Hamed, J. 2007: Differential reduction to the pole: Revisited. *Geophysics* 72(1), L13-L20.

Bain, J. & Weyand, J. A. 1993: Complex salt features resolved by integrating seismic, gravity and magnetics. *EAGE/EAPG Annual Meeting, Expanded abstracts*.

Bain, J., Weyand, J. & Weber, M. 1994: Resolving Complex Salt Features Using Gravity and Magnetics. *Fugro-LCT Technical Papers*.

Bainbridge, G., Musselman, C., Whitehead, N. & McDonald, N. 2002: Euler 3D Deconvolution (v5.1.5). Processing, analysis and visualization system for 3D inversion of potential field. Tutorial and User guide. *Geosoft Manual*. 66 pp.

Barbosa, V.C.F., Silva, J.B.C. & Medeiros, W.E. 1999: Stability analysis and improvement of structural index estimation in Euler deconvolution. *Geophysics* 64(1), 48-60.

Barbosa, V.C.F., Silva, J.B.C. & Medeiros, W.E. 2000: Making Euler deconvolution applicable to small ground magnetic surveys. *Journal of Applied Geophysics* 43(1), 55-68.

Barrère, C., Ebbing, J. & Gernigon, L. 2009a. Offshore prolongation of Caledonian structure and basement characterisation in the western Barents Sea from geophysical modelling, *Tectonophysics, 18 p*.

Barrère, C., Ebbing, J. & Gernigon, L. 2009b: 3D density and magnetic crustal characterisation of the southwestern Barents Shelf: implications for the offshore prolongation of the Norwegian Caledonides. *Geophysical Journal International*, in prep.

Barrère, C., Gernigon, L. & Ebbing, J. 2009c: The Bjørnøya Basin and Loppa High crustal structure, southwestern Barents Sea continental shelf post-Caledonian features imaged and modelled. *Journal of the Geological Society of London*, in prep.

Beicip-Franlab 2002: Tutorial - EasyDepth 2.0. The Basin Modeling line. *Beicip-Franlab*, 28 pp.

Bhattacharyya, B. 1966: Continuous spectrum of the total-magnetic field anomaly due to a rectangular prismatic body. *Geophysics 31*, 97-121.

Blakely, R. 1995: Potential Theory in Gravity and Magnetic Applications. *Cambridge University Press*, 461p.

Blakely, R.J. & Simpson, R.W. 1986: Approximating edges of source bodies from magnetic or gravity anomalies. *Geophysics* 51, 1494-1498.

Blakely, R.J., Wells, R.E., Yelin, T.S., Madin, I.P. & Beeson, M.H. 1995: Tectonic Setting of the Portland-Vancouver Area, Oregon and Washington - Constraints from Low-Altitude Aeromagnetic Data. *Geological Society of America Bulletin 107(9),* 1051-1062.

Breivik, A. J., Gudlaugsson, S. T. & Faleide, J. I. 1995: Ottar Basin, SW Barents Sea; a major upper Paleozoic rift basin containing large volumes of deeply buried salt. *Basin Research 7*, 299-312.

Breivik, A. J., Mjelde, R., Grogan, P., Shimamura, H., Murai, Y. & Nishimura, Y. 2005: Caledonide development offshore-onshore Svalbard based on ocean bottom seismometer, conventional seismic, and potential field data. *Tectonophysics 401,* 79-117.

Breivik, A.J., Faleide, J.I. & Gudlaugsson, S.T. 1998: Southwestern Barents Sea margin: late Mesozoic sedimentary basins and crustal extension, *Tectonophysics,* 293**,** 21-44.

Breivik, A.J., Mjelde, R., Grogan, P., Shimamura, H., Murai, Y. & Nishimura, Y. 2003: Crustal structure and transform margin development south of Svalbard based on ocean bottom seismometer data, *Tectonophysics* 369**,** 37-70.

Breivik, A.J., Mjelde, R., Grogan, P., Shimamura, H., Murai, Y., Nishimura, Y. & Kuwano, A. 2002: A possible Caledonide arm through the Barents Sea imaged by OBS data, *Tectonophysics* 355**,** 67-97.

Brocher, T. M. 2005: Compressional and Shear Wave Velocity Versus Depth in the San Fransisco Bay Area, California. Rules for USGS Bay Area Velocity Model 05.0.0. *U.S.G.S open-File Report* 05-1317, 1-58.

Bugge, T. & Fanavoll, S. 1995: The Svalis Dome, Barents Sea a geological playground for shallow stratigraphic drilling. *First Break* 13, 237-251.

Bugge, T., Elvebakk G., Fanavoll, S., Mangerud, G., Smelror, M., Weiss, H. M., Gjelberg J., Kristensen, S. E. & Nilsen, K. 2002: Shallow stratigraphic drilling applied in hydrocarbon exploration of the Nordkapp Basin, Barents Sea. *Marine and Petroleum Geology* 19, 13-37.

Bugge, T., Mangerud, G., Elvebakk, G., Mork, A., Nilsson, I., Fanavoll, S. & Vigran, J. O. 1995: The upper Palaeozoic succession on the Finnmark Platform, Barents Sea. *Norsk Geologisk Tidsskrift* 75, 3-30.

Bugge, T., Mangerud, G., Elvebakk, G., Mork, A., Nilsson, I., Fanavoll, S. & Vigran, J. O. 1995: The upper Palaeozoic succession on the Finnmark Platform, Barents Sea. *Norsk Geologisk Tidsskrift* 75, 3-30.

Burg, J.P. 1975: Maximum Entropy Spectral Analysis, *PhD thesis, Stanford University,* 123 pp.

Christensen, N.I. & Mooney, W.D. 1995: Seismic velocity structure and composition of the continental crust: A global view. *Journal of Geophysical Research - Solid Earth 100*, 9761-9788.

Chroston, P. N. 1986: Gravity anomalies on Varangerhalvøya, Finnmark. *Norges Geologiske Undersøkelse Bulletin 404*, 45-56.

Clark, D. 1997: Magnetic petrophysics and magnetic pretrology aids to geological interpretation of magnetic surveys. *AGSO Journal of Australian Geology and Geophysics* 17, 83-103.

Clark**,** S. A., Faleide, J. I., Ritzmann, O. and Mjelde, R. 2009: Multi-stage rift evolution of the SW Barents Sea from wide-angle seismic velocity modeling. EGU2009-12559.

Cooper, G.R.J. & Cowan, D.R. 2006: Enhancing potential field data using filters based on the local phase. Computers & Geosciences 32(10), 1585-1591.

Corfu, F., Torsvik, T.H., Andersen, T.B., Ashwal, L.D., Ramsay, D.M. & Roberts, R.J. 2006: Early Silurian mafic-ultramafic and granitic plutonism in contemporaneous flysch, Magerøy, northern Norway: U-Pb ages and regional significance, *Journal of the Geological Society London* 163**,** 291-301.

Dengo, C. & Røssland, K. 1992: Extensional tectonic history of the western Barents Sea. *In* Larsen, R.M. (ed), Structural and tectonic modelling and its application to petroleum geology: Norwegian Petroleum Society Special Publication, 91-107.

Dobrin, M. & Savit, C. 1988: *Introduction to geophysical prospecting. 4th edition*. McGraw-Hill, 867 pp.

Doré, A. 1995: Barents Sea geology, petroleum resources and commercial potential. *Arctic 48*, 207-221.

Doré, A. G., Lundin, E. R., Fichler, C. & Olesen, O. 1997: Patterns of basement structure and reactivation along the NE Atlantic margin. The role of basement reactivation in continental deformation. *Journal of the Geological Society, London 154*, p. 85-92.

Doré, A.G. 1991: The Structural Foundation and Evolution of Mesozoic Seaways between Europe and the Arctic. *Palaeogeography Palaeoclimatology Palaeoecology* 87(1-4), 441-492.

Drinkwater, N.J., Pickering, K.T. & Siedlecka, A. 1996: Deep-water fault-controlled sedimentation, Arctic Norway and Russia: Response to Late Proterozoic rifting and the opening of the Iapetus Ocean. *Journal of the Geological Society 153*, 427-436.

Engen, O., Frazer, L.N., Wessel, P. & Faleide, J.I. 2006: Prediction of sediment thickness in the Norwegian-Greenland Sea from gravity inversion, *Journal of Geophysical Research-Solid Earth*, 111, nr. B11, artikkelnr. B11403, doi:10.1029/2005JB003924, ISSN 0148-0227

Faleide, J. I., Gudlaugsson, S. T. & Jacquart, G. 1984: Evolution of the western Barents Sea. *Marine and Petroleum Geology 1*, 123-150.

Faleide, J. I., Solheim, A., Fiedler, A., Hjelstuen, B. O., Andersen, E. S. & Vanneste, K. 1996: Late Cenozoic evolution of the western Barents Sea-Svalbard continental margin. Impact of glaciations on basin evolution; data and models from the Norwegian margin and adjacent areas. *Global and Planetary Change 12*, 53-74.

Faleide, J. I., Vågnes, E. & Gudlaugsson, S. T. 1993: Late Mesozoic-Cenozoic evolution of the southwestern Barents Sea in a regional rift-shear tectonic setting. *Marine and Petroleum Geology 10*, 186-214.

Faleide, J.I., Gudlaugsson, S.T., Johansen, B., Myhre, A.M., Eldholm, O. & Norway, N.P.O.L.N. 1984: Free-air gravity anomaly maps of the Greenland Sea and the Barents

Sea.; Geo-scientific investigations in the Barents and Greenland Norwegian Seas. *Skrifter Norsk Polarinstitutt 180*, 63-67.

Fichler, C., Rueslåtten, H., Gram, C., Ingebrigtsen, A. & Olesen, O. 2007: Salt interpretation with special focus on magnetic data, Nordkapp Basin, Barents Sea. Expanded Abstract EGM 2007 International Workshop Innovation in EM, Grav and Mag Methods. a new Perspective for Exploration. Capri, Italy, 16-18 April 2007 .

Fichler, C., Rundovde, E., Johansen, S. & Sæther, B. M. 1997: Barents Sea tectonic structures visualized by ERS1 satellite gravity with indications of an offshore Baikalian trend. *First Break 15*, 355-363.

Flanagan G., Davis S., Campbell, C. & Doughtie, J. 1988: Integration of high sensitivity aeromagnetics and seismic to define salt and sediment structures in the Gulf of Mexico. 5*8th Annual International Meeting, Society of Exploration Geophysics, Expanded Abstracts*, 582-585.

Florio, G., Fedi, M. & Pasteka, R. 2006: On the application of Euler deconvolution to the analytic signal. *Geophysics 71(6)*, L87-L93.

Gabrielsen R., Færseth, R., Jensen, L., Kalheim, J. & Riis, F. 1990: Structural elements of the Norwegian Continental Shelf. Part 1.The Barents Sea region. *Norwegian Petroleum Directorate Bulletin 6*, 0-33.

Gabrielsen, R. & Færseth, R. 1989: The inner shelf of North Cape, Norway, and its implications for the Barents Shelf-Finnmark Caledonide boundary. *Norsk Geologisk Tidsskrift 69*, 57-62.

Gabrielsen, R. 1984: Long-lived fault zones and their influence on the tectonic development of the southwestern Barents Sea. *Journal of the Geological Society, London 141*, 651-662.

Gabrielsen, R. H., Klovjan, O. S., Rasmussen, A. & Stolan, T. 1992: Interaction between halokinesis and faulting; structuring of the margins of the Nordkapp Basin, Barents Sea region, *In* Larsen, R.M. et al. (eds.) Structural and tectonic modelling and its application to petroleum geology; proceedings. *Norwegian Petroleum Society (NPF) Special Publication 1*, 121-131.

Galitchanina, L.D., Glaznev, V.N., Mitrofanov, F.P. & Olesen, O. 1995: Surface density characteristics of the Baltic Shield and adjacent territories, *Norwegian Journal of Geology*, Special Publications**.**, 349-354.

Gardner G., Gardner, L. & Gregory, A. 1974: Formation velocity and density-the diagnostic basics for stratigraphic traps. *Geophysics 39*, 770-780.

Gayer, R.A., Rice, A.H.N., Roberts, D., Townsend, C. & Welbon, A. 1987: Restoration of the Caledonian Baltoscandian margin from balanced cross-sections: the problem of excess continental crust. *Transactions of the Royal Society of Edinburgh: Earth Sciences* 78, 197-217.

Gee, D. G. & Pease, V. 2004: The Neoproterozoic Timanide orogen of eastern Baltica; introduction. The Neoproterozoic Timanide Orogen of eastern Baltica. *Memoirs of the Geological Society of London 30*, 1-3.

Gee, D. G. & Teben'kov, A. 2004: Svalbard; a fragment of the Laurentian margin; The Neoproterozoic Timanide Orogen of eastern Baltica. *Memoirs of the Geological Society of London 30*, 191-206.

Gee, D. G., Bogolepova, K. & Lorenz, H., 2006: The Timanide, Caledonide and Uralide orogens in the Eurasian high Arctic, and relationships to the palaeo-continents Laurentia, Baltica and Siberia. In Gee, D.G & Stephenson, R.A. (eds.) European Lithosphere Dynamics. *Geological Society, London, Memoirs 32*, 507-520.

Gee, D.G., Fossen, H., Henriksen, N. & Higgins, A.K. 2008: From the early Paleozoic platforms of Baltica and Laurentia to the Caledonide orogen of Scandinavia and Greenland. *Episodes* 31(1), 44-51.

Geosoft, 2004: OASIS Montaj v 6.0 Mapping and processing system, The core software platform for working with large volume spatial data. Quick start tutorials. *Geosoft Incorporated*, 258 pp.

Geosoft, 2005a: OASIS Montaj MAGMAP Filtering. 2D frequency domain processing of potential Field Data tutorial. *Geosoft Incorporated*, 66 pp.

Geosoft, 2005b: Montaj Geophysics Levelling System, Processing and Enhancing Geophysicsl Data Extension for Oasis montja v6.2. Tutorial and user guide. *Geosoft Incorporated*, 68 pp.

Gernigon, L., Marello, L., Mogaard, J.O., Werner, S.C. & Skilbrei, J.R. 2007b: Barents Sea Aeromagnetic Survey BAS - 06: Acquisition-processing report and preliminary interpretation. NGU Report 2007.035, Geological Survey of Norway, Trondheim, 142 pp.

Gernigon, L., Olesen, O. & Continental-Shelf-Geophysics-team 2007: Challenging the Established Truths. Geoexpro 4, 40-44.

Gibson, R. I. & Millegan, P. 1998: Geologic applications of gravity and magnetics; case histories. *AAPG Studies in Geology 43 and* SEG Geophysical Reference Series 8, 175 p.

Gjelsvik, T. 1998: Nye aspekter ved forhold mellom den baikalske og den kaledonske deformasjonen og dets betydning for deformasjonshistorien i Barentshav-regionen, basert på strukturgeologisk kartlegging, Varanger-halvøyen, Finnmark, Nord-Norge. *Unpublished Cand. Scient. thesis, University of Bergen*, 112 pp.

Götze, H.J. & Lahmeyer, B. 1988: Application of 3-Dimensional Interactive Modeling in Gravity and Magnetics, *Geophysics*, 53**,** 1096-1108.

Grauch, V. J. S. & Hudson, M., R. 2007: Guides to understanding the aeromagnetic expression of faults in sedimentary basins: Lessons learned from the central Rio Grande rift, New Mexico. *Geosphere, 3, 6*, 596–623, doi: 10.1130/GES00128.1

Grauch, V.J.S., Hudson, M.R. & Minor, S.A. 2001: Aeromagnetic expression of faults that offset basin fill, Albuquerque basin, New Mexico. *Geophysics* 66(3), 707-720.

Grauch, V.J.S., Cordell, L. 1987: Limitations on determining density or magnetic boundaries from the horizontal gradient of gravity or pseudogravity data. Geophysics 52, 118– 121.

Grogan, P., Nyberg, K., Fotland, B., Myklebust, R., Dahlgren, S. & Riis, F. 1998: Cretaceous Magmatism South and East of Svalbard. Evidence from Seismic Reflection and Magnetic Data. *Polarforschung 68*, 25-34.

Gudlaugsson., S.T., Faleide, J. I., Johansen, S. E. & Breivik, A. J. 1994: Late Paleozoic structural development of the southwestern Barents Sea. Structure and Tectonic History of the Western Barents Sea (S. T. Gudlaugsson), *Dr. Philos. thesis*, University of Oslo.

Gudlaugsson, S. T., Faleide, J., Johansen, S. & Breivik, A. 1998: Late Palaeozoic structural development of the southwestern Barents Sea. *Marine and Petroleum Geology 15*, 73-102.

Guise, P.G. & Roberts, D. 2002: Devonian ages from $^{40}Ar/^{39}AR$ dating of plagioclase in dolerite dykes, eastern Varanger Peninsula, North Norway. *Norges Geologiske Undersøkelse* Bulletin 440, 27-37.

Gunn, P.J. 1997: Application of aeromagnetic surveys to sedimentary basin studies, *Journal of Australian Geology & Geophysics* 17**,** 133-144.

Hathaway, D.H., Wilson, R.M. & Reichmann, E.J. 1999: A synthesis of solar cycle prediction techniques. *Journal of Geophysical Research-Space Physics 104(A10)*, 22375-22388.

Herrevold, T., Gabrielsen, R.H. & Roberts, D. in press: The southeastern part of the Trollfjorden-Komagelva Fault Zone, Varanger Peninsula, Finnmark, North Norway. *Norwegian Journal of Geology*

Hospers, J. & Ediriweera, K.K. 1991: Depth and configuration of the crystalline basement in the Viking Graben area, Northern North Sea. *Journal of the Geological Society, London 148*, 261-265.

Hrouda, F., Smid, J. & Schulmann, K. 2001: Anisotropy of magnetic susceptibility and its carriers in salt domes of the SW Zagros Mts., Iran. *American Geophysical Union, Fall Meeting* 2001, abstract #GP41A-0247.

Hsu, S.-K. 2002: Imaging magnetic sources using Euler's equation. *Geophysical Prospecting 50*, 15-25.

Hsu, S. K., Sibuet, J. C. & Shyu, C. T. 1996: High-resolution detection of geologic boundaries from potential-field anomalies: An enhanced analytical signal technique. *Geophysics* 61, 373-386.

Hsu, S. K., Sibuet, J. C. & Shyu, C. T. 1996: High-resolution detection of geologic boundaries from potential-field anomalies: An enhanced analytical signal technique. *Geophysics* 61, 373-386.

Hudec, M.R., Jackson, M.P.A. & Schultz-Ela, D.D. 2009: The paradox of minibasin subsidence into salt: Clues to the evolution of crustal basins. *Geological Society of America Bulletin 121(1-2)*, 201-221.

Ivanova, N. M. 2001: The geological structure and petroleum potential of the Kola-Kanin Monocline, Russian Barents Sea. *Petroleum Geoscience 7*, 343-350.

Ivanova, N. M., Sakoulina, T. S. & Roslov, Y. V. 2006: Deep seismic investigation across the Barents-Kara region and Novozemelskiy fold belt (Arctic shelf). Seismic probing of continents and their margins. *Tectonophysics 420*, 123-140.

Jackson, M. P. & Talbot, C. J. 1986: External shapes, strain rates, and dynamics of salt structures. *Geological Society of America Bulletin 97*, 305-323.

Jakobsson, M., Cherkis, N.Z., Woodward, J., Macnab, R. & Coakley, B. 2000: New grid of Arctic bathymetry aids scientists and mapmakers, *Eos, Transactions, American Geophysical Union* 81**,** 89-96.

Jakobsson, M., Cherkis, N.Z., Woodward, J., Macnab, R. & Coakley, B., 2000. New grid of Arctic bathymetry aids scientists and mapmakers, *Eos, Transactions, American Geophysical Union, 81***,** 89-96.

Jensen, L. N. & Sørensen, K. 1992: Tectonic framework and halokinesis of the Nordkapp Basin, Barents Sea. Structural and tectonic modeling and its application to petroleum geology; proceedings. *Norwegian Petroleum Society (NPF) Special Publication 1,* 109-120.

Johansen, S., Ostisty, B., Birkeland, Ø., Fedorovski, Y., Martirosjan, V., Christensen, O., Cheredeev, S., Ignatenko, E.A. & Margulis, L. 1993: Hydrocarbon potential in the Barents Sea region. play distribution and potential. *In* Vorren, T.O., Bergsager, E., Dahl-Stamnes, Ø.A., Holter, E., Johansen, B., Lie, E., Lund, T.B. (eds.). Arctic Geology and Petroleum Potential. *Norwegian Petroelum Society, Special Publication 2,* Elsevier, Amsterdam, 273-320.

Juhojuntti, N., Juhlin, C. & Dyrelius, D. 2001: Crustal reflectivity underneath the Central Scandinavian Caledonides. *Tectonophysics 334(3-4),* 191-210.

Karpuz, M. R., Roberts, D., Moralev, V. & Terekhov, E. 1993a: Regional lineament framework of eastern Finnmark, Norway, western Kola Peninsula, Russia, and southern Barents Sea.; Proceedings of the Ninth thematic conference on Geologic remote sensing; exploration, environment, and engineering. *Proceedings of the Thematic Conference on Remote Sensing for Exploration Geology 9*, 733-750.

Karpuz, M.R., Roberts, D., Olesen, O., Gabrielsen, R.H. & Herrevold, T. 1993b: Application of multiple data sets to structural studies on Varanger Peninsula, Northern Norway. *International Journal of Remote Sensing 14*, 7979-1003.

Karpuz, M. R., Roberts, D., Moralev, V. M. & Terekhov, E. 1995: Regional lineaments of eastern Finnmark, Norway, and the western Kola Peninsula, Russia. Geology of the eastern Finmark-western Kola Peninsula region; proceedings of the International Barents symposium on "Geology and minerals in the Barents region". *Norges geologiske undersøkelse Special Publication 7*, 121-135.

Keating, P. 1998: Weighted Euler deconvolution of gravity data. *Geophysics 63*, 1595-1603.

Koyi, H., Talbot, C. J. & Torudbakken, B. O. 1993: Salt diapirs of the Southwest Nordkapp Basin; analogue modelling. New insights into salt tectonics; collection of invited papers reflecting the recent developments in the field of salt tectonics. *Tectonophysics 228*, 167-187.

Larssen, G. B., Elvebakk, G., Henriksen, L., Kristensen, S. E., Nilsson, I., Samuelsberg, T., Svånå, T., Stemmerik, L. & Worsley, D. 2005: Upper Palaeozoic lithostratigraphy of the southern part of the Norwegian Barents Sea. *Norge Geologiske Undersøkelse Bulletin 444*, 3-443.

Lauritsen, T., Blomstrand, L.B., Olesen, O. & Mørk, A. 2007: OSRAM II-Origin of sediment-Related AeroMagnetic II. Magnetic Susceptibility Measurements on Shallow Stratigraphic Cores from Finmark Platform, Nordkapp Basin and Svalis Dome. *Geological Survey of Norway (NGU) Report 2007.028*. 99 pp.

Levell, B.K. & Roberts, D. 1977: A re-investigation of the geology of north-west Varanger Peninsula, east Finnmark, north Norway. Norges Geologiske Undersøkelse Bulletin 334, 83-90.

Lippard, S. & Roberts, D. 1987: Faults systems in Caledonian Finnmark and the southern Barents Sea. *Norges Geologiske Undersøkelse Bulletin 410*, p. 55-64.

Lippard, S. 1987: Tectonic Development of the Sw Barents Sea with Special Reference to the Strategic Blocks. *Norsk Geologisk Tidsskrift* 67(4), 435-435.

Lønne, W. & Sellevoll, M.A. 1975: A reconnaissance gravity survey of Magerøy, Finnmark, Northern Norway. *Norges geologiske undersøkelse 319*, 1-15.

Løvaås, L., Mogaard, J., Olesen, O., Koziel, J. & Lynum, R. 2006: Southern Nordkapp Basin Aeromagnetic Survey 2006 (SNAS-06). Data acquisition and processing report. *Geological Survey of Norway (NGU) Report 2006.089*. 51 pp.

Ludwig, W., Nafe, J. & Drake, C. 1970: Seismic refraction. *In* Maxwell, A.E. (ed) The Sea, Volume 4. *Wiley-interscience, New York*, 53-84.

Luyendyk, A.P.J. 1997: Processing of airbone magnetic data. AGSO Journal of Australian Geology and Geophysics 17(2), 31-38.

Maher, H. D. J. 2001: Manifestations of Cretaceous High Arctic large igneous province in Svalbard. *Journal of Geology 109*, 91-104.

Mari, J.-L., Glangeaud, F. & Coppens, F. 2001: Traitement du signal pour géologues et géophysisiens-Techniques de base, 2. *Editions Technip*, 268 pp.

Marson, I. & Klingele, E. E. 1993: Advantages of using the vertical gradient of gravity for 3-D interpretation. *Geophysics 58*, 1588-1595.

Martinec, Z. 1994: The density contrast at the Mohorovičić discontinuity. *Geophysical Journal International 177*, 539-544.

Mathisen, O. 1976: A method for Bouguer reduction with rapid calculation of terrain corrections *Geographical Survey of Norway geodetic publications 18*, 40 p.

Mauring, E. & Kihle, A. 2006: Leveling aerogeophysical data using a moving differential median filter. *Geophysics 71(1)*, L5-L11.

Mauring, E., Beard, L.P., Kihle, O. & Smethurst, M.A. 2002: A comparison of aeromagnetic levelling techniques with an introduction to median levelling. *Geophysical Prospecting 50(1)*, 43-54.

McDonald, A. J., Fletcher, C. J., Carruthers, R. M., Wilson, D. & Evans, R. B. 1992: Interpretation of regional gravity and magnetic surveys of Wales, using shaded relief and Euler deconvolution techniques. *Geological Magazine 5*, 532-531.

Millegan, P.S. 1998: High-resolution aeromagnetic surveying. R.I. Gibson and P.S. Millegan (eds.) Geologic applications of gravity and magnetics: Case histories. Society of Exploration Geophysists and American Association of Petroleum Geologists, 18-19.

Miller, H.G. & Singh, V. 1994: Potential-Field Tilt - a New Concept for Location of Potential-Field Sources. Journal of Applied Geophysics 32(2-3), 213-217.

Mjelde, R., Breivik, A.J., Elstad, H., Ryseth, A.E., Skilbrei, J.R., Opsal, J.G., Shimamura, H., Murai, Y. & Nishimura, Y. 2002: Geological development of the Sorvestsnaget Basin,

SW Barents Sea, from ocean bottom seismic, surface seismic and gravity data, *Norwegian Journal of Geology*, 82**,** 183-202.

Mørk M.B.E., McEnroe S.A. and Olesen O. 2002. Magnetic susceptibility of Mesozoic and Cenozoic sediments off Mid Norway and the role of siderite: implications for interpretation of high-resolution aeromagnetic anomalies. *Marine and Petroleum Geology* **19**, 1115-1126.

Mudge, S. 1991: New developments in resolving detail in aeromagnetic data. *Exploration Geophysics 22*, 277-284.

Murphy, C. 2007. Interpreting FTG Gravity Data using Horizontal Tensor Components. Extended Abstract EGM 2007 International Worshop. Innovation in EM, Grav and Mag Methods:a new Perspective for Exploration, Capri, Italy, April 15-18.

Mushayandebvu, M.F., Lesur, V., Reid, A.B. & Fairhead, J.D. 2004: Grid Euler deconvolution with constraints for 2D structures. *Geophysics 69(2)*, 489-496.

Musset, A. E. & Khan, M. A. 2000: Looking into the Earth. *Cambridge University Press*, 470p.

Nabighian, M. N. 1972: The Analytic Signal of Two-Dimensional Magnetic Bodies with Polynomial Cross-Sections; Its Properties and Use for Automated Anomaly Interpretation. *Geophysics 37*, 505-517.

Nabighian, M. N. 1974: Additional comments on the analytic signal of two-dimensional magnetic bodies with polygonal cross-section. *Geophysics 39*, 85-92.

Nabighian, M. N. 1984: Toward a three-dimensional automatic interpretation of potential field data via generalized Hilbert transforms; fundamental relations. *Geophysics 49*, 780-786.

Nafe, J. E. & Drake C. 1957: Variation with depth in shallow and deep water marine sediments of porosity, density and the velocities of compressional and shear waves. *Geophysics 22*, 523-552.

Naidu, P. S. & Mathew, M. P. 1998: Analysis of geophysical potential fields. a digital signal processing approach. *In* Berkout, A.J. (ed). *Advances in Exploration Geophysics series, Elevier, Amsterdam 5*, 0-295.

Nettleton, L. L. 1976: Gravity and Magnetics in Oil prospecting. *McGraw-Hill, New York*, 462 pp.

Nilsen, K. T., Vendeville B. C., Johansen J. T. & A. 1994: An example of salt tectonics controlled by regional tectonics; the Nordkapp Basin, Norway. AAPG annual convention. *Annual Meeting Abstracts - American Association of Petroleum Geologists and Society of Economic Pale*, 1994, 225.

Nilsen, K. T., Vendeville, B. C. & Johansen, J. T. 1995: Influence of regional tectonics on halokinesis in the Nordkapp Basin, Barents Sea, *In* Jackson, M.P., Roberts, D.G. and Snelson, S. (eds), Salt tectonics: a global perspective. *AAPG Memoir 65*, 413-436.

Nyland, B., Jensen, L.N., Skagen, J., Skarpnes, O. & Vorren, T.O. 1992: Tertiary uplift and erosion in the Barents Sea: magnitude, timing and consequences. In Larsen, R.M., Brekke, H., Larsen, B.T. and Tallerås, E. (eds.). Structural and tectonic modeling and its apllication to petroleum geology. *Norwegian Petroleum Society Special Publication 1*, Elsevier, Amsterdam, 153-162.

Olesen O., Gernigon L., Ebbing, J., Mogaard, J., Pascal, C. and Wienecke, S., 2006: Interpretation of aeromagnetic data along the Jan Mayen Fracture Zone, JAS-05. *Geological Survey of Norway (NGU)* Report 2006.018. 162 pp.

Olesen, O., Gernigon, L., Hauge, J., Kihle, O., Koziel, J., Lauritsen, T., Myklebust, R., Skilbrei, J.R. & Usov, S. 2009: Magnetic anomaly map, Norway and adjacent areas. 1: 3 million. Geological Survey of Norway, Trondheim.

Olesen, O., Håbrekke, H., Kihle, O. & Smethurst, M. 1992: Finnmark fykke, aeromagnetisk anomalikart, M. 1:500.000. *Norges Geologiske Undersøkelse (NGU).*

Olesen, O., Håbrekke, H., Kihle, O. & Smethurst, M. 1992: Finnmark fykke, aeromagnetisk anomalikart, M. 1:500.000. *Norges Geologiske Undersøkelse (NGU)* .

Olesen, O., Roberts, D., Henkel, H., Lile, B.L. & Torsvik, T.H. 1990: Aeromagnetic and gravimetric interpretation of regional structural features in the Caledonides of West Finnmark and North Troms, northern Norway. *Norges geologiske undersøkelse Bulletin 419***,** 1-24.

Osmundsen, P.T., Sommaruga, A., Skilbrei, J.R. & Olesen, O. 2002: Deep structure of the Mid Norway rifted margin, *Norwegian Journal of Geology,* 82**,** 205-224.

Pilkington, M., Jansa, J. F. & Grieve, R. A. F. 1995: Geophysical studies of the Montagnais impact crater, Canada. *Meteoritics 30*, 446-450.

Pilkington, M., Miles, W. F., Ross, G. M. & Roest, W. R. 2000: Potential-field signatures of buried Precambrian basement in the Western Canada Sedimentary Basin: The Lithoprobe-Alberta basement transect-Le transect Lithoprobe du socle Albertain. *Canadian Journal of Earth Sciences = Revue Canadienne des Sciences de la Terre 37*, 1453-1471.

Popowski, T., Connard, G. & French, R., 2006. *GMSYS-3D: 3D Gravity and Magnetic Modeling for OasisMontaj - User Guide.* Northwest Geophysical Associates, Corvallis, Oregon, 32 pp.

Press, W.H., Teukolsky, S.A., Vetterling, W.T. & Flannery, B.P. 2002: Numerical Recipes in C++. The art of Scientific Computing Second Edition. Cambridge University Press. 972 pp

Prieto, C. 1993: Gulf of Mexico-understanding the magnetic response due to salt intrusion. International Geophysical Corporation Footnote Series.

Rafaelsen, B., Elvebakk, G., Andreassen, K., Stemmerik, L., Colpaert, A., Samuelsberg, T.J., 2008: From detached to attached carbonate buildup complexes — 3D seismic data from the upper Palaeozoic, Finnmark Platform, southwestern Barents Sea. *Sedimentary Geology*, 206, 17-32.

Ramberg, I.B. and Smithson, S.B. 1975.: Geophysical Interpretation of Crustal Structure along the Southeastern Coast of Norway and Skagerrak. *GSA Bulletin***,** 86(6), 769-774

Ravat, D. 1996: Analysis of the Euler method and its applicability in environmental magnetic investigations. *Journal of Environmental and Engineering Geophysics 1*, 229-238.

Ravat, D., Wang, B., Wildermuth, E. & Taylor, P. T. 2002: Gradients in the interpretation of satellite-altitude magnetic data; an example from central Africa. Earth's gravity and magnetic fields from space. *Journal of Geodynamics 33*, 131-142.

Reid, A., Allsop, J., Granser, H., Millet, A. & Somerton, I. 1990: Magnetic interpretation in three dimensions using Euler deconvolution. *Geophysics 55,* 80-91.

Rice, A. H.N., Gayer, R. A., Robinson, D. & Bevins, R. E. 1989a: Strike-slip restoration of the Barents Sea Caledonides terrane, Finnmark, North Norway. *Tectonics 8,* 247-264.

Rice, A.H.N., Bevins, R.E., Robinson, D. & Bevins, R.E. 1989b: Evolution of low-grade metamorphic zones in the Caledonides of Finnmark, N. Norway. *In* Gayer, R.A. (ed.) *The Caledonian geology of Scandinavia.* Graham & Trotman, London, 177-191.

Rice, A.H.N. 1994: Stratigraphic overlap of the Late Proterozoic Vadsø and Barents Sea Groups and correlation across the Trollfjorden-Komagelva Fault Zone, Finnmark, North Norway. *Norsk Geologisk Tidsskrift 74,* 48-57.

Rice, A.H.N. 2001: Field evidence for thrusting of the basement rocks coring tectonic windows in the Scandinavian Caledonides: an insight from the Kunes Nappe, Finnmark, Norway. *Norsk Geologisk Tidsskrift 81,* 321-328.

Rice, A.H.N., Frank, W. 2003: The early Caledonian (Finnmarkian) event reassessed in Finnmark: $^{40}Ar/^{39}Ar$ cleavage age data from NW Varangerhalvøya, N. Norway. Tectonophysics 374 (3-4), 219–236.

Rice, A.H.N., Ntaflos, T., Gayer, R.A. & Beckinsale, R.D. 2004: Metadolerite geochronology and dolerite geochemistry from East Finnmark, northern Scandinavian Caledonides. *Geological Magazine 141,* 301-318.

Riis, F. 1992: Dating and measuring of erosion, uplift and subsidence in Norway and the Norwegian shelf in glacial periods. *Norsk Geologisk Tidsskrift,* 72, 325–331.

Ritzmann, O., Hinz, K., Jokat, W., Reichert, C., Coffin, M. F., Duncan, R. A., Erzinger, J., Hinz, K. & Talwani, M. 1997: Crustal structure of the East Antarctic passive margin at 6 degrees E.; *Abstracts of the International Lithosphere program workshop on Volcanic margins.* p. 34-35.

Ritzmann, O., Maercklin, N., Faleide, J.I., Bungum, H., Mooney, W.D. & Detweiler, S.T. 2007: A three-dimensional geophysical model of the crust in the Barents Sea region: Model construction and basement characterization, *Geophysical Journal International,* 170**,** 417-435.

Roberts, D. 1972: Tectonic Deformation in the Barents Sea Region of Varanger Peninsula, Finnmark. *Norges Geologiske Undersøkelse 282,* 1-39.

Roberts, D. 1981: Geologisk kart over Norge, berggrunnskart NORDKAPP 1:250.000. *Norges geologiske undersøkelse (NGU), Trondheim.*

Roberts, D. 1985: The Caledonian fold bell in Finnmark: a synopsis. *Norske geologiske undersøkelse Bull*etin 403, 161-177.

Roberts, D. 1995: Principal features of the structural geology of Rybachi and Sredni Peninsulas, and some comparisons with Varanger Peninsula. *Norges geologiske undersøkelse Special Publication 7,* 247-258.

Roberts, D. 1996: Caledonian and Baikalian tectonic structures on Varanger Peninsula, Finnmark, and coastal areas of Kola Peninsula, NW Russia. *Norges geologiske undersøkelse Bulletin 431,* 59-65.

Roberts, D. 2003: The Scandinavian Caledonides; event chronology, palaeogeographic settings and likely modern analogues; *Tectonophysics 365*, 283-299.

Roberts, D. 2007: Palaeocurrent data from the Kalak Nappe Complex, northern Norway: a key element in models of terrane affiliation. *Norwegian Journal of Geology 87*, 319-328.

Roberts, D. 2009: Berggrunnskart Berlevåg 2336 1, M 1:50 000, revidert foreløpig utgave. *Norges geologiske undersøkelse*.

Roberts, D. & Andersen, T.B. 1985: Nordkapp. Beskrivelse til det bergrunnsgeologiske kartbladet M 1:250 000. *Norges Geologiske Undersøkelse Skrifter 61*, 1-49.

Roberts, D. & Gee, D.G. 1985: An introduction to the structure of the Scandinavian Caledonides. *In* Gee, D.G. & Sturt, B.A. (eds.) *The Caledonide orogen – Scandinavia and related areas.* John Wiley & Sons, Chichester, 55-68.

Roberts, D., Mitchell, J.G. & Andersen, T.B. 1991: A post-Caledonian dolerite dyke from Magerøya, North Norway: age and geochemistry. *Norsk Geologisk Tidsskrift 71*, 289-294.

Roberts, D. & Siedlecka, A. 2002: Timanian orogenic deformation along the northeastern margin of Baltica, Northwest Russia and Northeast Norway, and Avalonian-Cadomian connections. *Tectonophysics 352(1-2),* 169-184.

Roberts, D. & Olovyanishnikov, V. 2004: Structural and tectonic development of the Timanide orogen. *Geological Society London Memoirs* 30, 47–57.

Roberts, D. & Lippard, S. 2005: Inferred Mesozoic faulting in Finnmark. Current status and offshore links. *Norges Geologiske Undersøkelse Bulletin 443*, 55-60.

Roberts, R.J., Corfu, F., Torsvik, T.H., Ashwal, L.D. & Ramsay, D.M. 2006: Short-lived mafic magmatism at 560-570 Ma in the northern Norwegian Caledonides: U-Pb zircon ages from the Seiland Igneous Province, *Geological Magazine* 143**,** 887-903.

Roberts, R.J., Torsvik, T.H., Andersen, T.B. & Rehnstrom, E.F. 2003: The Early Carboniferous Mageroy dykes, northern Norway: palaeomagnetism and palaeogeography. *Geological Magazine 140(4)*, 443-451.

Robins, B. 1998: The mode of emplacement of the Honningsvåg Intrusive Suite, Magerøya, northern Norway, *Geological Magazine* 135**,** 231-244.

Roest, W. R., Verhoef, J. & Pilkington, M. 1992: Magnetic interpretation using the 3-D analytic signal. *Geophysics 57*, 116-125.

Rønnevik, H. C., Illing, L. V. & Hobson, G. D. 1981: Geology of the Barents Sea. *In* Illing, L.V. and Hobson, G.D. (eds.), Petroleum geology of the continental shelf of North-West Europe. *Proceedings of the second conference*, 395-406.

Rønnevik, H.C. & Jacobsen, H.P. 1984. Structural highs and basins in the western Barents Sea, Spence A.M. (ed.), Petroleum Geology of the north European margin. *Norsk Petroleum Forening, London*, Graham and Trotman, 19-32.

Saad, A. 1993: Interactive integrated interpretation of gravity, magnetic and seismic data-tools and examples. *Offshore Technology Conference abstract*, OTC#7079

Samuelsberg, T.J., Elvebakk, G. & Stemmerik, L. 2003: Late Palaeozoic evolution of the Finnmark Platform, southern Norwegian Barents Sea. *Norsk Geologisk Tidsskrift 83*, 351-362.

Siedlecka, A. & Roberts, D. 1992: The bedrock geology of Varanger Peninsula, Finmark, North Norway; an excursion guide. *Norges Geologiske Undersokelse Special Publication 5*, 1-45.

Siedlecka, A. & Roberts, D. 1996: Finnmark Fylke. Berggrunnsgeologi M 1:500 000. *Norges Geologiske Undersøkelse (NGU), Trondheim.*

Siedlecka, A. & Siedlecki, S. 1967: Some new aspects of the geology of the Varanger Peninsula (northern Norway). *Norges Geologiske Undersøkelse Bulletin 247*, 288-306.

Siedlecka, A. & Siedlecki, S. 1970: Rekognosering av den magnetiske anomali på østsiden av Nordkyhalvnøya. *Unpublished NGU report.*

Siedlecka, A. 1975: Late Precambrian stratigraphy and structure of the northeastern margin of the Fennoscandian Shield. *Norges geologiske undersøkelse 316*, 313-348.

Siedlecka, A. 1987: Development of the Upper Proterozoic Sedimentary Basins of Varanger Peninsula, North Norway. *Norsk Geologisk Tidsskrift 67(4)*, 437-437.

Siedlecka, A. 1984: SYLTEFJORD. Foreløpig berggrunnsgeologisk kart 2436, 1:50.000. Norges geologiske undersøkelse *(NGU), Trondheim.*

Siedlecki, S. 1980: Geologisk kart over Norge, berggrunnskart VADSØ-M. 1. 250.000. Norges geologiske undersøkelse (NGU), Trondheim.

Silva, I.A.B.C. & Barbosa, V.C.F. 2003: 3D Euler deconvolution: Theoretical basis for automatically selecting good solutions. *Geophysics 68(6)*, 1962-1968.

Simonov, A. G., M. & Yakovlev, Y. 1998: The Riphean oil of the Rybachiy Peninsula. Myth or key to a major direction for oil and gaz prospecting within the Barents Sea (in Russian). Bulletin of Murmansk´s State technical University, 1.

Skilbrei, J. R. 1993: An evaluation of magnetic top basement depth determinations from the southwestern Barents Sea. *Doktor ingeniøravhandling 1993:68*. Norges tekniske høgskole, Trondheim.

Skilbrei, J. R., Kihle, O., Olesen, O., Gellein, J., Sindre, A., Solheim, D. & Nyland, B. 2000: Gravity anomaly map of Norway and adjacent ocean areas, scale 1:3 Million: *Geological Survey of Norway (NGU)*, Trondheim.

Skilbrei, J.R. 1991: Interpretation of Depth to the Magnetic Basement in the Northern Barents Sea (South of Svalbard). *Tectonophysics 200(1-3)*, 127-141.

Skilbrei, J.R. 1992: Preliminary interpretation of aeromagnetic data from Spitsbergen, Svalbard Archipelago (76°-79°N): Implications for structure of the basement. *Marine Geology 106*, 53-68.

Skilbrei, J.R. 1993: Interpretation of geophysical data from the northwestern Barents Sea and Spitzbergen, Universitetet i Trondheim Norges Tekniske Høgskole.

Skilbrei, J.R., Habrekke, H., Christoffersen, T. & Myklebust, R.A. 1990: Aeromagnetic surveying at high latitudes, a case history from the northern Barents Sea. *First Break 8*, 2, 46-50.

Skilbrei, J.R., Kihle, O., Olesen, O., Gellein, J., Sindre, A., Solheim, D. & Nyland, B. 2000: Gravity map of Norway and adjacent ocean areas, scale 1:3 Million. *Geological survey of Norway (NGU).*

Skilbrei, J.R., Olesen, O., Osmundsen, P.T., Kihle, O., Aaro, S. & Fjellanger E. 2002: A study of basement structures and onshore-offshore correlations in Central Norway. *Norwegian Journal of Geology*, 82, 263-279.

Skilbrei, J.R., Olesen, O., Osmundsen, P.T., Kihle, O., Aaro, S. & Fjellanger, E. 1992: A study of basement structures and onshore-offshore correlations in Central Norway. *Norwegian Journal of Geology 82(4)*, 263-279.

Skilbrei, J.R., Skyseth, T. & Olesen, O. 1991: Petrophysical Data and Opaque Mineralogy of High-Grade and Retrogressed Lithologies - Implications for the Interpretation of Aeromagnetic Anomalies in Northern Vestranden, Central Norway. *Tectonophysics* 192(1-2), 21-31.

Skilbrei, J.R. 1995: Aspects of the geology of the southwestern Barents Sea from aeromagnetic data. *Norges geologiske undersøkelse Bulletin 427*, 64-67.

Slagstad, T., Barrère, C., Davidsen, B. & Ramstad, R.K., 2008. Petrophysical and thermal properties of pre-Devonian basement rocks on the Norwegian continental margin, *Norges geologiske undersøkelse Bulletin 448*, 1-6.

Slagstad, T., Barrère, C., Davidsen, B. & Ramstad, R.K. 2008: Petrophysical and thermal properties of pre-Devonian basement rocks on the Norwegian continental margin, *Norges geologiske undersøkelse Bulletin* 448, 1-6.

Spector, A. & Grant, F. S. 1970: Statistical models for interpreting aeromagnetic data. *Geophysics, 35*, 293-302.

Spector, A. & Grant, F. S. 1970: Statistical models for interpreting aeromagnetic data. *Geophysics, 35*, 293-302.

Stavrev, P. & Reid, A. 2007: Degrees of homogeneity of potential fields and structural indices of Euler deconvolution. *Geophysics* 72(1), L1-L12.

Stemmerik, L. & Worsley, D. 1989: Late Palaeozoic sequence correlations, North Greenland, Svalbard and the Barents Shelf. *In* Collison, J.D. (ed.), Correlation in hydrocarbon exploration. *Norwegian Petroleum Society, Graham and Trotman, London*, 99-111.

Stemmerik, L. & Worsley, D. 1989: Late Palaeozoic sequence correlations, North Greenland, Svalbard and the Barents Shelf. *In* Collison, J.D. (ed.), Correlation in hydrocarbon exploration. *Norwegian Petroleum Society, Graham and Trotman, London*, 99-111.

Stephens, M.B. & Gee, D., 1985: A tectonic model for the evolution of the eugeoclinal terranes in the central Scandinavian Caledonides. D. Gee & B.A. Sturt (eds.), The Caledonide Orogen—Scandinavia and Related Areas. Wiley, Chichester, 953-970.

Sundvoll, B. & Roberts, D. 2003: A likely Early Ordovician age for the regional penetrative cleavage in the Gaissa Nappe Complex, northern Norway. *Norges Geologiske Undersøkelse Bulletin 441*, 51-59.

Talwani, M. 1973. Computer Usage in the Computation of Gravity Anomalies. *Methods in Computational Physics 13*, 343-389.

Talwani, M. 1973: Computer Usage in the Computation of Gravity Anomalies. Methods in Computational Physics 13, 343-389.

Taylor, P.N. & Pickering, K.T. 1981: Rb–Sr isotopic age determination on the late Precambrian Kongsfjord Formation, and the timing of compressional deformation in the Barents Sea Group, East Finnmark. *Norges Geologiske Undersøkelse Bulletin 278*, 81-92.

Thompson, D. 1982: EULDPH. A new technique for making computer-assisted depth estimates from magnetic data. *Geophysics 47*, 31-37.

Thompson, D.T. 1982: EULDPH: A new technique for making computer-assisted depth estimates from magnetic data. *Geophysics* 47, 31-37.

Thurston, J.B. & Brown, R.J. 1994: Automated Source-Edge Location with a New Variable Pass-Band Horizontal-Gradient Operator. *Geophysics 59(4)*, 546-554.

Torsvik, T.H., Olesen, O., Trench, A., Andersen, T.B., Walderhaug, H.J. & Smethurst, M.A. 1992: Geophysical Investigation of the Honningsvag Igneous Complex, Scandinavian Caledonides. *Journal of the Geological Society 149*, 373-381.

Tsikalas, F. 1992: A study of seismic velocity, density and porosity in Barents Sea wells (N. Norway). *Unpublished Master Thesis*, University of Oslo, Norway, 169 pp.

Vendeville, B. & Jackson, M. P.1992. The rise of diapirs during thin-skinned extension. *Marine and Petroleum Geology 9*, 331-353.

Verduzco, B., Fairhead, J.D., Green, C.M. & MacKenzie, C. 2004: The meter reader-New insights into magnetic derivatives for structural mapping. *The Leading Edge* 23, 116-119.

Werner, S. 1953: Interpretation of magnetic anomalies of sheet-like bodies. *Sveriges Geologiska Arsbok*, 43, 6, 130 pp.

Wienecke, S., Ebbing, J. & Gernigon, L. 2007: 3D gravity modelling, isostasy and elastic thickness calculation in the Barents Sea, Geological Survey of Norway-NGU Report 2007.022, 1-56

Winograd, S. 1978: On Computing the Discrete Fourier Transform. *Mathematics of Computation* 32(141), 175-199.

Worsley, D. 2006: The post-Caledonian geological development of Svalbard and the Barents Sea. The Boreal Triassic conference, Longyearbyen, Svalbard, NGF *extended Abstract and Proceedings*.

Worsley, D., Agdestein, T., Gielberg, J.G., Kirkemo, K., Mork, A., Nilsson, I., Olaussen, S., Steel, R.J. & Stemmerik, L. 2001: The geological evolution of Bjørnøya, Arctic Norway: implications for the Barents Shelf. *Norsk Geologisk Tidsskrift 81(3)*, 195-234.

15 LIST OF FIGURES AND TABLES:

yellow lines underline the main structural features of the area (Gabrielsen et al. 1990). Grey lines represent the faults mapped at base Cretaceous level (Gabrielsen et al. 1990).

Figure 9.4 Bouguer anomalies along the BASAR-08 survey area and interpretation of the main anomaly highs and lows. Black and yellow lines underline the main structural features of the area (Gabrielsen et al. 1990). Grey lines represent the faults mapped at base Cretaceous level (Gabrielsen et al. 1990).

Figure 9.5 Interpretation of the main anomaly highs and lows from Bouguer (filled) and TMI (outlines) maps. Black and yellow lines underline the main structural features of the area (Gabrielsen et al. 1990). Grey lines represent the faults mapped at base Cretaceous level (Gabrielsen et al. 1990).

Figure 9.6 a) TMI grid with complete structural interpretation, b) 30 km high-pass filter with first-order tectonic elements and c) 30 km high-pass with complete structural interpretation. Blue curved lines are observed lineaments from the magnetic map and are most likely associated with Caledonian nappes, dark blue lines are major faults. Red lines show fault-related lineaments probably associated with high-magnetic material such as dykes (see text). Black and yellow lines underline the main structural features of the area (Gabrielsen et al. 1990). Grey lines represent the faults mapped at base Cretaceous level (Gabrielsen et al. 1990), black (BASAR-08) and blue (BAS-06) dotted lines represent second class lineaments with a more shallow origin, based on magnetic interpretation.

Figure 9.7 a) TILT derivative from TMI grid with principal possibly intruded faults, b) HD-TILT from TMI with complete structural interpretation and c) the complete structural interpretation. Blue curved lines are observed lineaments from the magnetic map and are most likely associated with Caledonian nappes, dark blue lines are major faults. Red lines show fault-related lineaments probably associated with high-magnetic material such as dykes (see text). Black and yellow lines underline the main structural features of the area (Gabrielsen et al. 1990). Grey lines represent the faults mapped at base Cretaceous level (Gabrielsen et al. 1990), black (BASAR-08) and blue (BAS-06) dashed lines represent second-order lineaments with a more shallow origin based on magnetic interpretation.

Figure 9.8 a) Structural elements with complete structural interpretation, b) Interpretation of the main anomaly highs and lows from Bouguer (filled) and TMI (outlines) maps with complete structural interpretation and c) Bouguer gravity with first-order tectonic elements and possibly intruded faults. Blue curved lines are observed lineaments from the magnetic map and are most likely associated with Caledonian nappes, dark blue are major faults. Red lines show fault-related lineaments probably associated with high-magnetic material such as dykes (see texte). Black and yellow lines underline the main structural features of the area (Gabrielsen et al. 1990). Grey lines represent the faults mapped at base Cretaceous level (Gabrielsen et al. 1990), black (BASAR-08) and blue (BAS-06) dashed lines represent second-order lineaments with a more shallow origin, based on magnetic interpretation.

Figure 9.9 Comparison between (a) the new and (b) the vintage magnetic data for the Nordkapp Basin. The BASAR-08 data (left) have a significantly higher resolution, showing various features such as salt structures and faults in much more details.

petrophysical values obtained by density and magnetic modelling. Figure 11.4a shows the location of the different basement units.

16 APPENDIX 1 CD CONTENT

16.1 Folders

Report
Presentations
Data
Figures & Maps

16.1.1 Report

NGU BASAR-08 report in PDF format

16.1.2 Presentations

Presentations showed to our partners in MS PowerPoint format (.ppt)

16.1.3 Data

- Profile

Profile data *BASAR08-BAS06_Mag_proc.** Geosoft database and ASCII file

Name	Format	Describtion
1 UMTE	10.0	UTM coordinates WGS84 UTM36N
2 UTMN	10.0	UTM coordinates WGS84 UTM36N
3 LATITUDE	24.2	geographical coordinates
4 LONGITUDE	16.2	geographical coordinates
5 ALT_gps	10.2	GPS altitude
6 ALT_R_ft	10.2	Radar altitude in feet
7 ALT_R_m	10.2	Radar altitude in metre
8 ALT_R_m_corr	14.2	corrected Radar altitude in metre
9 ALT_R_m_sensor	20.2	corrected Sensor altitude in metre
10 Date	10.2	Date
11 GPSTIME	18.2	Gpstime
12 Mag_raw	10.2	uncorrected recorded magnetic field
13 Mag_raw_NOSPK	14.2	Spike corrected recorded magnetic field
14 BMAG	10.2	Basemagentometre Lakselv/Hammerfest and Leknes(BAS06)
15 IGRF	10.2	IGRF field
16 MAG_anom	18.2	IGRF corrected and shifted magnetic field
17 MAG_anom_prelim	20.2	IGRF corrected magnetic field
18 Mag_anom_tlev	23.2	Tie-line leveled magnetic field
19 MAG_filt_BAS06	20.2	preliminary noise filtered raw magnetic (only BAS-06)
20 Mag_lag_head_BAS06	32.2	head corrected magnetic field (only BAS-06)
21 MAG_lev_all_rev1	24.2	levelled magnetic data, tie-lines and in-lines
22 MAG_lev_line_rev1	41.2	levelled magnetic data, in-lines
23 Mag_mic_Final	15.2	final TMI, microlevelled all lines, tie-lines and in-lines
24 Mag_mic_Final_rtp	10.2	final TMI reduced to pole
25 Mag_mic_Final_rtp_h30k	10.2	30 km high-pass filter of final TMIRTP
26 Mag_mic_line_rev1	36.2	microlevelled in-lines
27 MAG_tlev_stat	23.2	statistical tie-line levelling
28 MAG_tmic_rev1	20.1	microlevelled tie-lines
29 dcor_noise_full_lev_rev1	32.1	decorrogation noise full levelling
30 dcor_noise_rev1	17.1	decorrugation tie-lines

31 Dec	10.1	Declination
32 Inc	10.2	Inclination
33 NSAT	10.0	number of satellites

- Grids

Gridded data in UTM 36N, WGS84

Geosoft grid files

XYZ files

↵ Filtering

Various filtering of TMIRTP data

↵ Processing

Decorrugation grids subtracted from magnetic data during the processing workflow

16.1.4 Figures & Maps

Selected report figures in JPG format

Selected maps in PDF format

- Total magnetic field
- Total magnetic field reduced to pole
- 30 km high-pass filter from TMI field reduced to pole
- TILT derivative from TMI field reduced to pole
- Analytic signal from TMI field reduced to pole